

**CHAPTER 1**  
**INTRODUCTION**

## 1.1 Overview of This Manual

The following provides a brief description of each chapter in this technical manual.

### Chapter 1 Introduction

Before starting to describe the main subjects, this chapter explains basic photometric units used to measure or express properties of light such as wavelength and intensity. This chapter also describes the history of the development of photocathodes and photomultiplier tubes, as well as providing a brief guide to photomultiplier tubes which will be helpful for first-time users.

### Chapter 2 Basic Principles of Photomultiplier Tubes

This chapter describes the basic operating principles and mechanisms of photomultiplier tubes, including photoelectron emission, electron trajectories, and electron multiplication by use of secondary electron multipliers (dynodes).

### Chapter 3 Characteristics of Photomultiplier Tubes

Chapter 3 explains the types of photocathodes and dynodes, and their basic characteristics. This chapter also provides the definitions of various characteristics of photomultiplier tubes, their measurement procedures, and specific examples of typical photomultiplier tube characteristics.

In addition, this chapter describes photon counting and scintillation counting - light measurement techniques that have become more popular in recent years. Also listed are definitions of their characteristics, measurement procedures, and typical characteristics of major photomultiplier tubes.

### Chapter 4 MCP-PMTs (Microchannel Plate - Photomultiplier Tubes)

This chapter explains MCP-PMTs – photomultiplier tubes incorporating microchannel plates (MCPs) for their electron multipliers. The basic structure, operation, performance and examples of major characteristics are discussed.

### Chapter 5 Electron Multiplier Tubes

Chapter 5 describes electron multiplier tubes (sometimes called EMT), showing the basic structure, typical characteristics and handling precautions.

### Chapter 6 Position-Sensitive Photomultiplier Tubes

This chapter introduces recently developed position-sensitive photomultiplier tubes using grid type dynodes, mesh dynodes or fine-mesh dynodes combined with multianodes, and explains their structure, characteristics and applications.

## **Chapter 7 How to Use and Operate Photomultiplier Tubes**

To use photomultiplier tubes correctly, an optimum design is essential for the operating circuits (voltage-divider circuit and high-voltage power supply) and the associated circuit to which they are connected. In addition, magnetic or noise shielding may be necessary in some cases.

This chapter explains how to design an optimum electric circuit, including precautions for actual operation with photomultiplier tubes.

## **Chapter 8 Environmental Durability and Reliability**

In this chapter, photomultiplier tube performance and usage are discussed in terms of environmental durability and operating reliability. In particular, this chapter describes ambient temperature, humidity, magnetic field effects, mechanical strength, influence of electromagnetic fields and the countermeasures against these factors. Also explained are operating life, definitions concerning reliability and examples of typical photomultiplier tube characteristics.

## **Chapter 9 Application**

Chapter 9 introduces major applications of photomultiplier tubes, and explains how photomultiplier tubes are used in a variety of fields and applications. Moreover, this chapter shows how to evaluate characteristics of photomultiplier tubes which are required for each application along with their definitions and examples of data actually measured.

## 1.2 Photometric units

Before starting to describe photomultiplier tubes and their characteristics, this section briefly discusses photometric units commonly used to measure the quantity of light. This section also explains the wavelength regions of light (spectral range) and the units to denote them, as well as the unit systems used to express light intensity. Since information included here is just an overview of major photometric units, please refer to specialty books for more details.

### 1.2.1 Spectral regions and units

Electromagnetic waves cover a very wide range from gamma rays up to millimeter waves. So-called "light" is a very narrow range of these electromagnetic waves.

Table 1-1 shows designated spectral regions when light is classified by wavelength, along with the conversion diagram for light units. In general, what we usually refer to as light covers a range from  $10^2$  to  $10^6$  nanometers (nm) in wavelength. The spectral region between 350 and 700nm shown in the table is usually known as the visible region. The region with wavelengths shorter than the visible region is divided into near UV (shorter than 350nm), vacuum UV (shorter than 200nm) where air is absorbed, and extreme UV (shorter than 100nm). Even shorter wavelengths span into the region called soft X-rays (shorter than 10nm) and X-rays. In contrast, longer wavelengths beyond the visible region extend from near IR (750nm or up) to the infrared (several micrometers or up) and far IR (several tens of micrometers) regions.

| Wavelength | Spectral Range       | Frequency | Energy    |
|------------|----------------------|-----------|-----------|
| nm         |                      | (Hz)      | (eV)      |
|            | X-ray<br>Soft X-ray  |           |           |
| 10         | Extreme UV region    | $10^{16}$ | $10^2$    |
| $10^2$     |                      |           | 10        |
| 200        | Vacuum UV region     | $10^{15}$ |           |
| 350        | Ultraviolet region   |           |           |
| 750        | Visible region       |           |           |
| $10^3$     | Near infrared region |           | 1         |
|            | Infrared region      | $10^{14}$ |           |
| $10^4$     |                      |           | $10^{13}$ |
| $10^5$     | Far infrared region  |           | $10^{-2}$ |
| $10^6$     |                      |           | $10^{12}$ |

Table 1-1: Spectral regions and unit conversions

Light energy  $E$  (eV) is given by the following equation (Eq. 1-1).

$$E = h\nu = h \cdot \frac{c}{\lambda} = hc\bar{\nu} \quad \text{..... (Eq. 1-1)}$$

$h$ : Planck's constant  $6.626 \times 10^{-34}$  (J·S)

$\nu$ : Frequency of light (Hz)

$\bar{\nu}$ : Wave number ( $\text{cm}^{-1}$ )

$c$ : Velocity of light  $3 \times 10^8$  m/s

Here, velocity of light has relation to frequency  $\nu$  and wavelength  $\lambda$  as follow:

$$c = \nu\lambda.$$

When  $E$  is expressed in eV (electron volts) and  $\lambda$  in nm, the relation between eV and  $\lambda$  is given as follows:

$$E \text{ (eV)} = \frac{1240}{\lambda} \quad \text{..... (Eq. 1-2)}$$

From Eq. 1-2, it can be seen that light energy increases in proportion to the reciprocal of wavelength. This equation is helpful when discussing the relation between light energy (eV) and wavelength (nm), so remembering it is suggested.

## 1.2.2 Units of light intensity

This section explains the units used to represent light intensity and their definitions.

The radiant quantity of light or radiant flux is a pure physical quantity expressed in units of watts (W). In contrast, the photometric quantity of light or luminous flux is represented in lumens which correlate to the visual sensation of light.

The "watt (W)" is the basic unit of radiated light when it is measured as analog quantity, and the photon is the minimum unit of radiated light. The energy of one photon is given by the equation below.

$$P = h\nu = hc/\lambda \quad \text{..... (Eq. 1-3)}$$

From the relation  $W=J/\text{sec.}$ , the following calculation can be made by substituting specific values for the above equation.

$$1 \text{ watt} = 5.05 \lambda \text{ (}\mu\text{m)} \times 10^{18} \text{ photons/sec.}$$

This equation gives the number of photons (per second) from the radiant flux (W) measured, and will be helpful if you remember it.

Table 1-2 shows comparisons of radiant units with photometric units are listed. (Each unit is detailed in subsequent sections.)

| Quantity                               | Unit Name  | Symbol                                   |
|--|--|--|
| Radiant flux [Luminous flux]           | watts [lumens]   | W [lm]                                   |
| Radiant energy [Quantity of light]     | joules [lumen·sec.]  | J [lm·s]                                 |
| Irradiance [Illuminance]               | watts per square meter [lux]                                 | W/m <sup>2</sup> [lx]                    |
| Radiant emittance [Luminous emittance] | watts per square meter [lumens per square meter]             | W/m <sup>2</sup> [lm/m <sup>2</sup> ]    |
| Radiant intensity [Luminous intensity] | watts per steradian [candelas]                               | W/sr [cd]                                |
| Radiance [Luminance]                   | watts per steradian·square meter [candelas per square meter] | W/sr·m <sup>2</sup> [cd/m <sup>2</sup> ] |

**Table 1-2: Comparisons of radiant units with photometric units (shown in brackets [ ])**

## 1. Radiant flux [luminous flux]

Radiant flux is a unit to express radiant quantity, while luminous flux shown in brackets [ ] in Table 1-2 and the subhead just above is a unit to represent luminous quantity. (Units are shown this way in the rest of this chapter.) Radiant flux ( $\Phi_e$ ) is the flow of radiant energy ( $Q_e$ ) past a given point in a unit time period, and is defined as follows:

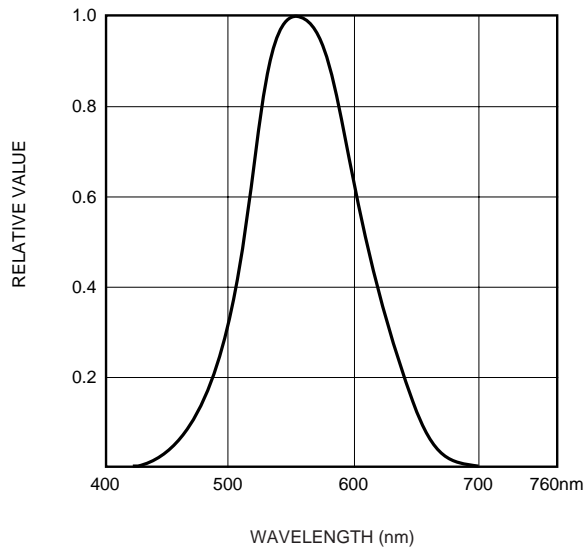
$$\Phi_e = dQ_e/dt \text{ (joules per sec. ; watts)} \dots\dots\dots \text{(Eq. 1-4)}$$

On the other hand, luminous flux ( $\Phi$ ) is measured in lumens and defined as follows:

$$\Phi = km \int \Phi_e(\lambda) v(\lambda) d\lambda \dots\dots\dots \text{(Eq. 1-5)}$$

- where  $\Phi_e(\lambda)$  : Spectral radiant density of a radiant flux, or spectral radiant flux  
 $km$  : Maximum sensitivity of the human eye (638 lumens/watt)  
 $v(\lambda)$  : Typical sensitivity of the human eye

The maximum sensitivity of the eye ( $km$ ) is a conversion coefficient used to link the radiant quantity and luminous quantity. Here,  $v(\lambda)$  indicates the typical spectral response of the human eye, internationally established as spectral luminous efficiency. A typical plot of spectral luminous efficiency versus wavelength (also called the luminosity curve) and relative spectral luminous efficiency at each wavelength are shown in Figure 1-1 and Table 1-3, respectively.



TPMOB0089EA

**Figure 1-1: Spectral luminous efficiency distribution**

| Wavelength (nm) | Luminous Efficiency | Wavelength (nm) | Luminous Efficiency |
|-----------------|---------------------|-----------------|---------------------|
| 400             | 0.0004              | 600             | 0.631               |
| 10              | 0.0012              | 10              | 0.503               |
| 20              | 0.0040              | 20              | 0.381               |
| 30              | 0.0116              | 30              | 0.265               |
| 40              | 0.023               | 40              | 0.175               |
| 450             | 0.038               | 650             | 0.107               |
| 60              | 0.060               | 60              | 0.061               |
| 70              | 0.091               | 70              | 0.032               |
| 80              | 0.139               | 80              | 0.017               |
| 90              | 0.208               | 90              | 0.0082              |
| 500             | 0.323               | 700             | 0.0041              |
| 10              | 0.503               | 10              | 0.0021              |
| 20              | 0.710               | 20              | 0.00105             |
| 30              | 0.862               | 30              | 0.00052             |
| 40              | 0.954               | 40              | 0.00025             |
| 550             | 0.995               | 750             | 0.00012             |
| 555             | 1.0                 | 60              | 0.00006             |
| 60              | 0.995               |                 |                     |
| 70              | 0.952               |                 |                     |
| 80              | 0.870               |                 |                     |
| 90              | 0.757               |                 |                     |

Table 1-3: Relative spectral luminous efficiency at each wavelength

## 2. Radiant energy (Quantity of light)

Radiant energy ( $Q_e$ ) is the integral of radiant flux over a duration of time. Similarly, the quantity of light ( $Q$ ) is defined as the integral of luminous flux over a duration of time. Each term is respectively given by Eq. 1-6 and Eq. 1-7.

$$Q_e = \int \Phi_e dt \text{ (watt-sec.)} \dots\dots\dots \text{(Eq. 1-6)}$$

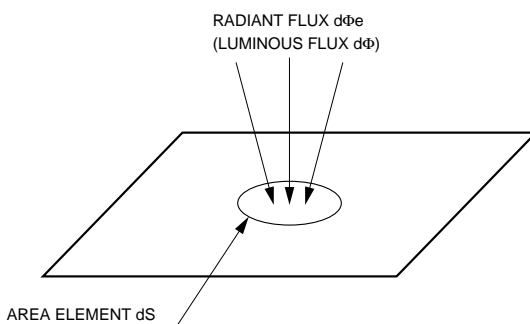
$$Q = \int \Phi dt \text{ (lumen-sec.)} \dots\dots\dots \text{(Eq. 1-7)}$$

## 3. Irradiance (Illuminance)

Irradiance ( $E_e$ ) is the radiant flux incident per unit area of a surface, and is also called radiant flux density. (See Figure 1-2.) Likewise, illuminance ( $E$ ) is the luminous flux incident per unit area of a surface. Each term is respectively given by Eq. 1-8 and Eq. 1-9.

$$\text{Irradiance } E_e = d\Phi_e/ds \text{ (watts per square meter; } W/m^2) \dots\dots\dots \text{(Eq. 1-8)}$$

$$\text{Illuminance } E = d\Phi/ds \text{ (lumen per square meter; } lm/m^2 \text{ or lux)} \dots\dots\dots \text{(Eq. 1-9)}$$



TPMOB0085EA

Figure 1-2: Irradiance (Illuminance)

**4. Radiant emittance (Luminous emittance)**

Radiant emittance ( $M_e$ ) is the radiant flux emitted per unit area of a surface. (See Figure 1-3.) Likewise, Luminous emittance ( $M$ ) is the luminous flux emitted per unit area of a surface. Each term is respectively expressed by Eq. 1-10 and Eq. 1-11.

Radiant emittance  $M_e = d\Phi_e/ds$  (watt per square meter;  $W/m^2$ ) ..... (Eq. 1-10)

Luminous emittance  $M = d\Phi/ds$  (lumen per square meter;  $lm/m^2$ ) ..... (Eq. 1-11)

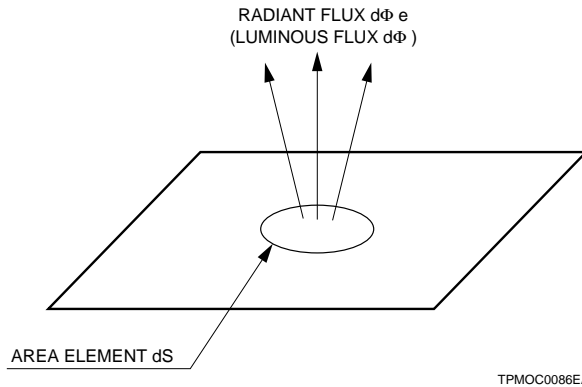


**Figure 1-3: Radiant emittance (Luminous emittance)**

**5. Radiant intensity (Luminous intensity)**

Radiant intensity ( $I_e$ ) is the radiant flux emerging from a point source, divided by the unit solid angle. (See Figure 1-4.) Likewise, luminous intensity ( $I$ ) is the luminous flux emerging from a point source, divided by the unit solid angle. These terms are respectively expressed by Eq. 1-12 and Eq. 1-13.

Radiant intensity  $I_e = d\Phi_e/dw$  (watts per steradian;  $W/sr$ ) ..... (Eq. 1-12)

Where

- $\Phi_e$  : radiant flux (watts)
- $w$  : solid angle (steradians)

Luminous intensity  $I = d\Phi/dw$ (candelas: cd) ..... (Eq. 1-13)

Where

- $\Phi$  : luminous flux (lumens)
- $w$  : solid angle (steradians)

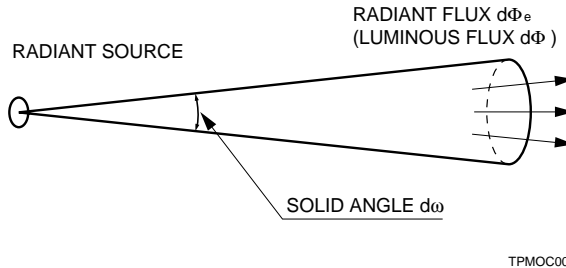


**Figure 1-4: Radiant intensity (Luminous intensity)**

### 6. Radiance (Luminance)

Radiance ( $L_e$ ) is the radiant intensity emitted in a certain direction from a radiant source, divided by unit area of an orthographically projected surface. (See Figure 1-5.) Likewise, luminance ( $L$ ) is the luminous flux emitted from a light source, divided by the unit area of an orthographically projected surface. Each term is respectively given by Eq. 1-14 and Eq. 1-15.

$$\text{Radiance } L_e = dI_e/ds \times \cos\theta \text{ (watts per steradian-m}^2\text{)} \dots\dots\dots \text{(Eq. 1-14)}$$

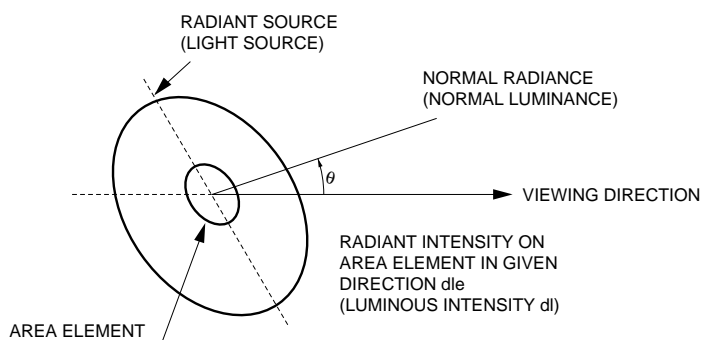
Where

- le: radiant intensity
- s : area
- $\theta$  : angle between viewing direction and small area surface

$$\text{Luminance } L = dI/ds \times \cos\theta \text{ (candelas/m}^2\text{)} \dots\dots\dots \text{(Eq. 1-15)}$$

Where

- I: luminous intensity (candelas)



TPMOC0088EA

**Figure 1-5: Radiant intensity (Luminous intensity)**

In the above sections, we discussed basic photometric units which are internationally specified as SI units for quantitative measurements of light. However in some cases, units other than SI units are used.

Tables 1-4 and 1-5 show conversion tables for SI units and non-SI units, with respect to luminance and illuminance. Refer to these conversion tables as necessary.

|             | Unit Name                           | Symbol               | Conversion Fomula   |
|-------------|-------------------------------------|----------------------|---|
| SI Unit     | nit<br>stilb<br>apostilb<br>lambert | nt<br>sb<br>asb<br>L | 1nt = 1cd/m <sup>2</sup><br>1sb = 1cd/cm <sup>2</sup> = 10 <sup>4</sup> cd/m <sup>2</sup><br>1asb = 1/π cd/m <sup>2</sup><br>1L = 1/π cd/cm <sup>2</sup> = 10 <sup>4</sup> /π cd/m <sup>2</sup> |
| Non SI Unit | foot lambert                        | fL                   | 1fL = 1/π cd/ft <sup>2</sup> = 3.426 cd/m <sup>2</sup>  |

**Table 1-4: Luminance units**

|             | Unit Name   | Symbol | Conversion Fomula                               |
|-------------|-------------|--------|---|
| SI Unit     | photo       | ph     | 1ph = 1 lm/cm <sup>2</sup> = 10 <sup>4</sup> lx |
| Non SI Unit | food candle | fc     | 1fc = 1 lm/ft <sup>2</sup> = 10.764 lx          |

**Table 1-5: Illuminance units**

## 1.3 History

### 1.3.1 History of photocathodes<sup>1)</sup>

The photoelectric effect was discovered in 1887 by Herts<sup>4)</sup> through experiments exposing a negative electrode to ultraviolet radiation. In the next year 1888, the photoelectric effect was conclusively confirmed by Hallwachs.<sup>5)</sup> In 1889, Elster and Geiter<sup>6)</sup> reported the photoelectric effect which was induced by visible light striking an alkali metal (sodium-potassium). Since then, a variety of experiments and discussions on photoemission have been made by many scientists. As a result, the concept proposed by Einstein (in the quantum theory in 1905),<sup>7)</sup> "Photoemission is a process in which photons are converted into free electrons.", has been proven and accepted.

During this historic period of achievement, Elster and Geiter produced a photoelectric tube in 1913. Then, a compound photocathode made of Ag-O-Cs (silver oxygen cesium, so-called S-1) was discovered in 1929 by Koller<sup>8)</sup> and Campbell.<sup>9)</sup> This photocathode showed photoelectric sensitivity about two orders of magnitude higher than previously used photocathode materials, achieving high sensitivity in the visible to near infrared region. In 1930, they succeeded in producing a phototube using this S-1 photocathode. In the same year, a Japanese scientist, Asao reported a method for enhancing the sensitivity of silver in the S-1 photocathode. Since then, various photocathodes have been developed one after another, including bialkali photocathodes for the visible region, multialkali photocathodes with high sensitivity extending to the infrared region and alkali halide photocathodes intended for ultraviolet detection.<sup>10)-13)</sup>

In addition, photocathodes using III-V compound semiconductors such as GaAs<sup>14)-19)</sup> and InGaAs<sup>20) 21)</sup> have been developed and put into practical use. These semiconductor photocathodes have an NEA (negative electron affinity) structure and offer high sensitivity from the ultraviolet through near infrared region. Currently, a wide variety of photomultiplier tubes utilizing the above photocathodes are available. They are selected and used according to the application required.

### 1.3.2 History of photomultiplier tubes

Photomultiplier tubes have been making rapid progress since the development of photocathodes and secondary emission multipliers (dynodes).

The first report on a secondary emissive surface was made by Austin et al.<sup>22)</sup> in 1902. Since that time, research into secondary emissive surfaces (secondary electron emission) has been carried out to achieve higher electron multiplication. In 1935, Iams et al.<sup>23)</sup> succeeded in producing a triode photomultiplier tube with a photocathode combined with a single-stage dynode (secondary emissive surface), which was used for movie sound pickup. In the next year 1936, Zworykin et al.<sup>24)</sup> developed a photomultiplier tube having multiple dynode stages. This tube enabled electrons to travel in the tube by using an electric field and a magnetic field. Then, in 1939, Zworykin and Rajchman<sup>25)</sup> developed an electrostatic-focusing type photomultiplier tube (this is the basic structure of photomultiplier tubes currently used). In this photomultiplier tube, an Ag-O-Cs photocathode was first used and later an Sb-Cs photocathode was employed.

An improved photomultiplier tube structure was developed and announced by Morton in 1949<sup>26)</sup> and in 1956.<sup>27)</sup> Since then the dynode structure has been intensively studied, leading to the development of a variety of dynode structures including circular-cage, linear-focused and box-and-grid types. In addition, photomultiplier tubes using magnetic-focusing type multipliers,<sup>28)</sup> transmission-mode secondary-emissive surfaces<sup>29)-31)</sup> and channel type multipliers<sup>32)</sup> have been developed.

At Hamamatsu Photonics, the manufacture of various phototubes such as types with an Sb-Cs photocathode was established in 1953 (then Hamamatsu TV Co., Ltd. – The company name was changed in 1983.). In 1959, Hamamatsu Photonics marketed side-on photomultiplier tubes (type No. 931A, 1P21 and R106 having

---

an Sb-Cs photocathode) which have been widely used in spectroscopy. Hamamatsu Photonics also developed and marketed side-on photomultiplier tubes (type No. R132 and R136) having an Ag-Bi-O-Cs photocathode in 1962. This photocathode had higher sensitivity in the red region of spectrum than that of the Sb-Cs photocathode, making them best suited for spectroscopy in those days. In addition, Hamamatsu Photonics put head-on photomultiplier tubes (type No. 6199 with an Sb-Cs photocathode) on the market in 1965.

In 1967, Hamamatsu Photonics introduced a 1/2-inch diameter side-on photomultiplier tube (type No. R300 with an Sb-Cs photocathode) which was the smallest tube at that time. In 1969, Hamamatsu Photonics developed and marketed photomultiplier tubes having a multialkali (Na-K-Cs-Sb) photocathode, type No. R446 (side-on) and R375 (head-on). Then, in 1974 a new side-on photomultiplier tube (type No. R928) was developed by Hamamatsu Photonics, which achieved much higher sensitivity in the red to near infrared region. This was an epoch-making event in terms of enhancing photomultiplier tube sensitivity. Since that time, Hamamatsu Photonics has continued to develop and produce a wide variety of state-of-the-art photomultiplier tubes. The current product line ranges in size from the world's smallest 3/8-inch tubes (R1635, etc.) to the world's largest 20-inch hemispherical tubes (R1449 and R3600). Hamamatsu Photonics also offers ultra-fast photomultiplier tubes using a microchannel plate for the dynodes (type No. R3809 with a time resolution as fast as 30 picoseconds) and mesh-dynode type photomultiplier tubes (R2490, etc.) that maintain an adequate gain of  $10^5$  even in high magnetic fields of up to one Tesla. More recently, Hamamatsu Photonics has developed subminiature metal can type photomultiplier tubes (R7400 series) using metal channel dynodes and various types of position-sensitive photomultiplier tubes capable of position detection. Hamamatsu Photonics is constantly engaged in research and development for manufacturing a wide variety of photomultiplier tubes to meet a wide range of application needs.

## 1.4 Using Photomultiplier Tubes

This section provides the first-time photomultiplier tube users with general information on how to choose the ideal photomultiplier tube (sometimes abbreviated as PMT), how to operate them properly and how to process the output signals. This section should be referred to as a quick guide. For more details, refer to the following chapters.

### 1.4.1 How to make the proper selection

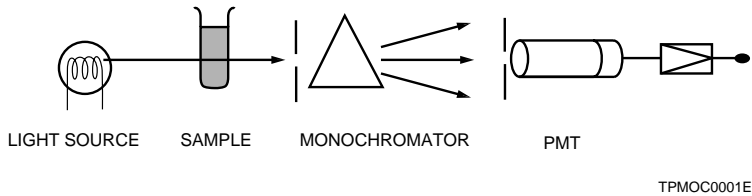


**Figure 1-6: Atomic absorption application**

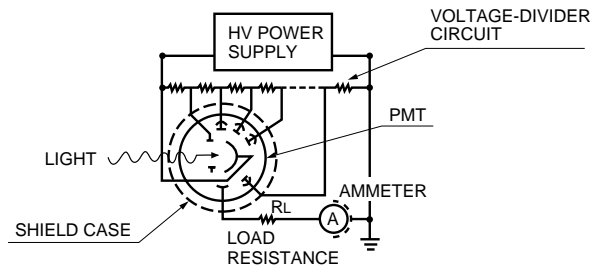
Figure 1-6 shows an application example in which a photomultiplier tube is used in absorption spectroscopy. The following parameters should be taken into account when making a selection.

| Incident light conditions   | Selection reference   |  |
|-----------------------------|---|--|
|                             | <Photomultiplier tubes>   | <Circuit Conditions>                                   |
| Light wavelength            | Window material<br>Photocathode spectral response                       |  |
| Light intensity             | Number of dynodes<br>Dynode type<br>Voltage applied to dynodes          | Signal processing method<br>(analog or digital method) |
| Light beam size             | Effective diameter (size)<br>Viewing configuration (side-on or head-on) |  |
| Speed of optical phenomenon | Time response   | Bandwidth of associated circuit                        |

It is important to know beforehand the conditions of the incident light to be measured. Then, choose a photomultiplier tube that is best suited to detect the incident light and also select the optimum circuit conditions that match the application. Referring to the table above, select the optimum photomultiplier tubes, operating conditions and circuit configurations according to the incident light wavelength, intensity, beam size and the speed of optical phenomenon. More specific information on these parameters and conditions are detailed in Chapter 2 and later chapters.

## 1.4.2 Basic operating method

As shown in Figure 1-7, operating a photomultiplier tube requires a stable source of high voltage (normally one to two kilovolts), voltage-divider circuit (or bleeder circuit) that distributes an optimum voltage to each dynode, and sometimes a shield case that protects the tube from magnetic or electric fields. The following equipment is available from Hamamatsu Photonics for setting up photomultiplier tube operation.



TPMOC0002EB

Figure 1-7: Basic operating method

### High-voltage power supply

A negative or positive high-voltage power supply of one to two kilovolts is usually required to operate a photomultiplier tube. There are two types of power supplies available: modular power supplies like that shown in Figure 1-8 and bench-top power supplies like that shown in Figure 1-9.



Figure 1-8: Modular high-voltage power supply

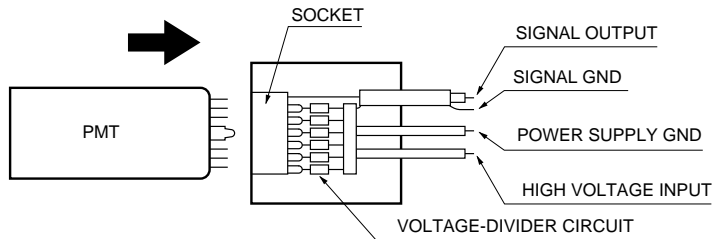


Figure 1-9: Bench-top high-voltage power supply

Since the gain of a photomultiplier tube is extremely high, it is very sensitive to variations in the high-voltage power supply. When the output stability of a photomultiplier tube should be maintained within one percent, the power supply stability must be held within 0.1 percent.

## Voltage-divider circuit

It is necessary to distribute voltage to each dynode independently. For this purpose, a divider circuit is usually used to divide the high voltage and provide a proper voltage gradient between each dynode. To allow easy operation of photomultiplier tubes, Hamamatsu provides socket assemblies that incorporate a photomultiplier tube socket and a matched divider circuit as shown in Figure 1-10 (D type socket assemblies \*1).

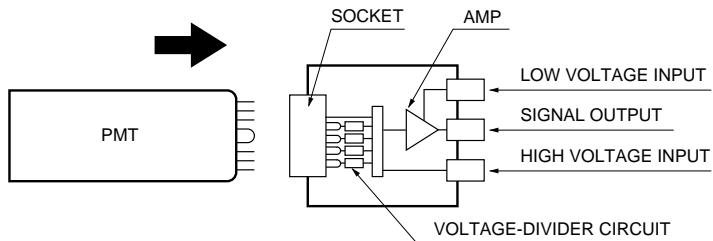


TACCC0001EB

**Figure 1-10: D type socket assembly**

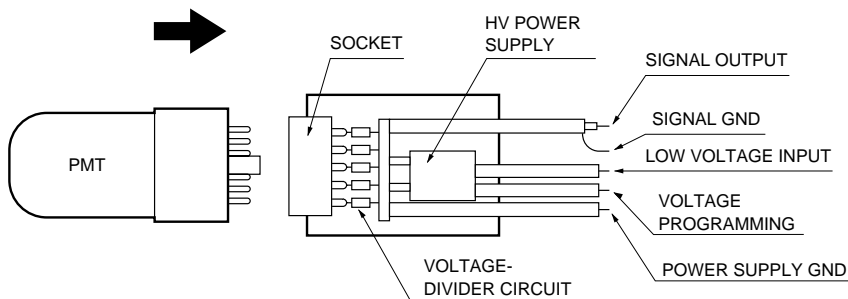
In addition, Hamamatsu offers socket assemblies that further include an amplifier (DA type socket assemblies \*2) or a power supply (DP type socket assemblies \*3), as shown in Figures 1-11 and 1-12 respectively.

- \*1 D type socket assemblies Built-in voltage divider
- \*2 DA type socket assemblies Built-in voltage divider and amplifier
- \*3 DP type socket assemblies Built-in voltage divider and power supply



TACCC0002EC

**Figure 1-11: DA type socket assembly**



TACCC0003EB

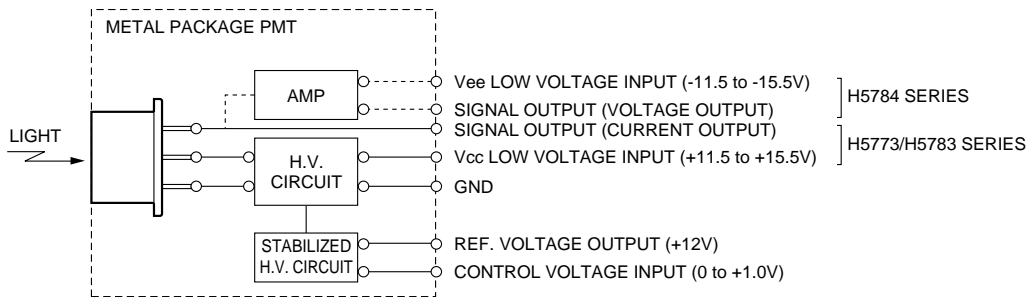
**Figure 1-12: DP type socket assembly**

## Shield

Photomultiplier tube characteristics may vary with external electromagnetic fields, ambient temperature, humidity, or mechanical stress applied to the tube. For this reason, it is necessary to use a magnetic or electric shield that protects the tube from such adverse environmental factors. Moreover, a cooled housing is sometimes used to maintain the tube at a constant temperature or at a low temperature, thus assuring more reliable operation.

## Integral power supply module

There are easy-to-use modules which incorporate a photomultiplier tube into a compact case, along with all necessary components such as a high-voltage power supply and operating circuit. (Figure 1-13)



TACCC0048EA

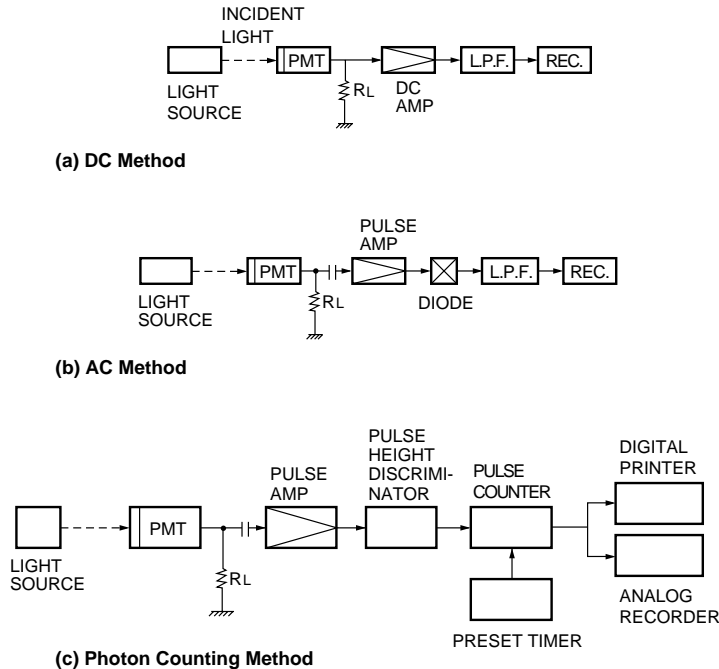
**Figure 1-13: Structure of an integral power supply module**

The description in this chapter is just an overview of operating a photomultiplier tube. For more detailed information, refer to Chapters 7 and 8.

### 1. 4. 3 Operating methods (associated circuits)

The output from a photomultiplier tube can be processed electrically as a constant current source. It is best, however, to connect it to an optimum circuit depending on the incident light and frequency characteristics required. Figure 1-14 shows typical light measurement circuits which are commonly used. The DC method and AC method (analog method) are mainly used in rather high light levels to moderate light levels. At very low light levels, the photon counting method is most effective. In this method, light is measured by counting individual photons which are the smallest unit of light.

The DC method shown in Figure 1-14 (a) detects DC components in the photomultiplier tube output by means of an amplifier and a lowpass filter. This method is suited for detection of relatively high light levels and has been widely used. The AC method shown in (b) extracts only AC components from the photomultiplier tube output via a capacitor and converts them into DC components by use of a diode. This method is generally used in lower light regions where the AC components are predominate in the output signal over the DC components. In the photon counting method shown in (c), the output pulses from the photomultiplier tube are amplified and only the pulses with an amplitude higher than the preset discrimination pulse height are counted as photon signals. This method allows observation of discrete output pulses from the photomultiplier tube, and is the most effective technique in detecting very low light levels.



TPMOC0004EA

Figure 1-14: Light measurement methods using PMT

These light measurement methods using a photomultiplier tube and the associated circuit must be optimized according to the intensity of incident light and the speed of the event to be detected. In particular, when the incident light is very low and the resultant signal is small, consideration must be given to minimize the influence of noise in the succeeding circuits. As stated, the AC method and photon counting method are more effective than the DC method in detecting low level light. When the incident light to be detected changes in a very short period, it is also important that the associated circuit be designed for a wider frequency bandwidth as well as using a fast response photomultiplier tube. Additionally, impedance matching at high frequencies must also be taken into account. Refer to Chapters 3 and 7 for more details on these precautions.

## References in Chapter 1

- 1) Society of Illumination: Lighting Handbook, Ohm-Sha (1987).
- 2) John W. T. WALSH: Photometry, DOVER Publications, Inc. New York
- 3) T. Hiruma: SAMPE Journal, 24, 35 (1988).  
A. H. Sommer: Photoemissive Materials, Robert E. Krieger Publishing Company(1980).
- 4) H. Herts: Ann. Physik, 31, 983 (1887).
- 5) W. Hallwachs: Ann. Physik, 33, 301 (1888).
- 6) J. Elster and H. Geitel: Ann. Physik, 38, 497 (1889).
- 7) A. Einstein: Ann. Physik, 17, 132 (1905).
- 8) L. Koller: Phys. Rev., 36, 1639 (1930).
- 9) N.R. Campbell: Phil. Mag., 12, 173 (1931).
- 10) P. Gorlich: Z. Physik, 101, 335 (1936).
- 11) A.H. Sommer: U. S. Patent 2,285, 062, Brit. Patent 532,259.
- 12) A.H. Sommer: Rev. Sci. Instr., 26, 725 (1955).
- 13) A.H. Sommer: Appl. Phys. Letters, 3, 62 (1963).
- 14) A.N. Arsenova-Geil and A. A. Kask: Soviet Phys.- Solid State, 7, 952 (1965).
- 15) A.N. Arsenova-Geil and Wang Pao-Kun: Soviet Phys.- Solid State, 3, 2632 (1962).
- 16) D.J. Haneman: Phys. Chem. Solids, 11, 205 (1959).
- 17) G.W. Gobeli and F.G. Allen: Phys. Rev., 137, 245A (1965).
- 18) D.G. Fisher, R.E. Enstrom, J.S. Escher, H.F. Gossenberger: IEEE Trans. Elect. Devices, Vol ED-21, No.10, 641(1974).
- 19) C.A. Sanford and N.C. Macdonald: J. Vac. Sci. Technol. B8(6), NOV/DEC 1853(1990).
- 20) D.G. Fisher and G.H. Olsen: J. Appl. Phys. 50(4), 2930 (1979).
- 21) J.L. Bradshaw, W.J. Choyke and R.P. Devaty: J. Appl. Phys. 67(3), 1, 1483 (1990).
- 22) H. Bruining: Physics and applications of secondary electron emission, McGraw-Hill Book Co., Inc. (1954).
- 23) H.E. Iams and B. Salzberg: Proc. IRE, 23, 55(1935).
- 24) V.K. Zworykin, G.A. Morton, and L. Malter: Proc. IRE, 24, 351 (1936).
- 25) V.K. Zworykin and J. A. Rajchman: Proc. IRE, 27, 558 (1939).
- 26) G.A. Morton: RCA Rev., 10, 529 (1949).
- 27) G.A. Morton: IRE Trans. Nucl. Sci., 3, 122 (1956).
- 28) Heroux, L. and H.E. Hinteregger: Rev. Sci. Instr., 31, 280 (1960).
- 29) E.J. Sternglass: Rev. Sci. Instr., 26, 1202 (1955).
- 30) J.R. Young: J. Appl. Phys., 28, 512 (1957).
- 31) H. Dormont and P. Saget: J. Phys. Radium (Physique Appliquee), 20, 23A (1959).
- 32) G.W. Goodrich and W.C. Wiley: Rev. Sci. Instr., 33, 761 (1962).

# MEMO

## CHAPTER 2

# BASIC PRINCIPLE OF PHOTOMULTIPLIER TUBES 1)-5)

A photomultiplier tube is a vacuum tube consisting of an input window, a photocathode and an electron multiplier sealed into an evacuated glass tube. Figure 2-1 shows the schematic construction of a photomultiplier tube.

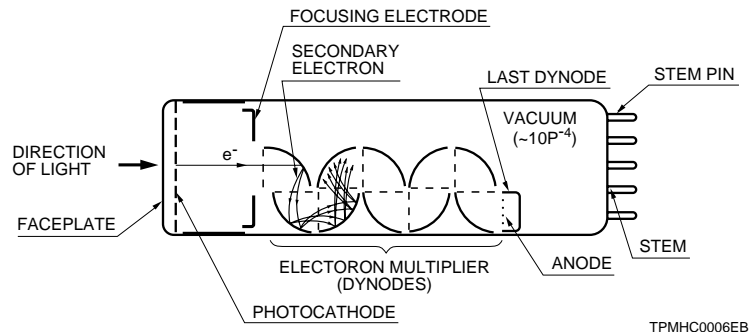


**Figure 2-1: Construction of a PMT**

Light which enters a photomultiplier tube is detected and produces an output signal through the following processes.

- (1) Light passes through the input window.
- (2) Excites the electrons in the photocathode so that photoelectrons are emitted into the vacuum (external photoelectric effect).
- (3) Photoelectrons are accelerated and focused by the focusing electrode onto the first dynode where they are multiplied by means of secondary electron emission. This secondary emission is repeated at each of the successive dynodes.
- (4) The multiplied secondary electrons emitted from the last dynode are finally collected by the anode.

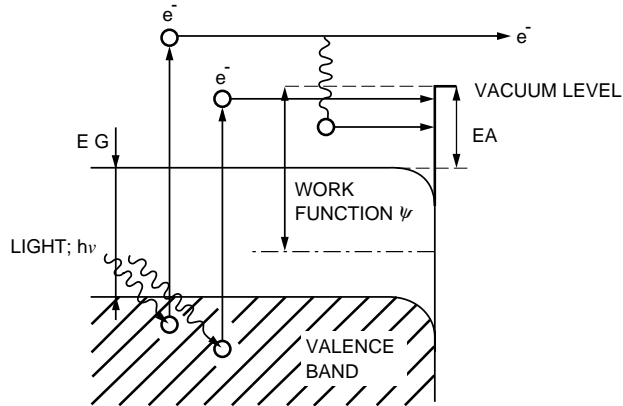
This chapter describes the principles of photoelectron emission, electron trajectory, and the design and function of electron multipliers. The electron multipliers used for photomultiplier tubes are classified into two types: normal discrete dynodes consisting of multiple stages and continuous dynodes such as microchannel plates. Since both types of dynodes differ considerably in operating principle, photomultiplier tubes using microchannel plates (MCP-PMTs) are separately described in Chapter 4. Furthermore, electron multipliers intended for use in particle and radiation measurement are discussed in Chapter 5.

## 2.1 Photoelectron Emission<sup>6) 7)</sup>

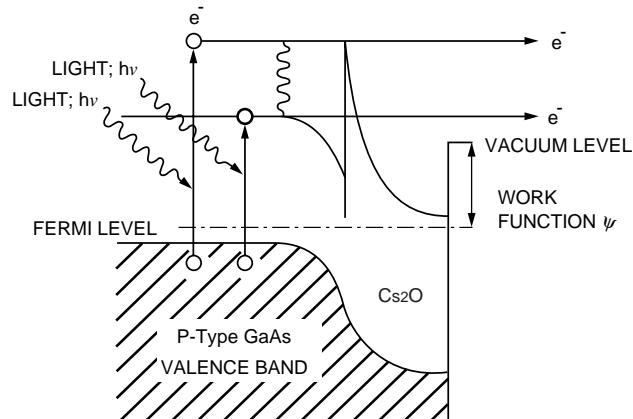
Photoelectric conversion is broadly classified into external photoelectric effects by which photoelectrons are emitted into the vacuum from a material and internal photoelectric effects by which photoelectrons are excited into the conduction band of a material. The photocathode has the former effect and the latter are represented by the photoconductive or photovoltaic effect.

Since a photocathode is a semiconductor, it can be described using band models as shown in Figure 2-2, (1) alkali photocathode and (2) III-V compound semiconductor photocathode.

(1) ALKALI PHOTOCATHODE



(2) III-V SEMICONDUCTOR PHOTOCATHODE



TPMOC0003EB

Figure 2-2: Photocathode band models

In a semiconductor band model, there exist a forbidden-band gap or energy gap (EG) that cannot be occupied by electrons, electron affinity (EA) which is an interval between the conduction band and the vacuum level barrier (vacuum level), and work function ( $\psi$ ) which is an energy difference between the Fermi level and the vacuum level. When photons strike a photocathode, electrons in the valence band absorb photon energy ( $h\nu$ ) and become excited, diffusing toward the photocathode surface. If the diffused electrons have enough energy to overcome the vacuum level barrier, they are emitted into the vacuum as photoelectrons. This can be expressed in a probability process, and the quantum efficiency  $\eta(\nu)$ , i.e., the ratio of output electrons to incident photons is given by

$$\eta(\nu) = (1-R) \frac{P_v}{k} \cdot \left( \frac{1}{1+1/kL} \right) \cdot P_s$$

where

- R : reflection coefficient
- k : full absorption coefficient of photons
- $P_v$ : probability that light absorption may excite electrons to a level greater than the vacuum level
- L : mean escape length of excited electrons
- $P_s$ : probability that electrons reaching the photocathode surface may be released into the vacuum
- $\nu$  : frequency of light

In the above equation, if we have chosen an appropriate material which determines parameters R, k and  $P_v$ , the factors that dominate the quantum efficiency will be L (mean escape length of excited electrons) and  $P_s$  (probability that electrons may be emitted into the vacuum). L becomes longer by use of a better crystal and  $P_s$  greatly depends on electron affinity (EA).

Figure 2-2 (2) shows the band model of a photocathode using III-V compound semiconductors.<sup>8)-10)</sup> If a surface layer of electropositive material such as  $\text{Cs}_2\text{O}$  is applied to this photocathode, a depletion layer is formed, causing the band structure to be bent downward. This bending can make the electron affinity negative. This state is called NEA (negative electron affinity). The NEA effect increases the probability ( $P_s$ ) that the electrons reaching the photocathode surface may be emitted into the vacuum. In particular, it enhances the quantum efficiency at long wavelengths with lower excitation energy. In addition, it lengthens the mean escape distance (L) of excited electrons due to the depletion layer.

Photocathodes can be classified by photoelectron emission process into a reflection mode and a transmission mode. The reflection mode photocathode is usually formed on a metal plate, and photoelectrons are emitted in the opposite direction of the incident light. The transmission mode photocathode is usually deposited as a thin film on a glass plate which is optically transparent. Photoelectrons are emitted in the same direction as that of the incident light. (Refer to Figures 2-3, 2-4 and 2-5. ) The reflection mode photocathode is mainly used for the side-on photomultiplier tubes which receive light through the side of the glass bulb, while the transmission mode photocathode is used for the head-on photomultiplier tubes which detect the input light through the end of a cylindrical bulb.

The wavelength of maximum response and long-wavelength cutoff are determined by the combination of alkali metals used for the photocathode and its fabrication process. As an international designation, photocathode sensitivity<sup>11)</sup> as a function of wavelength is registered as an "S" number by the JEDEC (Joint Electron Devices Engineering Council). This "S" number indicates the combination of a photocathode and window material and at present, numbers from S-1 through S-25 have been registered. However, other than S-1, S-11, S-20 and S-25 these numbers are scarcely used. Refer to Chapter 3 for the spectral response characteristics of various photocathodes and window materials.

## 2.2 Electron Trajectory

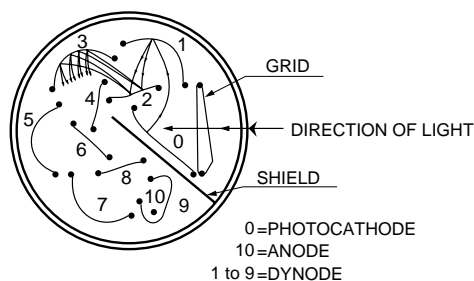
In order to collect photoelectrons and secondary electrons efficiently on a dynode and also to minimize the electron transit time spread, electrode design must be optimized through an analysis of the electron trajectory.<sup>12)-16)</sup>

Electron movement in a photomultiplier tube is influenced by the electric field which is dominated by the electrode configuration, arrangement, and also the voltage applied to the electrode. Conventional analysis of the electron trajectory has been performed by simulation models of an actual electrode, using methods such as rubber films and an electrolytic bath. Recently, however, numerical analysis using high-speed, large-capacity computers have come into use. This method divides the area to be analyzed into a grid-like pattern to give boundary conditions, and obtains an approximation by repeating computations until the error converges. By solving the equation for motion based on the potential distribution obtained using this method, the electron trajectory can be predicted.

When designing a photomultiplier tube, the electron trajectory from the photocathode to the first dynode must be carefully designed in consideration of the photocathode shape (planar or spherical window), the shape and arrangement of the focusing electrode and the supply voltage, so that the photoelectrons emitted from the photocathode are efficiently focused onto the first dynode. The collection efficiency of the first dynode is the ratio of the number of electrons landing on the effective area of the first dynode to the number of emitted photoelectrons. This is usually better than 60 to 90 percent. In some applications where the electron transit time needs to be minimized, the electrode should be designed not only for optimum configuration but also for higher electric fields than usual.

The dynode section is usually constructed from several to more than ten stages of secondary-emissive electrodes (dynodes) having a curved surface. To enhance the collection efficiency of each dynode and minimize the electron transit time spread, the optimum configuration and arrangement should be determined from an analysis of the electron trajectory. It is also necessary to design the arrangement of the dynodes in order to prevent ion or light feedback from the latter stages.

In addition, various characteristics of a photomultiplier tube can also be calculated by computer simulation. For example, the collection efficiency, uniformity, and electron transit time can be calculated using a Monte Carlo simulation by setting the initial conditions of photoelectrons and secondary electrons. This allows collective evaluation of photomultiplier tubes. Figures 2-3, 2-4 and 2-5 are cross sections of photomultiplier tubes having a circular-cage, box-and-grid, and linear-focused dynode structures, respectively, showing their typical electron trajectories.



TPMSC0001EB

Figure 2-3: Circular-cage type

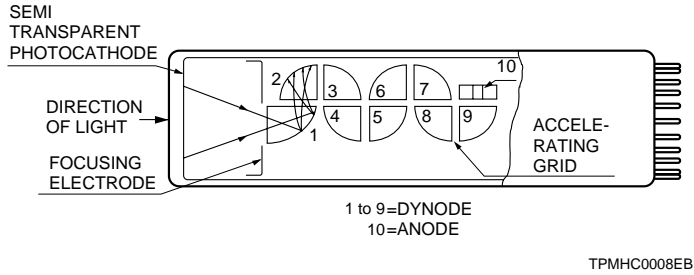


Figure 2-4: Box-and-grid type

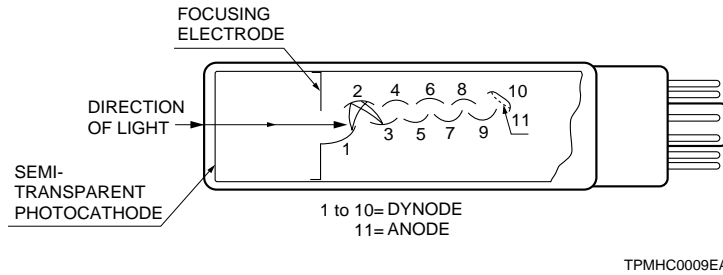
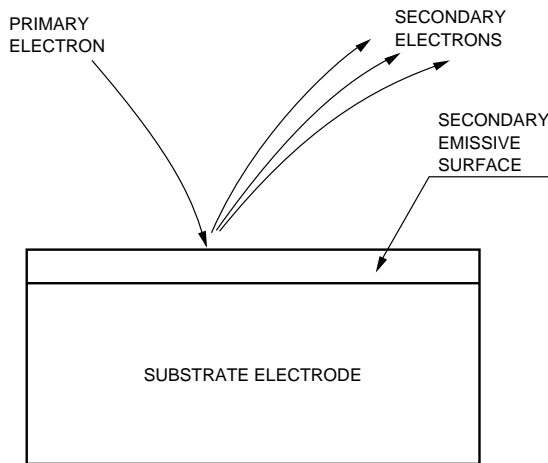


Figure 2-5: Linear-focused type

## 2.3 Electron Multiplier (Dynode Section)

As stated above, the potential distribution and electrode structure of a photomultiplier tube is designed to provide optimum performance. Photoelectrons emitted from the photocathode are multiplied by the first dynode through the last dynode (up to 19th dynode), with current amplification ranging from 10 to as much as 108 times, and are finally sent to the anode.

Major secondary emissive materials<sup>(17)-21)</sup> used for dynodes are alkali antimonide, beryllium oxide (BeO), magnesium oxide (MgO), gallium phosphide (GaP) and gallium arsenide phosphide (GaAsP). These materials are coated onto a substrate electrode made of nickel, stainless steel, or copper-beryllium alloy. Figure 2-6 shows a model of the secondary emission multiplication of a dynode.



TPMOC0066EA

Figure 2-6: Secondary emission of dynode

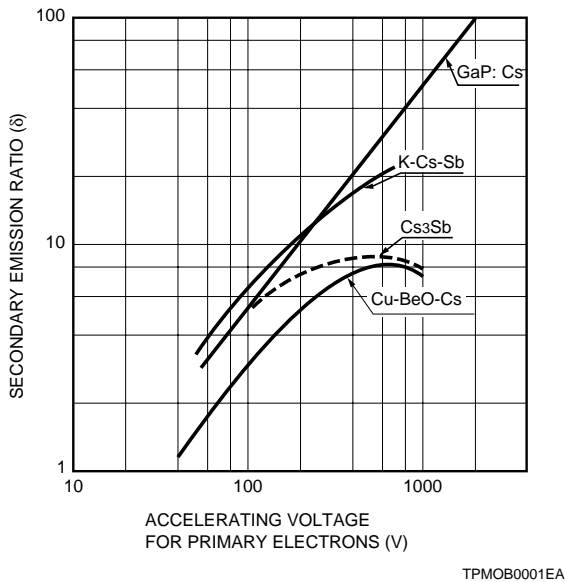


**Figure 2-7: Secondary emission ratio**

When a primary electron with initial energy  $E_p$  strikes the surface of a dynode,  $\delta$  secondary electrons are emitted. This  $\delta$ , the number of secondary electrons per primary electron, is called the secondary emission ratio. Figure 2-7 shows the secondary emission ratio  $\delta$  for various dynode materials as a function of the accelerating voltage for the primary electrons.

Ideally, the current amplification or gain of a photomultiplier tube having the number of dynode stages  $n$  and the average secondary emission ratio  $\delta$  per stage will be  $\delta^n$ . Refer to Section 3.2.2 in Chapter 3 for more details on the gain.

Because a variety of dynode structures are available and their gain, time response, uniformity, and collection efficiency differ depending on the number of dynode stages and other factors, it is necessary to select the optimum dynode type according to your application. These characteristics are described in Chapter 3, Section 3.2.1.

## 2.4 Anode

The anode of a photomultiplier tube is an electrode that collects secondary electrons multiplied in the cascade process through multi-stage dynodes and outputs the electron current to an external circuit.

Anodes are carefully designed to have a structure optimized for the electron trajectories discussed previously. Generally, an anode is fabricated in the form of a rod wire, metal plate or mesh electrode. One of the most important factors in designing an anode is that an adequate potential difference can be established between the last dynode and the anode in order to prevent space charge effects and obtain a large output current.

---

## References in Chapter 2

- 1) Hamamatsu Photonics: "Photomultiplier Tubes and Related Products" (1997, December revision)
- 2) Hamamatsu Photonics: "Characteristics and Uses of Photomultiplier Tubes" No.79-57-03 (1982).
- 3) S.K. Poultney: *Advances in Electronics and Electron Physics* 31, 39 (1972).
- 4) D.H. Seib and L.W. Ankerman: *Advances in Electronics and Electron Physics*, 34, 95 (1973).
- 5) J.P. Boutot, et al.: *Advances in Electronics and Electron Physics* 60, 223 (1983).
- 6) T. Hiruma: *SAMPE Journal*, 24, 6, 35-40 (1988).
- 7) T. Hayashi: *Bunkou Kenkyuu*, 22, 233 (1973). (Published in Japanese)
- 8) H. Sonnenberg: *Appl. Phys. Lett.*, 16, 245 (1970).
- 9) W.E. Spicer, et al.: *Pub. Astron. Soc. Pacific*, 84, 110 (1972).
- 10) M. Hagino, et al.: *Television Journal*, 32, 670 (1978). (Published in Japanese)
- 11) A. Honma: *Bunseki*, 1, 52 (1982). (Published in Japanese)
- 12) K.J. Van. Oostrum: *Philips Technical Review*, 42, 3 (1985).
- 13) K. Oba and Ito: *Advances in Electronics and Electron Physics*, 64B, 343.
- 14) A.M. Yakobson: *Radiotekh & Electron*, 11, 1813 (1966).
- 15) H. Bruining: *Physics and Applications of Secondary Electron Emission*, (1954).
- 16) J. Rodeny and M. Vaughan: *IEEE Transaction on Electron Devices*, 36, 9 (1989).
- 17) B. Gross and R. Hessel: *IEEE Transaction on Electrical Insulation*, 26, 1 (1991).
- 18) H.R. Krall, et al.: *IEEE Trans. Nucl. Sci.* NS-17, 71 (1970).
- 19) J.S. Allen: *Rev. Sci. Instr.*, 18 (1947).
- 20) A.M. Tyutikov: *Radio Engineering And Electronic Physics*, 84, 725 (1963).
- 21) A.H. Sommer: *J. Appl. Phys.*, 29, 598 (1958).

# MEMO

## **CHAPTER 3**

# **CHARACTERISTICS OF PHOTOMULTIPLIER TUBES**

*This chapter details various characteristics of photomultiplier tubes, including basic characteristics and their measurement methods. For example, Section 3.1 shows spectral response characteristics of typical photocathodes and also gives the definition of photocathode sensitivity and its measurement procedure. Section 3.2 explains dynode types, structures and typical characteristics. Section 3.3 describes various characteristics of photomultiplier tubes such as time response properties, operating stability, sensitivity, uniformity, signal-to-noise ratio as well as their definitions, measurement procedures and specific product examples. It also provides precautions and suggestions for actual use. Section 3.4 introduces the photon counting method, an effective technique for low-level light detection, including its principles, operating procedure, and various characteristics. In addition, 3.5 explains the principle of scintillation counting which is widely used in radiation measurements, along with the operating procedure and typical characteristics of photomultiplier tubes selected for this application.*

## 3.1 Basic Characteristics of Photocathodes

This section introduces photocathode and window materials which have been put into practical use up through the present and also explains the terms used to evaluate photocathodes such as quantum efficiency, radiant sensitivity, and luminous sensitivity.

### 3.1.1 Photocathode materials

Most photocathodes<sup>1)-15)</sup> are made of a compound semiconductor mostly consisting of alkali metals with a low work function. There are about ten kinds of photocathodes which are currently in practical use. Each photocathode is available with a transmission (semitransparent) type or a reflection (opaque) type, with different device characteristics. In the early 1940's, the JEDEC (Joint Electron Devices Engineering Council) introduced the "S number" to designate photocathode spectral response which is classified by the combination of the photocathode and window materials. Presently, since many photocathode and window materials are available, the "S number" is not frequently used except for S-1, S-20, etc. The photocathode spectral response is instead expressed in terms of photocathode materials. The photocathode materials commonly used in photomultiplier tubes are as follows.

#### (1) Cs-I

Cs-I is insensitive to solar radiation and therefore often called "solar blind". Its sensitivity falls sharply at wavelengths longer than 200 nanometers and it is exclusively used for vacuum ultraviolet detection. As window materials, MgF<sub>2</sub> crystals or synthetic silica are used because of high ultraviolet transmittance. Although Cs-I itself has high sensitivity to wavelengths shorter than 115 nanometers, the MgF<sub>2</sub> crystal used for the input window does not transmit wavelengths shorter than 115 nanometers. This means that the spectral response of a photomultiplier tube using the combination of Cs-I and MgF<sub>2</sub> covers a range from 115 to 200 nanometers. To measure light with wavelengths shorter than 115 nanometers using Cs-I, an electron multiplier having a first dynode on which Cs-I is deposited is often used with the input window removed.

#### (2) Cs-Te

Cs-Te is insensitive to wavelengths longer than 300 nanometers and is also called "solar blind" just as with Cs-I. A special Cs-Te photocathode processed to have strongly suppressed sensitivity in the visible part of the spectrum has been fabricated. With Cs-Te, the transmission type and reflection type show the same spectral response range, but the reflection type exhibits twice the sensitivity of the transmission type. Synthetic silica or MgF<sub>2</sub> is usually used for the input window.

#### (3) Sb-Cs

This photocathode has sensitivity in the ultraviolet to visible range, and is widely used in many applications. Because the resistance of the Sb-Cs photocathode is lower than that of the alkali photocathode described later on, it is suited for applications where light intensity to be measured is relatively high so that a large current can flow in the cathode, and is also used where changes in the photocathode resistance due to cooling affects measurements. Sb-Cs is chiefly used for the reflection type photocathode.

#### (4) Bialkali (Sb-Rb-Cs, Sb-K-Cs)

Since two kinds of alkali metals are employed, these photocathodes are called "bialkali". The transmission type of these photocathodes has a spectral response range similar to the Sb-Cs photocathode, but has higher sensitivity and lower dark current. It also provides sensitivity that matches the emission of a NaI(Tl) scintillator, thus being widely used for scintillation counting in radiation measurements. On the other hand, the reflection-type bialkali photocathodes are intended for different applications and therefore are fabricated by a different process using the same materials. As a result, they offer enhanced sensitivity on the long wavelength side, providing a spectral response from the ultraviolet region to around 700 nanometers.

**(5) High temperature, low noise bialkali (Sb-Na-K)**

As with the above bialkali photocathodes, two kinds of alkali metals are used. The spectral response range of this photocathode is almost identical with that of the above bialkali photocathodes, but the sensitivity is somewhat lower. This photocathode can withstand operating temperatures up to 175°C while normal photocathodes are guaranteed to no higher than 50°C. For this reason, it is ideally suited for use in oil well logging where photomultiplier tubes are often subjected to high temperatures. In addition, when used at room temperatures, this photocathode exhibits very low dark current, thus making it very useful in low-level light detection, for instance in photon counting applications where low noise is a prerequisite.

**(6) Multialkali (Sb-Na-K-Cs)**

Since three or more kinds of alkali metals are employed, this photocathode is sometimes called a "trialkali". It has high sensitivity, wide spectral response from the ultraviolet through near infrared region around 850 nanometers, and is widely used in broad-band spectrophotometers. Furthermore, Hamamatsu also provides a multialkali photocathode with long wavelength response extending out to 900 nanometers, which is especially useful in the detection of chemiluminescence in NO<sub>x</sub>, etc.

**(7) Ag-O-Cs**

The transmission type photocathode using this material is sensitive from the visible through near infrared region, from 300 to 1200 nanometers, while the reflection type shows a slightly narrower region, spectral range from 300 to 1100 nanometers. Compared to other photocathodes, this photocathode shows lower sensitivity in the visible region, but has sensitivity at longer wavelengths in the near infrared region. Thus, both the transmission type and reflection type Ag-O-Cs photocathodes are chiefly used for near infrared detection.

**(8) GaAs (Cs)**

A GaAs crystal activated with cesium is also used as a photocathode. The spectral response of this photocathode covers a wide range from the ultraviolet through 930 nanometers with a plateau curve from 300 to 850 nanometers, showing a sudden cutoff at the near infrared limit. It should be noted that if exposed to incident light with high intensity, this photocathode tends to suffer sensitivity degradation when compared with other photocathodes.

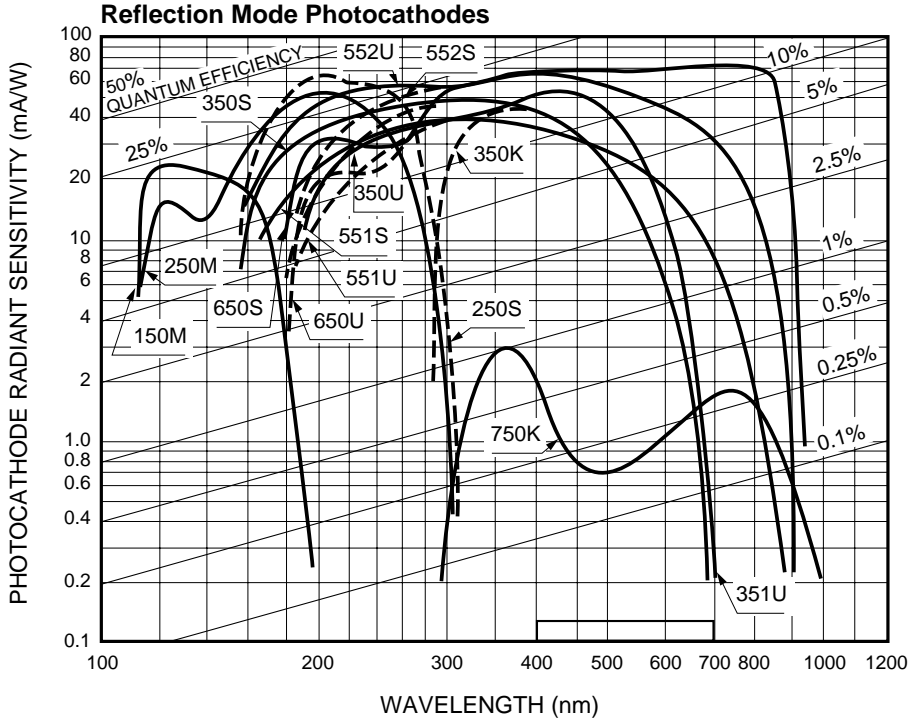
**(9) InGaAs (Cs)**

This photocathode provides a spectral response extending further into the infrared region than the GaAs photocathode. Additionally, it offers a superior signal-to-noise ratio in the neighborhood of 900 to 1000 nanometers in comparison with the Ag-O-Cs photocathode.

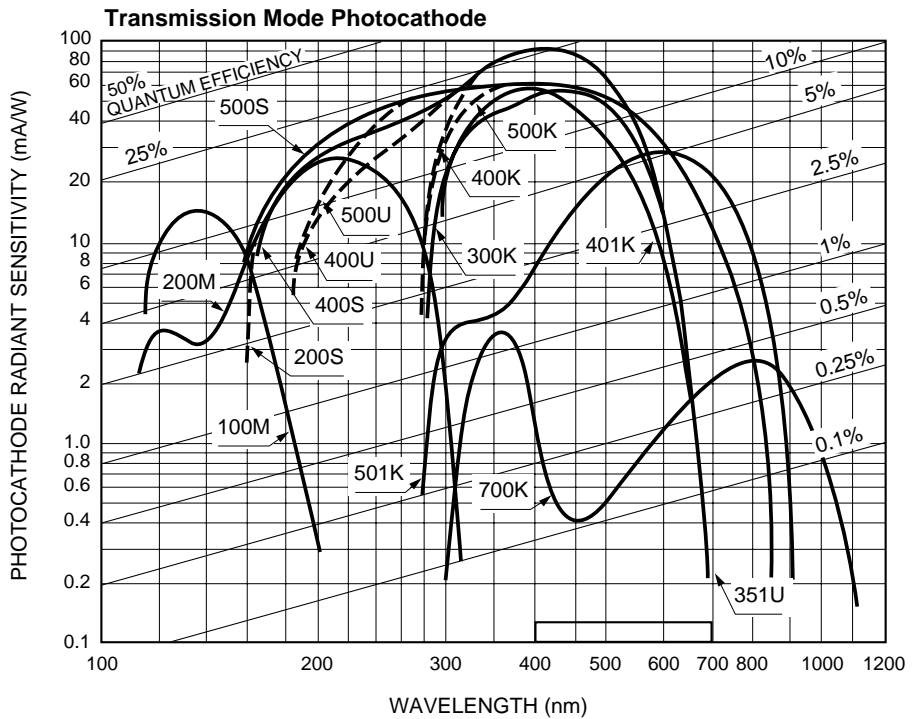
**(10) InP/InGaAsP(Cs), InP/InGaAs(Cs)**

These are field-assisted photocathodes utilizing a PN junction by growing InP/InGaAsP or InP/InGaAs on a p-InP substrate, and utilized in practical use by means of our unique semiconductor micro-process technology.<sup>16) 17)</sup> These photocathodes are sensitive to long wavelengths extending to 1.4μm or even 1.7μm which have up till now been impossible to detect with a photomultiplier tube. Since these photocathodes produce large amounts of dark current when used at room temperatures, they must be cooled to about -80°C during operation.

Typical spectral response characteristics of major photocathodes are illustrated in Figure 3-1<sup>1)</sup> and Table 3-1.<sup>1)</sup> The JEDEC "S numbers" being frequently used are also listed in Table 3-1. The definition of photocathode radiant sensitivity expressed in the ordinate of Figure 3-1 is explained in Section 3.1.3, "Spectral response characteristics". Note that Figure 3-1 and Table 3-1 show typical characteristics and actual data may differ from tube to tube.



TPMOB0052EA



TPMOB0052EA

Figure 3-1: Typical photocathode spectral response characteristics

**Transmission mode photocathodes**

|   | Curve Code<br>(S number) | Photocathode Material     | Window<br>Material | Spectral Response      |                             |                            |
|---|--------------------------|---------------------------|--------------------|------------------------|-----------------------------|----------------------------|
|   |                          |                           |                    | Spectral Range<br>(mm) | Peak Wavelength             |                            |
|   |                          |                           |                    |                        | Radiant<br>Sensitivity (nm) | Quantum<br>Efficiency (nm) |
| * | 100M                     | Cs-I                      | MgF <sub>2</sub>   | 115 to 200             | 140                         | 130                        |
| * | 200S                     | Cs-Te                     | Sythetic silica    | 160 to 320             | 210                         | 200                        |
| * | 200M                     | Cs-Te                     | MgF <sub>2</sub>   | 115 to 320             | 210                         | 200                        |
| – | 201S                     | Cs-Te                     | Sythetic silica    | 160 to 320             | 240                         | 220                        |
| – | 201A                     | Cs-Te                     | Sapphire           | 150 to 320             | 250                         | 220                        |
| * | 300K (S-11)              | Sb-Cs                     | Bolosilicate       | 300 to 650             | 440                         | 410                        |
| * | 400K                     | Bialkali                  | Bolosilicate       | 300 to 650             | 420                         | 390                        |
| * | 400U                     | Bialkali                  | UV                 | 185 to 650             | 420                         | 390                        |
| * | 400S                     | Bialkali                  | Sythetic silica    | 160 to 650             | 420                         | 390                        |
| * | 401K                     | High temperature bialkali | Bolosilicate       | 300 to 650             | 375                         | 360                        |
| – | 402K                     | Bialkali                  | Bolosilicate       | 300 to 650             | 375                         | 360                        |
| * | 500K (S-20)              | Multialkali               | Bolosilicate       | 300 to 850             | 420                         | 360                        |
| * | 500U                     | Multialkali               | UV                 | 185 to 850             | 420                         | 290                        |
| * | 500S                     | Multialkali               | Sythetic silica    | 160 to 850             | 420                         | 280                        |
| * | 501K (S-25)              | Multialkali               | Bolosilicate       | 300 to 900             | 650                         | 600                        |
| * | 700K (S-1)               | Ag-O-Cs                   | Bolosilicate       | 300 to 1200            | 800                         | 780                        |

\* : Spectral response curves are shown in Figure 3-1.

– : Spectral response curves are not shown in Figure 3-1.

**Table 3-1: Quick reference for typical spectral response characteristics (1)**

## Reflection mode photocathodes

|   | Curve Code<br>(S number) | Photocathode Material     | Window<br>Material | Spectral Response      |                             |                            |
|---|--------------------------|---------------------------|--------------------|------------------------|-----------------------------|----------------------------|
|   |                          |                           |                    | Spectral Range<br>(mm) | Peak Wavelength             |                            |
|   |                          |                           |                    |                        | Radiant<br>Sensitivity (nm) | Quantum<br>Efficiency (nm) |
| * | 150M                     | Cs-I                      | MgF <sub>2</sub>   | 115 to 195             | 120                         | 120                        |
| * | 250S                     | Cs-Te                     | Sythetic silica    | 160 to 320             | 200                         | 200                        |
| * | 250M                     | Cs-Te                     | MgF <sub>2</sub>   | 115 to 320             | 200                         | 190                        |
| * | 350K (S-4)               | Sb-Cs                     | Bolosilicate       | 300 to 650             | 400                         | 350                        |
| * | 350K (S-5)               | Sb-Cs                     | UV                 | 185 to 650             | 340                         | 270                        |
| * | 350S (S-19)              | Sb-Cs                     | Sythetic silica    | 160 to 650             | 340                         | 210                        |
| - | 351U (Extended S-5)      | Sb-Cs                     | UV                 | 185 to 700             | 450                         | 235                        |
| - | 451U                     | Bialkali                  | UV                 | 185 to 730             | 340                         | 320                        |
| - | 452U                     | Bialkali                  | UV                 | 185 to 750             | 350                         | 315                        |
| - | 453K                     | Bialkali                  | Bolosilicate       | 300 to 650             | 400                         | 360                        |
| - | 453U                     | Bialkali                  | UV                 | 185 to 650             | 400                         | 330                        |
| - | 454K                     | Bialkali                  | Bolosilicate       | 300 to 680             | 450                         | 430                        |
| - | 455U                     | Bialkali                  | UV                 | 185 to 680             | 420                         | 400                        |
| - | 456U                     | Low dark current bialkali | UV                 | 185 to 680             | 375                         | 320                        |
| - | 457U                     | Bialkali                  | Bolosilicate       | 300 to 680             | 450                         | 450                        |
| - | 550U                     | Multialkali               | UV                 | 185 to 850             | 530                         | 250                        |
| - | 550S                     | Multialkali               | Sythetic silica    | 160 to 850             | 530                         | 250                        |
| * | 551U                     | Multialkali               | UV                 | 185 to 870             | 330                         | 280                        |
| * | 551S                     | Multialkali               | Sythetic silica    | 160 to 870             | 330                         | 280                        |
| * | 552U                     | Multialkali               | UV                 | 185 to 900             | 400                         | 260                        |
| * | 552S                     | Multialkali               | Sythetic silica    | 160 to 900             | 400                         | 215                        |
| - | 554U                     | Multialkali               | UV                 | 185 to 900             | 450                         | 370                        |
| - | 555U                     | Multialkali               | UV                 | 185 to 850             | 400                         | 320                        |
| - | 556U                     | Multialkali               | UV                 | 185 to 930             | 420                         | 320                        |
| - | 557U                     | Multialkali               | UV                 | 185 to 900             | 420                         | 400                        |
| - | 558K                     | Multialkali               | Bolosilicate       | 300 to 800             | 530                         | 510                        |
| * | 650U                     | GaAs(Cs)                  | UV                 | 185 to 930             | 300 to 800                  | 300                        |
| * | 650S                     | GaAs(Cs)                  | Sythetic silica    | 160 to 930             | 300 to 800                  | 280                        |
| - | 651U                     | GaAs(Cs)                  | UV                 | 185 to 910             | 350                         | 270                        |
| * | 750K                     | Ag-O-Cs                   | Bolosilicate       | 300 to 1100            | 730                         | 730                        |
| - | 850U                     | InGaAs(Cs)                | UV                 | 185 to 1010            | 400                         | 330                        |
| * | —                        | InP/nGaAsP(Cs)            | Bolosilicate       | 300 to 1400            | —                           | —                          |
| * | —                        | InP/InGaAsP(Cs)           | Bolosilicate       | 300 to 1700            | —                           | —                          |

\* : Spectral response curves are shown in Figure 3-1.

- : Spectral response curves are not shown in Figure 3-1.

**Table 3-1: Quick reference for typical spectral response characteristics (2)**

### 3.1.2 Window materials

As stated in the preceding section, most photocathodes have high sensitivity down to the ultraviolet region. However, because ultraviolet radiation tends to be absorbed by the window material, the short wavelength limit is determined by the ultraviolet transmittance of the window material.<sup>18)-22)</sup> The window materials commonly used in photomultiplier tubes are as follows:

#### (1) MgF<sub>2</sub> crystal

The crystals of alkali halide are superior in transmitting ultraviolet radiation, but have the disadvantage of deliquescence. A magnesium fluoride (MgF<sub>2</sub>) crystal is used as a practical window material because it offers very low deliquescence and allows transmission of vacuum ultraviolet radiation down to 115 nanometers.

#### (2) Sapphire

Sapphire is made of Al<sub>2</sub>O<sub>3</sub> crystal and shows an intermediate transmittance between the UV-transmitting glass and synthetic silica in the ultraviolet region. Sapphire glass has a short wavelength cutoff in the neighborhood of 150 nanometers, which is slightly shorter than that of synthetic silica.

#### (3) Synthetic silica

Synthetic silica transmits ultraviolet radiation down to 160 nanometers and in comparison to fused silica, offers lower absorption in the ultraviolet region. Since silica has a thermal expansion coefficient greatly different from that of a Kovar alloy used for the stem pins (leads) of photomultiplier tubes, it is not suited for use as the bulb stem. Because of this, a borosilicate glass is used for the bulb stem and then a graded seal using glasses with gradually different thermal expansion coefficient are connected to the synthetic silica bulb, as shown in Figure 3-2. Because of this structure, the graded seal is very fragile so that sufficient care should be taken when handling the tube. In addition, helium gas may permeate through the silica bulb and cause the noise to increase. Avoid operating or storing such tubes in environments where helium is present.

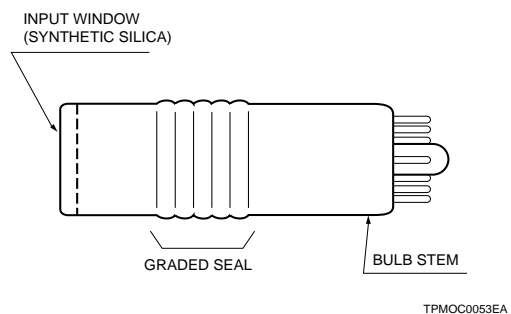


Figure 3-2: Grated seal

#### (4) UV glass (UV-transmitting glass)

As the name implies, this transmits ultraviolet radiation well. The short wavelength cutoff of the UV glass extends to 185 nanometers.

#### (5) Borosilicate glass

This is the most commonly used window material. Because the borosilicate glass has a thermal expansion coefficient very close to that of the Kovar alloy which is used for the leads of photomultiplier tubes, it is often called "Kovar glass". The borosilicate glass does not transmit ultraviolet radiation shorter than 300 nanometers. It is not suited for ultraviolet detection shorter than this range. Moreover, some types of head-on photomultiplier tubes using a bialkali photocathode employ a special borosilicate glass (so-called "K-free glass") containing a very small amount of potassium (K<sup>40</sup>) which may cause unwanted noise counts. The K-free glass is mainly used for photomultiplier tubes designed for scintillation counting where low background counts are desirable. For more details on background noise caused by K<sup>40</sup>, refer to Section 3.3.6, "Dark current".

Spectral transmittance characteristics of various window materials are shown in Figure 3-3.

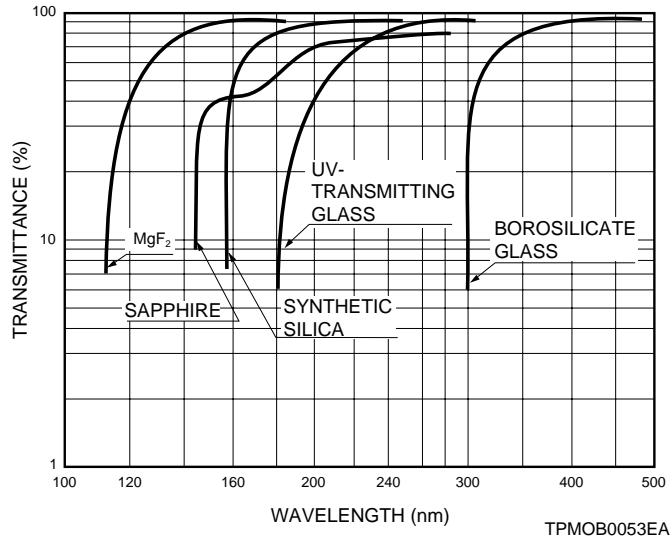


Figure 3-3: Spectral transmittance of window materials

### 3. 1. 3 Spectral response characteristics

The photocathode of a photomultiplier converts the energy of incident photons into photoelectrons. The conversion efficiency (photocathode sensitivity) varies with the incident light wavelength. This relationship between the photocathode and the incident light wavelength is referred to as the spectral response characteristics. In general, the spectral response characteristics are expressed in terms of radiant sensitivity and quantum efficiency.

#### (1) Radiant sensitivity

Radiant sensitivity is the photoelectric current from the photocathode divided by the incident radiant flux at a given wavelength, expressed in units of amperes per watts (A/W). Furthermore, relative spectral response characteristics in which the maximum radiant sensitivity is normalized to 100% are also conveniently used.

#### (2) Quantum efficiency

Quantum efficiency is the number of photoelectrons emitted from the photocathode divided by the number of incident photons. Quantum efficiency is symbolized by  $\eta$  and generally expressed in percent. Incident photons give energy to electrons in the valence band of a photocathode but not all electrons given energy are emitted as photoelectrons. This photoemission takes place under a certain probability process. Photons at shorter wavelengths carry higher energy compared to those at longer wavelengths and contribute to an increase in the photoemission probability. As a result, the maximum quantum efficiency occurs at a wavelength slightly shorter than that of the radiant sensitivity.

#### (3) Measurement and calculation of spectral response characteristics

To measure radiant sensitivity and quantum efficiency, a standard phototube or semiconductor detector which is precisely calibrated is used as a secondary standard. At first, the incident radiant flux  $L_p$  at the wavelength of interest is measured with the standard phototube or semiconductor detector. Next, the pho-

tomultiplier tube to be measured is set in place and the photocurrent  $I_k$  is measured. Then the radiant sensitivity  $S_k$  of the photomultiplier tube can be calculated from the following equation:

$$S_k = \frac{I_k}{L_p} (A/W) \dots\dots\dots (Eq. 3-1)$$

The quantum efficiency  $\eta$  can be obtained from  $S_k$  using the following equation:

$$\eta(\%) = \frac{h \cdot c}{\lambda \cdot e} \cdot S_k = \frac{1240}{\lambda} \cdot S_k \cdot 100\% \dots\dots\dots (Eq. 3-2)$$

$$h : 6.626276 \times 10^{-34} \text{ J}\cdot\text{s}$$

$$c : 2.997924 \times 10^8 \text{ m}\cdot\text{s}^{-1}$$

$$e : 1.602189 \times 10^{-19} \text{ C}$$

where  $h$  is Planck's constant,  $\lambda$  is the wavelength of incident light ( nanometers),  $c$  is the velocity of light in vacuum and  $e$  is the electron charge. The quantum efficiency  $\eta$  is expressed in percent.

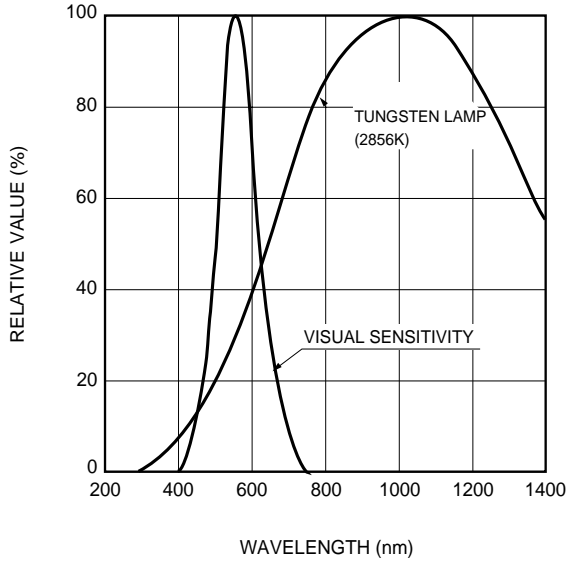
#### (4) Spectral response range (short wavelength limit, long wavelength limit)

The wavelength at which the spectral response drops on the short wavelength side is called the short wavelength limit or cutoff while the wavelength at which the spectral response drops on the long wavelength side is called the long wavelength limit or cutoff. The short wavelength limit is determined by the window material, while the long wavelength limit depends on the photocathode material. The range between the short wavelength limit and the long wavelength limit is called the spectral response range.

In this handbook, the short wavelength limit is defined as the wavelength at which the incident light is abruptly absorbed by the window material. The long wavelength limit is defined as the wavelength at which the photocathode sensitivity falls to 1 percent of the maximum sensitivity for alkali and Ag-O-Cs photocathodes, and 0.1 percent of the maximum sensitivity for multialkali photocathodes. However, these wavelength limits will depend on the actual operating conditions such as the amount of incident light, photocathode sensitivity, dark current and signal-to-noise ratio of the measurement system.

### 3.1.4 Luminous sensitivity

The spectral response measurement of a photomultiplier tube requires an expensive, sophisticated system and much time is required, it is therefore more practical to evaluate the sensitivity of common photomultiplier tubes in terms of luminous sensitivity. The illuminance on a surface one meter away from a point light source of one candela (cd) is one lux. One lumen equals the luminous flux of one lux passing an area of one square meter. Luminous sensitivity is the output current obtained from the cathode or anode divided by the incident luminous flux (lumen) from a tungsten lamp at a distribution temperature of 2856K. In some cases, a visual-compensation filter is interposed between the photomultiplier tube and the light source, but in most cases it is omitted. Figure 3-4 shows the visual sensitivity and relative spectral distribution of a 2856K tungsten lamp.



TPMOB0054EB

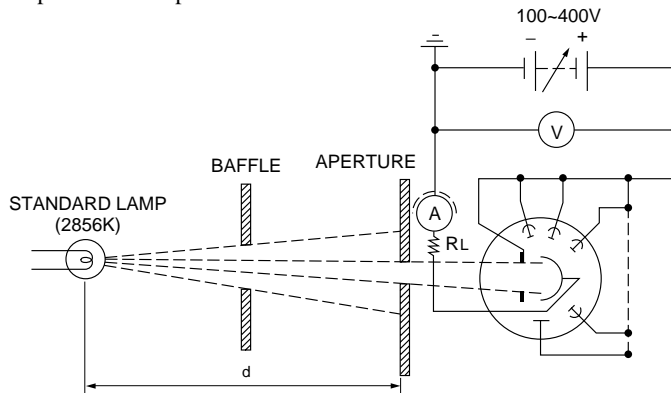
Figure 3-4: Response of eye and spectral distribution of 2856 K tungsten lamp

Luminous sensitivity is a convenient parameter when comparing the sensitivity of photomultiplier tubes categorized in the same types. However, it should be noted that "lumen" is the unit of luminous flux with respect to the standard visual sensitivity and there is no physical significance for photomultiplier tubes which have a spectral response range beyond the visible region (350 to 750 nanometers). To evaluate photomultiplier tubes using Cs-Te or Cs-I photocathodes which are insensitive to the spectral distribution of a tungsten lamp, radiant sensitivity at a specific wavelength is measured.

Luminous sensitivity is divided into two parameters: cathode luminous sensitivity which shows the photocathode property and anode luminous sensitivity which indicates the performance of the whole photomultiplier tube.

**(1) Cathode luminous sensitivity**

Cathode luminous sensitivity<sup>23) 25)</sup> is defined as the photoelectron current from the photocathode (cathode current) per luminous flux from a tungsten lamp operated at a distribution temperature of 2856K. In this measurement, each dynode is shorted to the same potential as shown in Figure 3-5, so that the photomultiplier tube is operated as a bipolar tube.



TPMOC0054EA

Figure 3-5: Cathode luminous sensitivity measuring diagram

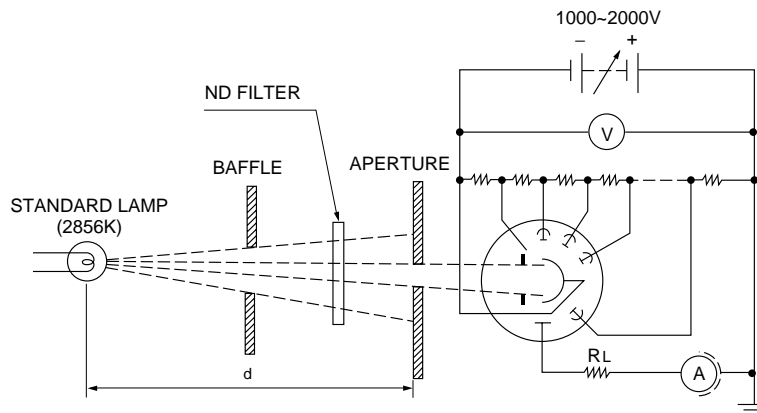
The incident luminous flux used for measurement is in the range of  $10^{-5}$  to  $10^{-2}$  lumens. If the luminous flux is too large, measurement errors may occur due to the surface resistance of the photocathode. Consequently, the optimum luminous flux must be selected according to the photocathode size and material.

A picoammeter is usually used to measure the photocurrent which is as small as several nanoamperes to several microamperes. Sufficient countermeasures against leakage current and possible noise source must be taken. In addition, be careful to avoid contamination on the socket or bulb stem and to keep the ambient humidity at a low level so that an adequate electrical safeguard is provided.

The photomultiplier tube must be operated at a supply voltage which establishes a complete saturation in the supply voltage vs. cathode current characteristics. A voltage of 90 to 400 volts is usually applied for this purpose. Cathode saturation characteristics are discussed in Section 3.3.2, "Linearity". The ammeter is connected to the cathode via a serial load resistance ( $R_L$ ) of 100 kilohms to one megohm for circuitry protection.

## (2) Anode luminous sensitivity

Anode luminous sensitivity<sup>(23) (25)</sup> is defined as the anode output current per luminous flux incident on the photocathode. In this measurement, a proper voltage distribution is given to each electrode as illustrated in Figure 3-6. Although the same tungsten lamp that was used to measure the cathode luminous sensitivity is used again, the light flux is reduced to  $10^{-10}$  to  $10^{-5}$  lumens using a neutral density filter. The ammeter is connected to the anode via the series resistance. The voltage-divider resistors used in this measurement must have minimum tolerance and good temperature characteristics.



TPMOC0055EA

Figure 3-6: Anode luminous sensitivity measuring diagram

### (3) Blue sensitivity and red-to-white ratio

Blue sensitivity and red-to-white ratio are often used for simple comparison of the spectral response of photomultiplier tubes.

Blue sensitivity is the cathode current obtained when a blue filter is placed in front of the photomultiplier tube under the same conditions for the luminous sensitivity measurement. The blue filter used is a Corning Cs No.5-58 polished to half stock thickness. Since the light flux entering the photomultiplier tube has been transmitted through the blue filter once, it cannot be directly represented in lumens. Therefore at Hamamatsu Photonics, it is conveniently expressed in units of A/lm-b (amperes per lumen-blue). The spectral transmittance of this blue filter matches well the emission spectrum of a NaI(Tl) scintillator (peak wavelength 420 nanometers) which is widely used for scintillation counting. Photomultiplier tube sensitivity to the scintillation flash has a good correlation with the anode sensitivity using this blue filter. Furthermore, the blue sensitivity is an important factor to determine energy resolution in scintillation measurement. Refer to Section 3.5 for more details, "Scintillation counting".

The red-to-white ratio is used to evaluate photomultiplier tubes with a spectral response extending to the near infrared region. This parameter is defined as the quotient of the cathode sensitivity measured with a red or near infrared filter interposed under the same conditions for cathode luminous sensitivity divided by the cathode luminous sensitivity without a filter. The filter used is a Toshiba IR-D80A for Ag-O-Cs photocathodes or a Toshiba R-68 for other photocathodes. If other types of filters are used, the red-to-white ratio will vary. Figure 3-7 shows the spectral transmittance of these filters.

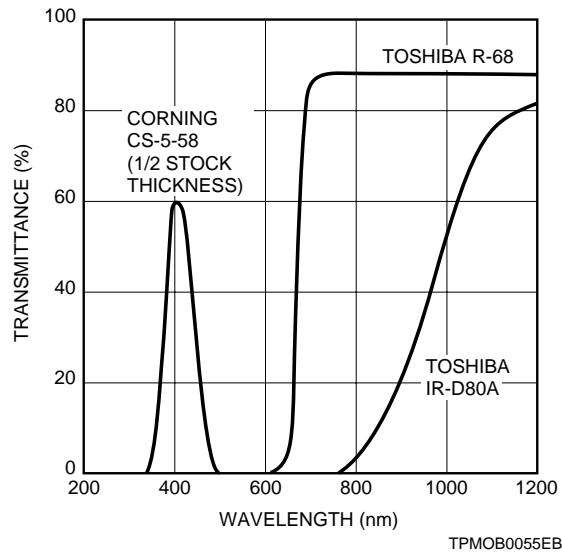
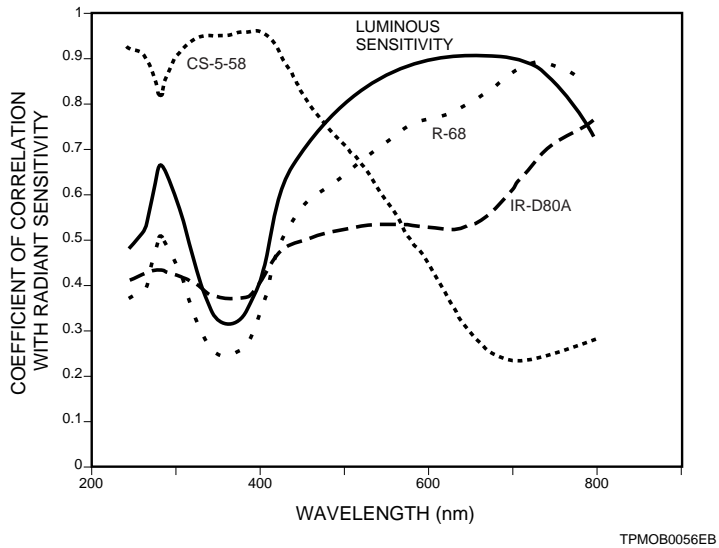


Figure 3-7 Typical spectral transmittance of optical filters.

### 3.1.5 Luminous sensitivity and spectral response

There is a correlation between luminous sensitivity and spectral response to some extent at a specific wavelength. Figure 3-8 describes the correlation between luminous sensitivity, blue sensitivity (CS-5-58) and red-to-white ratio (R-68, IR-D80A) as a function of wavelength.



**Figure 3-8: Correlation between luminous sensitivities and radiant sensitivity**

It can be seen from the figure that the radiant sensitivity of a photomultiplier tube has a good correlation with the blue sensitivity at wavelengths shorter than 450 nanometers, with the luminous sensitivity at 700 to 800 nanometers, with the red-to-white ratio using the Toshiba R-68 filter at 700 to 800 nanometers, and with the red-to-white ratio using the Toshiba IR-D80A filter at 800 nanometers or longer. From these correlation values, it is possible to select a photomultiplier tube with optimum sensitivity at a certain wavelength by simply measuring the sensitivity using a filter which has the best correlation value at that wavelength rather than making troublesome measurements of the spectral response.

## 3.2 Basic Characteristics of Dynodes

This section introduces typical dynode types currently in use and describes their basic characteristics: collection efficiency and gain (current amplification).

### 3.2.1 Dynode types and features

There are a variety of dynode types available and each type exhibits different gain, time response, uniformity and secondary-electron collection efficiency depending upon the structure and the number of stages. It is essential to select the optimum type in accordance with your application. Figure 3-9 illustrates the cross sectional views of typical dynodes and their features are briefly discussed in the following sections. MCP-PMT's incorporating a microchannel plate for the dynode and photomultiplier tubes using a fine-mesh dynode are detailed in Chapter 4 and Chapter 6, respectively.

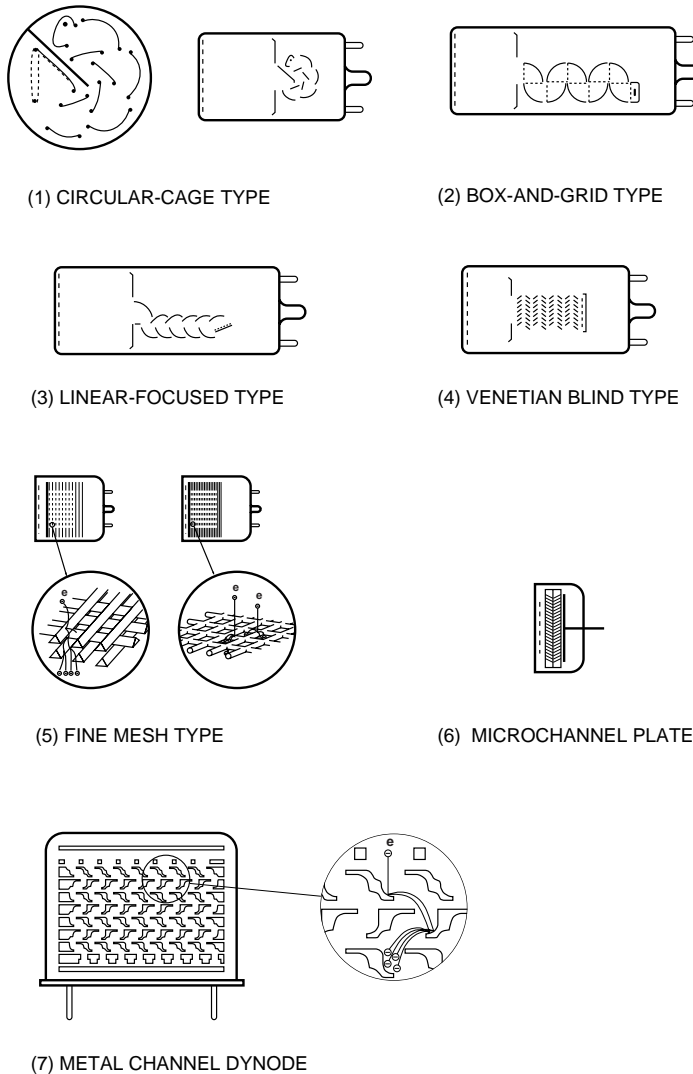


Figure 3-9: Types of electron multipliers

**(1) Circular-cage type**

The circular-cage type has an advantage of compactness and is used in all side-on photomultiplier tubes and in some head-on photomultiplier tubes. The circular-cage type also features fast time response.

**(2) Box-and-grid type**

This type, widely used in head-on photomultiplier tubes, is superior in photoelectron collection efficiency. Accordingly, photomultiplier tubes using this dynode offer high detection efficiency and good uniformity.

**(3) Linear-focused type**

As with the box-and-grid type, the linear-focused type is widely used in head-on photomultiplier tubes. Its prime features include fast time response, good time resolution and excellent pulse linearity.

**(4) Venetian blind type**

The venetian blind type allows a simple design for photoelectron collection and is ideally suited for use in head-on photomultiplier tubes with a large photocathode diameter.

**(5) Mesh type**

This type of dynode uses mesh electrodes stacked in close proximity to each other. There are two types: coarse mesh type and fine mesh type. Both are excellent in output linearity and have good immunity to magnetic fields. When used with a cross wire anode or multianode, it is possible to detect the position of incident light. Fine mesh types are developed primarily for photomultiplier tubes which are used in high magnetic fields. (For further details, refer to Chapter 6.)

**(6) MCP (Microchannel plate)**

A microchannel plate (MCP) with 1mm thickness is used as a dynode. This dynode exhibits dramatically improved time resolution as compared to other discrete dynodes. It also assures stable gain even in highly magnetic fields and provides position-sensitive capability when combined with a special anode. (For more details, refer to Chapter 6.)

**(7) Metal channel dynode**

Our long experience with micromachining technology and computer simulation of electron trajectories allowed fabricating extremely thin electrodes and assembling them in a precisely stacked configuration. Since each dynode is in close proximity to each other, the overall length is very short ensuring excellent time characteristics and stable gain even in magnetic fields. (A detailed description is given in Chapter 6.)

The electrical characteristics of a photomultiplier tube depend not only on the dynode type but also on the photocathode size and focusing system. As a general guide, Table 3-2 summarizes typical performance characteristics of head-on photomultiplier tubes (up to 5-inch diameter) classified by the dynode type. Magnetic characteristics listed are measured in a magnetic field in the direction of the most sensitive tube axis.

| Dynode Type    | Rise Time (ns) | Pulse Linearity at 2% (mA) | Magnetic Immunity (mT) | Uniformity | Collection Efficiency | Features                               |
|----------------|----------------|----------------------------|------------------------|------------|-----------------------|--|
| Circular-cage  | 0.9 to 3.0     | 1 to 10                    | 0.1                    | Poor       | Good                  | Compact, high speed                    |
| Box-and-grid   | 6 to 20        |                            |                        | Good       | Very good             | High collection efficiency             |
| Linear-focused | 0.7 to 3       | 10 to 250                  |                        | Poor       | Good                  | High speed, high linearity             |
| Venetian blind | 6 to 18        | 10 to 40                   |                        | Good       | Poor                  | Suited for large diameter              |
| Fine mesh      | 1.5 to 5.5     | 300 to 1000                | *700 to 1200 or more   | Good       | Poor                  | High magnetic immunity, high linearity |
| MCP            | 0.1 to 0.3     | 700                        | 15 to *1200 or more    | Good       | Poor                  | high speed                             |
| Metal channel  | 0.65 to 1.5    | 30                         | 1 to 20**              | Good       | Good                  | Compact, high speed                    |

\* In magnetic field parallel to tube axis  
 \*\*Metal package PMT

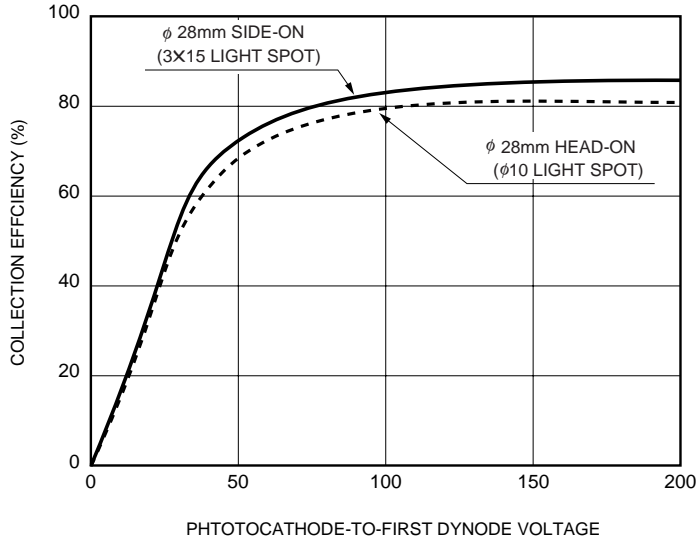
**Table 3-2: Typical characteristics of head-on photomultiplier tubes classified by dynode type**

## 3. 2. 2 Collection efficiency and current amplification (gain)

### (1) Collection efficiency

The electron multiplier of a photomultiplier tube is designed with consideration to the electron trajectories so that electrons are efficiently multiplied at each dynode. However, some electrons may deviate from their favorable trajectories, not contributing to multiplication.

In general, the probability that photoelectrons may land on the effective area of the first dynode is termed the collection efficiency ( $\alpha$ ). This effective area is the area of the first dynode where photoelectrons can be multiplied effectively at the successive dynode stages without deviating from their favorable trajectories. Although there exist secondary electrons which do not contribute to multiplication at the second dynode or latter dynodes, they will tend to have less of an affect on the total collection efficiency as the number of secondary electrons emitted increases greatly. Thus the photoelectron collection efficiency at the first dynode is important. Figure 3-10 shows collection efficiency as a function of cathode-to-first dynode voltage. If the cathode-to-first dynode voltage is inappropriate, the photoelectrons will not enter the effective area of the first dynode, thereby degrading collection efficiency.



TPMOB0057JC

**Figure 3-10: Collection efficiency vs. photocathode-to-first dynode voltage**

From Figure 3-10, it can be seen that the cathode-to-first dynode voltage should be higher than 70 volts. The collection efficiency influences energy resolution, detection efficiency and signal-to-noise ratio in scintillation counting. The detection efficiency is the ratio of the detected signal to the input signal of a photomultiplier tube. In photon counting this is expressed as the product of the photocathode quantum efficiency and the collection efficiency.

**(2) Gain**

Secondary emission ratio  $\delta$  is a function of the interstage voltage of dynodes E, and is given by the following equation:

$$\delta = a \cdot E^k \dots\dots\dots \text{(Eq. 3-3)}$$

Where a is a constant and k is determined by the structure and material of an electrode and has a value from 0.7 to 0.8.

The photoelectron current  $I_k$  emitted from the photocathode strikes the first dynode where secondary electrons  $I_{d1}$  are released. At this point, the secondary emission ratio  $\delta_1$  at the first dynode is given by

$$\delta_1 = \frac{I_{d1}}{I_k} \dots\dots\dots \text{(Eq. 3-4)}$$

These electrons are multiplied in a cascade process from the first dynode  $\rightarrow$  second dynode  $\rightarrow$  .... the n-th dynode. The secondary emission ratio  $\delta_n$  of n-th stage is given by

$$\delta_n = \frac{I_{dn}}{I_{d(n-1)}} \dots\dots\dots \text{(Eq. 3-5)}$$

The anode current  $I_p$  is given by the following equation:

$$I_p = I_k \cdot \alpha \cdot \delta_1 \cdot \delta_2 \dots \delta_n \dots\dots\dots \text{(Eq. 3-6)}$$

Then

$$\frac{I_p}{I_k} = \alpha \cdot \delta_1 \cdot \delta_2 \dots \delta_n \dots\dots\dots \text{(Eq. 3-7)}$$

where  $\alpha$  is the collection efficiency. (See Section 3.4.2.)

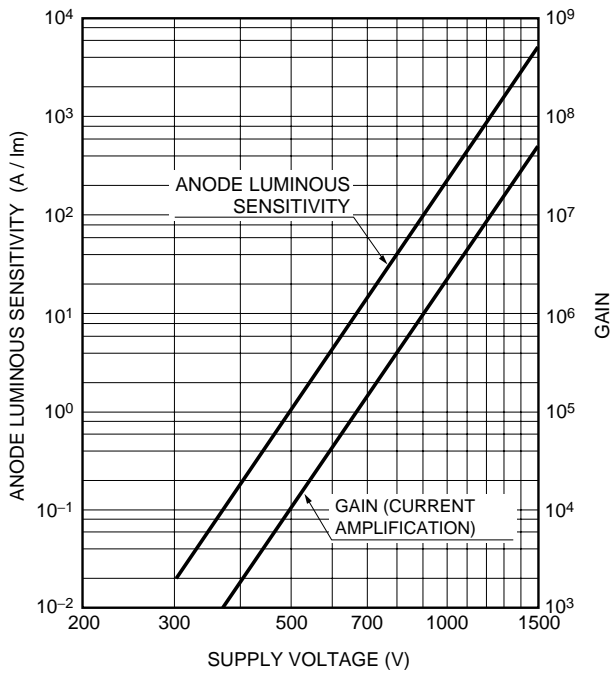
The product of  $\alpha, \delta_1, \delta_2 \dots \delta_n$  is called the gain  $\mu$ , and is given by the following equation:

$$\mu = \alpha \cdot \delta_1 \cdot \delta_2 \dots \delta_n \dots \dots \dots \text{(Eq. 3-8)}$$

Accordingly, in the case of a photomultiplier tube with  $\alpha=1$  and the number of dynode stages = n, which is operated using an equally-divided divider, the gain  $\mu$  changes in relation to the supply voltage V, as follows:

$$\mu = (a \cdot E^k)^n = a^n \left( \frac{V}{n+1} \right)^{kn} = A \cdot V^{kn} \dots \dots \dots \text{(Eq. 3-9)}$$

where A should be equal to  $a^n / (n+1)^{kn}$ . From this equation, it is clear that the gain  $\mu$  is proportional to the kn exponential power of the supply voltage. Figure 3-11 shows typical gain vs. supply voltage. Since Figure 3-11 is expressed in logarithmic scale for both the abscissa and ordinate, the slope of the straight line becomes kn and the current multiplication increases with the increasing supply voltage. This means that the gain of a photomultiplier tube is susceptible to variations in the high-voltage power supply used to operate the photomultiplier tube, such as drift, ripple, temperature stability, input regulation, and load regulation.



TPMOB0058EB

Figure 3-11: Gain vs. supply voltage

## 3.3 Characteristics of Photomultiplier Tubes

This section describes important characteristics for photomultiplier tube operation and their evaluation methods, and photomultiplier tube usage.

### 3.3.1 Time characteristics

The photomultiplier tube is a photodetector that has an exceptionally fast time response.<sup>1) 23)-27)</sup> The time response is primarily determined by the transit time required for the photoelectrons emitted from the photocathode to reach the anode while being multiplied and also the transit time difference between each photoelectron. Accordingly, fast response photomultiplier tubes are designed to have a spherical inner window and carefully engineered electrodes so that the transit time difference in the tube can be minimized.

Table 3-3 lists the timing characteristics of 2-inch diameter head-on photomultiplier tubes categorized by their dynode structure. As can be seen from the table, the linear-focused type exhibits the best time characteristics, while the box-and-grid and venetian blind types provide rather poor properties. Therefore, fast response photomultiplier tubes usually employ linear-focused dynodes.

Unit : ns

| Dynode Type    | Rise Time   | Fall Time | Pulse Width (FWHM) | Electron Transit Time | T.T.S.       |
|----------------|-------------|-----------|--------------------|-----------------------|--------------|
| Linear-focused | 0.7 to 3    | 1 to 10   | 1.3 to 5           | 16 to 50              | 0.37 to 1.1  |
| Circular-cage  | 3.4         | 10        | 7                  | 31                    | 3.6          |
| Box-and-grid   | to 7        | 25        | 13 to 20           | 57 to 70              | to 10        |
| Venetian blind | to 7        | 25        | 25                 | 60                    | to 10        |
| Fine mesh      | 2.5 to 2.7  | 40        | 5                  | 15                    | to 0.9       |
| Metal channel  | 0.65 to 1.5 | 1 to 3    | 1.5 to 3           | 4.7 to 8.8            | 0.26 to 0.28 |

Table 3-3: Typical time characteristics (2-inch dia. photomultiplier tubes)

The time response is mainly determined by the electrode structure, but also depends on the supply voltage. Increasing the electric field intensity or supply voltage improves the electron transit speed and thus shortens the transit time. In general, the time response improves in inverse proportion to the square root of the supply voltage. Figure 3-12 shows typical time characteristics vs. supply voltage.

For the detection of high-speed phenomenon, wiring from the photomultiplier tube to external circuits such as a voltage-divider circuit and an anode signal processing circuit must be as short as possible to minimize stray capacitance and inductance. These circuit systems are discussed later in Chapter 7. In addition, some fast response photomultiplier tubes have a coaxial anode to suppress output waveform distortion.

The following explains definitions of time characteristics and their measurement methods.

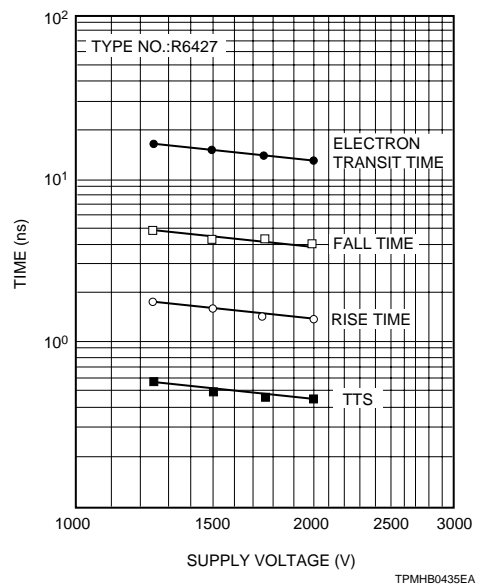
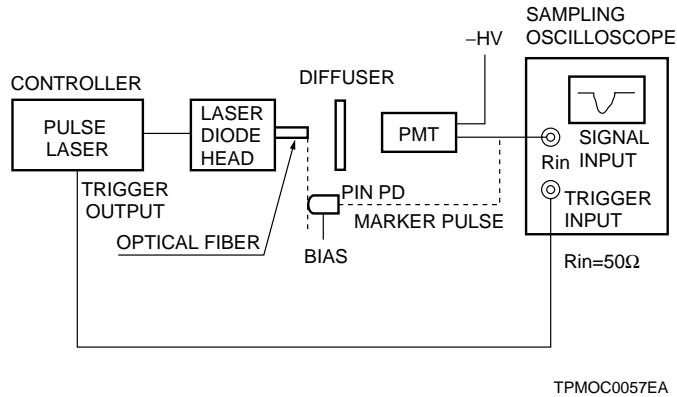


Figure 3-12: Time characteristics vs. supply voltage

### (1) Rise time, fall time and electron transit time

Figure 3-13 shows a schematic diagram for time response measurements and Figure 3-14 illustrates the definitions of the rise time, fall time and electron transit time of a photomultiplier tube output.



**Figure 3-13: Measurement block diagram for rise/fall times and electron transit time**

A pulsed laser diode is used as the light source. Its pulse width is 55 picoseconds (800 nanometers) which is sufficiently short compared to that attainable from a photomultiplier tube. Thus it can be regarded as a delta-function light source. A sampling oscilloscope is used to sample the photomultiplier tube output many times so that a complete output waveform is created. When measuring a photomultiplier tube with a bialkali photocathode, an SHG (second harmonic generator) is used to produce a light pulse with a wavelength of 400 nanometers which is twice the fundamental frequency of the light from the laser diode. At this point, the pulse width will be 30 picoseconds. The output pulse waveform obtained from the photomultiplier tube is composed of waveforms which are produced by electrons emitted from every position of the photocathode. Therefore, the rise and fall times are mainly determined by the electron transit time difference and also by the electric field distribution and intensity (supply voltage) between the electrodes.

As indicated in Figure 3-14, the rise time is defined as the time for the output pulse to increase from 10 to 90 percent of the peak pulse height. Conversely, the fall time is defined as the time required to decrease from 90 to 10 percent of the peak output pulse height. In time response measurements where the rise and fall times are critical, the output pulse tends to suffer waveform distortion, causing an erroneous signal. To prevent this problem, proper impedance matching must be provided including the use of a voltage-divider circuit with damping resistors. (See Chapter 7.)

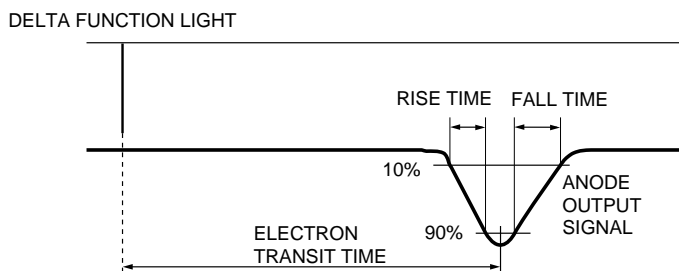
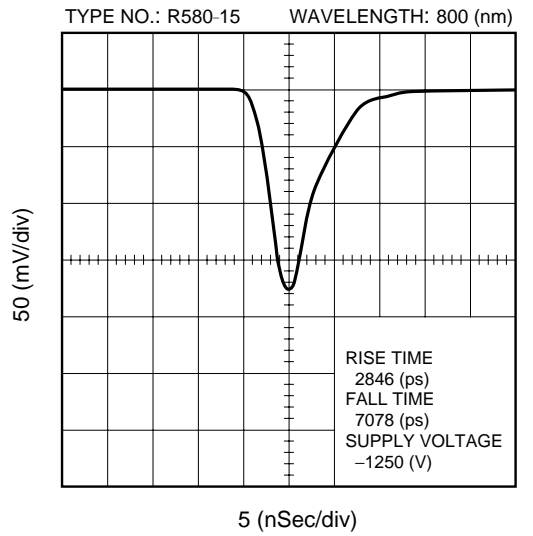


**Figure 3-14: Definitions of rise/fall times and electron transit time**

Figure 3-15 shows an actual output waveform obtained from a photomultiplier tube. In general, the fall time is two or three times longer than the rise time. This means that when measuring repetitive pulses, care must be taken so that each output pulse does not overlap. The FWHM (full width at half maximum) of the output pulse will usually be about 2.5 times the rise time.

The transit time is the time interval between the arrival of a light pulse at the photocathode and the appearance of the output pulse. To measure the transit time, a PIN photodiode is placed as reference (zero second) at the same position as the photomultiplier tube photocathode. The time interval between the instant the PIN photodiode detects a light pulse and the instant the output pulse of the photomultiplier tube reaches its peak amplitude is measured. This transit time is a useful parameter in determining the delay time of a measurement system in such applications as fluorescence lifetime measurement using repetitive light pulses.

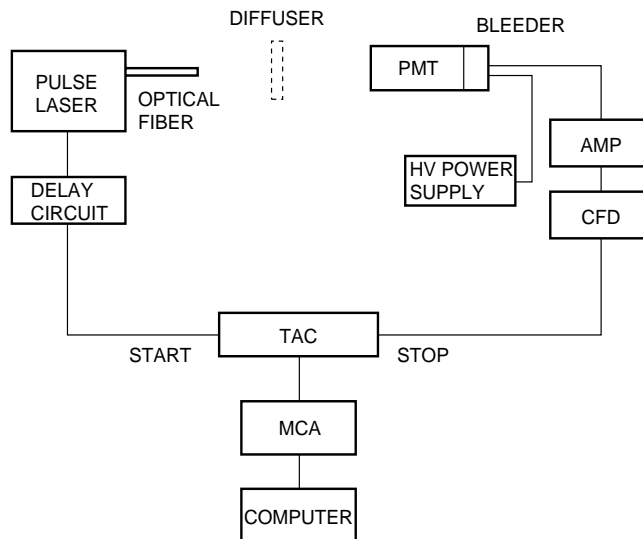


TPMOB0090EA

Figure 3-15: Example of output waveform

(2) TTS (transit time spread)

When a photocathode is fully illuminated, the transit time of each photoelectron pulse has a fluctuation. This fluctuation is called TTS (transit time spread). A block diagram for TTS measurement is shown in Figure 3-16 and typical measured data is shown in Figure 3-17.



TPMOC0058EB

Figure 3-16: Block diagram for TTS measurement

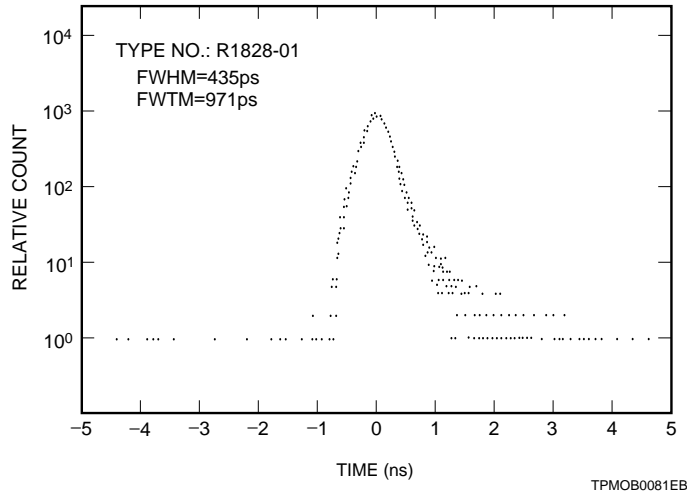


Figure 3-17: TTS data example

In this measurement, a trigger signal from the pulsed laser is passed through the delay circuit and then fed as the start to the TAC (time-to-amplitude converter) which converts the time difference into pulse height. Meanwhile, the output from the photomultiplier tube is fed as the stop signal to the TAC via the CFD (constant fraction discriminator) which reduces the time jitter resulting from fluctuation of the pulse height. The TAC generates a pulse height proportional to the time interval between the "start" and "stop" signals. This pulse is fed to the MCA (multichannel analyzer) for pulse height analysis. Since the time interval between the "start" and "stop" signals corresponds to the electron transit time, a histogram displayed on the MCA, by integrating individual pulse height values many times in the memory, indicates the statistical spread of the electron transit time.

At Hamamatsu Photonics, the TTS is usually expressed in the FWHM of this histogram, but it may also be expressed in standard deviation. When the histogram shows a Gaussian distribution, the FWHM is equal to a value which is 2.35 times the standard deviation. The TTS improves as the number of photoelectrons per pulse increases, in inverse proportion to the square root of the number of photoelectrons. This relation is shown in Figure 3-18.

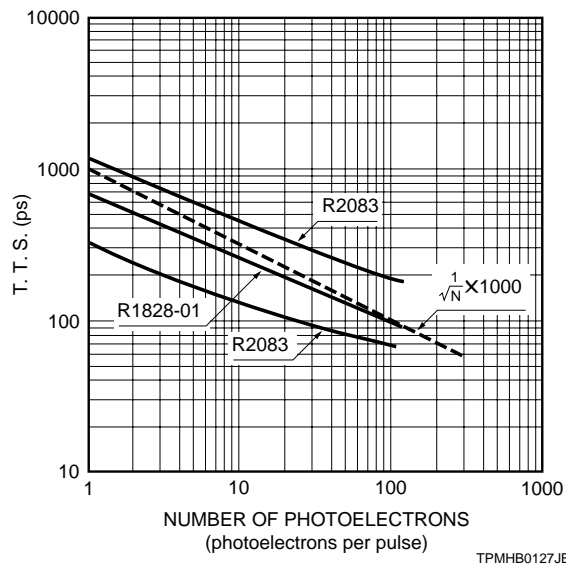
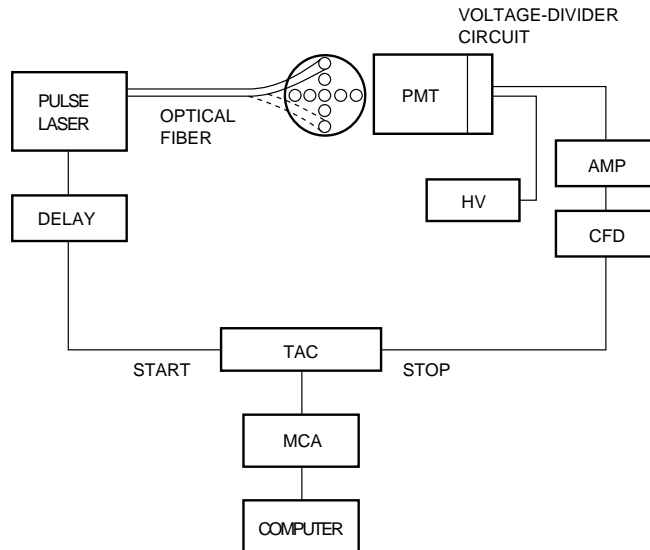


Figure 3-18: TTS vs. number of photoelectrons

### (3) CTTD (cathode transit time difference)

The CTTD (cathode transit time difference) is the difference in transit time when the incident light position on the photocathode is shifted. In most time response measurements the entire photocathode is illuminated. However, as illustrated in Figure 3-19, the CTTD measurement employs an aperture plate to shift the position of a light spot entering the photocathode, and the transit time difference between each incident position is measured.



TPMOC0059JB

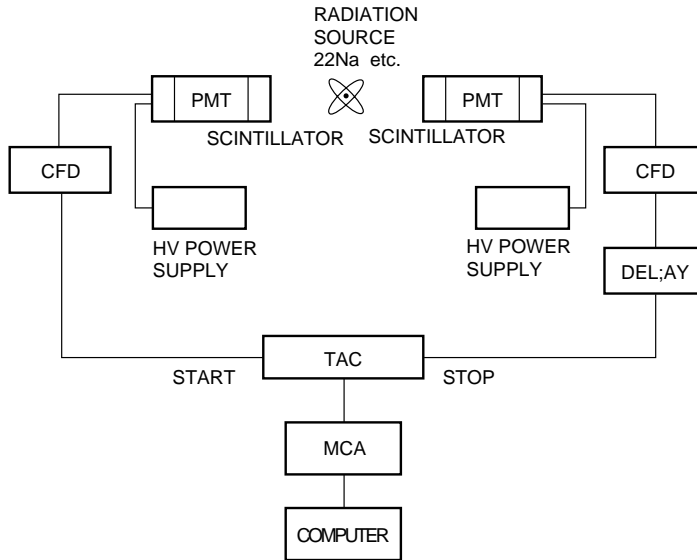
**Figure 3-19: Block diagram for CTTD measurement**

Basically, the same measurement system as for TTS measurement is employed, and the TTS histogram for each of the different incident light positions is obtained. Then the change in the peak pulse height of each histogram, which corresponds to the CTTD, is measured. The CTTD data of each position is represented as the transit time difference with respect to the transit time measured when the light spot enters the center of the photocathode.

In actual applications, the CTTD data is not usually needed but rather primarily used for evaluation in the photomultiplier tube manufacturing process. However, the CTTD is an important factor that affects the rise time, fall time and TTS described previously and also CRT (coincident resolving time) discussed in the next section.

**(4) CRT (coincident resolving time)**

As with the TTS, this is a measure of fluctuations in the transit time. The CRT measurement system resembles that used for positron CT (See Section 9.3.) or TOF (time of flight) measurement (See Section 9.7.). Therefore, the CRT is a very practical parameter for evaluating the performance of photomultiplier tubes used in the above fields or similar applications. Figure 3-20 shows a block diagram of the CRT measurement.



TPMOC0060JA

**Figure 3-20: Block diagram for CRT measurement**

As a radiation source <sup>22</sup>Na, <sup>68</sup>Ge-Ga or <sup>60</sup>Co is commonly used, while for the scintillator a BGO, BaF<sub>2</sub>, CsF or plastic scintillator is used. A proper combination of radiation source and scintillator should be selected according to the application. The radiation source is placed in the middle of a pair of photomultiplier tubes and emits gamma-rays in opposing directions at the same time. A coincident flash occurs from each of the two scintillators coupled to the photomultiplier tube. The signal detected by one photomultiplier tube is fed as the start signal to the TAC, while the signal from the other photomultiplier tube is fed as the stop signal to the TAC via the delay circuit used to obtain proper trigger timing. Then, as in the case of the TTS measurement, the output pulse from the TAC is analyzed by the MCA and this operation is repeated many times so that a CRT spectrum is created. This spectrum statistically displays the time fluctuation of the signals that enter the TAC. This fluctuation mainly results from the TTS of the two photomultiplier tubes. As can be seen from Figures 3-12 and 3-18, the TTS is inversely proportional to the square root of the number of photoelectrons per pulse and also to the square root of the supply voltage. In general, therefore, the higher the radiation energy and the supply voltage, the better the CRT will be. If the TTS of each photomultiplier tube is  $\tau_1$  and  $\tau_2$ , the CRT is given by

$$C.R.T. = (\tau_1^2 + \tau_2^2)^{1/2} \dots\dots\dots (Eq. 3-10)$$

The CRT characteristic is an important parameter for TOF measurements because it affects the position resolution.

### 3.3.2 Linearity

The photomultiplier tube provides good linearity<sup>1) 24) 27) 28)</sup> in anode output current over a wide range of incident light levels including the photon counting region. In other words, it offers a wide dynamic range. However, if the incident light amount is too large, the output begins to deviate from the ideal linearity. This is primarily caused by anode linearity characteristics, but it may also be affected by cathode linearity characteristics when a photomultiplier tube with a transmission mode photocathode is operated at a low supply voltage and large current. Both cathode and anode linearity characteristics are dependent only on the current value if the supply voltage is constant, while being independent of the incident light wavelength.

#### (1) Cathode linearity

| Photocathode Materials | Spectral Response [Peak Wavelength] (nm)      | Upper Limit of Linearity (Average Current) |
|------------------------|---|--|
| Ag-O-Cs                | 300 to 1200 [800]                             | 1 $\mu$ A                                  |
| Sb-Cs                  | up to 650 [440]                               | 1 $\mu$ A                                  |
| Sb-Rb-Cs/Sb-K-Cs       | up to 650 [420]                               | 0.1 $\mu$ A/0.01 $\mu$ A                   |
| Sb-Na-K                | up to 650 [375]                               | 10 $\mu$ A                                 |
| Sb-Na-K-Cs             | up to 850 [420], up to 900 [600] extended red | 10 $\mu$ A                                 |
| Ga-As                  | up to 930 [300~700]                           | (*) 0.1 $\mu$ A                            |
| Cs-Te                  | up to 320 [210]                               | 0.1 $\mu$ A                                |
| Cs-I                   | up to 200 [140]                               |  |

(\*) Linearity considerably degrades if this current is exceeded.

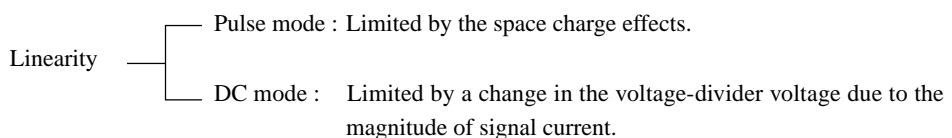
**Table 3-4: Photocathode materials and cathode linearity limits**

The photocathode is a semiconductor and its electrical resistance depends on the photocathode materials. As listed in Table 3-4, therefore, the cathode linearity also differs depending on the photocathode materials. It should be noted that Table 3-4 shows characteristics only for transmission mode photocathodes. In the case of reflection mode photocathodes which are formed on a metal plate and thus have a sufficiently low resistivity, the linearity will not be a significant problem. To reduce the effect of photocathode resistivity on the linearity without degrading the collection efficiency, it is generally recommended to apply a voltage of more than 100 volts between the photocathode and the first dynode. (Refer to Section 3.2.2.) For semiconductors, the photocathode surface resistivity increases as the temperature decreases. Thus, consideration must be given to the temperature characteristics of the photocathode resistivity when cooling the photomultiplier tube.

#### (2) Anode linearity

The anode linearity is limited by two factors: the voltage-divider circuit and space charge effects due to a large current flowing in the dynodes.

As shown below, the linearity in DC mode operation is mainly limited by the voltage-divider circuit, while the pulse mode operation is limited by space charge effects.



The linearity limit caused by the voltage-divider circuit is described in Chapter 7. The pulse linearity is chiefly dependent on the peak anode current. When an intense light pulse enters a photomultiplier tube, a large current flows in the latter dynode stages, increasing the space charge density, as a result current saturation occurs. The extent of these effects depends on the dynode structure, as indicated in Table 3-2. The space charge effects also depend on the electric field distribution and intensity between each dynode. The mesh type dynodes offer superior linearity because they have a structure resistant to the space charge effects. Each dynode is arranged in close proximity providing a higher electric field strength and the dynode area is large so that the signal density per unit area is lower. In general, any dynode type provides better linearity when the supply voltage is increased, or in other words, when the electric field strength between each dynode is enhanced.

Figure 3-21 shows the relationship between the linearity and the anode peak current with the supply voltage as a parameter for a Hamamatsu photomultiplier tube R2059. The linearity can be improved by use of a special voltage-divider (called "a tapered voltage-divider") designed to increase the interstage voltages at the latter dynode stages. Because such a tapered voltage-divider must have an optimum electric field distribution and intensity that match each dynode, determining the proper voltage distribution ratio is not simple but a rather complicated operation.

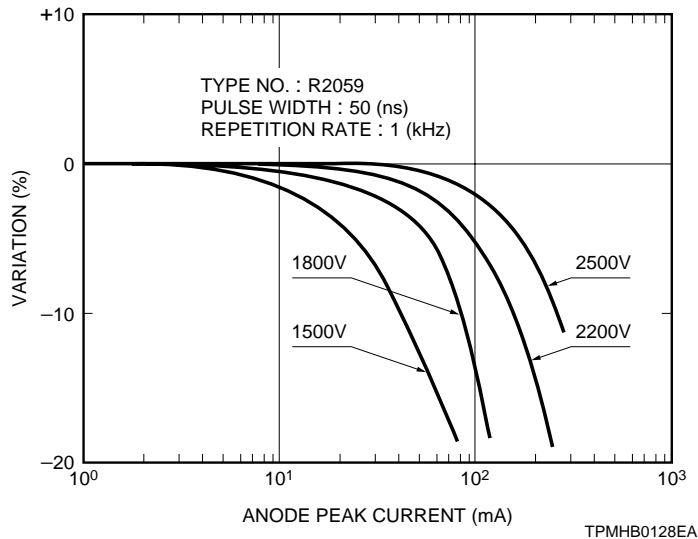
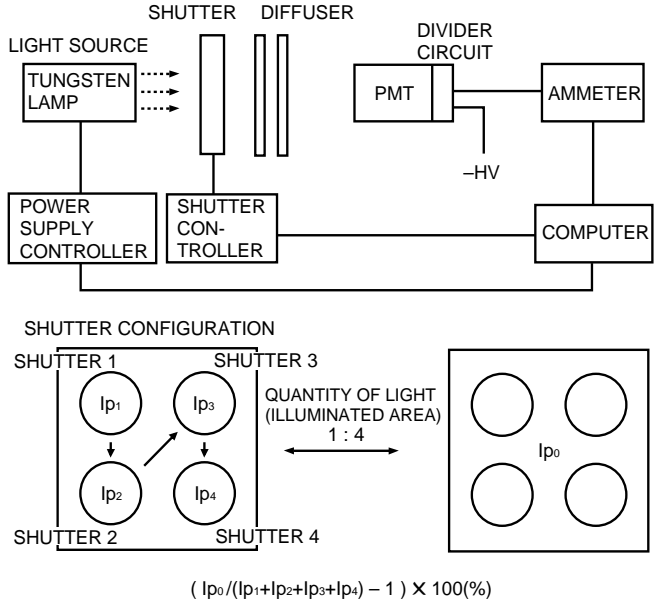


Figure 3-21: Voltage dependence of linearity

**(3) Linearity measurement**

The linearity measurement methods include the DC mode and the pulse mode. Each mode is described below.

**(a) DC mode**



TPMOC0061EB

**Figure 3-22: Block diagram for DC mode linearity measurement**

This section introduces the DC linearity measurement method used by Hamamatsu Photonics. As Figure 3-22 shows, an aperture plate with four apertures equipped with shutters is installed between the light source and the photomultiplier tube. Each aperture is opened in the order of 1, 2, 3 and 4, finally all four apertures are opened, and the photomultiplier tube outputs are measured (as  $I_{p1}$ ,  $I_{p2}$ ,  $I_{p3}$ ,  $I_{p4}$  and  $I_{p0}$ , respectively). Then the ratio of  $I_{p0}$  to  $(I_{p1} + I_{p2} + I_{p3} + I_{p4})$  is calculated as follows:

$$(I_{p0} / (I_{p1} + I_{p2} + I_{p3} + I_{p4}) - 1) \times 100(\%) \dots\dots\dots \text{(Eq. 3-11)}$$

This value represents a deviation from linearity and if the output is within the linearity range,  $I_{p0}$  becomes

$$I_{p0} = I_{p1} + I_{p2} + I_{p3} + I_{p4} \dots\dots\dots \text{(Eq. 3-12)}$$

Repeating this measurement by changing the intensity of the light source (i.e. changing the photomultiplier tube output current) gives a plot as shown in Figure 3-23. This indicates an output deviation from linearity. This linearity measurement greatly depends on the magnitude of the current flowing through the voltage-divider circuit and its structure.

As a simple method, linearity can also be measured using neutral density filters which are calibrated in advance for changes in the incident light level.



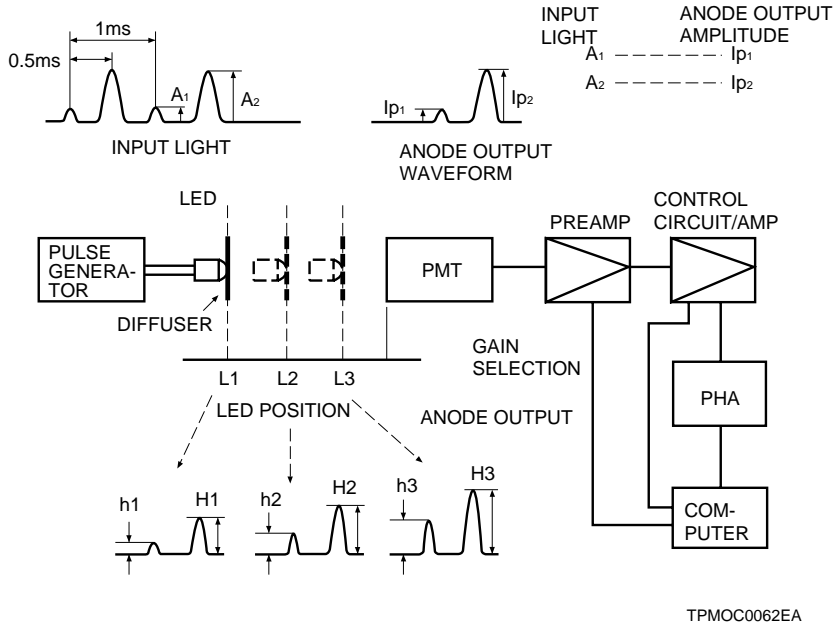


**Figure 3-24: Block diagram for pulse mode linearity measurement**

By repeating this measurement while varying the distance between the LED light source and the photomultiplier tube so as to change the output current of the photomultiplier tube, linearity curves like those shown in Figure 3-25 can be obtained. There are several other methods for measuring linearity, the above methods are just examples.

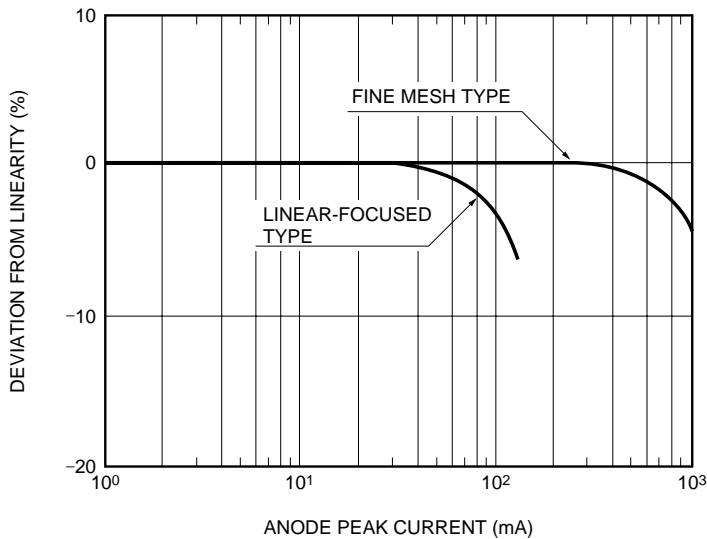


**Figure 3-25: Pulse linearity**

### 3.3.3 Uniformity

Uniformity is the variation of the output sensitivity with respect to the photocathode position. Anode output uniformity is thought to be the product of the photocathode uniformity and the electron multiplier (dynode section) uniformity.

Figure 3-26 shows anode uniformity data measured at wavelengths of 400 nanometers and 800 nanometers. This data is obtained with a light spot of 1mm diameter scanned over the photocathode surface.

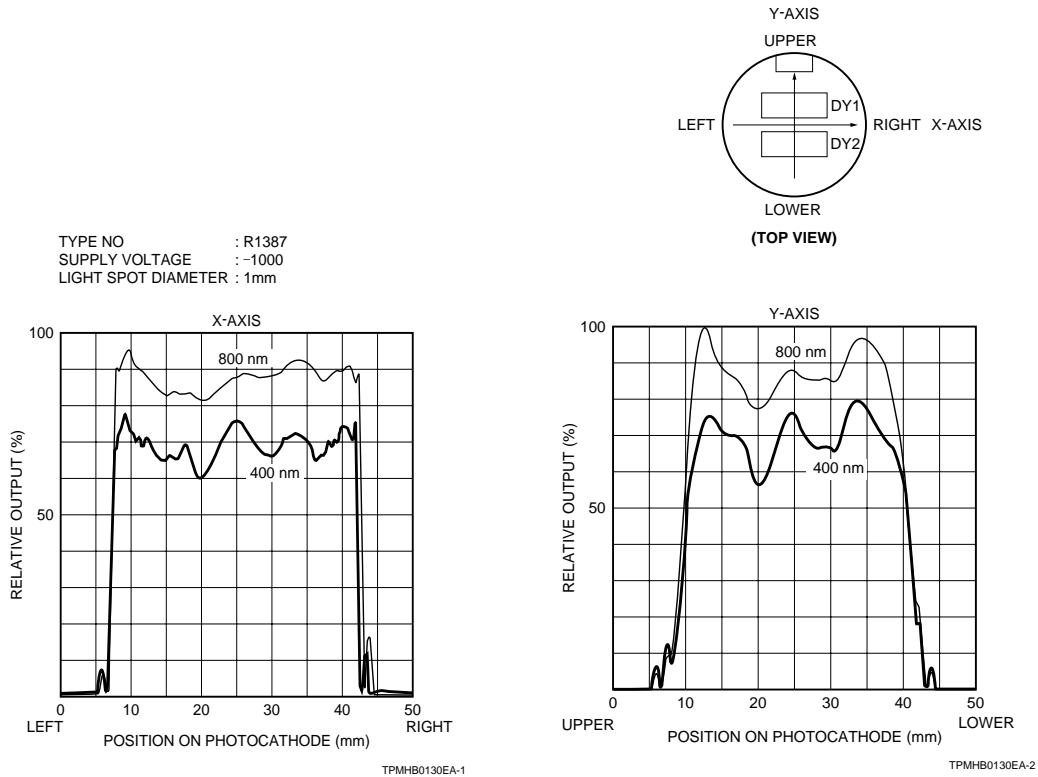


**Figure 3-26: Difference of uniformity with wavelength**

In general, both photocathode uniformity and anode uniformity deteriorate as the incident light shifts to a longer wavelength, and especially as it approaches the long-wavelength limit. This is because the cathode sensitivity near the long-wavelength limit greatly depends on the surface conditions of the photocathode and thus fluctuations increase. Moreover, if the supply voltage is too low, the electron collection efficiency between dynodes may degrade and adversely affect uniformity. It is therefore necessary to apply more than 100 volts between the photocathode and the first dynode, and more than 50 volts between each dynode.

Head-on photomultiplier tubes provide better uniformity in comparison with side-on types. In such applications as gamma cameras (See Section 9.2.) used for medical diagnosis where good position detecting ability is demanded, uniformity is an important parameter in determining equipment performance. Therefore, the photomultiplier tubes used in this field are specially designed and selected for better uniformity. Figure 3-27 shows typical uniformity data for a side-on tube. The same measurement procedure as for head-on tubes is used. Uniformity is also affected by the dynode structure. As can be seen from Table 3-2, the box-and-grid type, venetian blind type and mesh type offer better uniformity.

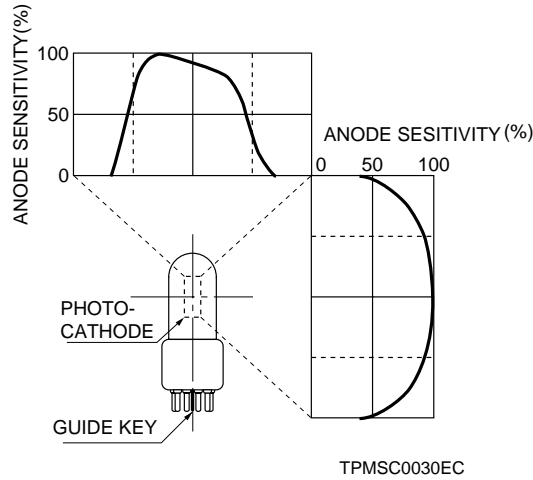


Figure 3-27: Uniformity of a side-on photomultiplier tube

Considering actual photomultiplier tube usage, uniformity is evaluated by two methods: one measured with respect to the position of incidence (spatial uniformity) and one with respect to the angle of incidence (angular response). The following sections explain their measurement procedures and typical characteristics.

(1) Spatial uniformity

To measure spatial uniformity, a light spot is scanned in two-dimensions over the photocathode of a photomultiplier tube and the variation in output current is graphically displayed. Figure 3-28 shows a schematic diagram for the spatial uniformity measurement.

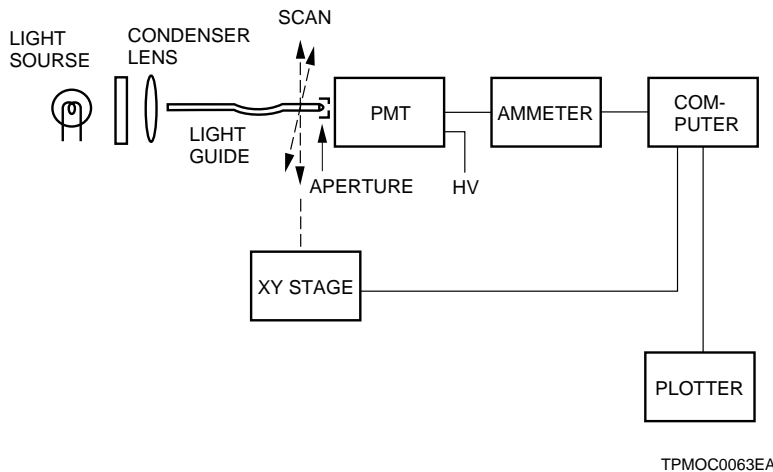
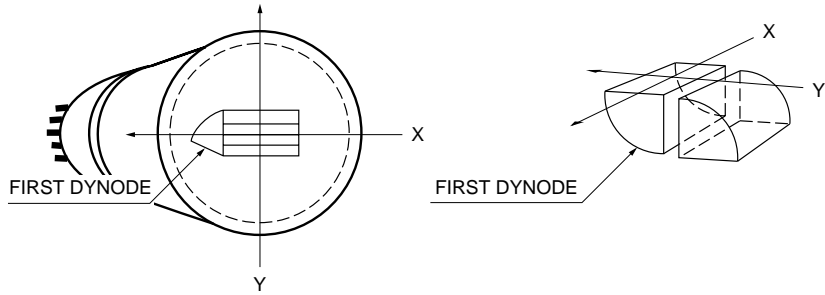


Figure 3-28: Schematic diagram for spatial uniformity measurement

For convenience, the photocathode is scanned along the X-axis and Y-axis. The direction of the X-axis or Y-axis is determined with respect to the orientation of the first dynode as shown in Figure 3-29.

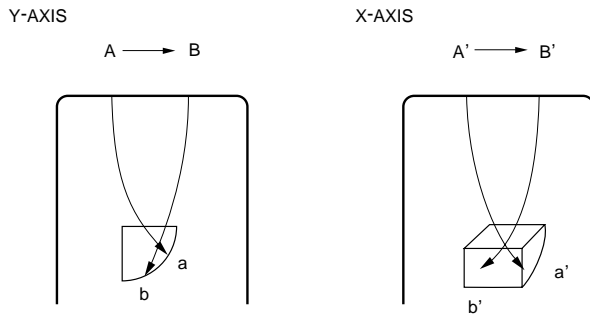
The degree of loss of electrons in the dynode section significantly depends on the position of the first dynode on which the photoelectrons strike. Refer to Figure 3-26 for specific uniformity data.



TPMHB0131EB

**Figure 3-29: Spatial uniformity measurement for head-on types**

While the photocathode is scanned by the light spot, the emitted photoelectrons travel along the X-axis or Y-axis of the first dynode as shown in Figure 3-30.



TPMHC0053EA

**Figure 3-30: Position of photoemission and the related position on the first dynode**

This method for measuring spatial uniformity is most widely used because the collective characteristics can be evaluated in a short time. In some cases, spatial uniformity is measured by dividing the photocathode into a grid pattern, so that sensitivity distribution is displayed in two or three dimensions.

The spatial uniformity in anode output ranges from 20 to 40 percent for head-on tubes, and may exceed those values for side-on tubes. To minimize the influence of the uniformity, placing a diffuser in front of the input window of a photomultiplier tube or using a photomultiplier tube with a frosted glass window will prove effective.

## (2) Angular response

Photomultiplier tube sensitivity somewhat depends on the angle of incident light on the photocathode. This dependence on the angle of incidence is called the angular response.<sup>28)-30)</sup> To measure the angular response, the entire photocathode is illuminated with collimated light, and the output current is measured while rotating the photomultiplier tube. A schematic diagram for the angular response measurement is shown in Figure 3-31 and specific data is plotted in Figure 3-32. As the tube is rotated, the projected area of the photocathode is reduced. This means that the output current of a tube, even outputs having no dependence on the angle of incidence, are plotted as a cosine curve. Commonly, the photocathode sensitivity improves at larger angles of incidence and thus the output current is plotted along a curve showing higher sensitivity than the cosine ( $\cos \theta$ ) curve. This is because the incident light transmits across a longer distance at large angles of incidence. In addition, this increase in sensitivity usually becomes larger at longer wavelengths.

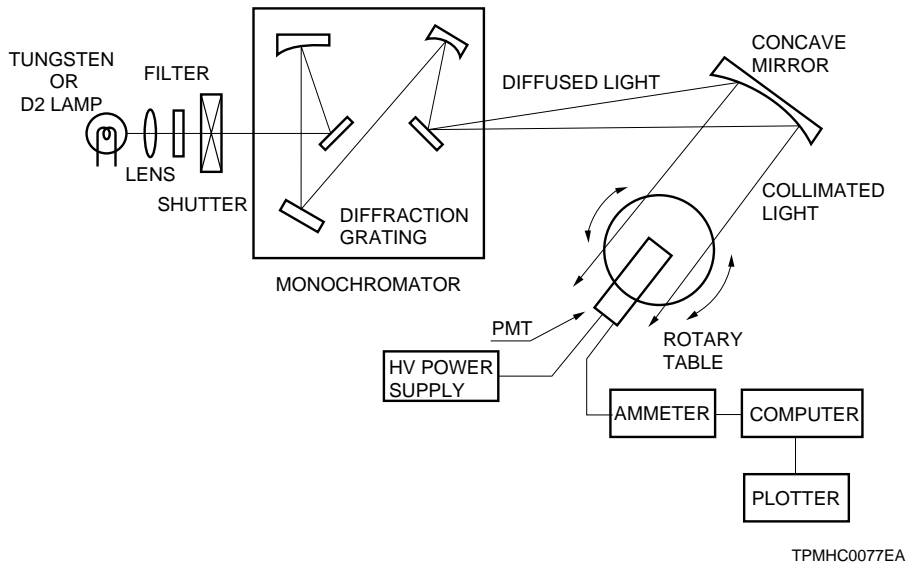


Figure 3-31: Schematic diagram for angular response measurement

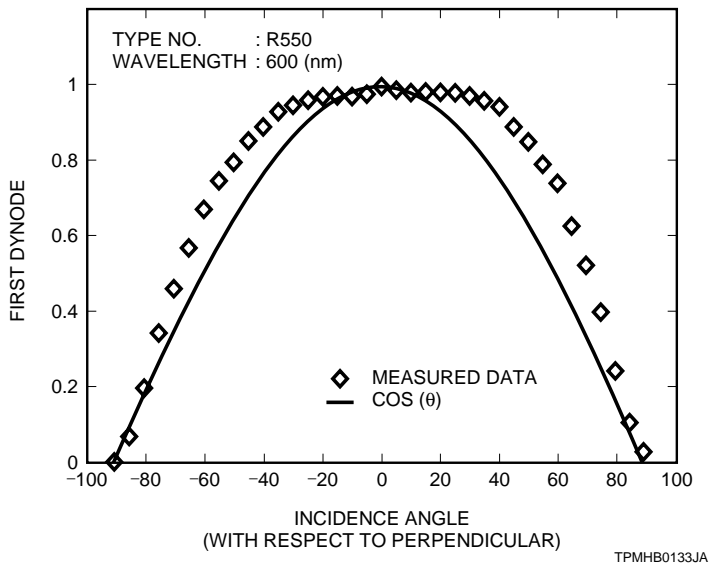


Figure 3-32: Typical angular response

### 3. 3. 4 Stability

The output variation of a photomultiplier tube with operating time is commonly termed as "drift" or "life" characteristics. On the other hand, the performance deterioration resulting from the stress imposed by the supply voltage, current, and ambient temperature is called "fatigue".

#### (1) Drift (time stability) and life characteristics

Variations (instability) over short time periods are mainly referred to as drift<sup>1) 31)</sup>, while variations (instability) over spans of time longer than  $10^3$  to  $10^4$  hours are referred to as the life characteristics. Since the cathode sensitivity of a photomultiplier tube exhibits good stability even after long periods of operating time, the drift and life characteristics primarily depend on variations in the secondary emission ratio. In other words, these characteristics indicate the extent of gain variation with operating time.

Drift per unit time generally improves with longer operating time and this tendency continues even if the tube is left unused for a short time after operation. It is therefore instrumental to perform aging or warm-up of the tube to stabilize the drift.

At Hamamatsu Photonics, drift is usually measured in the DC mode by illuminating a photomultiplier tube with a continuous light and recording the output current with the operating time. Figure 3-33 shows specific drift data for typical Hamamatsu photomultiplier tubes. In most cases, the drift of a photomultiplier tube tends to vary largely during initial operation and stabilizes as operating time elapses. In pulsed or intermittent operation (cyclic on/off operation), the drift shows a variation pattern similar to those obtained with continuous light if the average output current is of the same level as the output current in the DC mode.

In addition, there are other methods for evaluating the drift and life characteristics, which are chiefly used for photomultiplier tubes designed for scintillation counting. For more details refer to Section 3.5, "Scintillation counting".

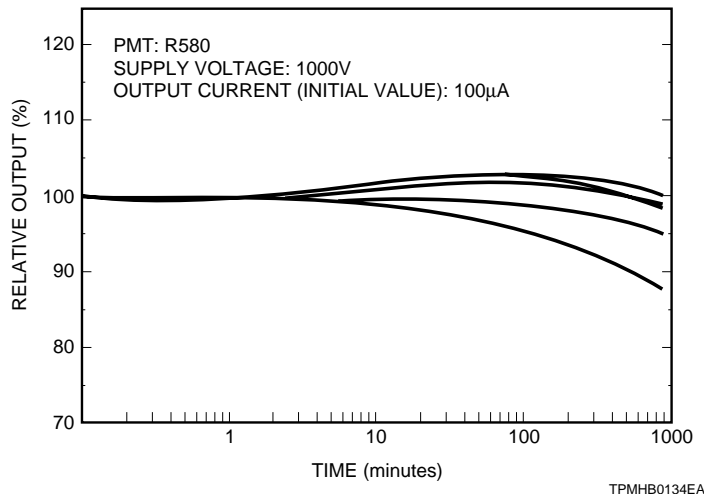


Figure 3-33: Examples of drift data

#### (2) Aging and warm-up

In applications where output stability within several percent is required, it is necessary to carry out aging or warm-up.

**(a) Aging**

Aging is a technique in which a photomultiplier tube is continuously operated for a period ranging from several hours to several tens of hours, with the anode output current not exceeding the maximum rating. Through this aging, drift can be effectively stabilized. In addition, if the tube is warmed up just before actual use, the drift will be further stabilized.

**(b) Warm-up**

For stable operation of a photomultiplier tube, it is essential to warm up the tube for about 30 to 60 minutes. The warm-up period should be longer at the initial phase of photomultiplier tube operation, particularly in intermittent operation then, after a long period of operation warm up can be shortened. At a higher anode current the warm-up period can be shortened and at a lower anode current it should be longer. As one common method, the photomultiplier tube is operated at a voltage near the actual operating voltage and warmed up for about one hour with an anode current of several microamperes. However, in low current operation (average anode current: within one hundred up to several hundred nanoamperes), just applying a voltage to the photomultiplier tube prior to use for a period of one to two hours in the dark state serves as a warm-up to some extent.

**3.3.5 Hysteresis**

When the incident light or the supply voltage is changed in a step function, a photomultiplier tube may not produce an output comparable with the same step function. This phenomenon is known as "hysteresis".<sup>1) 32)</sup> Hysteresis is observed as two behaviors: "overshoot" in which the output current first increases greatly and then settles and "undershoot" in which the output current first decreases and then returns to a steady level. Hysteresis is further classified into "light hysteresis" and "voltage hysteresis" depending on the measurement conditions. Some photomultiplier tubes have been designed to suppress hysteresis by coating the insulator surface of the electrode supports with a conductive material so as to minimize the electrostatic charge on the electrode supports without impairing their insulating properties.

**(1) Light hysteresis**

When a photomultiplier tube is operated at a constant voltage, it may exhibit a temporary variation in the anode output after the incident light is changed in a step function. This variation is called light hysteresis. Figure 3-34 shows the Hamamatsu test method for light hysteresis and typical hysteresis waveforms.

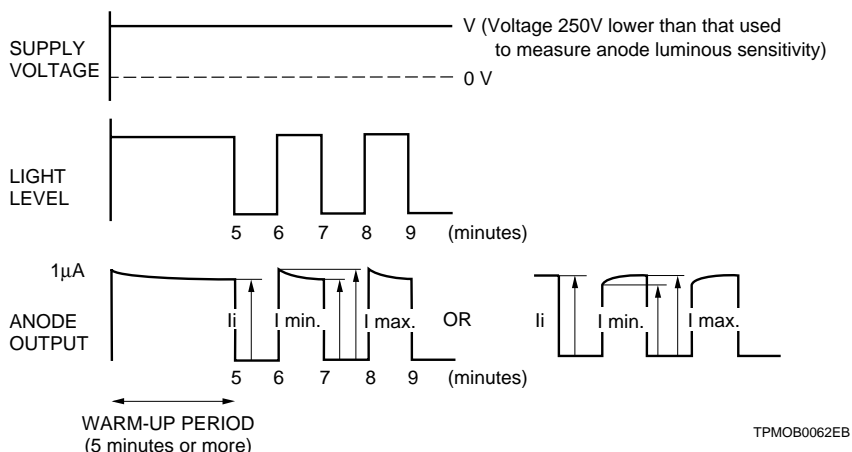


**Figure 3-34: Light hysteresis**

As shown in Figure 3-34, a photomultiplier tube is operated at a voltage  $V$ , which is 250 volts lower than the voltage used to measure the anode luminous sensitivity. The tube is warmed up for five minutes or more at a light level producing an anode current of approximately one microampere. Then the incident light is shut off for one minute and then input again for one minute. This procedure is repeated twice to confirm the reproducibility. By measuring the variations of the anode outputs, the extent of light hysteresis can be expressed in percent, as follows:

$$\text{Light hysteresis } H_L = ((I_{MAX} - I_{MIN}) / I_i) \times 100(\%) \quad \text{..... (Eq. 3-17)}$$

where  $I_{MAX}$  is the maximum output value,  $I_{MIN}$  is the minimum output value and  $I_i$  is the initial output value.

Table 3-5 shows typical hysteresis data for major Hamamatsu photomultiplier tubes. Since most photomultiplier tubes have been designed to minimize hysteresis, they usually only display a slight hysteresis within  $\pm 2$  percent. It should be noted that light hysteresis behaves in different patterns or values, depending on the magnitude of the output current.

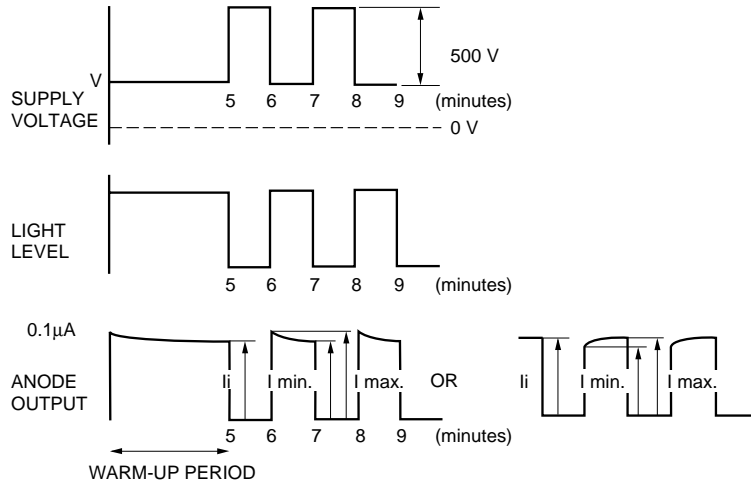
## (2) Voltage hysteresis

When the incident light level cycles in a step function, the photomultiplier tube is sometimes operated with a feedback circuit that changes the supply voltage in a complimentary step function so that the photomultiplier tube output is kept constant. In this case, the photomultiplier tube output may overshoot or undershoot immediately after the supply voltage is changed. This phenomenon is called voltage hysteresis and should be suppressed to the minimum possible value. Generally, this voltage hysteresis is larger than light hysteresis and even tubes with small light hysteresis may possibly exhibit large voltage hysteresis. Refer to Table 3-5 below for typical hysteresis data.

| PMT   | Light Hysteresis $H_L$ (%) | Voltage Hysteresis $H_v$ (%) | Tube Diameter (mm) |
|-------|----------------------------|------------------------------|--------------------|
| R6350 | 0.3                        | 0.5                          | 13mm side-on       |
| R212  | 0.2                        | 1.0                          | 28mm side-on       |
| R928  | 0.1                        | 1.0                          | 28mm side-on       |
| R647  | 0.9                        | 2.5                          | 13mm head-on       |
| R6249 | 0.4                        | 2.0                          | 28mm head-on       |
| R1306 | 0.07                       | 0.06                         | 52mm head-on       |

**Table 3-5: Typical hysteresis data for major Hamamatsu photomultiplier tubes**

Figure 3-35 shows a procedure for measuring voltage hysteresis, commonly used by Hamamatsu Photonics. A photomultiplier tube is operated at a voltage  $V$ , which is 700 volts lower than the voltage used to measure the anode luminous sensitivity. The tube is warmed up for five minutes or more at a light level producing an anode current of approximately 0.1 microampere.



TPMOB0063EA

**Figure 3-35: Voltage hysteresis**

Then the incident light is shut off for one minute while the supply voltage is increased in 500 volt step. Then the light level and supply voltage are returned to the original conditions. This procedure is repeated to confirm the reproducibility. By measuring the variations in the anode outputs, the extent of voltage hysteresis is expressed in percent, as follows:

$$\text{Voltage hysteresis } H_V = ((I_{MAX} - I_{MIN}) / I_i) \times 100(\%) \dots\dots\dots (\text{Eq. 3-18})$$

where  $I_{MAX}$  is the maximum output value,  $I_{MIN}$  is the minimum output value and  $I_i$  is the initial output value.

In general, the higher the change in the supply voltage, the larger the voltage hysteresis will be. Other characteristics are the same as those for light hysteresis.

**(3) Reducing the hysteresis**

When a signal light is blocked for a long period of time, applying a dummy light to the photomultiplier tube to minimize the change in the anode output current is effective in reducing the possible light hysteresis. Voltage hysteresis may be improved by use of HA coating. (Refer to Section 8.8.2.)

### 3.3.6 Dark current

A small amount of current flows in a photomultiplier tube even when operated in a completely dark state. This output current is called the dark current<sup>1) 23) 25) 33)</sup> and ideally it should be kept as small as possible because photomultiplier tubes are used for handling minute amounts of light and current.

#### (1) Causes of dark current

Dark current may be categorized by cause as follows:

- (a) Thermionic emission current from the photocathode and dynodes
- (b) Leakage current (ohmic leakage) between the anode and other electrodes inside the tube and/or between the anode pin and other pins on the bulb stem
- (c) Photocurrent produced by scintillation from glass envelope or electrode supports
- (d) Field emission current
- (e) Ionization current from residual gases (ion feedback)
- (f) Noise current caused by cosmic rays, radiation from radioisotopes contained in the glass envelopes and environmental gamma rays

Dark current increases with an increasing supply voltage, but the rate of increase is not constant. Figure 3-36 shows a typical dark current vs. supply voltage characteristic.

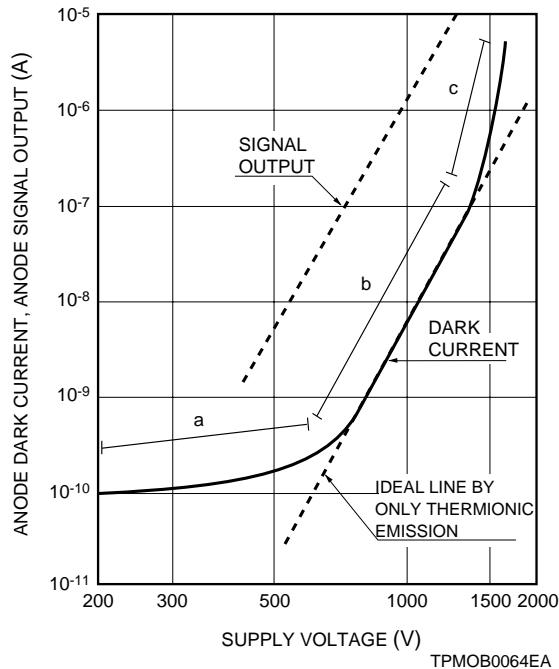


**Figure 3-36: Typical dark current vs. supply voltage characteristic**

This characteristic is related to three regions of the supply voltage: a low voltage region (a in Figure 3-36), a medium voltage region (b in Figure 3-36), and a high voltage region (c in Figure 3-36). Each region is largely controlled by the leakage current, thermionic emission, glass scintillation, field emission and glass or electrode support scintillation, respectively. In general, region b provides the best signal-to-noise ratio, so operating the photomultiplier tube in this region would prove ideal.

Ion feedback<sup>34)</sup> and noise<sup>34) 35) 36)</sup> originating from cosmic rays and radioisotopes will sometimes be a problem in pulse operation.

Furthermore, when a photocathode is exposed to room illumination, the dark current will return to the original level by storing the tube in a dark state for one to two hours. However, if exposed to sunlight or extremely intense light (10000 lux or higher), the tube may be damaged to some extent and not recoverable. This should therefore be avoided. It is recommended that the photomultiplier tube be stored in a dark state before use.

The dark current data furnished with Hamamatsu photomultiplier tubes is measured after the tube has been stored in a dark state for 30 minutes. This "30-minute storage in a dark state" condition allows most photomultiplier tubes to approach the average dark current level attained after being stored for a long period in a dark state. This is also selected in consideration of work efficiency in measuring the dark current. If the tube is stored for a greater length of time in a dark state, the dark current will decrease further. The following sections explain each of the six causes of dark current listed above.

#### a) Thermionic emission

Since the photocathode and dynode surfaces are composed of materials with a very low work function, they emit thermionic electrons even at room temperatures. This effect has been studied by W. Richardson, and is stated by the following equation.<sup>3) 37)</sup>

$$i_s = AT^{5/4} e^{(-e\psi/KT)} \dots\dots\dots \text{(Eq. 3-19)}$$

where,

|                        |                          |
|------------------------|--------------------------|
| $\psi$ : work function | T : absolute temperature |
| e : electron charge    | A : constant             |
| K : Boltzmann constant |                          |

It can be seen from this equation that the thermionic emission is a function of the photocathode work function and absolute temperature. Thus the magnitude of the work function and the photocathode material govern the amount of thermionic emission. When the photocathode work function is low, the spectral response extends to the right with lower energy or longer wavelengths, but with an increase in the thermionic emission. In general, the Ag-O-Cs photocathode with a spectral response in the longest wavelength range (See Figure 3-1.) exhibits the highest dark current. In contrast, the photocathodes for the ultraviolet range (Cs-Te, Cs-I) with the shortest wavelength limit provide the lowest dark current.

Eq. 3-19 also implies that the dark current decreases with decreasing temperature. Therefore, as shown in Figure 3-37, cooling a photomultiplier tube is an effective technique for reducing the dark current. The dark current resulting from the thermionic emission can be considerably reduced by cooling.

However, when the dark current reduces down to a level where the leakage current predominates, this effect becomes limited. Although thermionic emission occurs both from the photocathode and dynodes, the thermionic emission from the photocathode has a much larger effect on the dark current. This is because the photocathode is larger in size than each dynode and also because the dynodes, especially at the latter stages, contribute less to the output current. Consequently, the dark current caused by the thermionic emission vs. the supply voltage characteristic will be nearly identical with the slope of gain vs. supply voltage.

Figure 3-38 describes temperature characteristics for dark pulses measured in the photon counting method. In this case as well, the number of dark pulses decrease by cooling the photocathode.

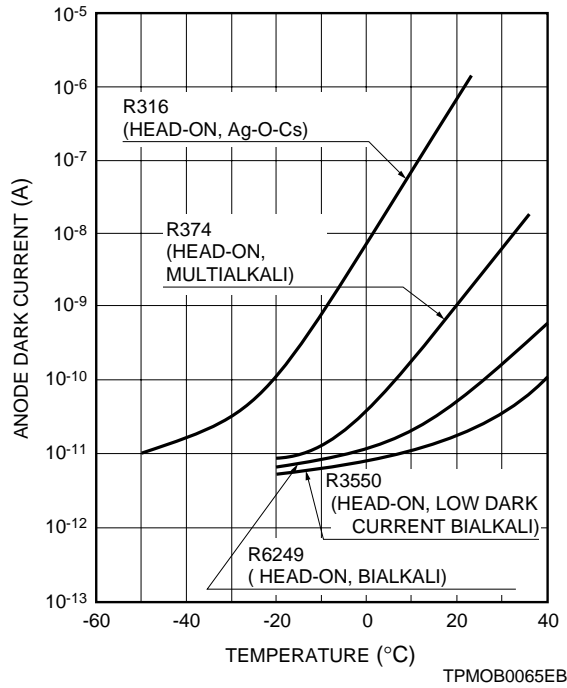


Figure 3-37: Temperature characteristics of anode dark current

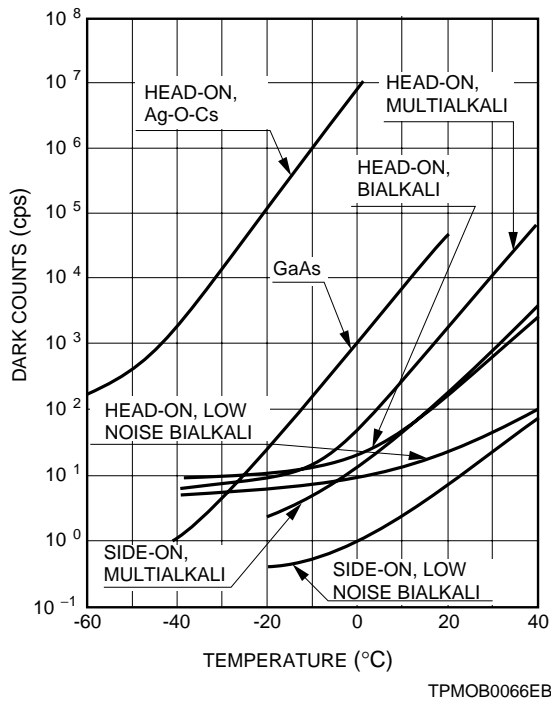


Figure 3-38: Temperature characteristics for dark current pulse

**b) Leakage current (ohmic leakage)**

Photomultiplier tubes are operated at high voltages from 500 up to 3000 volts, but they handle very low currents from several nanoamperes to less than 100 microamperes. Therefore, the quality of the insulating materials used in the tubes is very important. For instance, if the insulation resistance is around  $10^{12}$  ohms, the leakage current may reach the nanoampere level. The relationship between the leakage current from the insulating materials and the supply voltage is determined by Ohm's law, i.e., current value (I) = supply voltage (V)/insulation resistance (R), regardless of the gain of the photomultiplier tube as seen in Figure 3-36. On the other hand, the dark current resulting from thermionic emission varies exponentially with the supply voltage. Thus, as mentioned in the previous section, the leakage current has relatively more effect on the dark current as the supply voltage is lowered.

A leakage current may be generated between the anode and the last dynode inside a tube. It may also be caused by imperfect insulation of the glass stem and base, and between the socket anode pin and other pins. Since contamination from dirt and moisture on the surface of the glass stem, base, or socket increases the leakage current, care should be taken to keep these parts clean and at low humidity. If contaminated, they can be cleaned with alcohol in most cases. This is effective in reducing the leakage current.

**c) Scintillation from the glass envelope or electrode support materials**

Some electrons emitted from the photocathode or dynodes may deviate from their normal trajectories and do not contribute to the output signal. If these stray electrons impinge on the glass envelope, scintillations may occur slightly and result in dark pulses. In general, a photomultiplier tube is operated with a negative high voltage applied to the photocathode and is housed in a metal case at ground potential. This arrangement tends to cause stray electrons to impinge on the glass envelope. However, this problem can be minimized by a technique called "HA coating". Refer to Section 8.8.2 for further details on HA coating.

**d) Field emission**

If a photomultiplier tube is operated at an excessive voltage, electrons may be emitted from the electrodes by the strong electric field. Subsequently the dark current increases abruptly. This phenomenon occurs in region c in Figure 3-36 and shortens the life of the photomultiplier tube considerably. Therefore, the maximum supply voltage is specified for each tube type and must be observed. As long as a photomultiplier tube is operated within this maximum rating there will be no problem. But for safety, it is recommended that the tube be operated at a voltage 20 to 30 percent lower than the maximum rating.

**e) Ionization current of residual gases (ion feedback)**

The interior of a photomultiplier tube is kept at a vacuum as high as  $10^{-6}$  to  $10^{-5}$  pascals (about  $10^{-7}$  Torrs). Even so, there exist residual gases that cannot be ignored. The molecules of these residual gases may be ionized by collisions with electrons. The positive ions that strike the front stage dynodes or the photocathode produce many secondary electrons, resulting in a large noise pulse. During high current operation, this noise pulse is usually identified as an output pulse appearing slightly after the main photocurrent. This noise pulse is therefore called an afterpulse<sup>38) 39) 40)</sup> and may cause a measurement error in pulsed operation.

**f) Noise current caused by cosmic rays, radiation from radioisotopes contained in the glass envelopes and environmental gamma rays**

Many types of cosmic rays are always falling on the earth. Among them, muons ( $\mu$ ) can be a major source of photomultiplier tube noise. When muons pass through the glass envelope, Cherenkov radiation may occur, releasing a large number of photons. In addition, most glasses contain potassium

oxide ( $K_2O$ ) which also contains a minute amount of the radioactive element  $^{40}K$ .  $^{40}K$  may emit beta rays and result in noise. Furthermore, environmental gamma rays emitted from radioisotopes contained in buildings may be another noise source. However, because these dark noises occur much less frequently, they are negligible except for such cases as liquid scintillation counting where the number of signal counts is exceptionally small.

## (2) Expression of dark current

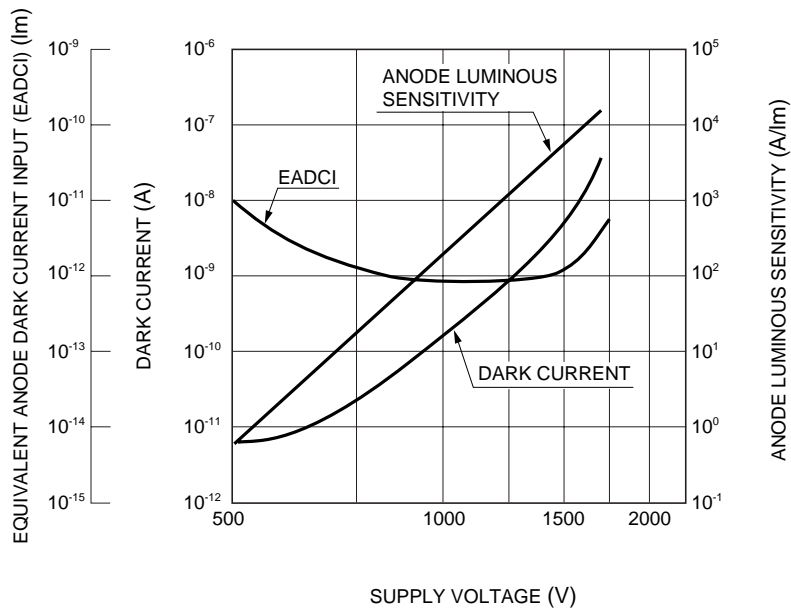
Dark current is a critical factor that governs the lower detection limit in low light level measurements. There are various methods or terms used to express the dark current. The following introduces some of them.

### a) DC expression

In general, Hamamatsu photomultiplier tubes are supplied with the dark current data measured at a constant voltage. The dark current may be measured at a voltage that produces a certain anode sensitivity. In this case, the dark current is expressed in terms of equivalent dark current or EADCI (equivalent anode dark current input). The equivalent dark current is simply the dark current measured at the voltage producing a specific anode luminous sensitivity, and is a convenient parameter when the tube is operated with the anode sensitivity maintained at a constant value. The EADCI is the value of the incident light flux required to produce an anode current equal to the dark current and is represented in units of lumens or watts as follows:

$$\text{EADCI (lm)} = \text{Dark current (A)} / \text{Anode luminous sensitivity (A/lm)} \dots\dots (\text{Eq. 3-20})$$

When representing the EADCI in watts (W), a specified wavelength is selected and the dark current is divided by the anode radiant sensitivity (A/W) at that wavelength. Figure 3-39 illustrates an example of EADCI data along with the anode dark current and anode luminous sensitivity. A better signal-to-noise ratio can be obtained when the tube is operated in the supply voltage region with a small EADCI. It is obvious from this figure that the supply voltage region in the vicinity of 1000 volts displays a small, flat EADCI curve, yet offers an adequate anode sensitivity of three orders of magnitude.



TPMOB0040EA

Figure 3-39: Example of EADCI

**b) AC expression**

In low-level-light measurements, the DC components of dark current can be subtracted. The lower limit of light detection is determined rather by the fluctuating components or noise. In this case, the noise is commonly expressed in terms of ENI (equivalent noise input). The ENI is the value of incident light flux required to produce an output current equal to the noise current, i.e., the incident light level that provides a signal-to-noise ratio of unity. When the ENI is expressed in units of watts (W) at the peak wavelength or at a specific wavelength, it is also referred to as the NEP (noise equivalent power).

Because the noise is proportional to the square root of the circuit bandwidth, the ENI<sup>23)</sup> is defined as follows:

$$\text{ENI} = (2e \cdot I_d \cdot \mu \cdot B)^{1/2} / S \quad (\text{Eq. 3-21})$$

where

- e: electron charge ( $1.6 \times 10^{-19}$  coulombs)
- $I_d$ : anode dark current (A)
- $\mu$ : current amplification
- B: circuit bandwidth (Hz)
- S: anode radiant sensitivity (A/W)

Commonly,  $\Delta f = 1 \text{ Hz}$  is used and the ENI value ranges from  $10^{-15}$  to  $10^{-16}$  (W) at the peak wavelength.

The ENI is a parameter to be considered when the frequency band width B of the circuit is low (up to several thousand hertz). However, it is not so important in a high frequency band because the noise originating from the signal light becomes predominant. (See 3.4, "Photon counting".)

### 3. 3. 7 Signal-to-noise ratio of photomultiplier tubes

When observing the output waveform of a photomultiplier tube, two types of noise components can be seen: one is present even without light input, and the other is generated by the input of signal light. Normally, these noise components are governed by the dark current caused by the photocathode thermionic emission, and the shot noise resulting from the signal current, respectively. Both of these noise sources are discussed here.

The signal-to-noise ratio referred to in the following description is expressed in r.m.s. (root mean square). When signal and noise waveforms like those shown in Figure 3-40 are observed, they can be analyzed as follows:

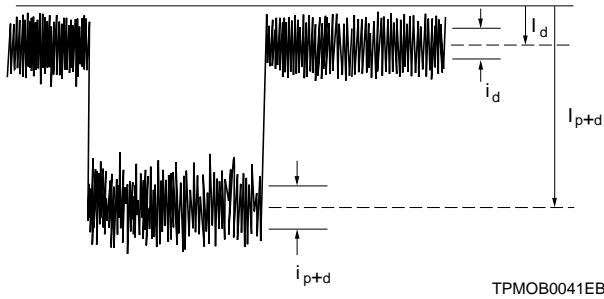


Figure 3-40: Example of signal-to-noise ratio

- Mean value of noise component :  $I_d$
- AC component of noise :  $i_d$  (r.m.s.)
- Mean value of signal (noise component included) :  $I_{p+d}$
- AC component of signal (noise component included) :  $i_{p+d}$  (r.m.s.)

Using these factors, the signal-to-noise ratio<sup>25) 41) 42)</sup> is given by

$$SN \text{ ratio} = I_p / i_{p+d} \dots\dots\dots (Eq. 3-22)$$

where  $I_p$  is the mean value of the signal component only, which is obtained by subtracting  $I_d$  from  $I_{p+d}$ .

If the dark current  $I_d$  is low enough to be ignored ( $I_p \gg I_d$ ), the signal-to-noise ratio will be

$$SN \text{ ratio} \approx I_p / i_p \dots\dots\dots (Eq. 3-23)$$

where  $I_p$  is the mean value of the signal component and  $i_p$  is the AC component (r.m.s.) of the signal.  $i_p$  consists of a component associated with the statistical fluctuation of photons and the photoemission process and a component created in the multiplication process. The noise component produced in the multiplication process is commonly expressed in terms of the NF (noise figure). The NF is defined as follows:

$$NF = (S/N)_{in}^2 / (S/N)_{out}^2 \dots\dots\dots (Eq. 3-24)$$

where  $(S/N)_{in}$  is the signal-to-noise ratio on the photomultiplier tube input side and  $(S/N)_{out}$  is the signal-to-noise ratio on the photomultiplier tube output side. With a photomultiplier tube having  $n$  dynode stages, the NF from the cascade multiplication process is given by the following equation:

$$NF = (1/\alpha) \cdot (1 + 1/\delta_1 + 1/\delta_1\delta_2 + \dots + 1/\delta_1\delta_2 \dots \delta_n) \dots\dots\dots (Eq. 3-25)$$

where  $\alpha$  is the collection efficiency (Refer to 3.2.2.),  $\delta_1, \delta_2 \dots \delta_n$  are the secondary emission ratios at each stage.

With  $\alpha=1$  and  $\delta_1, \delta_2, \delta, \dots, \delta_n=\delta$ , Eq. 3-25 is simplified as follows:

$$NF \approx \delta/(\delta-1) \dots\dots\dots (Eq. 3-26)$$

Thus by adding the NF to the AC component  $i_p$ ,  $i_p$  is expressed by the following equation:

$$i_p = \mu \cdot (2 \cdot e \cdot I_k \cdot B \cdot NF)^{1/2} \dots\dots\dots (Eq. 3-27)$$

where  $\mu$  is the gain,  $e$  is the electron charge,  $I_k$  is the cathode current and  $B$  is the bandwidth of the measurement system. From this equation and Eq. 3-25,  $i_p$  becomes

$$i_p = \mu \cdot \{2 \cdot e \cdot I_k \cdot B \cdot (1/\alpha) \cdot (1+1/\delta_1+1/\delta_1\delta_2+\dots+1/\delta_1\delta_2\dots\delta_n)\}^{1/2} \dots\dots\dots (Eq. 3-28)$$

On the other hand, the average anode current  $I_p$  is expressed in the following equation:

$$I_p = I_k \cdot \alpha \cdot \mu \dots\dots\dots (Eq. 3-29)$$

From Eqs. 3-28 and 3-29, the signal-to-noise ratio becomes

$$\begin{aligned} SN \text{ ratio} &= I_p/i_p \\ &= \left( \frac{I_k \alpha}{2eB} \cdot \frac{1}{1+1/\delta_1+1/\delta_1\delta_2+\dots+1/\delta_1\delta_2\dots\delta_n} \right)^{1/2} \end{aligned}$$

This equation can be simplified using Eq. 3-26, as follows:

$$SN \text{ ratio} \approx \left( \frac{I_k}{2eB} \cdot \frac{1}{\delta/(\delta-1)} \right)^{1/2} \dots\dots\dots (Eq. 3-30)$$

From this relationship, it is clear that the signal-to-noise ratio is proportional to the square root of the cathode current  $I_k$  and is inversely proportional to the square root of the bandwidth  $B$ .

To obtain a better signal-to-noise ratio, the shot noise should be minimized and the following points observed:

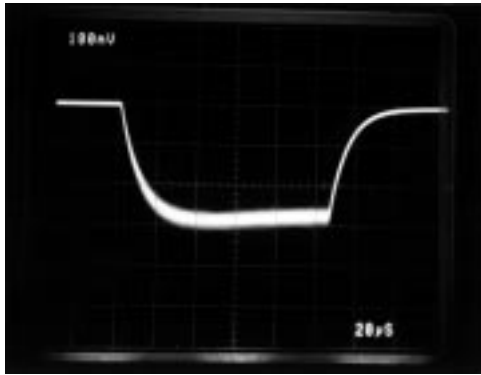
- (1) Use a photomultiplier tube that has as high a quantum efficiency as possible in the wavelength range to be measured.
- (2) Design the optical system for better light collection efficiency so that the incident light is guided to the photomultiplier tube with minimum loss.
- (3) Use a photomultiplier tube that has an optimum configuration for light collection.
- (4) Narrow the bandwidth as much as possible, as long as no problems occurs in the measuring system.

By substituting  $\delta = 6$  into Eq. 3-30, which is the typical secondary emission ratio of a normal photomultiplier tube, the value  $\delta/(\delta-1)$  will be 1.2, a value very close to 1. Consequently, if the noise in the multiplication process is disregarded, the signal-to-noise ratio can be rearranged as follows:

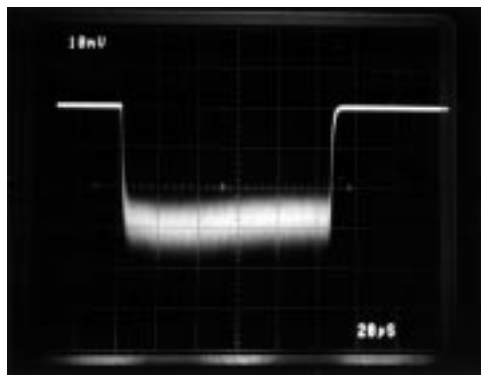
$$SN \text{ ratio} = (I_k/2eB)^{1/2} \approx 1.75 \times 10^3 \sqrt{\frac{I_k(\mu A)}{B(MHz)}} \dots\dots\dots (Eq. 3-31)$$

Figure 3-41 shows the output voltage waveforms obtained while the light level and load resistance are changed under certain conditions. These prove that the relation in Eq. 3-30 is correct.

(a)  $R_l=20k\Omega$



(b)  $R_l=2k\Omega$  (Bandwidth is 10 times wider than (a))



(c) Light level is 10 times higher than (b)

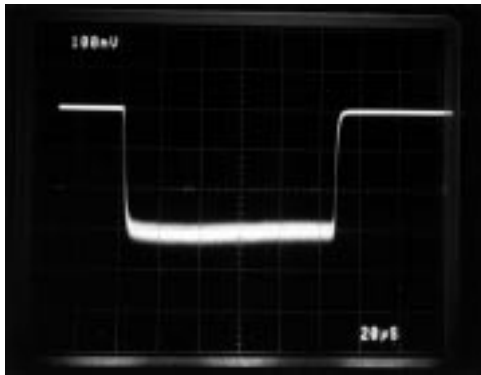


**Figure 3-41: Change in the signal-to-noise ratio for R329 when the light level and load resistance are changed**

In the above relationship however, the dark current is not involved. Taking into account the contribution of the dark current and the noise current of the amplifier circuit, the intrinsic signal-to-noise ratio will be as follows:

$$\text{SN ratio} = \frac{I_k}{(2eB \cdot \delta / (\delta - 1) \cdot (I_k + 2I_d) + N_A^2)^{1/2}} \dots\dots\dots (\text{Eq. 3-32})$$

In cases in which the noise of the amplifier circuit is negligible ( $N_A=0$ ), the signal-to-noise ratio becomes

$$\text{SN ratio} = \frac{I_k}{(2eB \cdot \delta / (\delta - 1) \cdot (I_k + 2I_d))^{1/2}} \dots\dots\dots (\text{Eq. 3-33})$$

where  $I_k = \eta \cdot e \cdot P \cdot \lambda \dots / hc$ , and each symbol stands for the following:

- |                                     |  |
|-------------------------------------|--|
| $I_k$ : cathode current (A)         | $e$ : electron charge (C)              |
| $\lambda$ : wavelength (m)          | $h$ : Planck's constant (J·s)          |
| $c$ : velocity of light (m/s)       | $\eta$ : quantum efficiency            |
| $P$ : power (W)                     | $B$ : bandwidth (Hz)                   |
| $\delta$ : secondary emission ratio | $N_A$ : noise of amplifier circuit (A) |
| $I_d$ : dark current (A)            |  |

### 3.3.8 Afterpulsing

When a photomultiplier tube is operated in a pulse detection mode as in scintillation counting or in laser pulse detection, extraneous pulses with small amplitudes may be observed. Since these pulses appear after the signal output pulse, they are called afterpulses. Afterpulses often disturb accurate measurement of low level signals following a large amplitude pulse, degrades energy resolution in scintillation counting (See "3.5"), or causes errors in pulse counting applications.

#### Types of afterpulses

There are two types of afterpulses: one is output with a very short delay (several nanoseconds to several tens of nanoseconds) after the signal pulse and the other appears with a longer delay ranging up to several microseconds, each being generated by different causes. In general, the latter pulses appearing with a long delay are commonly referred to as afterpulses.

Most afterpulses with a short delay are caused by elastic scattering electrons on the first dynode. The probability that these electrons may be produced can be reduced to about one-tenth in some types of photomultiplier tubes, by providing a special electrode near the first dynode. Usually, the time delay of this type of afterpulse is small and hidden by the time constant of the subsequent signal processing circuit, so that it does not create significant problems in most cases. However, this should be eliminated when measuring very short fluorescence lifetime in time-correlated photon counting.

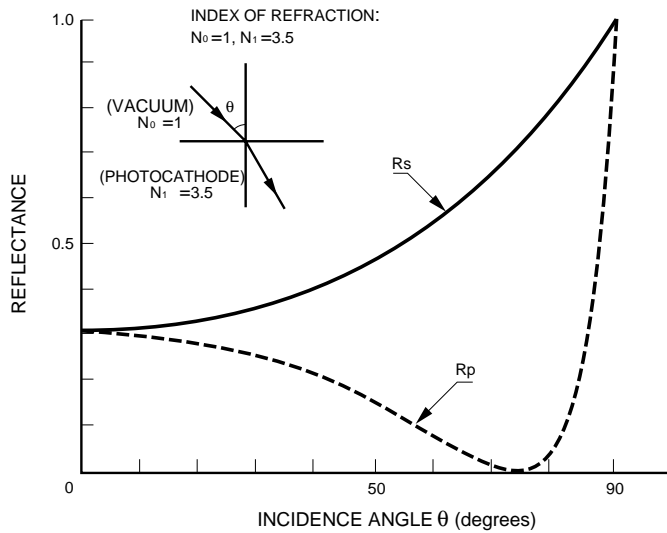
In contrast, afterpulses with a longer delay are caused by the positive ions which are generated by the ionization of residual gases in the photomultiplier tube. These positive ions return to the photocathode (ion feedback) and produce many photoelectrons which result in afterpulses. The amplitude of this type of afterpulse depends on the type of ions and the position where they are generated. The time delay with respect to the signal output pulse varies ranging from several hundred nanoseconds to over a few microseconds, and depends on the supply voltage for the photomultiplier tube. Helium gas is known to produce afterpulses because it easily penetrates through a silica bulb, so use caution on the operating environments. Afterpulses can be reduced temporarily by aging (See 3.3.4, "Stability"), but this is not a permanent measure.

In actual measurements, the frequency of afterpulses and the amount of charge may sometimes be a problem. The amount of output charge tends to increase when the photomultiplier tube is operated at a higher supply voltage to obtain a high gain even though the number of generated ions is the same. In pulse counting applications such as photon counting, the frequency of afterpulses with an amplitude higher than a certain threshold level will only be a problem.

As explained, afterpulses appear just after the signal pulse. Another extraneous pulse may be observed just before the signal pulse output. But, this pulse is very close to the signal pulse and has a low amplitude, causing no problems.

### 3. 3. 9 Polarized-light dependence

Photomultiplier tube sensitivity may be affected by polarized light.<sup>43) 44)</sup> It is therefore necessary to take this characteristic into account when polarized light is to be measured. Also it should be noted that light may be polarized at such optical devices as a monochromator. When polarized light enters the photocathode of a photomultiplier tube, the photocathode reflectance varies with the angle of incidence. This effect is also greatly dependent on the polarization component as shown in Figure 3-42. In this figure,  $R_p$  is the polarization component parallel to the photocathode surface (P component) and  $R_s$  is the polarization component perpendicular to the photocathode surface (S component). It is clear that the photocathode reflectance varies with the angle of incidence. Because this figure shows the calculated examples with the assumption that the absorption coefficient at the photocathode is zero, the actual data will be slightly more complicated.



TPMSB0045EA

Figure 3-42: Angle dependence of reflectance

If the polarization plane of the incident light has an angle  $\theta$  with respect to the perpendicular of the photocathode surface, the photocurrent  $I_\theta$  is given by the following expression:

$$I_\theta = I_s \cos^2 \theta + I_p \sin^2 \theta = \frac{1}{2} (I_p + I_s) \left( 1 - \frac{I_p - I_s}{I_p + I_s} \cdot \cos^2 \theta \right) \dots \dots \dots \text{(Eq. 3-34)}$$

where

- $I_s$ : Photocurrent produced by polarized component perpendicular to the photocathode
- $I_p$ : Photocurrent produced by polarized component parallel to the photocathode

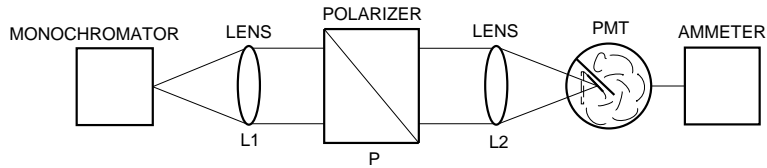
while

$$I_0 = \frac{I_p + I_s}{2}, P = \frac{I_p - I_s}{I_p + I_s} \dots \dots \dots \text{(Eq. 3-35)}$$

then substituting Eq. 3-35 into Eq. 3-34 gives the following relationship

$$\theta = I_0 (1 - P \cdot \cos^2 \theta) \dots \dots \dots \text{(Eq. 3-36)}$$

$P$  is called the polarization factor and indicates the polarized-light dependence of a photomultiplier tube, and is measured using the optical system like that shown in Figure 3-43.



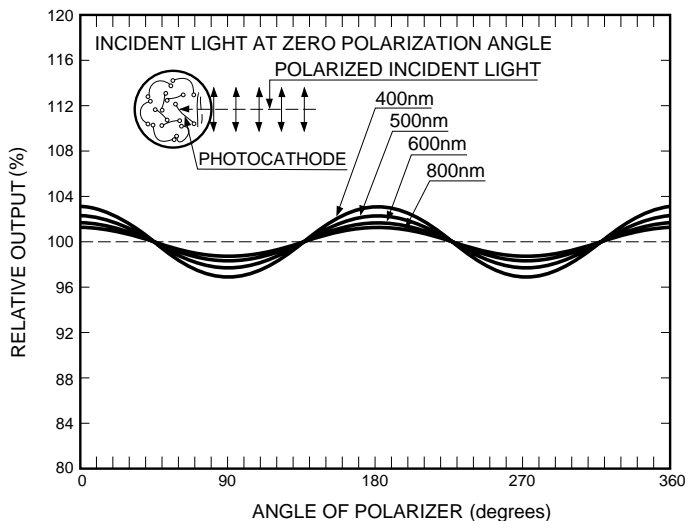
TPMOC0047EA

**Figure 3-43: Optical system used for measuring polarized-light dependence**

In the above measurement, monochromatic light from the monochromator is collimated by  $L_1$  (collimator lens) and is linearly polarized by the polarizer (P). The polarized light is then focused onto the photomultiplier tube through  $L_2$  (condenser lens). The dependence on the polarized light is measured by recording the photomultiplier tube output in accordance with the rotating angle of the polarizer.

In this case, it is necessary to remove the polarization component of the light source. This is done by interposing a diffuser plate such as frosted glass or by compensating for the photomultiplier tube output values measured when the tube is at 0 degree and is then rotated to 90 degrees with respect to the light axis.

Figure 3-44 illustrates the polarized-light dependence of a side-on photomultiplier tube with a reflection type photocathode. In principle, this dependence exists when the light enters slantways with respect to the photocathode surface. In actual operation, the polarization factor P is almost zero when the light enters perpendicular to the photocathode surface.



TPMSB0046EA

**Figure 3-44: Typical polarization-light dependence of a side-on photomultiplier tube**

In the case of reflection-type photocathode photomultiplier tubes, because the photocathode is arranged at a certain angle with respect to the input window, the sensitivity is affected by polarized light. Figure 3-45 indicates the relative output of a reflection-type photocathode photomultiplier tube as a function of the angle of incident light. It can be seen that the polarization factor P becomes smaller as the direction of the incident light nears the perpendicular of the photocathode surface.

The reflection-type photocathode photomultiplier tubes usually exhibit a polarization factor of about 10 percent or less, but tubes specially designed to minimize the polarization-light dependence offer three percent or less. A single crystal photocathode such as gallium arsenide (GaAs) has high reflectance and show a polarization factor of around 20 percent, which is higher than that of alkali antimonide photocathodes.

The polarization that provides the maximum sensitivity is the component perpendicular to the tube axis (P component). In contrast, the polarization that gives the minimum sensitivity is the component parallel to the tube axis (S component), independent of the type of tube and wavelength of incident light. As can be seen from Figure 3-42, this is probably due to a change in the photocathode transmittance. The S component increases in reflectance as the angle of incidence becomes larger, whereas the P component decreases. Moreover, as the wavelength shifts to the longer side, the reflectance generally decreases and the polarization factor P becomes smaller accordingly, as shown in Figure 3-44.

In applications where the polarized-light dependence of a photomultiplier tube cannot be ignored, it will prove effective to place a diffuser such as frosted glass or tracing paper in front of the input window of the photomultiplier tube or to use a photomultiplier tube with a frosted window.

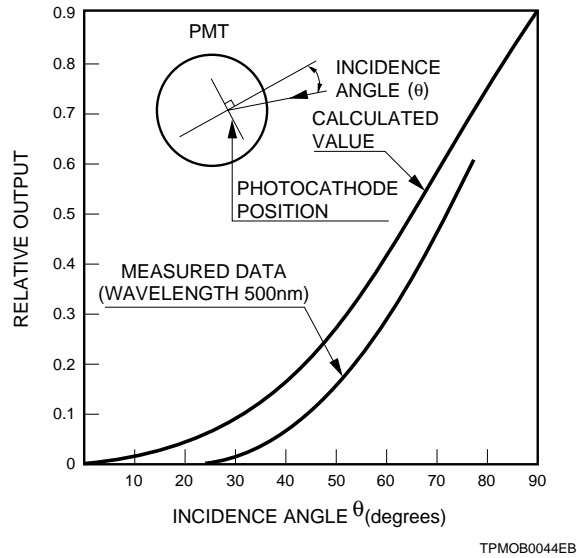


Figure 3-45: Relative output vs. incident angle of polarized light

## 3.4 Photon Counting<sup>25) 41) 45)-52)</sup>

Photon counting is an effective technique used to detect very-low-level-light such as Raman spectroscopy, fluorescence analysis, and chemical or biological luminescence analysis where the absolute magnitude of the light is extremely low. This section describes the principles of photon counting, its operating methods, detection capabilities, and advantages as well as typical characteristics of photomultiplier tubes designed for photon counting.

### 3.4.1 Analog and digital (photon counting) modes

The methods of processing the output signal of a photomultiplier tube can be divided broadly into analog and digital modes, depending on the incident light intensity and the bandwidth of the output processing circuit.

As Figure 3-46 shows, when light strikes the photocathode of a photomultiplier tube, photoelectrons are emitted. These photoelectrons are multiplied by the cascade process of secondary emission through the dynodes (normally  $10^6$  to  $10^7$  times) and finally reach the anode connecting with an output processing circuit.

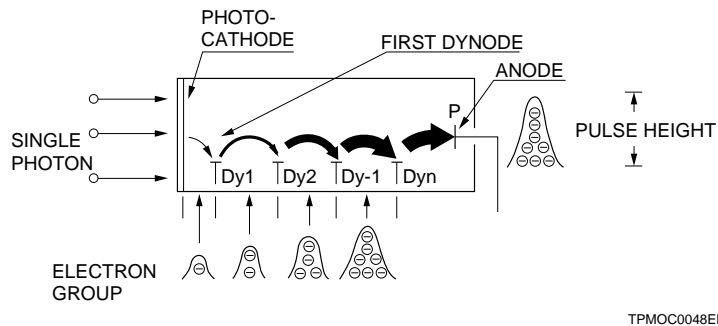


**Figure 3-46: Photomultiplier tube operation in the photon counting mode**

When observing the output signal of a photomultiplier tube with an oscilloscope while varying the incident light level, output pulses like those shown in Figure 3-47 are seen. At higher light levels, the output pulse intervals are narrow so that they overlap each other, producing an analog waveform (similar to (a) and (b) of Figure 3-47). If the light level becomes very low, the ratio of AC component (fluctuation) in the signal increases, and finally the output signal will be discrete pulses (like (c) of Figure 3-47). By discriminating these discrete pulses at a proper binary level, the number of the signal pulses can be counted in a digital mode. This is commonly known as photon counting.

In analog mode measurements, the output signal is the mean value of the signals including the AC components shown in Figure 3-47 (a). In contrast, the photon counting method can detect each pulse shown in Figure 3-47 (c), thus the number of counted pulses equals the signal. This photon counting mode uses a pulse height discriminator that separates the signal pulses from the noise pulses, enabling high-precision measurement with a higher signal-to-noise ratio in comparison with the analog mode. Therefore photon counting is exceptionally effective in detecting low level light.

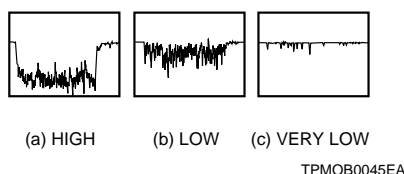


**Figure 3-47: photomultiplier tube output waveforms observed at different light levels**

### 3. 4. 2 Principle of photon counting

When light incident on a photomultiplier tube becomes very low and reaches a state in which no more than two photoelectrons are emitted within the time resolution (pulse width) of the photomultiplier tube, this light level is called the single photoelectron region and photon counting is performed in this region. Quantum efficiency, an important parameter for photon counting, signifies the probability of photoelectron emission when a single photon strikes the photocathode.

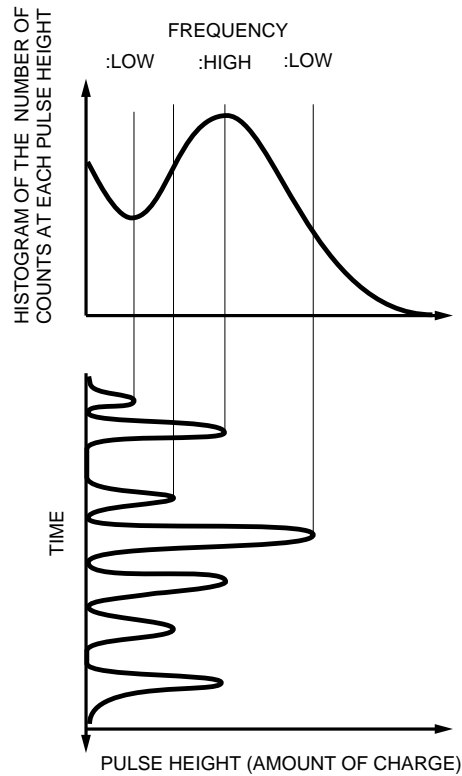
In this single photoelectron region, the number of emitted electrons per photon is one or zero and the quantum efficiency can be viewed as the ratio of the number of photoelectrons emitted from the photocathode to the number of incident photons per unit time. The probability that the photoelectrons emitted from the photocathode (primary electrons) will impinge on the first dynode and contribute to gain is referred to as collection efficiency. Some photoelectrons may not contribute to gain because they deviate from the normal trajectories and are not collected by the first dynode. Additionally, in the photon counting mode, the ratio of the number of counted pulses (output pulses) to the number of incident photons is called detection efficiency or photomultiplier tube counting efficiency and is expressed by the following relation:

$$\text{Detection efficiency (counting efficiency) in the photon counting region} = (N_d/N_p) = \eta \times \alpha \quad \dots \text{(Eq. 3-37)}$$

where  $N_d$  is the counted value,  $N_p$  is the number of incident photons,  $\eta$  is the quantum efficiency of the photocathode and  $\alpha$  is the collection efficiency of the dynodes. The detection efficiency greatly depends on the threshold level used for binary processing.

The number of secondary electrons released from the first dynode is not constant. It is around several secondary electrons per primary electron, with a broad probability seen as a Poisson distribution. Therefore the average number of electrons per primary electron  $\delta$  corresponds to the secondary-electron multiplication factor of the dynode. Similarly, this process is repeated through the second and subsequent dynodes until the final electron bunch reaches the anode. In this way the output multiplied in accordance with the number of photoelectrons from the photocathode appears at the anode. If the photomultiplier tube has  $n$  stage dynodes, the photoelectrons emitted from the photocathode are multiplied in cascade up to  $\delta^n$  times and derived as an adequate electron bunch from the anode. In this process, each output pulse obtained at the anode exhibits a certain distribution in pulse height because of fluctuations in the secondary multiplication factor at each dynode (statistical fluctuation due to cascade multiplication), non-uniformity of multiplication depending on the dynode position and electrons deviating from their favorable trajectories. Figure 3-48 illustrates a histogram of photomultiplier tube output pulses. The abscissa indicates the pulse height and the anode output pulses are integrated with time. This graph is known as the pulse height distribution.

Figure 3-48 also shows the relation between the pulse height distribution and the actual output pulses obtained with a photomultiplier tube. The pulse height distribu-



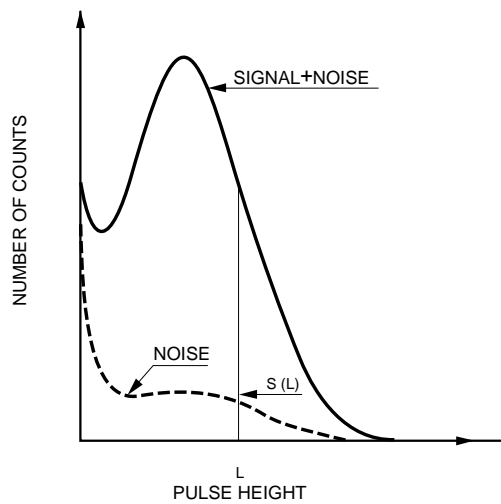
TPMOC0049EB

**Figure 3-48 : Photomultiplier tube output and its pulse height distribution**

tion is usually taken with a multichannel analyzer (MCA) frequently used in scintillation counting applications.

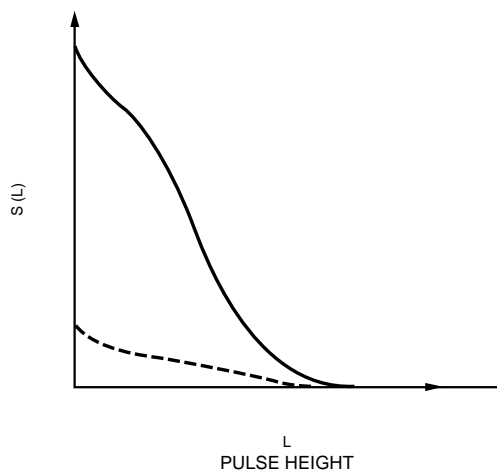
Figure 3-49 (a) shows examples of the pulse height distribution obtained with a photomultiplier tube. The output pulses are present even if no light falls on the photomultiplier tube. (These are called dark current pulses or noise pulses.) The broken line indicates the distribution of the dark current pulses, with a tendency to build up somewhat in the lower pulse height region (left side). These dark pulses mainly originate from the thermal electron emission at the photocathode and also at the dynodes. The thermal electrons from the dynodes are multiplied less than those from the photocathode and are therefore distributed in the lower pulse height region.

Figure 3-49 (b) indicates the distribution of the total number of counted pulses  $S(L)$  with amplitudes greater than a threshold level  $L$  shown in (a). (a) and (b) have differential and integral relations to each other. Item (b) is a typical integral curve taken with a photon counting system using a photomultiplier tube.



(a) DIFFERENTIAL SPECTRUM

TPMOB0046EA-1



(b) INTEGRAL SPECTRUM

TPMOB0046EA-2

**Figure 3-49: Differential and integral representations of pulse height distribution**

### 3. 4. 3 Operating method and characteristics for photon counting

This section discusses specific circuit configurations used to perform photon counting and the basic characteristics involved in photon counting.

#### (1) Circuit configuration

Figure 3-50 shows a typical circuit configuration for photon counting and a pulse waveform obtained at each circuit.

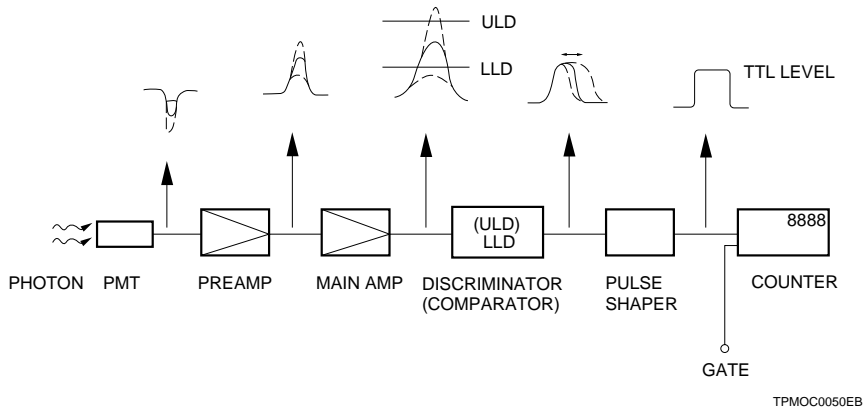


**Figure 3-50: Circuit configuration for photon counting**

In the above system, current output pulses from a photomultiplier tube are converted to a voltage by a wide-band preamplifier and amplified. These voltage pulse are fed to a discriminator and then to a pulse shaper. Finally the number of pulses is counted by a counter. The discriminator usually employs a comparator IC that compares the input voltage pulses with the preset reference voltage (threshold level) and eliminates those pulses with amplitudes lower than this value. In general, the LLD (lower level discrimination) level is set at the lower pulse height side. The ULD (upper level discrimination) level may also be often set at the higher pulse height side to eliminate noise pulses with higher amplitudes. The counter is usually equipped with a gate circuit, allowing measurement at different timings and intervals.

#### (2) Basic characteristics in photon counting

##### a) Pulse height distribution and plateau characteristics

If a multichannel pulse height analyzer is available, a proper threshold level can be set in the pulse height distribution. Because the dark current pulses are usually distributed in the lower pulse height region, setting the LLD level in the vicinity of the valley ( $L_1$ ) of the distribution can effectively eliminate such noise pulses without sacrificing the detection efficiency. In actual operation, however, using a pulse height analyzer is not so popular. Other methods using plateau characteristics are more commonly employed instead. By counting the total number of pulses with amplitudes higher than the preset threshold level while varying the supply voltage for the photomultiplier tube, plots similar to those shown in Figure 3-52 can be obtained. These plots are called the plateau characteristics. The pulse height obtained at the supply voltage giving the maximum rising gradient in the signal plateau characteristic corresponds to the  $L_1$  level in Figure 3-51. From this relation, the pulse height for the LLD level can be predicted.

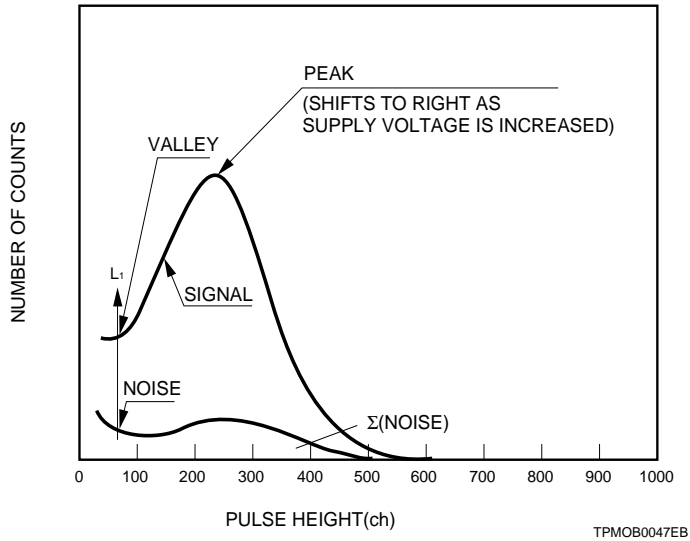


Figure 3-51: Typical example of pulse height distribution

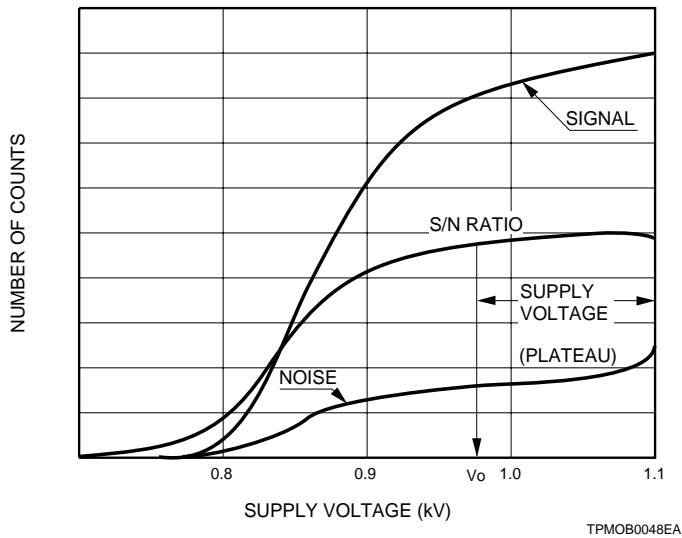


Figure 3-52: Plateau characteristics

### b) Setting the photomultiplier tube supply voltage

The signal-to-noise ratio is an important factor from the viewpoint of accurate measurements. Here the signal-to-noise ratio is defined as the ratio of the mean value of the signal count rate to the fluctuation of the counted signal and noise pulses (expressed in standard deviation or root mean square). The signal-to-noise ratio curve shown in Figure 3-52 is plotted by varying the supply voltage, the same procedure which is used to obtain the plateau characteristics. This figure implies that the photomultiplier tube should be operated in the range between the voltage ( $V_0$ ) at which the plateau region begins and the maximum supply voltage.

**c) Count rate linearity**

The photon counting mode offers excellent linearity over a wide range. The lower limit of the count rate linearity is determined by the number of dark current pulses, and the upper limit by the maximum count rate. The maximum count rate further depends on pulse-pair resolution, which is the minimum time interval at which each pulse can be separated. The reciprocal of this pulse pair resolution would be the maximum count rate. However, since most events in the photon counting region usually occur at random, the counted pulses may possibly overlap. Considering this probability of overlapping, the actual maximum count rate will be about one-tenth of the calculated above. The loss of count rate from pulse overlapping is given by

$$\xi = \frac{n\tau}{1+n\tau} \dots\dots\dots \text{(Eq. 3-38)}$$

where

- n: true count rate(cps)
- τ: pulse pair resolution(s)

Figure 3-53 shows the typical linearity taken using a system with a pulse pair resolution of 8 nanoseconds.

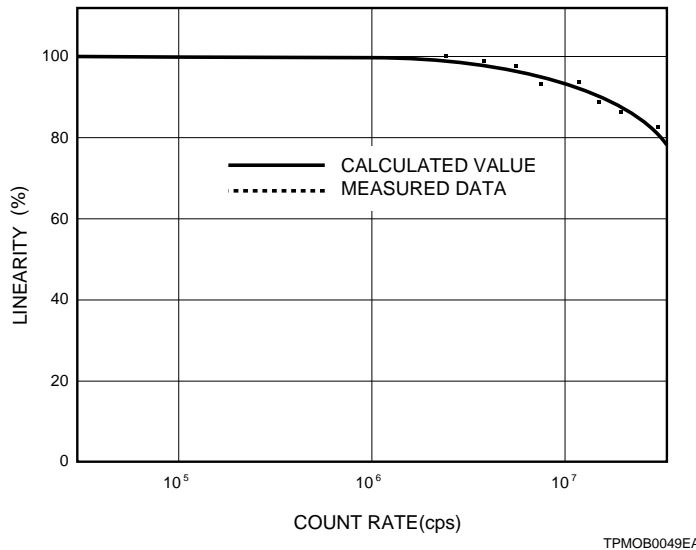


**Figure 3-53: Linearity of count rate**

**d) Setting the threshold level**

In photon counting, it is most important to determine where to set the threshold level. In general, the optimum threshold level may be determined according to the suggestions listed below. But setting threshold is not simple and therefore careful selection must be made in accordance with individual needs.

- (1) To optimize the signal-to-noise ratio and stabilize the count rate with respect to gain variations of the photomultiplier tube, the threshold level should be set near the valley or the plateau region of the pulse height distribution.
- (2) Setting the threshold level at the lowest possible level gives the best detection efficiency. Practically, however, setting it near the valley or the plateau region is recommended.
- (3) To optimize the elimination rate between the signal and noise, the threshold level should be set at the middle of the peak and valley in the pulse height distribution.

### e) Advantages of photon counting

Photon counting has many advantages in comparison with the analog mode. Among them, stability and signal-to-noise ratio are discussed in this section.

#### (I) Stability

One of the significant advantages photon counting offers is operating stability. The photon counting mode is resistant to variations in supply voltage and photomultiplier tube gain. If the supply voltage is set within the plateau region, a change in the voltage has less effect on the output counts. In the analog mode, however, it affects the output current considerably. Immunity to variations in the supply voltage means that the photon counting mode also assures high stability against gain fluctuation of the photomultiplier tube. Normally the photon counting mode offers several times higher immunity to such variations than the analog mode. (Refer to Figure 3-54.)

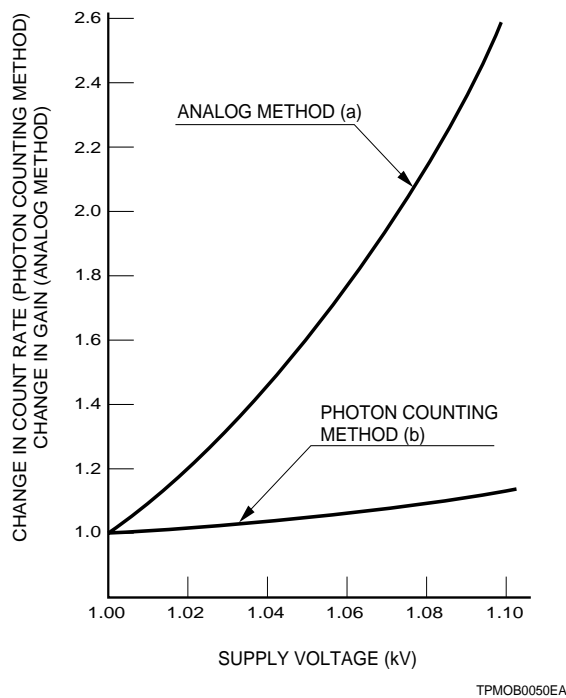


Figure 3-54: Stability versus changes in supply voltage

#### (II) Signal-to-noise ratio

When signal light strikes the photocathode of a photomultiplier tube, photoelectrons are emitted and directed to the dynode section where secondary electrons are produced. The number of photoelectrons produced per unit time and also the number of secondary electrons produced are determined by statistical probability of events which is represented by a Poisson distribution. Thus they are accompanied by statistical fluctuations (AC current components) expressed as a binomial distribution, having an effect on the signal-to-noise ratio. The signal-to-noise ratio is also described in Section 3.3.7. The AC component noise which is superimposed on the signal can be categorized by origin as follows

- (1) Shot noise resulting from signal light
- (2) Shot noise resulting from background light
- (3) Shot Noise resulting from dark current

In the analog mode, the signal-to-noise ratio<sup>41) 42) 45) 46) - 50) 51)</sup> of the photomultiplier tube output including these shot noises becomes

$$\text{SN ratio(current)} = \frac{I_{ph}}{\sqrt{2eNF\{I_{ph}+2(I_b+I_d)\}}} \dots\dots\dots (\text{Eq. 3-39})$$

where

- I<sub>ph</sub>: signal current produced by incident light (A)
- e: electron charge (c)
- F: noise figure of the photomultiplier tube (A)
- I<sub>b</sub>: cathode current resulting from background light (A)
- I<sub>d</sub>: cathode current resulting from dark current (A)
- B: Bandwidth of measurement system (Hz)

Here the true signal current I<sub>ph</sub> is obtained by subtracting I<sub>b</sub>+I<sub>d</sub> from the total current. The noise originating from the latter-stage amplifier is considered to be negligible because the typical gain μ of a photomultiplier tube is sufficiently large.

The signal-to-noise ratio in the photon counting mode is given by the following equation.

$$\text{SN ratio} = \frac{N_s\sqrt{T}}{\sqrt{N_s+2(N_b+N_d)}} \dots\dots\dots (\text{Eq. 3-40})$$

where

- N<sub>s</sub>: number of counts/sec resulting from incident light per second
- N<sub>b</sub>: number of counts/sec resulting from background light per second
- N<sub>d</sub>: number of counts/sec resulting from dark current per second
- T: measurement time(sec)

Here the number of counts/sec of true signals N<sub>s</sub> is obtained by subtracting N<sub>b</sub>+N<sub>d</sub> from the total number of counts.

From the common equivalent relation between the time and frequency, if B=1 (Hz) and T=0.5 (sec), then the signal-to-noise ratio will be as follows:

in the analog mode

$$\text{SN ratio(current)} = \frac{I_{ph}}{\sqrt{2eNF\{I_{ph}+2(I_b+I_d)\}}} \dots\dots\dots (\text{Eq. 3-41})$$

in the photon counting mode

$$\text{SN ratio} = \frac{N_s}{\sqrt{2\{N_s+2(N_b+N_d)\}}} \dots\dots\dots (\text{Eq. 3-42})$$

Through the above analysis, it is understood that the photon counting mode provides a better signal-to-noise ratio by a factor of the noise figure NF. Since the dark current includes thermal electrons emitted from the dynodes in addition to those from the photocathode, its pulse height distribution will be an exponential spectrum shifted toward the lower pulse height side. Therefore, the dark current component can be effectively eliminated by use of a pulse height discriminator while maintaining the signal component, assuring further improvement in the signal-to-noise ratio. In addition, because only AC pulses are counted, the photon counting mode is not influenced by the DC leakage current. Amplifier noises can totally be eliminated by a discriminator.

### 3. 4. 4 Characteristics of photomultiplier tubes for photon counting

Table 3-6 lists typical characteristics<sup>52)</sup> of Hamamatsu photomultiplier tubes currently available for photon counting.

| Wavelength Range   | Diameter/ Configuration inch (mm) | Type No.  | Spectral Response (nm) | Sensitive Area (mm) | Photocathode Quantum Efficiency |                 | Dark Count |            |                  | Rise Time (ns) | Remarks                            |
|--------------------|-----------------------------------|-----------|------------------------|---------------------|---------------------------------|-----------------|------------|------------|------------------|----------------|------------------------------------|
|                    |                                   |           |                        |                     | QE (%)                          | Wavelength (nm) | Typ (cps)  | Max. (cps) | Temperature (°C) |                |                                    |
| VUV to UV          | 28 (1-1/8), side-on               | R7154P    | 160~320                | 8X24                | 35                              | 200             | 5          | 20         | 25               | 2.2            | MgF <sub>2</sub> : R1220P          |
| UV to Visible      | 28 (1-1/8), head-on               | R2707-01  | 160~650                | 5X8                 | 22                              | 390             | 10         | 30         | 25               | 1.7            | Low dark count                     |
|                    | 13 (1/2), side-on                 | R6350P    | 185~680                | 4X13                | 20                              | 270             | 10         | 30         | 25               | 1.4            |                                    |
|                    | 13 (1/2), side-on                 | R6353P    | 185~680                | 4X13                | 23                              | 330             | 10         | 30         | 25               | 1.4            |                                    |
|                    | 28 (1-1/8), side-on               | R1527P    | 185~680                | 8X24                | 19                              | 300             | 10         | 50         | 25               | 2.2            | Low dark count                     |
|                    | 28 (1-1/8), side-on               | R2693P    | 185~650                | 18X16               | 20                              | 300             | 15         | 50         | 25               | 1.2            | Semi-transparent photocathode      |
|                    | 28 (1-1/8), side-on               | R4220P    | 185~710                | 8X24                | 23                              | 320             | 10         | 50         | 25               | 2.2            | High sensitivity<br>Low dark count |
|                    | 15 (3/5), head-on                 | R7400P-06 | 160~650                | 8 dia.              | 20                              | 360             | 80         | 400        | 25               | 0.78           | Metal package type                 |
|                    | 15 (3/5), head-on                 | R7400P-03 | 185~650                | 8 dia.              | 20                              | 360             | 80         | 400        | 25               | 0.78           | Metal package type                 |
| Visible            | 10 (3/8), head-on                 | R1635P    | 300~650                | 8 dia.              | 26                              | 390             | 100        | 400        | 25               | 0.8            |                                    |
|                    | 13 (1/2), head-on                 | R647P     | 300~650                | 10 dia.             | 26                              | 390             | 80         | 400        | 25               | 2.5            |                                    |
|                    | 13 (1/2), head-on                 | R2557     | 300~650                | 10 dia.             | 20                              | 375             | 10         | 30         | 25               | 2.2            | Low dark count                     |
|                    | 19 (3/4), head-on                 | R5610     | 300~650                | 15 dia.             | 20                              | 375             | 15         | 45         | 25               | 1.5            | Low dark count                     |
|                    | 25 (1), head-on                   | R1924P    | 300~650                | 21 dia.             | 26                              | 390             | 100        | 300        | 25               | 2.0            |                                    |
|                    | 25 (1), head-on                   | R3550     | 300~650                | 21 dia.             | 20                              | 375             | 20         | 60         | 25               | 2.0            | Low dark count                     |
|                    | 28 (1-1/8), head-on               | R6249P    | 300~650                | 25 dia.             | 25                              | 390             | 120        | 300        | 25               | 4.0            |                                    |
|                    | 28 (1-1/8), head-on               | R7205-01  | 300~650                | 25 dia.             | 22                              | 390             | 10         | 30         | 25               | 1.7            | Low dark count                     |
|                    | 51 (2), head-on                   | R329P     | 300~650                | 46 dia.             | 26                              | 390             | 200        | 600        | 25               | 2.6            |                                    |
|                    | 15 (3/5), head-on                 | R7400P    | 300~650                | 8 dia.              | 20                              | 360             | 80         | 400        | 25               | 0.78           | Metal package type                 |
| Visible to Near IR | 28 (1-1/8), head-on               | R3206-01  | 300~850                | 10 dia.             | 20.3                            | 340<br>800      | 300        | 1000       | 25               | 1.7            | Low dark count                     |
|                    | 28 (1-1/8), head-on               | R2228P    | 300~900                | 25 dia.             | 8.1.5                           | 600<br>800      | 150        | 500        | -20              | 15.0           |                                    |
|                    | 51 (2), head-on                   | R2257P    | 300~900                | 46 dia.             | 10.2                            | 600<br>800      | 600        | 2000       | 25               | 2.6            |                                    |
|                    | 51 (2), head-on                   | R3310-02  | 300~1010               | 10X10               | 13.0.25                         | 340<br>1000     | 30         | 150        | -20              | 3.0            |                                    |
|                    | 15 (3/5), head-on                 | R7400P-01 | 300~850                | 8 dia.              | 19.0.19                         | 370<br>800      | 500        | 1000       | 25               | 0.78           | Metal package type                 |
| UV to Near IR      | 13 (1/2), head-on                 | R1463P    | 185~850                | 10 dia.             | 22.0.3                          | 270<br>800      | 900        | 1000       | 25               | 2.5            |                                    |
|                    | 28 (1-1/8), head-on               | R1104P    | 185~850                | 25 dia.             | 23.0.3                          | 270<br>800      | 4500       | 7000       | 25               | 15.0           | High gain                          |
|                    | 51 (2), head-on                   | R943-02   | 160~930                | 10X10               | 22.12                           | 300<br>800      | 20         | 50         | -20              | 3.0            |                                    |
|                    | 13 (1/2), side-on                 | R6358P    | 185~850                | 4X13                | 24.13                           | 240<br>600      | 20         | 50         | 25               | 1.4            |                                    |
|                    | 28 (1-1/8), side-on               | R928P     | 185~900                | 8X24                | 25.2.7                          | 260<br>800      | 500        | 1000       | 25               | 2.2            |                                    |
|                    | 28 (1-1/8), side-on               | R2949     | 185~900                | 8X6                 | 25.2.7                          | 260<br>800      | 300        | 500        | 25<br>-20        | 2.2            | UV to near IR<br>Low dark count    |
|                    | 28 (1-1/8), side-on               | R2658P    | 185~1010               | 3X12                | 14.0.13                         | 330<br>1000     | 50         | 300        | -20              | 2.0            | InGaAs photo-cathode               |
|                    | 28 (1-1/8), side-on               | R4632     | 185~850                | 8X24                | 26.11                           | 270<br>600      | 50         | 100        | 25               | 2.2            | Low dark count in near IR          |
|                    | 15 (3/5), head-on                 | R7400P-04 | 185~850                | 8 dia.              | 20.0.19                         | 280<br>300      | 500        | 1000       | 25               | 0.78           | Metal package type                 |

Table 3-6: Typical characteristics of photomultiplier tubes for photon counting

### 3.5 Scintillation Counting

Radiation of various types is widely utilized for non-destructive inspection and testing such as in medical diagnosis, industrial inspection, material analysis and other diverse fields. In such applications, radiation detectors play an important role. There are various methods for detecting radiation.<sup>34) 53) 54)</sup> For example, typical detectors include proportional counters, semiconductor detectors that make use of gas and solid ionization respectively, radiation-sensitive films, cloud chambers, and scintillation counters.

In scintillation counting, the combination of a scintillator and photomultiplier tube is one of the most commonly used detectors for practical applications.<sup>55) 56)</sup> Scintillation counting has many advantages over other detection methods, for example, a wide choice of scintillator materials, fast time response, high detection efficiency, and a large detection area. This section gives definitions of photomultiplier tube characteristics required for scintillation counting and explains their measurement methods and typical data.

#### 3.5.1 Scintillators and photomultiplier tubes<sup>28)</sup>

When ionizing radiation enters a scintillator, it produces a fluorescent flash with a short decay time. This is known as scintillation. In the case of gamma rays, this scintillation occurs as a result of excitation of the bound electrons by means of free electrons inside the scintillator. These free electrons are generated by the following three mutual interactions: the photoelectric effect, Compton effect, and pair production. The probability of occurrence of these interactions depends on the type of scintillators and the energy level of the gamma rays. Figure 3-55 shows the extent of these interactions when gamma-ray energy is absorbed by a NaI(Tl) scintillator.

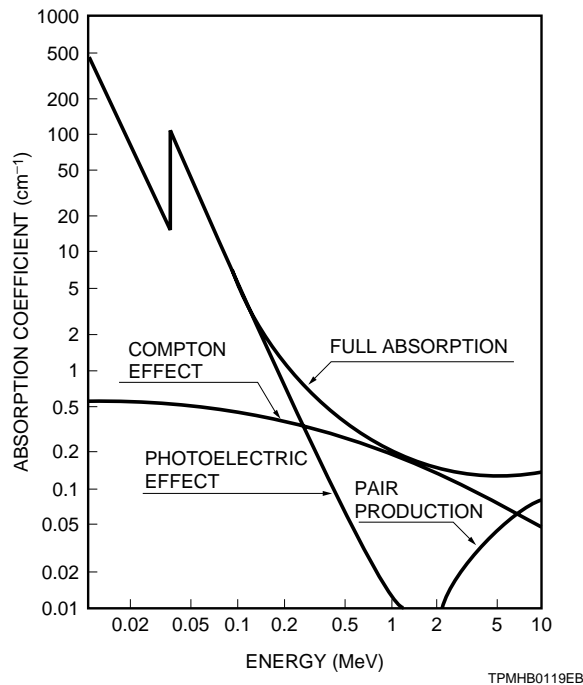
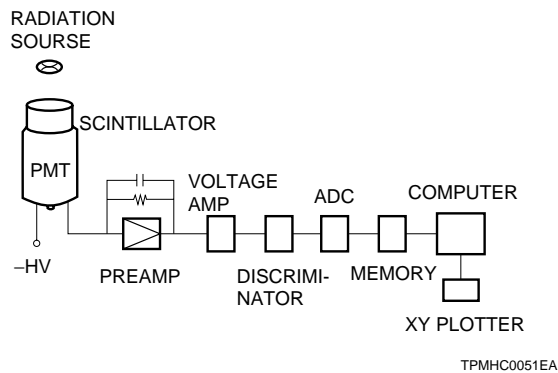


Figure 3-55: Gamma-ray absorption characteristics of NaI(Tl) scintillator

From Figure 3-55, it is clear that the photoelectric effect predominates at low energy levels of gamma rays, but pair production increases at high energy levels. Of these three interactions, the amount of scintillation produced by the photoelectric effect is proportional to gamma-ray energy because all the energy of the gamma ray is given to the orbital electrons. The photomultiplier tube outputs an electrical charge in proportion to the amount of this scintillation, as a result, the output pulse height from the photomultiplier tube is essentially proportional to the incident radiation energy. Accordingly, a scintillation counter consisting of a scintillator and a photomultiplier tube provides accurate radiation energy distribution and its dose rate by measuring the photomultiplier tube output pulse height and count rate. To carry out energy analysis, the current output from the photomultiplier tube is converted into a voltage output by an integrating preamplifier and fed to a PHA (pulse height analyzer) for analyzing the pulse height.<sup>53)</sup> A typical block diagram for scintillation counting is shown in Figure 3-56.



**Figure 3-56: Block diagram for scintillation counting**

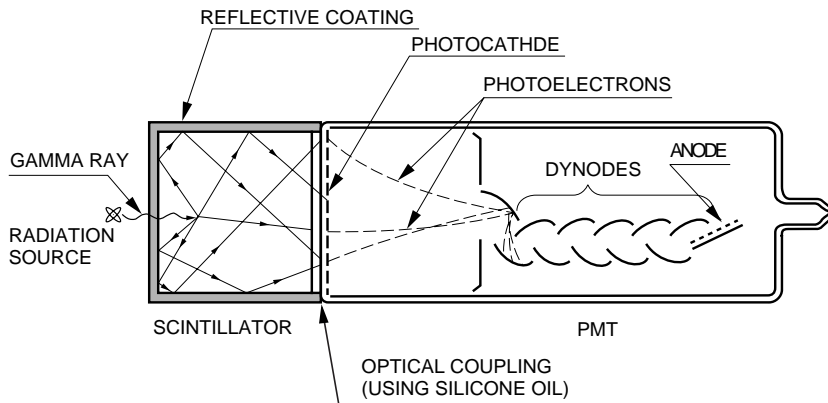
Scintillators are divided into inorganic scintillators and organic scintillators. Most inorganic scintillators are made of a halogen compound such as NaI(Tl), BGO, BaF<sub>2</sub>, CsI(Tl) and ZnS. Of these, the NaI(Tl) scintillator is most commonly used. These inorganic scintillators offer advantages of excellent energy conversion efficiency, high absorption efficiency and a good probability for the photoelectric effect compared to organic scintillators. Unfortunately however, they are not easy to handle because of deliquescence and vulnerability to shock and impact.

Organic scintillators include plastic scintillators, liquid scintillators and anthracene, an organic crystal. These scintillators display a short decay time and have no deliquescence. In addition, plastic scintillators are easy to handle and available in various types varying from small or thin sizes to large sizes with special configurations. In the detection of gamma rays, however, organic scintillators have a low absorption coefficient and exhibit less probability for the photoelectric effect. Accordingly, they are not suited for energy analysis applications. Table 3-7 lists typical characteristics and applications of major scintillators which have been developed up to the present.<sup>56)</sup>

| Scintillators    | Density (g/cm <sup>3</sup> ) | Emission Intensity (NaI(Tl) normalized at 100) | Emission Time (ns) | Peak Emission Wavelength (nm) | Applications                                   |
|------------------|------------------------------|--|--------------------|-------------------------------|--|
| NaI(Tl)          | 3.67                         | 100  | 230                | 410                           | Surveymeter, area monitor, gamma camera, SPECT |
| BGO              | 7.13                         | 15   | 300                | 480                           | PET, X-ray CT                                  |
| CsI(Tl)          | 4.51                         | 45 to 50                                       | 1000               | 530                           | Surveymeter, area monitor, X-ray CT            |
| Pure CsI         | 4.51                         | <10  | 10                 | 310                           | High energy physics                            |
| BaF <sub>2</sub> | 4.88                         | 20   | 0.9/630            | 220/325                       | TOF, PET                                       |
| GSO:Ce           | 6.71                         | 20   | 30                 | 310/430                       | Area monitor, oil well logging                 |
| Plastic          | 1.03                         | 25   | 2                  | 400                           | Area monitor, neutron detection                |
| LSO              | 7.35                         | 70   | 40                 | 420                           | PET  |
| PWO              | 8.28                         | 0.7  | 15                 | 470                           | High energy physics                            |
| YAP              | 5.55                         | 40   | 30                 | 380                           | Surveymeter, compact gamma camera              |

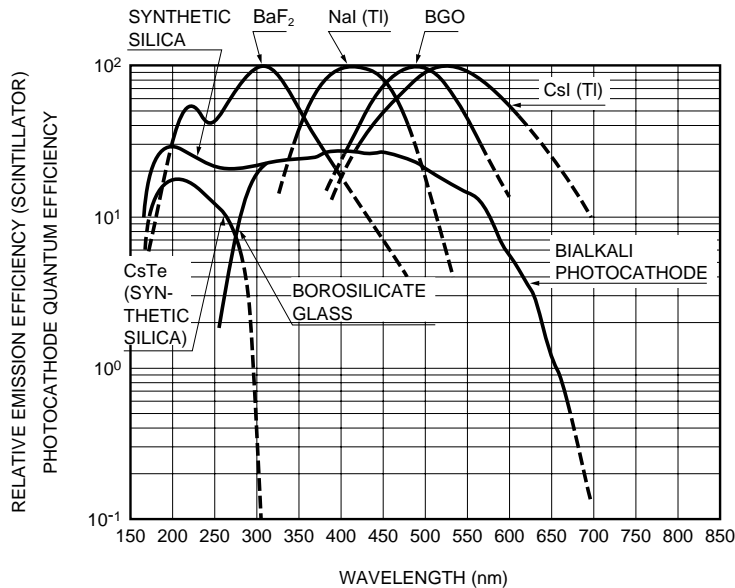
**Table 3-7: Typical characteristics and applications of scintillators**

A scintillator is attached to a photomultiplier tube with coupling material as shown in Figure 3-57. The coupling material is used in place of an air layer in order to minimize optical loss between the scintillator and the photocathode faceplate. Silicon oil having an index of refraction close to that of the glass faceplate is most widely used as a coupling material. However, selecting the proper material which provides good transmittance over the emission spectrum of the scintillator is necessary. Figure 3-58 indicates typical emission spectra of major scintillators and photocathode spectral responses of various photomultiplier tubes.



TPMHC0052EB

**Figure 3-57: Gamma-ray detection using a NaI(Tl) scintillator and a photomultiplier tube**



TPMHB0120EA

Figure 3-58: Photocathode quantum efficiency and emission spectra of major scintillators

### 3.5.2 Various characteristics

#### (1) Energy resolution

Figure 3-56 shows typical pulse height distributions for various kinds of gamma ray sources (<sup>55</sup>Fe, <sup>57</sup>Co, <sup>137</sup>Cs, <sup>60</sup>Co) taken with a photomultiplier tube coupled to an NaI(Tl) crystal. (The same measurement method as shown in Figure 3-56 is used.)

When gamma-ray energy incident on the scintillator increases and the average number of resultant photons per unit disintegration becomes large, the shape of the photopeak distribution closely approximates a Gaussian distribution, which is expressed by the following equation:

$$P(X) = \frac{1}{\sqrt{2\pi\sigma^2}} \exp\left(-\frac{(X-\bar{X})^2}{2\sigma^2}\right) \dots\dots\dots \text{(Eq. 3-43)}$$

where  $\sigma$  is the standard deviation ( $\sigma = \text{FWHM}/2.35$ ) and  $X$  is the average number of photons produced. The energy resolution or pulse height resolution (PHR)  $R$  is defined as the ratio of the FWHM ( $\Delta P$ ) to the pulse height ( $P$ ) at the peak count rate, as follows.  $R$  is usually stated in percent.

$$R = \frac{\Delta P}{P} \dots\dots\dots \text{(Eq. 3-44)}$$

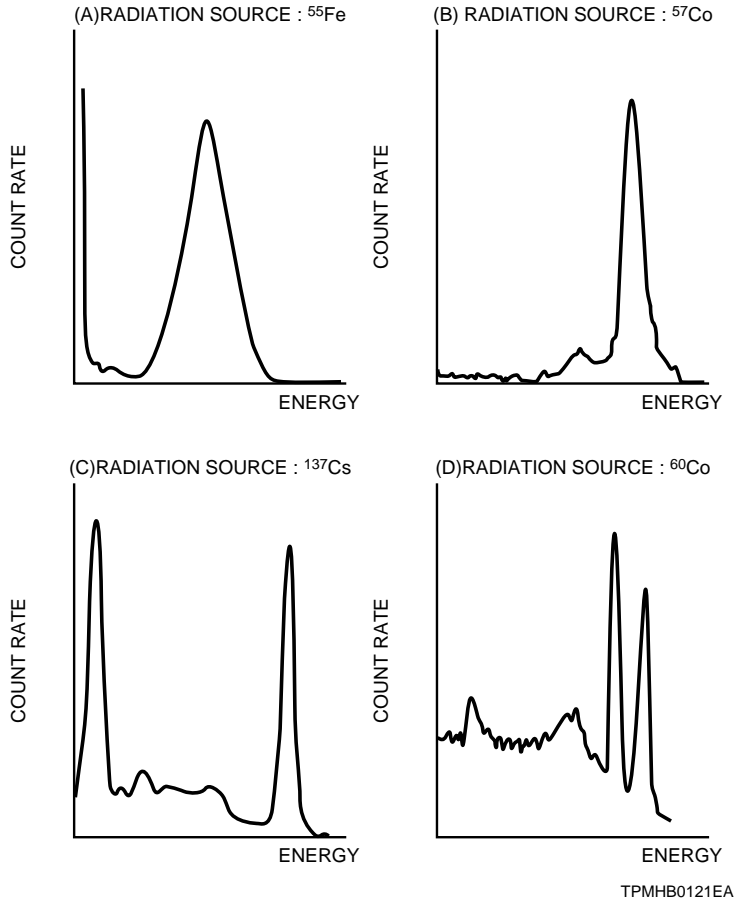


**Figure 3-59: Typical pulse height distributions**

The following factors affect the energy resolution.

- (1) Energy conversion efficiency of the scintillator
- (2) Intrinsic energy resolution of the scintillator
- (3) Light collection efficiency of the photomultiplier tube photocathode
- (4) Quantum efficiency ( $\eta$ ) of the photomultiplier tube photocathode
- (5) Collection efficiency ( $\alpha$ ) at first dynode and gain

Generally, energy resolution is given by

$$R^2(E) = R_s^2(E) + R_p^2(E) \dots\dots\dots (Eq. 3-45)$$

where

$$R_p^2(E) = \frac{5.56}{N\eta\alpha} \left( \frac{\delta}{\delta-1} \right) \dots\dots\dots (Eq. 3-46)$$

in which N is the average number of photons incident on the photocathode per unit disintegration and σ is the secondary emission yield at each dynode (assumed to be constant here).

In the above equations, Rs(E) is the energy resolution of the scintillator and Rp(E) is that of the photomultiplier tube, both of which depend on the energy (E) of the incident gamma ray. Rp<sup>2</sup>(E) is inversely proportional to E.

When a 2-inch diameter by 2-inch length NaI(Tl) scintillator and a 2-inch diameter photomultiplier tube (Hamamatsu R878) are used, the following values will typically be obtained for R, Rs and Rp:

With E=122keV (<sup>57</sup>Co), R ≈ 10%, Rs≈7 or 8%, Rp ≈ 7%

With E=662keV (<sup>137</sup>Cs), R ≈ 7%, Rs ≈ 6%, Rp ≈ 3.5%

Along with using a scintillator with high conversion efficiency and good inherent energy resolution, to obtain higher energy resolution, good optical coupling should be provided to reduce optical loss. For this purpose, as mentioned previously it is helpful to couple the scintillator and the photomultiplier tube using silicon oil having an index of refraction close to that of the faceplate of the photomultiplier tube.

When the intensity distribution of light entering the photomultiplier tube is always constant over the photocathode, the photomultiplier tube uniformity has no effect on the energy resolution. However, if the light flash from the scintillator fluctuates with respect to the incident position on the photocathode, the photomultiplier tube uniformity may degrade the energy resolution. To avoid this problem, a light-guide is sometimes placed between the scintillator and the photomultiplier tube so that the light flash from the scintillator is diffused and allowed to enter uniformly over the photocathode. But this technique is not necessary when using a photomultiplier tube with normal uniformity.

| γ-ray source      | Energy (keV) | NaI(Tl) + PMT | BGO + PMT   |
|-------------------|--------------|---------------|-------------|
| <sup>55</sup> Fe  | 5.9          | 40 to 50%     | —           |
| <sup>241</sup> Am | 59.5         | 12 to 15%     | 70 to 150%  |
| <sup>57</sup> Co  | 122          | 8.5 to 10%    | 35 to 50%   |
| <sup>22</sup> Na  | 511          | 7.5 to 9.0%   | 13 to 25%   |
| <sup>137</sup> Cs | 662          | 6.5 to 8.5%   | 11 to 20%   |
| <sup>60</sup> Co  | 1,170        | 5 to 6.5%     | 8.5 to 11%  |
|                   | 1,330        | 4.5 to 5.5%   | 8.0 to 9.5% |

**Table 3-8: Energy resolution for typical gamma-ray sources, obtained with a NaI(Tl) or BGO scintillator**

Energy resolution is one of the most important characteristics in radiation measurement such as gamma cameras and gamma counters. Therefore photomultiplier tubes used in these applications are usually tested for energy resolution. Table 3-8 summarizes energy resolution for typical gamma rays measured with a NaI(Tl)/photomultiplier tube or a BGO/photomultiplier tube combination device. As shown in the table, each of the data exhibits a certain variation in energy resolution. This is due to the non-uniformity of the physical size of the scintillator or photomultiplier tube and also the performance variations between individual photomultiplier tubes. If necessary, it is possible to select only those photomultiplier tubes that meet specific specifications.

## (2) Relative pulse height

In scintillation counting, when a photomultiplier tube is operated at a constant supply voltage and the gain of the measuring circuit is fixed, the pulse height that gives the peak of the pulse height distribution is referred to as the relative pulse height (RPH). This is commonly stated in terms of the channel number at which the maximum count rate of the pulse height distribution is obtained with a pulse height analyzer.<sup>28)</sup> The same measurement setup is used as shown in Figure 3-56. This relative pulse height essentially means the collective gain of a photomultiplier tube used in scintillation counting. It usually shows a good correlation with measurement data taken by users (instrument manufacturers) and thus is often used for simple evaluation of a photomultiplier tube.

When measured with a NaI(Tl) scintillator, the relative pulse height provides a close correlation with blue sensitivity because the emission spectrum of the NaI(Tl) resembles the spectral transmittance of the Corning filter CS No.5-58 which is used for the blue sensitivity measurement. (Refer to Section 3.1.5.)

## (3) Linearity

Output current linearity of a photomultiplier tube with respect to the amount of scintillation flash is another important parameter to discuss. Since linearity of general-purpose photomultiplier tubes has already been described earlier, this section explains how to measure linearity related to scintillation counting. Figure 3-60 shows a typical pulse height distribution for the  $^{226}\text{Ra}$  taken with a NaI(Tl) and Figure 3-61 indicates the relationship between each peak channel and the gamma-ray energy. Because  $^{226}\text{Ra}$  releases various kinds of radiation ranging in energy from 10.8keV to 2.2MeV, it is used for linearity measurements over a wide energy range.

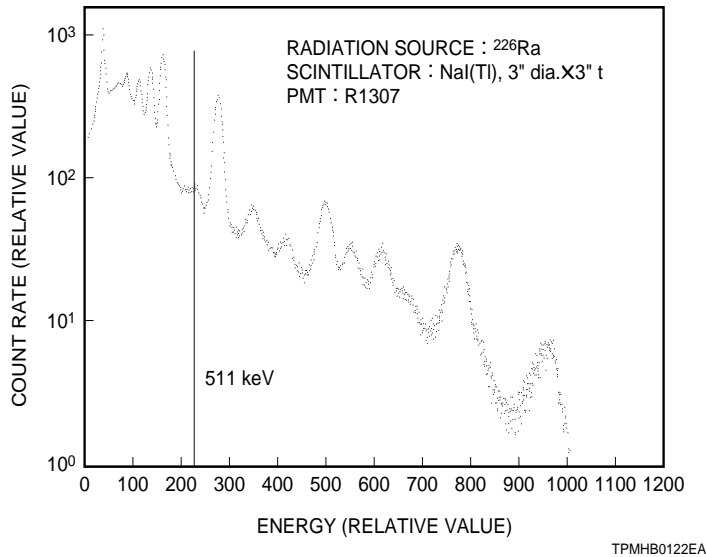
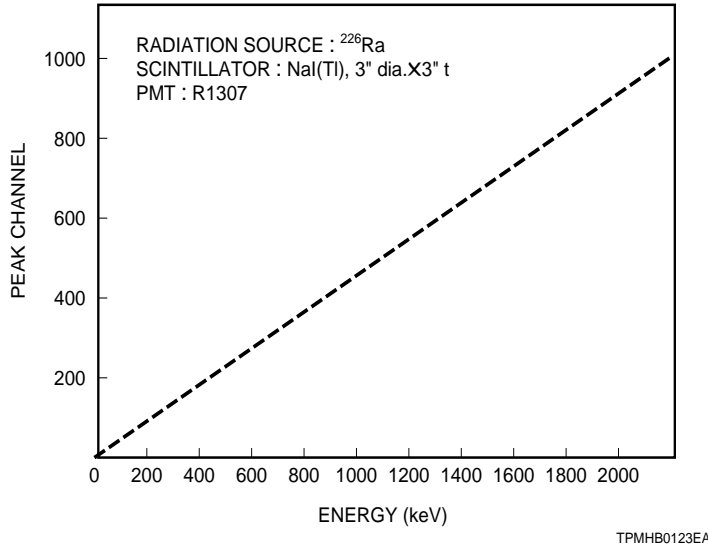


Figure 3-60: Pulse height distribution for the  $^{226}\text{Ra}$  taken with a NaI(Tl)



**Figure 3-61: Relation between peak channel and gamma-ray energy**

Amount of emission from a NaI(Tl) scintillator equals about 30 photons per 1keV of gamma-ray energy. Accordingly, some 20,000 photons (662keV X 30) are generated with <sup>137</sup>Cs and some 40,000 photons (1330keV X 30) are generated with <sup>60</sup>Co. Photomultiplier tube linearity and measurement methods using normal light sources have been discussed in Section 3.3.2. When <sup>60</sup>Co is used for linearity measurements under the conditions that the photomultiplier tube gain is at 10<sup>6</sup> and the decay constant (τ s) of the NaI(Tl) scintillator is 250 nanoseconds at room temperature, the photomultiplier tube output current I<sub>p</sub> is given by

$$\begin{aligned}
 I_p &= \frac{N \times h \times m \times e}{\tau_s} \\
 &= 4 \times 10^4 \times 0.25 \times 10^6 \times \frac{1.6 \times 10^{-19}}{250 \times 10^{-9}} \dots\dots\dots \text{(Eq. 3-47)} \\
 &= 6.4 \times 10^{-3} \text{(A)}
 \end{aligned}$$

where

- μ: gain of photomultiplier tube
- N: amount of light flash per event produced from scintillator
- e: electron charge
- η: quantum efficiency of photocathode (assumed to be 25%)

Thus in this measurement the photomultiplier tube must have a pulse linearity over 6.4 milliamperes. In particular, care should be taken with respect to the linearity range when measuring radiation at higher energy levels as the photomultiplier tube produces a large amount of light flash.

**(4) Uniformity**

The uniformity of a photomultiplier tube affects the performance of systems utilizing scintillation counting, especially in such equipment as Anger cameras used to detect the incident position of radiation. Uniformity of a photomultiplier tube is commonly defined as the variation in the output current with respect to the photocathode position on which a light spot is scanned.

However, another evaluation method like that illustrated in Figure 3-62<sup>28)</sup> provides more useful data which allows users to predict the direct effects of uniformity on the equipment.

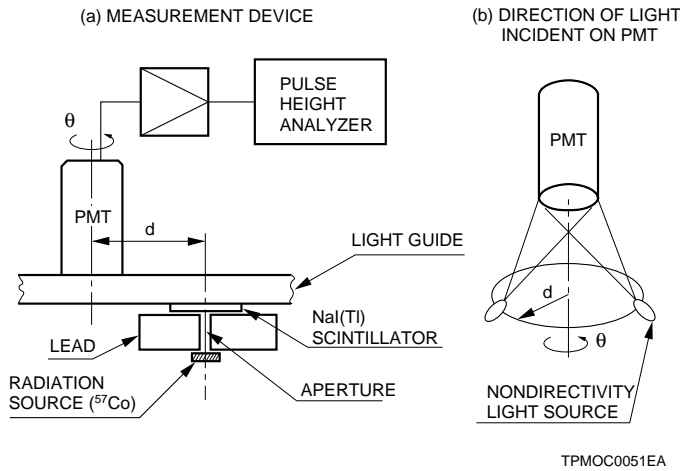


**Figure 3-62: Measurement method for azimuth uniformity**

In Figure 3-62, the photomultiplier tube is set at a distance ( $d$ ) from a light source. The output variations of the photomultiplier tube are measured as the light source is rotated around the tube (by changing angle  $\theta$ ). The same procedure is repeated at different values of  $d$ . Then plotting the positions ( $d, \theta$ ) of the light source providing equal output gives a graph similar to a contour map (Figure 3-63).

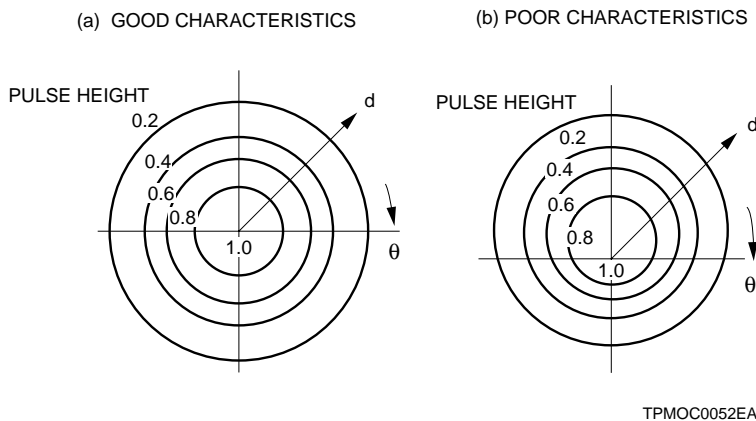


**Figure 3-63: Examples of azimuth uniformity data**

Uniformity data evaluated by this method is called the azimuth uniformity. If photomultiplier tubes with poor azimuth uniformity are installed in an Anger camera, position distortion may occur in the detection area, degrading spatial resolution. Since the azimuth uniformity requires a long time to test, it is not practical to measure this data for every photomultiplier tube. Usually, only a sample of photomultiplier tubes are measured to provide reference data.

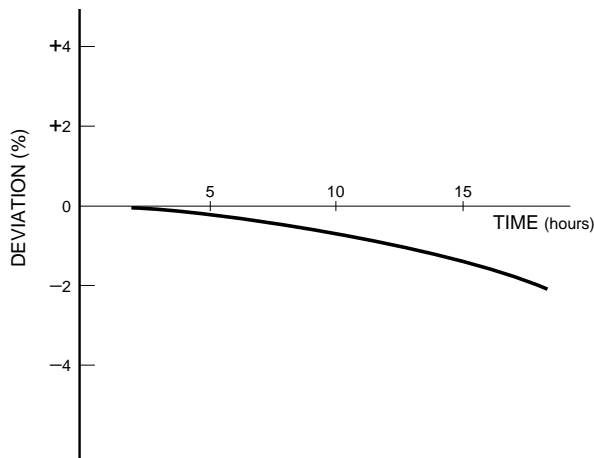
## (5) Stability

There are two types of stability tests used in scintillation counting: long term stability<sup>28)</sup> and short term stability.<sup>28)</sup> Both stability tests employ a  $^{137}\text{Cs}$  radiation source and a NaI(Tl) scintillator. The variation in the photopeak obtained from a photomultiplier tube is measured with a pulse height analyzer (PHA). These stability tests differ slightly from those applied to the general-purpose photomultiplier tubes which were discussed in the previous section.

### a) Long term stability

The long term stability is also referred to as the photopeak drift. In this stability test, the photomultiplier tube is allowed to warm up for one hour with the photopeak count rate maintained at 1kcps. After this, the variation rate of the photopeak pulse height (channel number) is measured for a period of 16 hours.

The same measurement setup shown in Figure 3-56 is used and the variation occurring in the peak channel is recorded as the time elapses. Typical photomultiplier tube data is shown in Figure 3-64 below.



TPMOB0067EA

**Figure 3-64: Long term stability of a typical photomultiplier tube**

There are a few tube types that exhibit somewhat a tendency to increase during the period of 16 hours. However, most photomultiplier tubes tend to show decreasing values, with a variation rate within plus or minus several percent. This tendency is analogous to the drift characteristic explained earlier, but this test method is more practical for scintillation applications. Numerically, the long term stability DLTS is defined as the mean deviation of the peak pulse height (or mean gain deviation) with respect to the mean pulse height, expressed in percent as given by the equation below. It usually has a value of 1 or 2 percent.

$$D_{LTS} = \frac{\sum_{i=1}^n |P_i - \bar{P}|}{n} \cdot \frac{100}{\bar{P}} \dots\dots\dots (Eq. 3-48)$$

where

$\bar{P}$ : mean value of photopeak pulse height (channel)

$P_i$ : peak pulse height at the  $i$ -th reading

$n$ : total number of readings for 16 hours

**b) Short term stability**

The short term stability is also referred to as the count rate stability. The variation in the photopeak pulse height is measured when the photopeak count rate is increased from 10kcps to 1kcps. If the photopeak pulse height at a count rate of 10kcps is given by A and that at 1kcps by B, the short term stability DSTS is stated by the following relationship. This value is expected to be about  $\pm 1$  percent.

$$D_{STS} = (1 - \frac{B}{A}) \times 100(\%) \dots\dots\dots (Eq. 3-49)$$

This instability is caused by the abrupt change in output current resulting from the changing count rate, and is closely related to the hysteresis effect in photomultiplier tubes.

**(6) Noise**

In scintillation counting, a signal pulse is usually produced by multiple photoelectrons simultaneously emitted from the photocathode, which create a higher pulse height than most dark current pulses do. Use of a discriminator effectively eliminates most dark current pulses with lower amplitudes. Accordingly, only noise pulses with higher amplitudes will be a problem in scintillation counting. To remove this type of noise pulse, the coincident counting technique is commonly used.

Noise pulses with higher amplitudes may be caused by radiation released from natural radioactive elements contained in a reinforced concrete building or in the atmosphere. These noise pulses may be a significant problem, particularly in low-level-radiation measurements. Concrete used to construct a building usually contains Rn, Th and <sup>40</sup>Fe, and steel contains U, Th and <sup>60</sup>Co. Radioactive floating dust and Rn or Th gases may be present in the atmosphere, and a scintillator may also contain minute amounts of <sup>40</sup>K and <sup>208</sup>Tl. Furthermore, borosilicate glass used to fabricate the faceplate of a photomultiplier tube contains potassium of which <sup>40</sup>K comprises 0.118 percent. The <sup>40</sup>K releases gamma rays of 1.46MeV.

Figure 3-65 shows background noise measured with a Hamamatsu R877 photomultiplier tube (5-inch diameter, borosilicate glass, bialkali photocathode) coupled to a NaI(Tl) scintillator (5-inch diameter X 2-inch length), (1) n Figure 3-65 is measured without taking any countermeasures, while (2) is measured by shielding the tube with two lead blocks of 100 and 50 millimeter thickness, each being placed respectively in the lower section and upper section. (3) is data taken with an R877-01 that employs a so-called K-free glass containing a very minute amount of potassium for its faceplate and side bulb envelope.

Since these measurements were made using the setup in which the peak of <sup>137</sup>Cs (662keV) becomes 300 channels, the energy range measured covers from about several thousand keV to 2.2MeV. In this energy range, the background noise that is as high as 470cps during normal measurement, can be drastically reduced to 26cps (about 1/20) by shielding the tube with lead blocks. Consequently, it has been proven that most background noise originate from environmental radiation. In addition, use of the R877-01 with K-free glass (Refer to Section 3.1.2.) further reduces the total noise counts down to about 16cps. Particularly, in the energy range from 1.2 to 1.6MeV where noise counts mainly result from the <sup>40</sup>K (1.46MeV), the noise count of 3.3cps measured with the R877 (normal borosilicate glass) is reduced to 0.9cps with the R877-01 (K-free glass).

The external parts of a photomultiplier tube and the scintillator, are usually maintained at ground potential. Therefore, a cathode ground scheme with the high voltage applied to the anode is often used in scintillation counting.

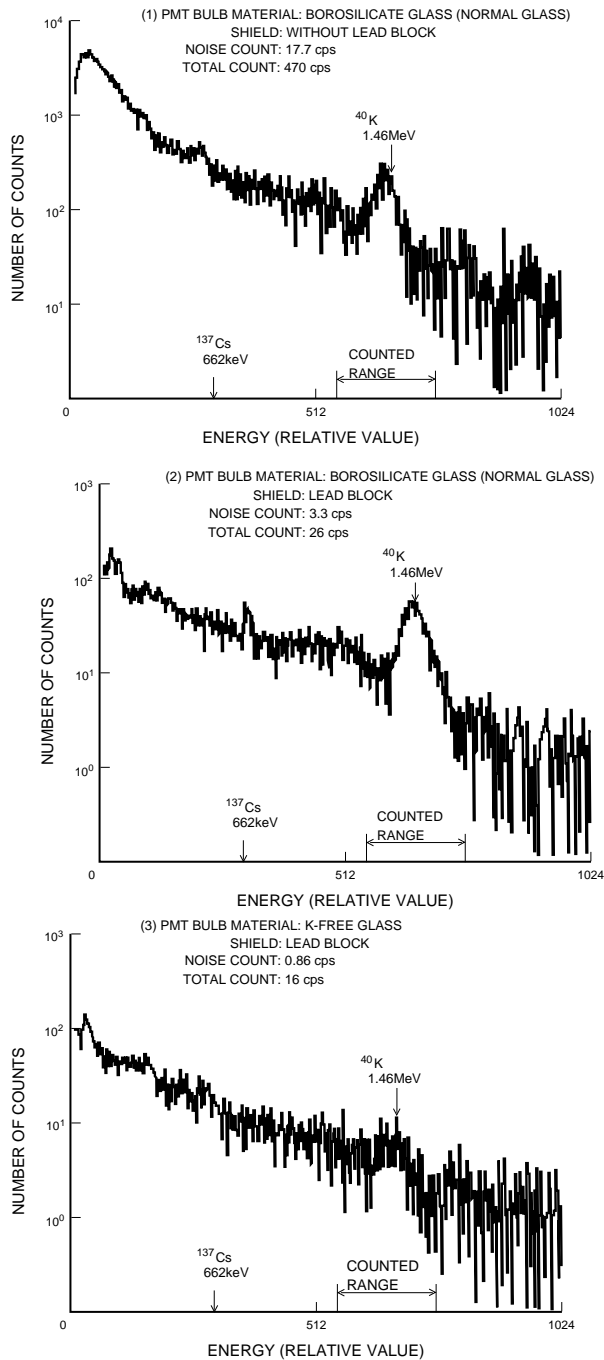
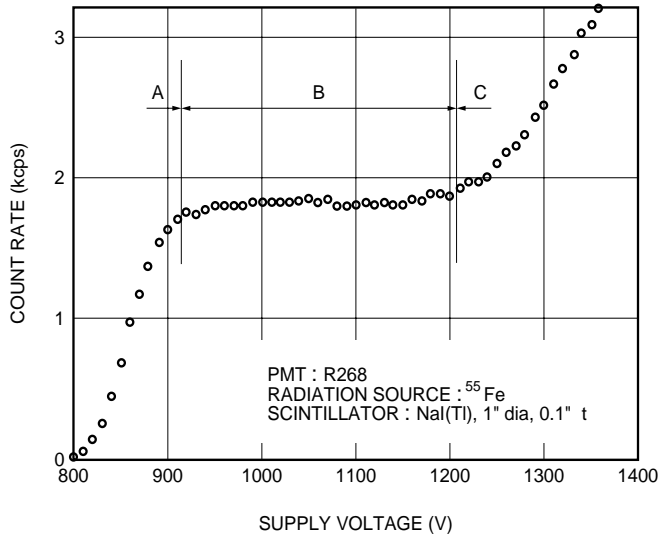


Figure 3-65: Background noise

### (7) Plateau characteristic

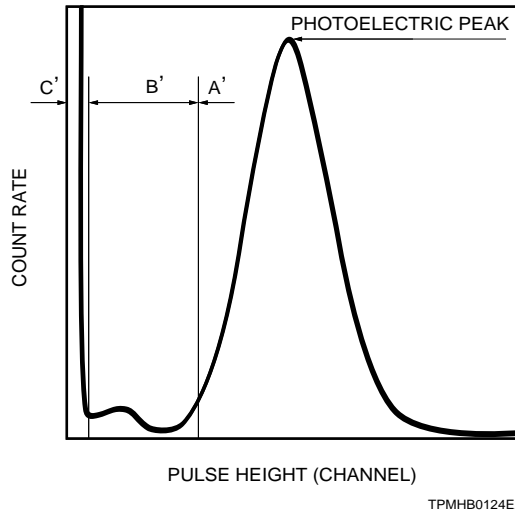
The plateau characteristic is useful in simple scintillation counting which does not use a pulse height analyzer. The plateau characteristic is measured by setting a discrimination level and counting all pulses with amplitudes greater than that level. This operation is done while changing the supply voltage for the photomultiplier tube. The measured data is plotted on a graph in which the abscissa indicates the supply voltage and the ordinate indicates the total number of counted pulses with amplitudes greater than the discrimination level. Figures 3-66 (a) and (b) show the typical plateau characteristic and pulse height distribution when a NaI(Tl) scintillator and  $^{55}\text{Fe}$  radiation source are used.

With the discrimination level kept at a constant value, as the photomultiplier tube supply voltage is increased, the output pulses are counted in order from the photopeak region to the valley and the dark current regions. Plotting the count rate versus the photomultiplier tube supply voltage gives a curve like that shown in Figure 3-66 (a), which consists of three regions (regions A, B and C). Region B is referred to as the plateau and the supply voltage should be set within this region. The count rate will not vary even if the supply voltage is changed within this region, showing a constant photopeak count rate. The wider the plateau region, the less the count rate will be affected by fluctuations in the dark current. This plateau region corresponds to the valley of a pulse height distribution, i.e., region B' in Figure 3-66 (b). photomultiplier tubes with better energy resolution and lower dark current provide a wider region B'. Since the plateau region is expressed in terms of supply voltage range, photomultiplier tubes with smaller gain and lower noise tend to have a wider plateau range. With this method, however, it should be noted that energy analysis cannot be carried out because all pulses with amplitudes higher than the discrimination level are counted.



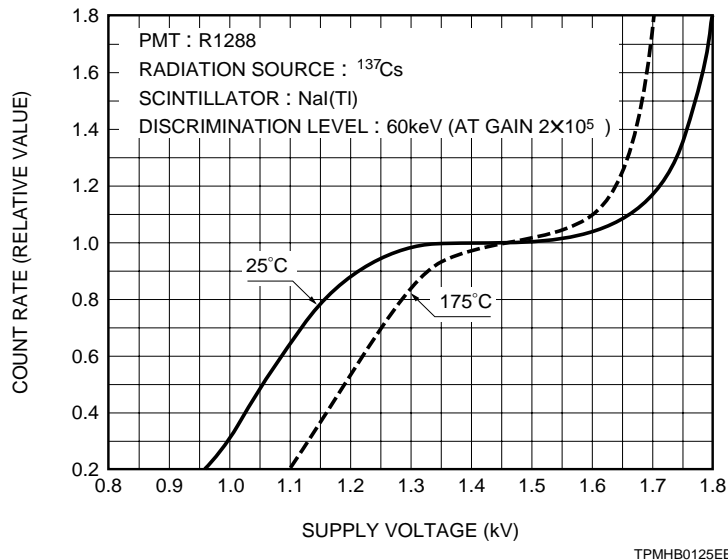
TPMHB0124EA

Figure 3-66: Plateau characteristic (a)



**Figure 3-66: Plateau characteristic (b)**

As an application example, plateau characteristics are widely employed to evaluate photomultiplier tubes designed for use in oil well logging where geological information is obtained based on the signal produced by Compton scattering. In this case, photomultiplier tubes are also evaluated using a  $^{137}\text{Cs}$  radiation source and a NaI(Tl) scintillator. Typical plateau characteristics are shown in Figure 3-67.



**Figure 3-67: Typical plateau characteristics of a photomultiplier tube designed for high temperature operation**

To measure the data shown in Figure 3-67, a photomultiplier tube designed for high temperature operation is used. The plateau characteristic taken at  $175^\circ\text{C}$  is shown along with that obtained at  $25^\circ\text{C}$ . It can be seen from the figure that the supply voltage at which the signal appears (corresponding to region A in Figure 3-66 (a)) shifts to the higher voltage side. This is because the gain of the photomultiplier tube decreases as the temperature increases. On the other hand, since the dark current increases with temperature, the count rate sharply increases (corresponding to region C in Figure 3-66 (a)) at a lower supply voltage. Consequently, the plateau width (supply voltage range) measured at a higher temperature becomes narrow in comparison with that obtained at room temperatures ( $+25^\circ\text{C}$ ).

## References in Chapter 3

- 1) Hamamatsu Photonics Catalog: Photomultiplier Tubes.
- 2) T. Hiruma, SAMPE Journal. 24, 35 (1988).
- 3) A. H. Sommer: Photoemissive Materials, Robert E. Krieger Publishing Company (1980).
- 4) T. Hirohata and Y. Mizushima: Japanese Journal of Applied Physics. 29, 8, 1527 (1990).
- 5) T. Hirohata, T. Ihara, M. Miyazaki, T. Suzuki and Y. Mizushima: Japanese Journal of Applied Physics. 28, 11, 2272 (1989).
- 6) W.A. Parkhurst, S. Dallek and B.F. Larrick: J. Electrochem. Soc, 131, 1739 (1984).
- 7) S. Dallek, W.A. Parkhurst and B.F. Larrick: J. Electrochem. Soc, 133, 2451 (1986).
- 8) R.J. Cook: Phys. Rev. A25, 2164; 26,2754 (1982).
- 9) H.J. Kimble and L. Mandel: Phys. Rev. A30, 844 (1984).
- 10) M. Miyao, T. Wada, T. Nitta and M. Hagino: Appl. Surf. Sci. 33/34, 364 (1988).
- 11) Tailing Guo: J. Vac. Sci. Technol. A7, 1563 (1989).
- 12) Huairong Gao: J. Vac. Sci. Technol. A5, 1295 (1987).
- 13) C.A. Sanford and N.C. MacDonald: J. Vac. Sci. Technol. B 6. 2005 (1988).
- 14) C.A. Sanford and N.C. MacDonald: J. Vac. Sci. Technol. B 7. 1903 (1989).
- 15) M. Domke, T. Mandle, C. Laubschat, M. Prietsch and G.Kaindl: Surf. Sci. 189/190, 268 (1987).
- 16) M. Niigaki, T. Hirohata, T. Suzuki, H. Kan and T. Hiruma: Appl. Phys. Lett. 71 (17) 27, Oct. 1997
- 17) K. Nakamura, H. Kyushima: Japanese Journal of Applied Physics, 67, 5, (1998)
- 18) D. Rodway: Surf. Sci. 147, 103 (1984).
- 19) "Handbook of Optics": McGraw-Hill (1978).
- 20) James A. R. Samson: "Techniques of Vacuum Ultraviolet Spectroscopy" John Wiley & Sons, Inc (1967).
- 21) C.R. Bamford: Phys. Chem. Glasses, 3, 189 (1962).
- 22) Corning Glass Works Catalog.
- 23) IEEE ET-61A 1969.5.8.
- 24) IEEE STD 398-1972.
- 25) IEC PUBLICATION 306-4, 1971.
- 26) H. Kume, K. Koyama, K. Nakatsugawa, S. Suzuki and D. Fatlowitz: Appl. Opt, 27, 1170 (1988).
- 27) T. Hayashi: "PHOTOMULTIPLIER TUBES FOR USE IN HIGH ENERGY PHYSICS".  
Hamamatsu Photonics Technical Publication (APPLICATION RES-0791-02).
- 28) Hamamatsu Photonics Technical Publication "USE OF PHOTOMULTIPLIER TUBES IN SCINTILLATION APPLICATIONS" (RES-0790)
- 29) T.H. Chiba and L. Mmandel: J. Opt. Soc. Am. B,5, 1305 (1988).
- 30) D.P. Jones: Appl. Opt. 15,14 (1976).
- 31) D.E. Persyk: IEEE Trans. Nucl. Sci. 38, 128 (1991).
- 32) Mikio Yamashita: Rev. Sci. Instrum., 49, 9 (1978).
- 33) "Time-Correlated Single-Photon Counting": Academic Press, Inc (1985).
- 34) G.F.Knoll: "RADIATION DETECTION and MEASUREMENT", John Wiley & Sons, Inc. (1979).
- 35) C.E. Miller, et al.: IEEE Trans. Nucl. Sci. NS-3, 91 (1956).
- 36) A.T. Young: Appl. Opt., 8, 12, (1969).
- 37) R.L. Bell: "Negative Electron Affinity Devices", Clarendon Press. Oxford (1973).
- 38) G.A. Morton et al.: IEEE Trans. Nucl. Sci. NS-14 No.1, 443 (1967).
- 39) R. Staubert et al.: Nucl. Instrum. & Methods 84, 297 (1970).
- 40) S.J. Hall et al.: Nucl. Instrum. & Methods 112, 545 (1973).
- 41) Illes P. Csorba "Image Tubes" Howard W. Sams & Co (1985).
- 42) F. Robber: Appl. Opt., 10, 4 (1971).
- 43) S.A. Hoenig and A. Cutler: Appl. Opt. 5,6, 1091 (1966).
- 44) H. Hora: Phys. Stat. Soli Vol (a), 159 (1971).
- 45) R. Foord, R. Jones, C. J. Oliver and E. R. Pike: Appl. Opt., 8, 10, (1969).
- 46) R. Foord, R. Jones, C.J. Oliver and E.R. Pike: Appl. Opt. 1975, 8 (1969).

- 
- 47) J.K. Nakamura and S.E. Schmarz: Appl. Opt., 1073, 7, 6 (1968).
  - 48) J.K. Nakamura and S. E. Schwarz: Appl. Opt., 7, 6 (1968).
  - 49) R.R. Alfano and N. Ockman: Journal of the Optical Society of America, 58, 1 (1968).
  - 50) T. Yoshimura, K. Hara and N. Wakabayashi: Appl. Optics, 18, 23 (1979).
  - 51) T.S. Durrani and C. A. Greated: Appl. Optics, 14, 3 (1975).
  - 52) Hamamatsu Photonics Technical Publication: Photon Counting (1990).
  - 53) Nicholas Tsoulfanidis: "Measurement and Detection of Radiation", Hemispherev Publication Corporation (1983).
  - 54) William J. Price: "Nuclear Radiation Detection", McGraw-Hill Book Company Inc. (1964).
  - 55) H. Kume, T. Watanabe, M. Iida, T. Matsushita and S. Suzuki: IEEE Trans. Nucl. Sci, NS-33[1], 364 (1986).
  - 56) R.L. Heath, R. Hofstadter and E. B. Hughes: Nucl. Inst. and Meth, 162, 431 (1979).
  - 57) Emil Kowalski: "Nuclear Electronics", Springer-Verlag Berlin (1970).

# MEMO

# **CHAPTER 4**

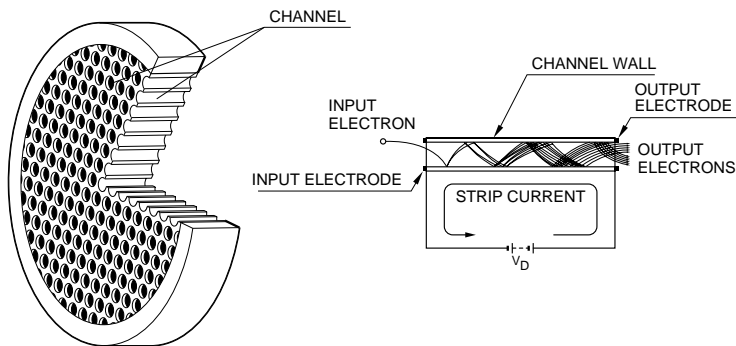
## **MCP-PMT**

*With the advent of the microchannel plate<sup>1)</sup> (abbreviated as MCP hereafter), photomultiplier tubes have evolved as more versatile devices. MCP-PMTs - photomultiplier tubes that incorporate an MCP in place of the conventional discrete dynodes - offer wide-bandwidth measurements up to the picosecond region as well as low-light-level detection in the photon counting region. This chapter describes these ultra-fast and high-sensitivity MCP-PMTs.<sup>2)</sup>*

## 4.1 Structure

### 4.1.1 Structure of MCPs

Figure 4-1 illustrates the schematic structure of an MCP. The MCP consists of a two-dimensional array of a great number of glass capillaries (channels) bundled in parallel and formed into the shape of a thin disk. Each channel has an internal diameter ranging from 6 to 20 microns with the inner wall processed to have the proper electrical resistance and secondary emissive properties. Accordingly, each channel acts as an independent electron multiplier. The cross section of a channel and its principle of multiplication are illustrated in Figure 4-1 (b). When a primary electron impinges on the inner wall of a channel, secondary electrons are emitted. Being accelerated by the electric field created by the voltage  $V_D$  applied across both ends of the MCP, these secondary electrons bombard the channel wall again to produce additional secondary electrons. This process is repeated many times along the channel and as a result, a large number of electrons are released from the output end.



TMCP0002EB

(a) Schematic structure of an MCP

(b) Principle of multiplication

**Figure 4-1: Schematic structure of an MCP and its principle of multiplication**

MCPs are quite different in structure and operation from conventional discrete dynodes and therefore offer the following outstanding features:

- 1) High gain despite compact size
- 2) Fast time response
- 3) Two-dimensional detection with high spatial resolution
- 4) Stable operation even in high magnetic fields
- 5) Sensitive to charged particles, ultraviolet radiation, X rays, gamma rays, and neutrons
- 6) Low power consumption

There are various types of detectors that utilize the advantages offered by MCPs, for example image intensifiers for low-light-level imaging, fast time response photomultiplier tubes that incorporate an MCP (MCP-PMTs), position-sensitive multianode photomultiplier tubes, streak tubes for ultra-fast photometry, and photon counting imaging tubes for ultra-low light level imaging.

### 4. 1. 2 Structure of MCP-PMT

Figure 4-2 shows the cross section of a typical MCP-PMT. This tube consists of an input window, photocathode, MCP, and anode. The photoelectrons emitted from the photocathode enter the channels of the MCP and impinge on the inner wall where they are multiplied by means of secondary emission. This process is repeated along the channels, and finally a large number of electrons are collected by the anode as an output signal. The MCP is arranged at a distance of 2 millimeters or less from the photocathode, forming a close-proximity structure. A photograph of an actual MCP-PMT complete with housing is shown in Figure 4-3.

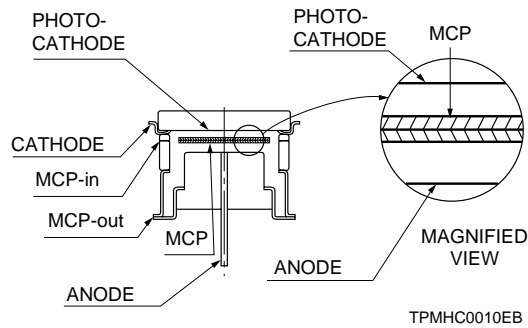


**Figure 4-2 Cross section of a typical MCP-PMT**



**Figure 4-3 External view of an MCP-PMT**

### 4. 1. 3 Voltage -divider circuit and housing structure

Figure 4-4 shows a basic voltage-divider circuit used to operate an MCP-PMT (with a two-stage MCP) and the configuration of the housing that contains the MCP-PMT with the voltage-divider circuit.

As shown in the figure, a negative high voltage is normally applied to the photocathode, and the voltage-divider circuit gives a voltage gradient between the photocathode, MCP-in, MCP-out, and the anode by dividing the high voltage with properly selected resistors. The voltage-divider circuit and housing are designed with careful consideration given to prevent "ringing" which may be caused by high-frequency signals, so that the output waveform distortion is suppressed to a minimum level.

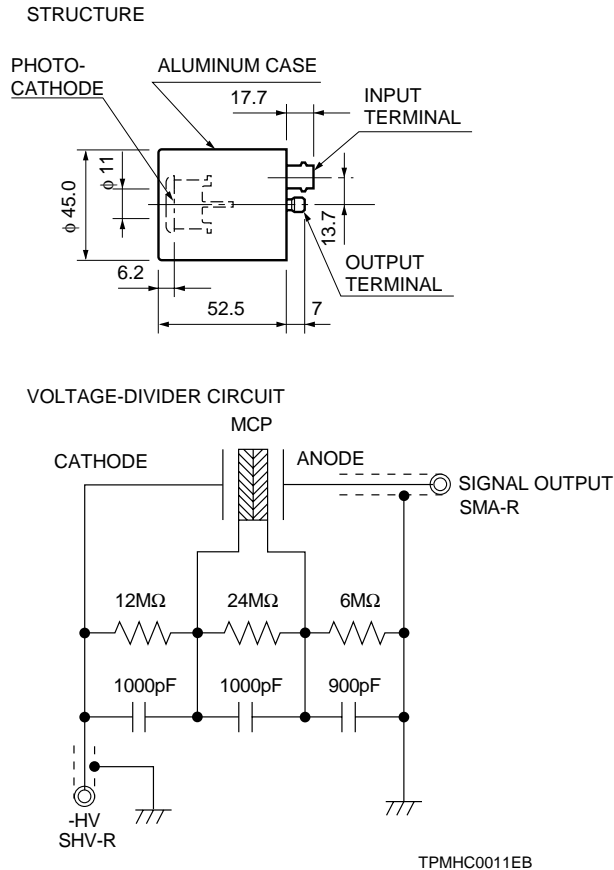


Figure 4-4: Housing configuration and operating circuit for MCP-PMT

## 4.2 Basic characteristics of MCP-PMTs

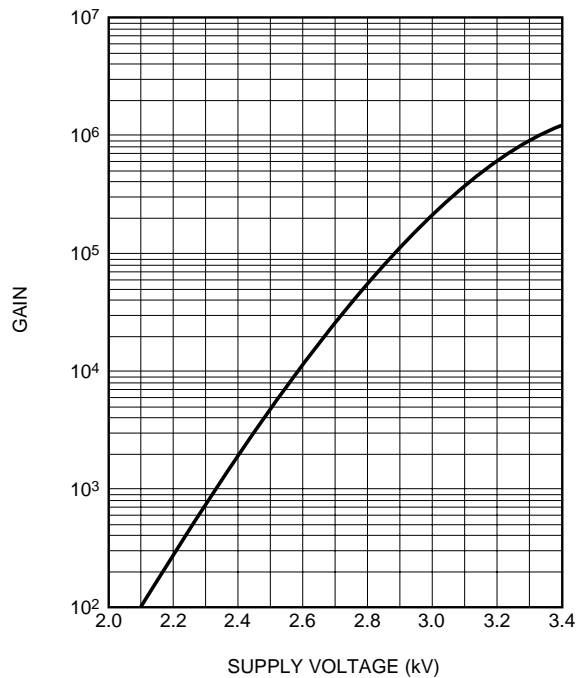
### 4.2.1 Gain characteristics<sup>1)</sup>

The gain of an MCP-PMT depends on the number of MCPs incorporated in the tube. Figure 4-5 shows a typical current amplification curve of an MCP-PMT.

The gain<sup>1)</sup> ( $\mu$ ) of an MCP is determined by the length-to-diameter ratio  $\alpha$  ( $=L/d$ ) of a channel, and approximated as follows:

$$\mu = \text{EXP}(G \cdot \alpha)$$

where  $G$  is the secondary emission characteristics called the gain factor. This gain factor is an inherent characteristics of the channel wall material and presented by a function of the electric field intensity inside the channel.



TPMHB0077EB

**Figure 4-5: Typical gain of an MCP-PMT (using a two-stage MCP of 6 $\mu$ m channel diameter)**

In general, the gain rising point moves to the higher voltage side as  $\alpha$  is made greater. This also allows obtaining a higher gain. However, if the gain becomes higher than 10<sup>4</sup>, noise begins to increase significantly due to ion feedback effects causing a serious problem. To avoid this,  $\alpha$  is usually selected to be around 40 so that a single MCP provides a gain of about 10<sup>4</sup> at 1kV supply voltage.

As shown in Figure 4-5 above, a higher gain can be obtained from a two-stage MCP-PMTs. This gain level enables photon counting measurements.

### 4. 2. 2 Dead time<sup>1)</sup>

When an MCP is irradiated by a pulsed electron current, a positive charge is generated at the MCP output end in accordance with the released electron current. This phenomenon deforms the potential distribution and enfeebles the electric fields so that the subsequent electron multiplication is suppressed. This charge is neutralized by the strip current flowing through the channel wall. However, a certain amount of time is required for neutralization because the strip current is small due to the high resistance of the MCP. The gain of signals entering within this period is usually low. The time required for neutralization is referred to as the dead time or recovery time. If the output charge per channel is given by  $Q_{out}$  and the strip current per channel by  $I_s$ , then the dead time  $t_d$  is given by the following relation:

$$t_d = Q_{out} / I_s$$

The dead time can be shortened by using a low resistance MCP which allows the strip current  $I_s$  to flow in large quantities. This also improves saturation characteristics.

When an MCP-PMT is operated in such a way that the next electron enters the MCP within this dead time, various types of output saturation occur as described in 4.2.3. If the MCP-PMT is operated at saturated levels, it cannot exhibit adequate performance, and also degrades the photocathode sensitivity and MCP gain.

### 4. 2. 3 Saturation characteristics<sup>1)</sup>

In general, the saturation of a photodetector is defined as the phenomenon in which the amount of output signal is no longer proportional to the incident light intensity. In the case of MCP-PMTs, this saturation is caused by the dead time as described in 4.2.2, disturbed potential distribution and space charge effects inside the MCP, being different from those of normal photomultiplier tubes using multiple stages of discrete dynodes.

#### (1) Saturation in DC operation

An MCP has a high resistance ranging from several tens to several hundreds of megohms, which limits the output current from the MCP. Because of this, output current saturation occurs as the input current increases, as shown in Figure 4-6 (a) and (b). This is mainly caused by a decrease in the electric field intensity due to variations in the potential distribution at the output end of the MCP which results from large amounts of secondary electrons from the MCP.

The decrease in the electric field intensity is recovered by the strip current flowing through the channel wall. Saturation in DC operation usually begins to occur when the output current reaches 5 or 6 percent of the strip current.

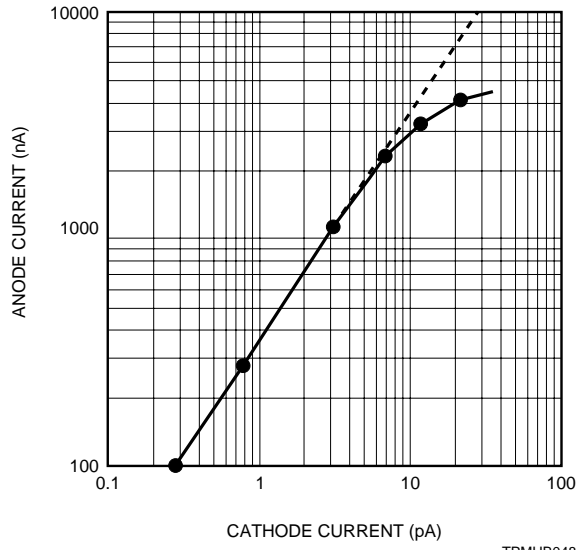


Figure 4-6 (a): Saturation characteristics of MCP-PMT in DC operation

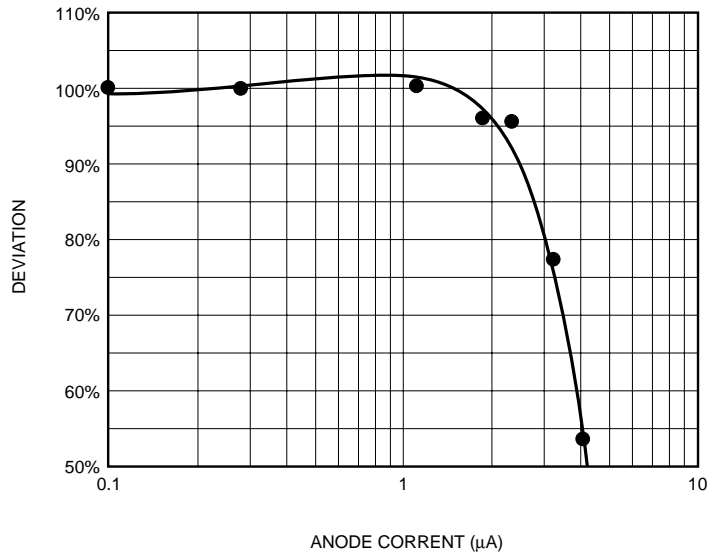
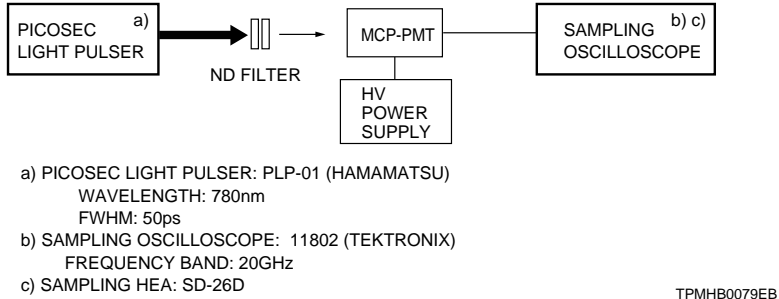


Figure 4-6 (b): Saturation characteristics of MCP-PMT (R3809U-05) in DC operation

## (2) Pulse gain saturation characteristics (pulse linearity)

When pulsed light in an extremely short duration enters the MCP-PMT, the output linearity can be maintained to some extent. Figure 4-7 shows the linearity data of an MCP-PMT when it detects pulsed light.



**Figure 4-7 (a): Block diagram for MCP-PMT pulse linearity measurement**

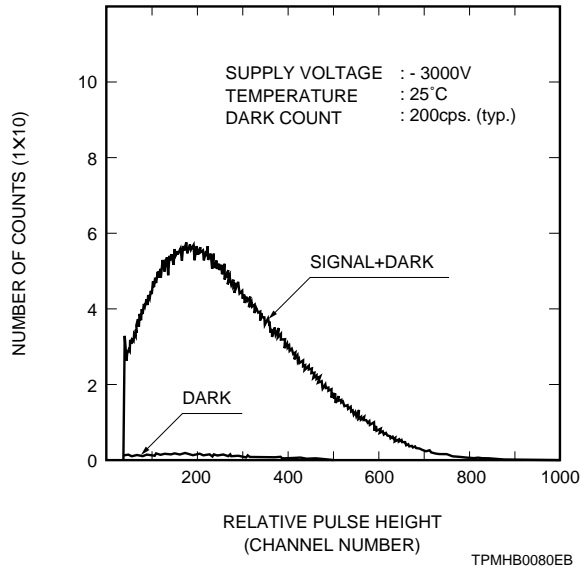
### **Figure 4-7 (b): Typical pulse linearity of an MCP-PMT (R3809U-50)**

Figure 4-7 (a) shows a block diagram for measuring pulse linearity. A picosecond light pulser (Hamamatsu PLP-01) is used as the light source. The intensity of the pulsed light is adjusted by ND (neutral density) filters and input to the MCP-PMT. Figure 4-7 (b) shows a typical pulse linearity plot for a proximity-focused MCP-PMT measured at a pulse repetition rate of 300Hz to 30kHz. Pulse currents up to 350 milliamperes can be extracted at a repetition rate of 300Hz or less. The maximum pulse current at a low repetition rate is determined by the product of the number of electrons released from one channel governed by space charge effects and the number of MCP channels. On the contrary, the maximum pulse current at a high repetition rate is determined by the ratio of the strip current to the total amount of charge which is the product of the charge per pulse and the repetition rate.

When the repetition rate is too high, the MCP gain begins to drop because the next pulse enters within the dead time, causing the output saturation.

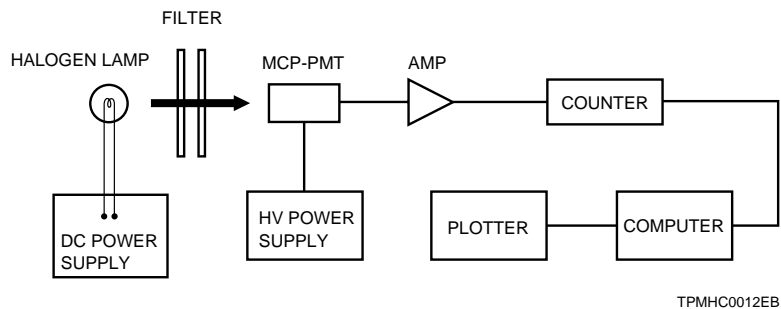
### (3) Saturation gain characteristics in photon counting mode

Figure 4-8 shows pulse height distributions of photoelectron signals and dark current pulses taken with an MCP-PMT in the photon counting mode. Since the MCP is operated in the saturation range, a distinct pulse height distribution for the signals is obtained.



**Figure 4-8: Typical pulse height distribution in single photon counting**

Figure 4-9 illustrates a block diagram for measuring the count-rate pulse linearity in photon counting. Light intensity is reduced by neutral density filters down to the single photoelectron level. The number of single photoelectron pulses is counted by the counter circuit connected to the MCP-PMT, and the count rate is measured and plotted while changing the number of incident photons.



**Figure 4-9: Block diagram for measuring count-rate linearity in photon counting mode**

Figure 4-10 shows count-rate linearity data measured in photon counting mode. A good linearity is maintained up to  $10^7$  counts/second (cps).

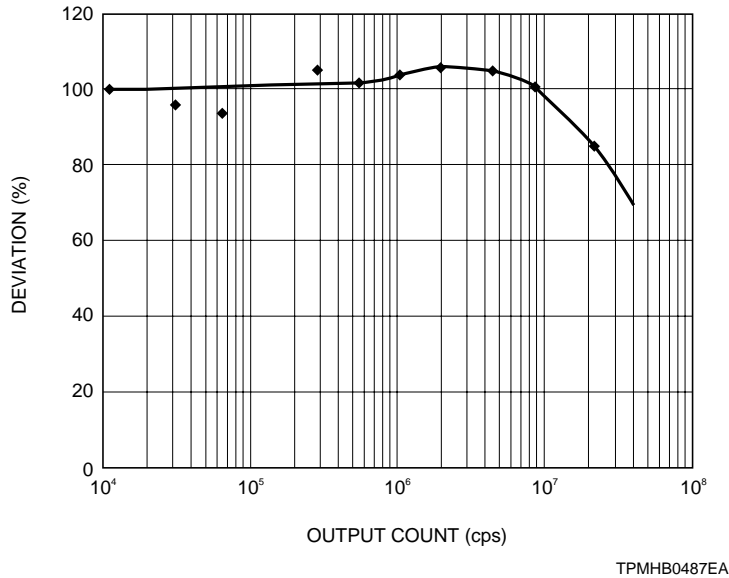


Figure 4-10: MCP-PMT (R3809U-50) count-rate linearity in photon counting mode

#### 4. 2. 4 Time characteristics<sup>2)</sup>

As discussed in the previous chapter on photomultiplier tube time characteristics, the signal pulse broadens along time in the multiplication process from the photocathode to the anode. This is due to the emission-angle distribution and initial-velocity distribution of photoelectrons and secondary electrons, as well as the effects of the accelerating lens. Since MCP-PMTs employ an MCP in place of conventional dynodes, the electron transit time in the secondary electron multiplication process is very short, thus resulting in a significant improvement in the transit time spread. In addition, because a nearly parallel electric field is applied between the photocathode, MCP and anode, the emission-angle distribution and initial-velocity distribution of photoelectrons can be virtually ignored.

##### (1) Rise/fall times

The rise and fall times of an MCP-PMT are evaluated from the output waveform when the MCP-PMT detects a light pulse whose width is sufficiently short compared to the time response of the MCP-PMT. These parameters are especially important when observing the waveform of ultra-short pulsed light. For the measurement method, refer to Section 3.3.1, "Time characteristics". Figure 4-11 shows an actual waveform obtained with an MCP-PMT.

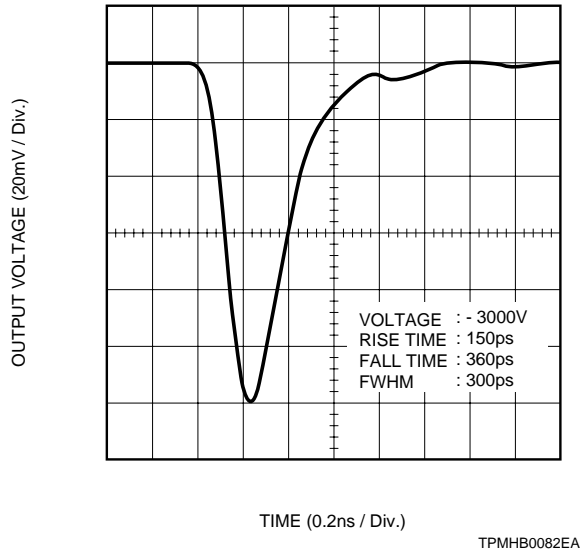


Figure 4-11: Pulse response waveform of MCP-PMT (R3809U-50)

## (2) Transit time

The transit time is the time delay between the input of a light pulse at the photomultiplier tube and the appearance of the output pulse from the photomultiplier tube. For the measurement method, refer to Section 3.3.1, "Time characteristics".

## (3) TTS (transit time spread)

When a light pulse enters an MCP-PMT, the photocathode converts the light energy into an electron pulse which travels to the anode while being multiplied. The transit time of each pulse differs depending on each event. The distribution of this transit time is referred to as the transit time spread or TTS. The TTS of an MCP-PMT is measured with the incident light intensity reduced down to single photon levels. The TTS is an important parameter, especially in the time-correlated photon counting technique<sup>3)</sup> where the measurement of timing is of prime consideration. For the measurement method, refer to Section 3.3.1, "Time characteristics".

At Hamamatsu Photonics, TTS is evaluated with the measurement system shown in Figure 4-12. In this system, the IRF (instrument response function) value is measured as the time characteristic for the entire system including the MCP-PMT. This is because the measurement system uses a laser pulse with approximately 35 picosecond pulse width, which act as a time jitter equal to the TTS of the MCP-PMT. The relation between the TTS and IRF is given by the following equation.

$$(\text{IRF})^2 = (\text{TTS})^2 + \text{Tw}^2 + \text{Tj}^2$$

TW : laser pulse width

Ti : other time jitter in the measurement system

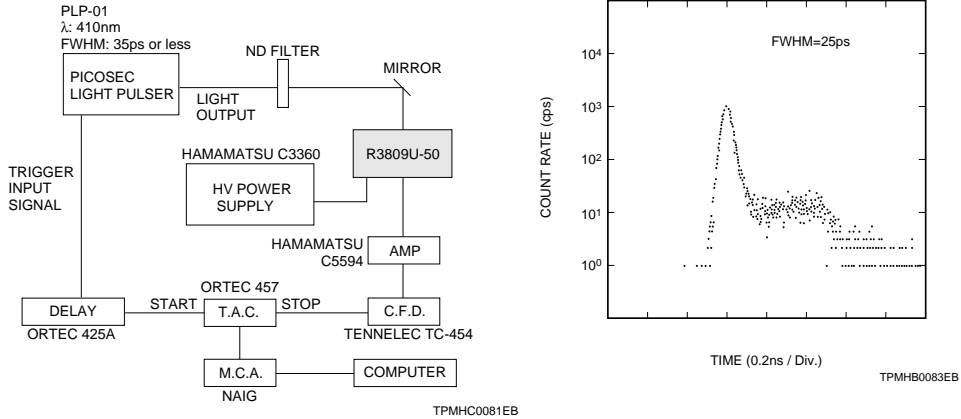


Figure 4-12: IRF measurement using MCP-PMT (R3809U-50)

To evaluate the TTS of an MCP-PMT more accurately, the measurement system shown in Figure 4-13 is used and excellent data of 25.0 picoseconds has been obtained. This system uses a laser pulse with a 5 picosecond pulse width which is shorter than the TTS of the MCP-PMT, therefore enabling accurate measurements.

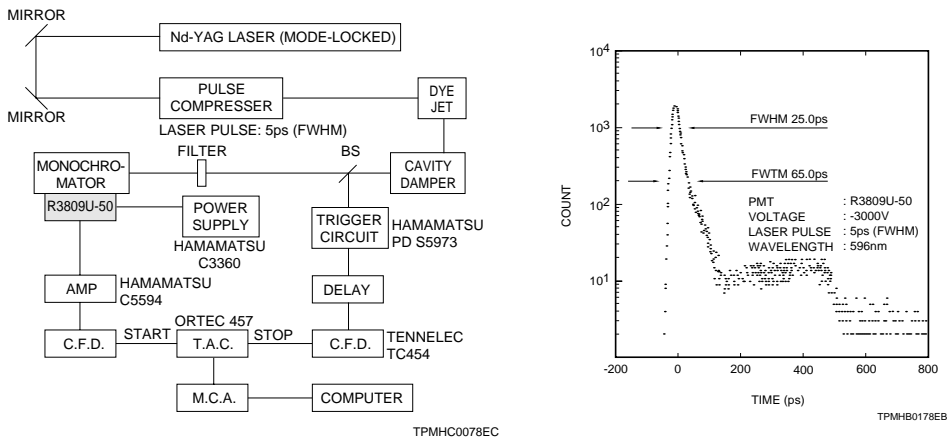


Figure 4-13: Accurate TTS measurement of MCP-PMT (R3809U-50)

**(4) Cathode transit time difference**

In most photomultiplier tubes, the electron transit time differs with the position of photocathode illumination. When the entire photocathode is uniformly illuminated, the difference in transit time with respect to position is referred to as the cathode transit time difference or CTTD. The CTTD usually affects the TTS, but in the case of proximity-focused MCP-PMTs, it has little effect on the TTS. For the measurement method, refer to Section 3.3.1, "Time characteristics".

**(5) Time characteristics of various products**

Time characteristics of various MCP-PMTs are summarized in Table 4-1 below. The less the number of MCP stages and the smaller the channel diameter, the better the time characteristics. Compared to conventional MCP-PMTs using 12mm channel MCPs, the R3809U series using 6mm channel MCPs has improved the rise time by 70 picoseconds and the IRF by 25 picoseconds. The fall time does not show a correlation with the rise time. This is probably due to the difference in electrostatic capacity between the

MCP and the anode. The gated MCP-PMT is slightly inferior in time characteristics compared to other types. This is presumably because the electric field between the gate mesh and the cathode is weak so that the photoelectron emission angle and initial velocity distribution tend to affect the time characteristics adversely to some extent.

| MCP-PMT Type No                | Rise Time | Fall Time | Transit Time | IRF (FWHM) |
|--------------------------------|-----------|-----------|--------------|------------|
| R3809U-50 (6 $\mu$ m/2-stages) | 150ps     | 360ps     | 400ps        | 45ps       |
| R5916U-50 (6 $\mu$ m/2-stages) | 180ps     | 700ps     | 350ps        | 95ps       |
| R7024U (6 $\mu$ m/2-stages)    | 110ps     | 120ps     | 400ps        | –          |

**Table 4-1: Comparison of MCP-PMT time characteristics**

Here, let us introduce the R7024 MCP-PMT which offers significant improvements in rise and fall times. The structure of the R7024 is shown in Figure 4-14. This tube has been developed specifically for use in ultra-fast photometry. A mesh electrode is provided between the MCP and the anode as shown in the figure, and the signal output method differs from ordinary MCP-PMTs. The mesh between the MCP and the anode cancels out the displacement current generated at the time that the secondary electrons emitted from the MCP are accelerated towards the anode. Figure 4-15 shows a typical output waveform from the R7024. Ultrafast time response with 110 picosecond rise time and 120 picosecond fall time is obtained.

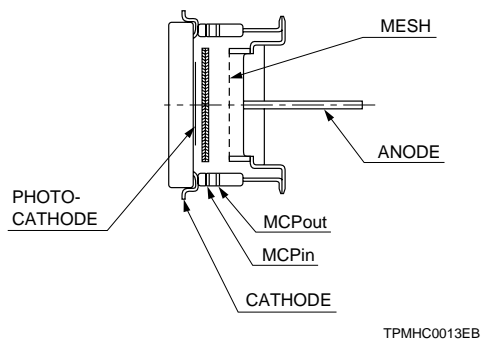


**Figure 4-14: Structure of the R7024**

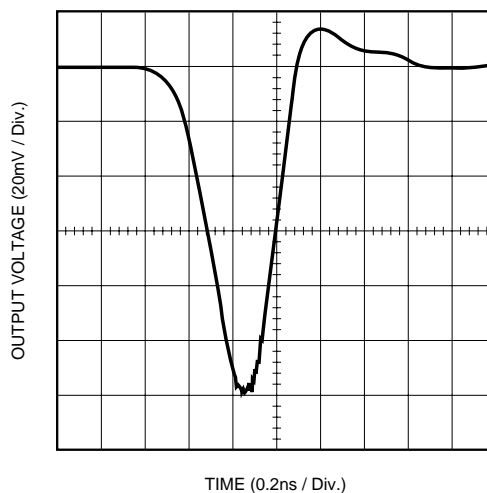


**Figure 4-15: Time response waveform of the R7024U**

### 4. 2. 5 Magnetic characteristics<sup>2)</sup>

As stated in the section on photomultiplier tubes designed for use in highly magnetic environments, the following points are essential to improve magnetic characteristics.

- (1) The distance between the photocathode, dynodes and anode should be shortened to minimize the electron transit distance.
- (2) The electrodes should be designed to apply a parallel electric field from the photocathode to the anode so that the secondary electrons do not converge but travel in parallel to the tube axis.
- (3) A high electric field intensity should be applied.

The MCP-PMT meets all the above requirements and thus provides superior magnetic characteristics. Figure 4-16 shows typical magnetic characteristics of an MCP-PMT. The extent of the effect of a magnetic field on the output depends on the direction of the magnetic field with respect to the MCP axis. In magnetic fields parallel to the tube axis, the MCP-PMT can operate at up to 2.0 Tesla (20 kilogausses), but in magnetic fields perpendicular to the tube axis, the output drops drastically if fields exceed 0.07 Tesla (700 gauss).

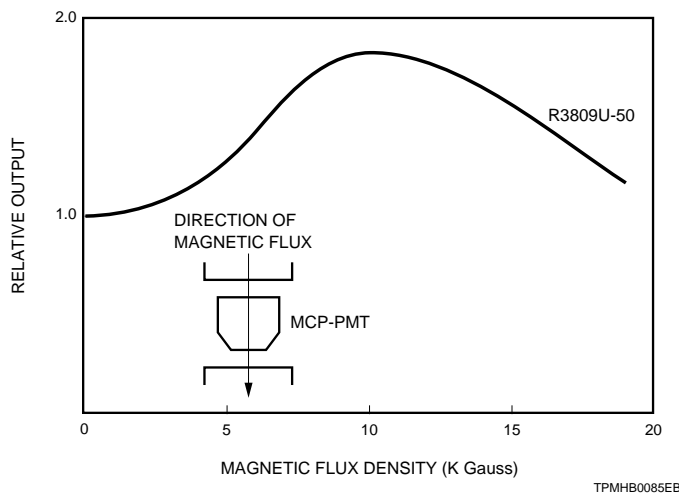


**Figure 4-16 (1): Typical magnetic characteristics of an MCP-PMT  
(in magnetic fields parallel to tube axis)**

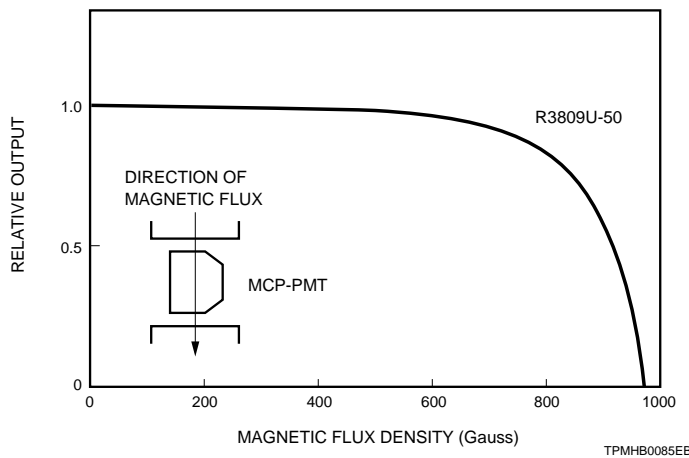


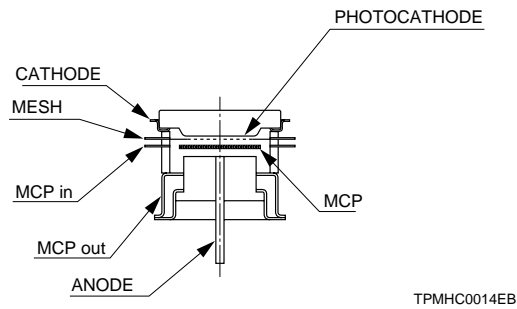
**Figure 4-16 (2): Typical magnetic characteristics of an MCP-PMT  
(in magnetic fields perpendicular to tube axis)**

### 4.3 Gated MCP-PMT<sup>2)</sup>

In applications in fields such as fluorescence lifetime measurement, laser Raman spectroscopy, and laser radar, photodetectors with a gate function are often required for more precise measurements. The gate function should have the following performance characteristics:

- (1) Highest possible gating speed
- (2) Large switching ratio (gate on/off ratio)
- (3) Low switching noise

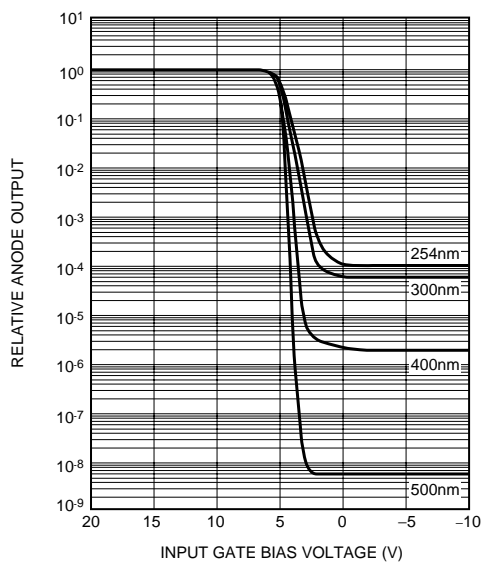
Figure 4-17 illustrates the structure of a gated MCP-PMT (R5916U-50). This tube basically consists of a photocathode, gate mesh, MCP and anode. The gating function is performed by controlling the gate mesh which is positioned in close proximity to the photocathode as shown in Figure 4-17. Applying a reverse potential with respect to the photocathode potential to the gate mesh sets the "off" mode, while applying a forward potential sets the gate operation "on" mode.



TPMHC0014EB

**Figure 4-17: Structure of an MCP-PMT with gate mesh**

Figure 4-18 shows the basic characteristic of the gate function for a typical switching ratio taken with a gated MCP-PMT operating under static conditions. This data was measured with the photocathode potential maintained at 0 volts and proves that the switching ratio is better than  $10^{-8}$  (incident light wavelength: 500 nanometers).



TPMH0244EA

**Figure 4-18: Switching ratio characteristic under static operating conditions**

Figure 4-19 shows the dynamic gate performance obtained with a gated MCP-PMT when a gate pulse is applied while continuous light is allowed to strike the tube. The gate operation starts in as little as one nano-second.

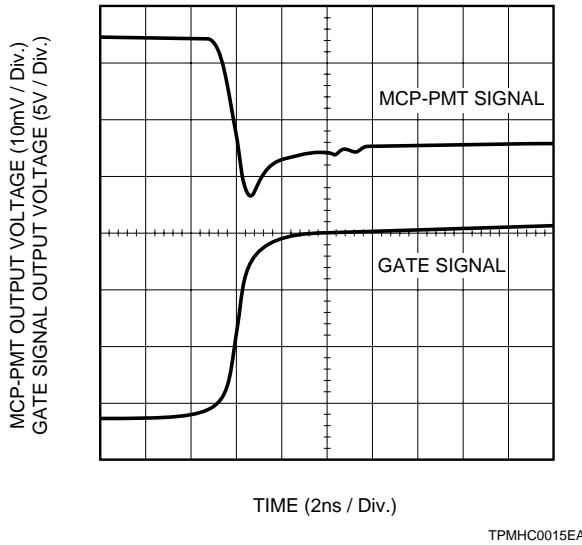


**Figure 4-19: Dynamic gate characteristic**

As explained above, the gated MCP-PMT offers significant improvement in gate speed and switching ratio in comparison with conventional photomultiplier tubes.

### 4.4 Multianode MCP-PMT<sup>4)</sup>

The previous sections mainly discussed MCP-PMTs having a single anode. A variety of MCP-PMTs with independent multianodes have been developed and utilized in practical use. These multianode MCP-PMTs offer simultaneous, two-dimensional (or one-dimensional) detection as well as fast response speed and low-light-level detection. The structure of a typical multianode MCP-PMT is illustrated in Figure 4-20.

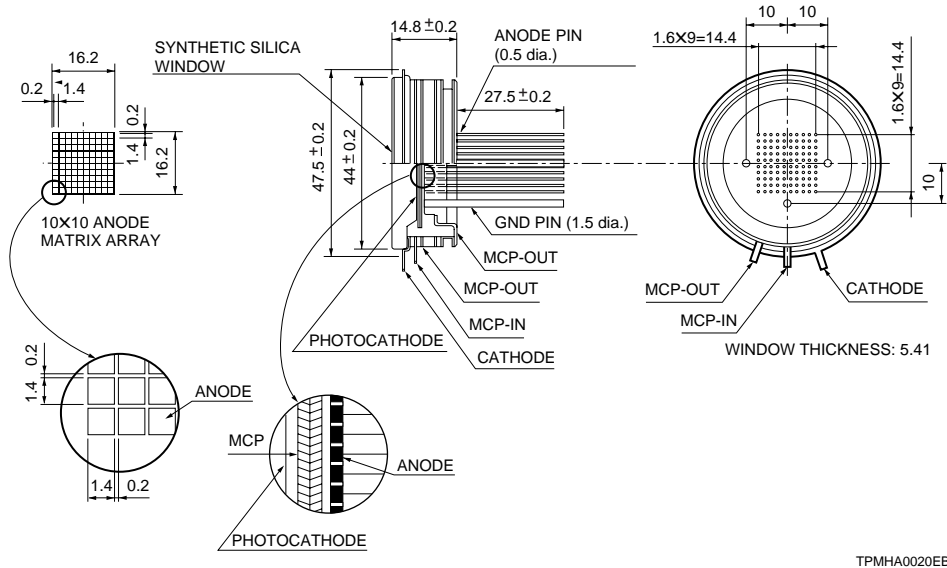


Figure 4-20: Multianode MCP-PMT with 10X10 anode format

Figures 4-21 (a) to (c) show the spatial resolutions of various multianode MCP-PMTs. These consist of the output profile of each anode when a light spot of approximately 20μm diameter is scanned over the photocathode.

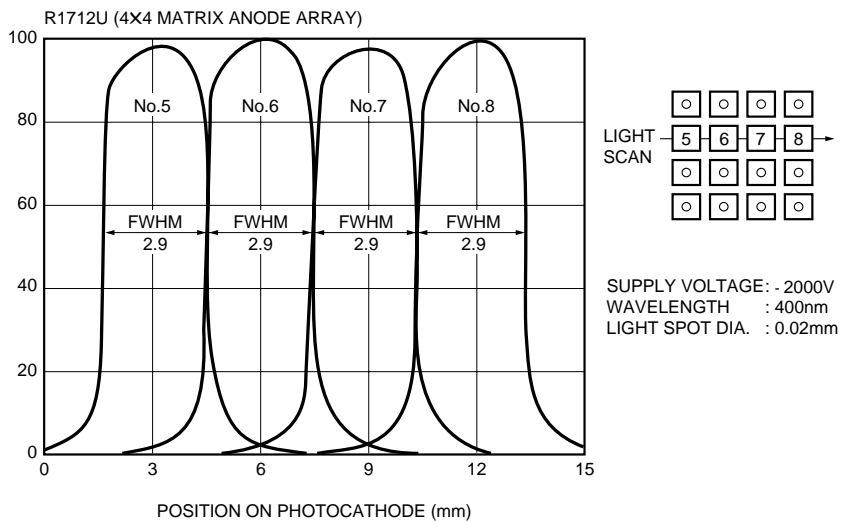


Figure 4-21 (a): Spatial resolution of 454 multianode MCP-PMT

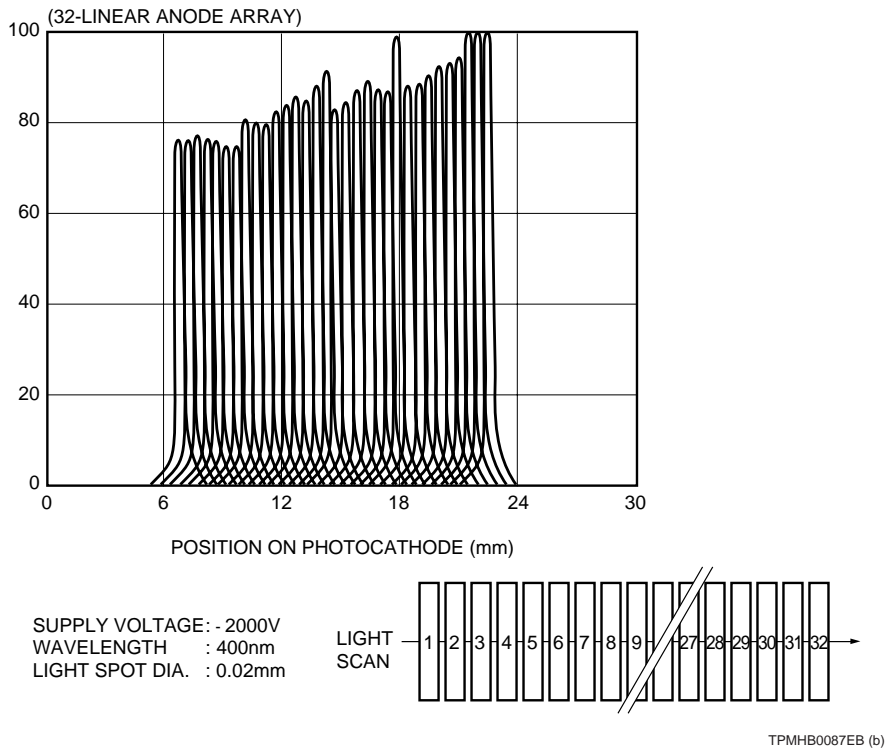


Figure 4-21 (b): Spatial resolution of 32-linear array multianode MCP-PMT

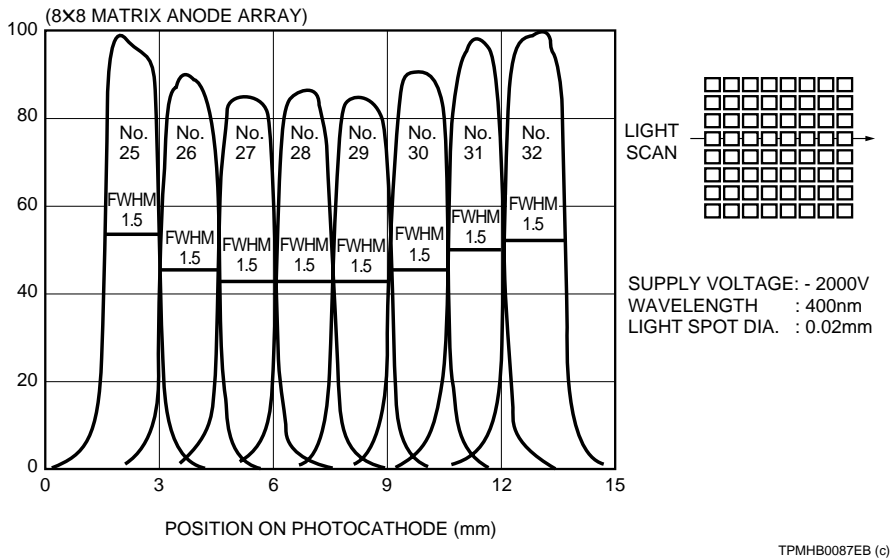


Figure 4-21 (c): Spatial resolution of 858 multianode MCP-PMT

The following applications are possible by making use of the advantages of multianode MCP-PMTs.

- (1) Simultaneous, two-dimensional detection of a luminous body which is spatially spread at low light levels
- (2) Simultaneous, multichannel time-resolved spectroscopy using optical fibers
- (3) Multichannel readout from scintillating fibers

As listed in Table 4-2, the family of multianode MCP-PMTs includes a 4X4 matrix anode type, 8X8 matrix anode type, 10X10 matrix anode type, and a 32 linear anode type. Furthermore, multianode MCP-PMT assemblies equipped with connectors and cables are available. The anode configurations listed in Table 4-2 are just typical examples. Other anode configurations and the number of anodes are also available upon request.

| Type No        | Anode Format     | Type No        | Anode Format       |
|----------------|------------------|----------------|--------------------|
| R4110U-XX-M016 | 4X4 matrix anode | R4110U-XX-M100 | 10X10 matrix anode |
| R4110U-XX-M064 | 8X8 matrix anode | R4110U-XX-L032 | 32-linear anode    |

**Table 4-2: Examples of multianode MCP-PMTs**

## References in Chapter 4

- 1) Hamamatsu Photonics Technical Information: MCP assembly, No.TMCP9001E01
- 2) Hamamatsu Photonics Catalog: Ultrafast MCP-PMT R3809U (FEB. 1992).  
Hamamatsu Photonics Catalog: Microchannel Plate - Photomultiplier Tubes (MCP-PMTs), No.T-112-02 (FEB. 1990)  
H. Kume et al.: Ultrafast Microchannel Plate - Photomultiplier Tubes, Applied Optics, Vol. No. 27 (Mar. 15, 1988).
- 3) Hamamatsu Photonics Technical Information: Applications of MCP-PMTs to Time Correlated Single Photon Counting and Related Procedures. No. ET-03 (FEB. 1991).  
Desmond V. O'connor, David Phillips: Time-Correlated Single Photon Counting, Academic Press (Harcourt Brace Jovanovich, Publishers), The Royal Institution, London, UK.
- 4) Hamamatsu Photonics Catalog: Multianode MCP-PMT Series, No.T-1000 (FEB. 1989).

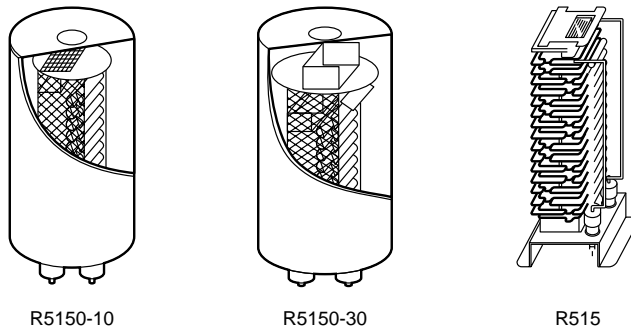
# **CHAPTER 5 ELECTRON MULTIPLIER TUBES**

*Electron multiplier tubes (EMT) are mainly used in various models of mass spectrometers<sup>1)2)3)</sup> for detection of ions, electrons, soft X-rays, and vacuum ultraviolet (VUV) radiation.*

## 5.1 Electron Multiplier Tubes

### 5.1.1 Electron multiplier tube structure

The structure of an electron multiplier tube is basically identical with the dynode assembly and anode used in a photomultiplier tube. The actual details of the structure differ depending on the materials to be detected and the equipment in which the electron multiplier tube is installed. (See Figure 5-1.)



TEMC0018EA



**Figure 5-1: Electron multiplier tube structure**

An electron multiplier tube is operated in a vacuum, and the ions, electrons, VUV radiation, or soft X-rays to be detected are guided so as to enter the first dynode. The first dynode excited by such particles or radiation emits secondary electrons or photoelectrons. These generated electrons are multiplied in a cascade just as is done in a photomultiplier tube and finally reach the anode. In most electron multiplier tubes, voltage-divider resistors are incorporated to supply an optimum voltage between each dynode.

### 5.1.2 Composition of the secondary emissive surface

The dynodes of electron multiplier tubes are made of copper containing several percent beryllium. The surface of these copper-beryllium electrodes is activated and a thin film of beryllium oxide is formed on the dynode structure, which emits secondary electrons in response to ions, electrons, VUV radiation and X-rays. This beryllium oxide layer is chemically very stable. Even if exposed to air, it provides stable characteristics with extremely low deterioration.

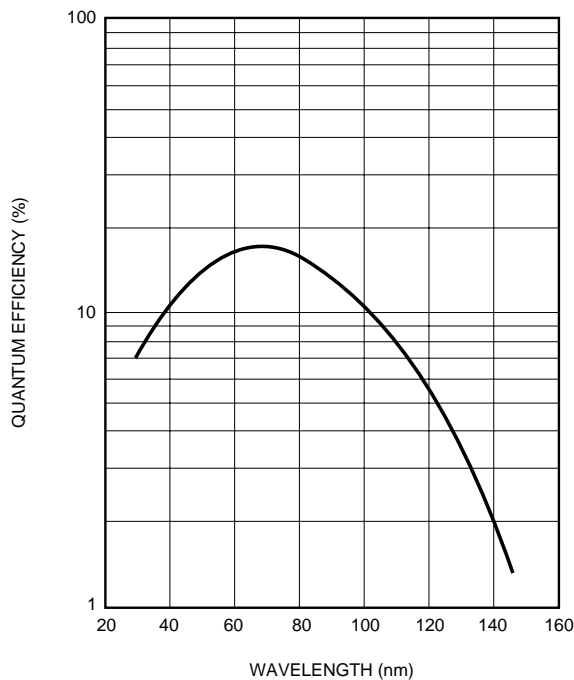
### 5.1.3 Dynode types

Three kinds of dynodes of box-and-grid, linear-focused and mesh types are commonly used for electron multiplier tubes. (See 3.2.) The number of dynode stages is usually from 15 to 25 depending on the required gain.

## 5.2 Characteristics of Electron Multiplier Tubes

### 5.2.1 First dynode sensitivity

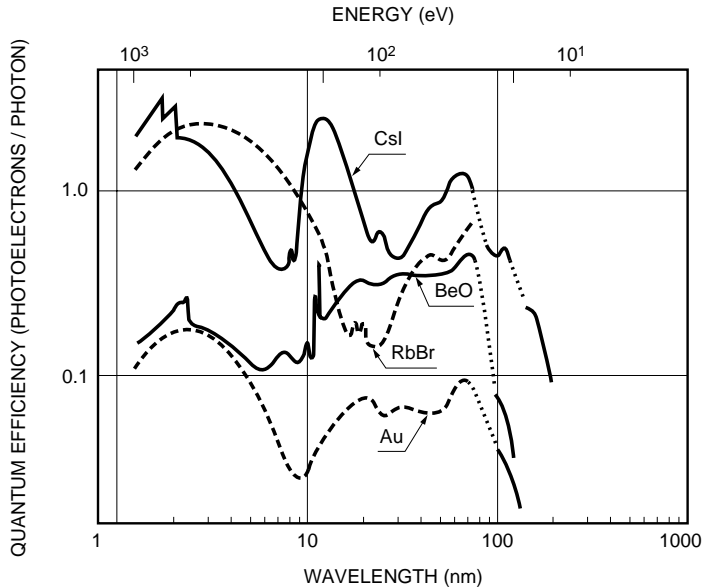
Beryllium oxide (BeO) widely used in the first dynode of electron multiplier tubes is sensitive to soft X-ray to ultraviolet radiation at nearly 300 nanometers. Electron multiplier tubes are effectively used in a wavelength range shorter than the cutoff wavelength of the MgF2 window (approximately 115 nanometers). A typical spectral response for beryllium oxide is shown in Figure 5-2, covering a range from 30 to 140 nanometers.



TEMB0012EA

Figure 5-2: Spectral response characteristic of beryllium oxide

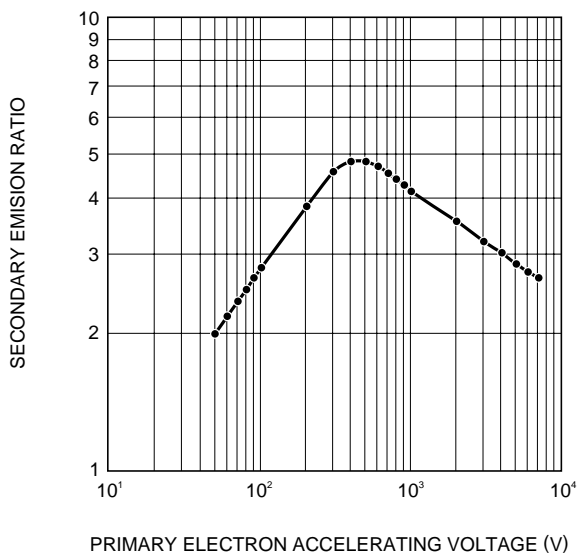
Various spectral response characteristics are available by replacing the first dynode with another type evaporated with a substance optimized for the target wavelength range and operating conditions. Figure 5-3 shows typical spectral response characteristics of beryllium oxide (BeO), cesium iodide (CsI), rubidium bromide (RbBr) and gold (Au) used for the first dynode.



TEMB0013EA

**Figure 5-3: Spectral response characteristics of various evaporative substances**

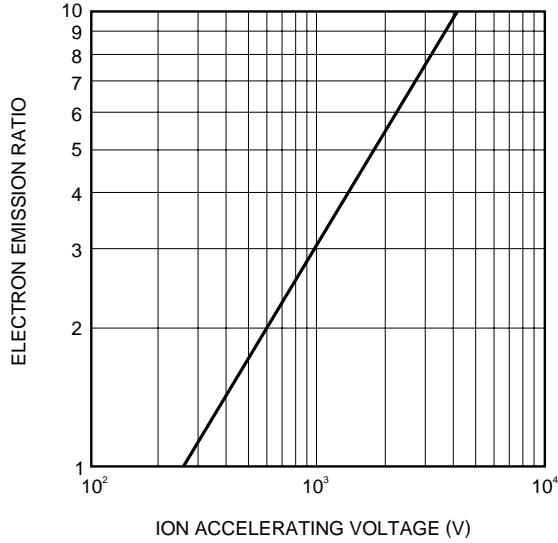
The first dynode of electron multiplier tubes is sensitive to electrons with energy, such as Auger electrons, secondary electrons and reflected electrons. (See 2.3.) Since beryllium oxide has a high work function, the high secondary electron emission ratio is much lower than that obtained with alkali-antimonide used for photomultiplier tube dynodes. Figure 5-4 shows typical secondary emission ratio versus primary electron accelerating voltage. The secondary emission ratio peaks at a primary electron accelerating voltage of about 400 volts.



TEMB0031EA

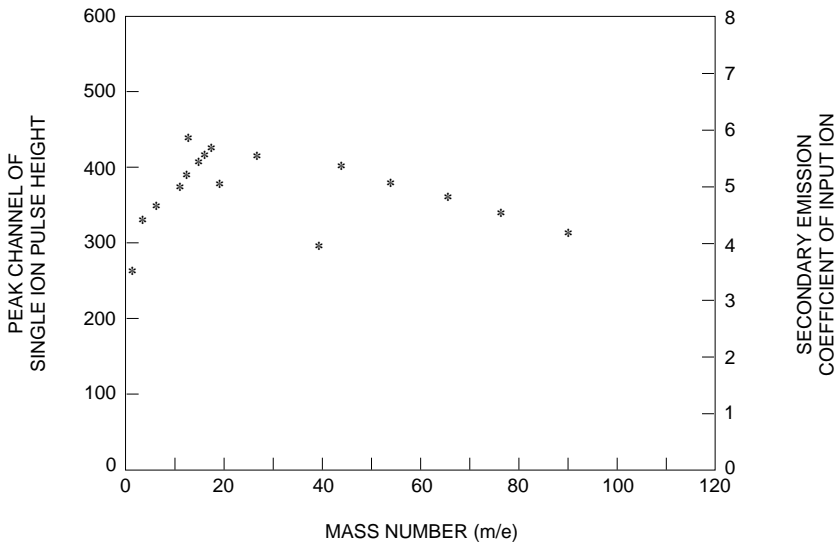
**Figure 5-4: Secondary emission ratio vs. primary electron accelerating voltage for beryllium oxide**

The first dynode of electron multiplier tubes is also sensitive to ions. Typically, several electrons are emitted in response to one ion, although this ratio depends slightly on the state of the secondary electron emissive surface on the first dynode. The number of emitted electrons is also affected by the molecular weight ( $m/e$ ) and ion accelerating voltage. Figure 5-5 shows the relation between the electron emission ratio and the accelerating voltage for nitrogen ion. In Figure 5-6, typical electron emission ratios at an accelerating voltage of 200 volts are plotted along various kinds of ions.



TEMB0032EA

Figure 5-5: Electron emission ratio vs. accelerating voltage for nitrogen ion



TEMB0011EA

Figure 5-6: Electron emission ratios for various kinds of ions at 200V accelerating voltage

### 5.2.2 Gain

As in the case of photomultiplier tubes, the current amplification or gain ( $\mu$ ) of an electron multiplier tube is theoretically expressed as follows. (See also 3.2.)

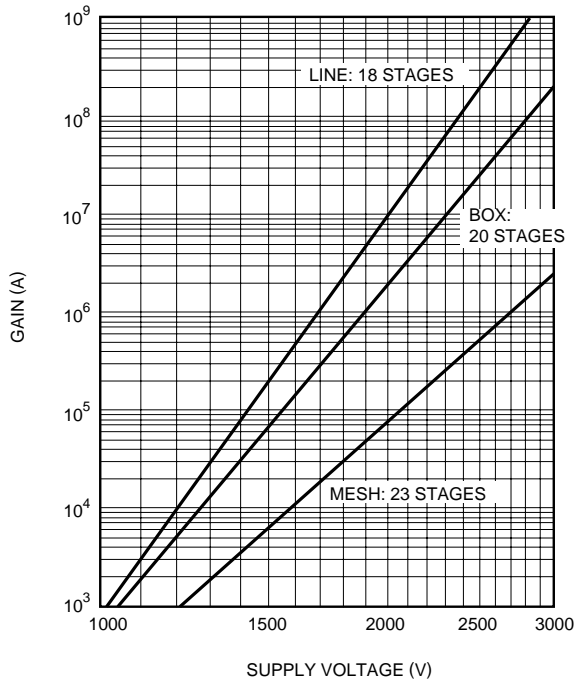
$$\text{Gain } (\mu) = A \cdot E_{bb}^{kn} \dots\dots\dots (\text{Eq. 5-1})$$

$E_{bb}$ : supply voltage

$k$  : constant determined by electrode structure and material

$n$  : number of dynode stages

It is clear from this equation that the gain  $\mu$  is proportional to the  $kn$ -th power of the supply voltage. Typical gain versus supply voltage characteristics are plotted in Figure 5-7. Since this graph is on logarithmic scales, the slope of each straight line indicates  $kn$ .



TEMB0033EA

Figure 5-7: Gain versus supply voltage characteristics

### 5.2.3 Dark current and noise

The secondary electron emissive surface of the dynodes used for electron multiplier tubes has a high work function and therefore exhibits exceptionally low dark current. Even so, small amounts of dark current may be generated by the following factors:

1. Thermionic emission current from the secondary electron emissive surface
2. Leakage current from electrode support materials
3. Field emission current

The dark current of an electron multiplier tube is very low. It is usually less than one picoampere when operated at a supply voltage providing a gain of  $10^6$ .

In ion detection, a sample is ionized by thermal electrons generated from the filament of a lamp such as tungsten lamp. This filament also emits ultraviolet rays and X-rays which then enter the electron multiplier tube along with sample ions. The signals generated by these extraneous rays do not originate from the electron multiplier tube itself. However, they must be handled as noise just like noise of other detectors.

To reduce noise caused by ultraviolet rays and X-rays, some types of electron multipliers have a shield plate above the first dynode, in order to allow only sample ions to enter the first dynode. This design is often called the "off-axis structure". Figure 5-8 shows noise measured with an electron multiplier tube with the off-axis structure. The signal at a molecular weight of 5 (m/e), where no ions exist, appears as noise. This noise level is nearly equal to the intrinsic noise of the electron multiplier tube.

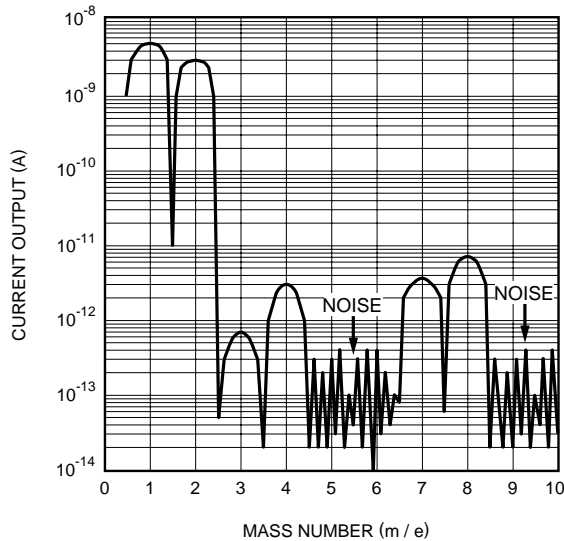


**Figure 5-8 Filament noise measured with an electron multiplier tube with the off-axis structure**

Because electron multiplier tubes are used in a vacuum, the noise level also depends on the vacuum level. Generally, the higher the vacuum level (for example,  $10^{-5}$  Pa), the less the noise will be. In contrast, the noise increases as the vacuum level degrades. Figure 5-9 shows the relation between the noise count and the vacuum level at which an electron multiplier is operated.

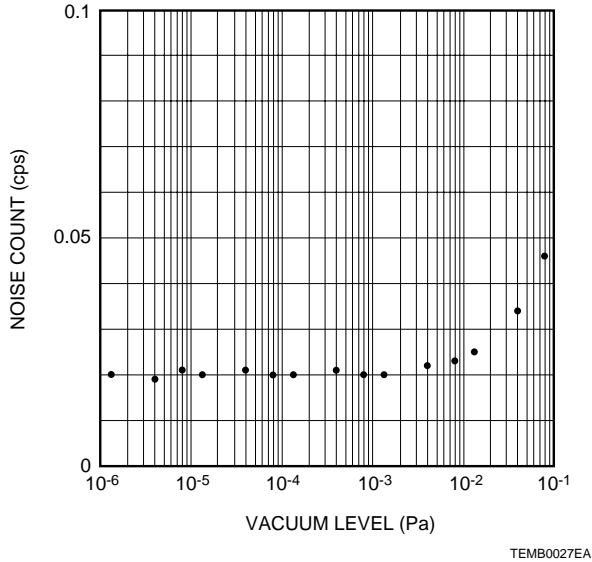


Figure 5-9: Noise count versus vacuum level for typical electron multiplier tube

## 5.2.4 Pulse counting

In applications where high sensitivity is required, the pulse counting technique which counts the number of output pulses is frequently utilized. The principle and advantages of this technique are almost identical with the photon counting technique. (Refer to Section 3.4.) Figure 5-10 shows typical pulse height distribution measured with nitrogen single ions, etc.

As stated previously, the secondary surface of the dynodes used for electron multiplier tubes is made of beryllium oxide (BeO) having a high work function. The dark count is therefore suppressed as low as 0.01 counts per second.

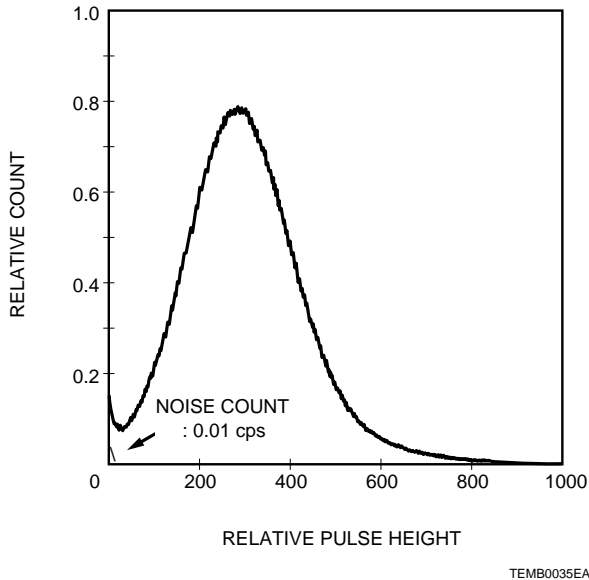
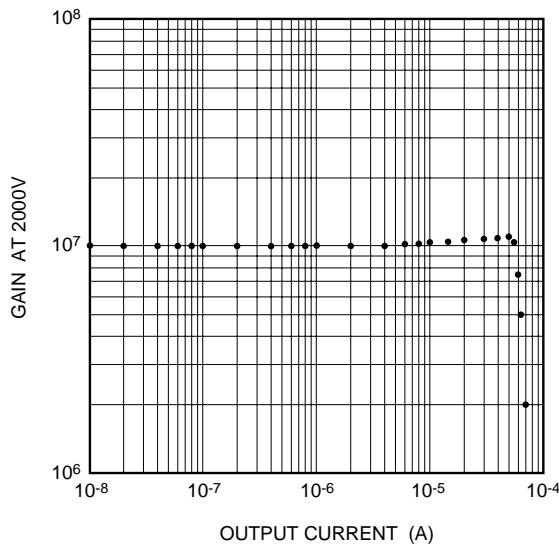


Figure 5-10: Pulse height distribution measured by input of UV, electrons and nitrogen ions

### 5.2.5 Linearity

Electron multiplier tubes usually incorporate voltage-divider resistors between each successive dynode. This resistor is about 1 megohm per stage, so the total resistance comes to 20 megohms. The value of a linear output current is limited by the voltage-divider current flowing through these voltage-divider resistors. (See Section 7.1.)

Figure 5-11 shows a linearity plot of an electron multiplier tube operated in DC mode. As the output current increases, the gain abruptly drops after increasing slightly. This is a typical pattern for linearity dependent on the voltage-divider current. The linearity can be improved by applying a higher voltage or reducing the total value of the voltage-divider resistors in order to increase the voltage-divider current. To suppress the undesired increase in the gain which tends to occur when the output current becomes large, the resistor value between the last stage and ground should be made smaller.



TEMB0026EA

**Figure 5-11: Linearity of typical electron multiplier tube in DC operation**

In general, the linearity in pulse counting mode is determined by the electron multiplier tube performance and the pulse pair resolution of the signal processing circuit. (See 3.4.) To maintain high pulse count linearity, it is necessary to use an electron multiplier tube having linear focused dynodes with high-speed response.

### 5.2.6 Life characteristics

The life of electron multiplier tubes is affected by the gain, output current and operating vacuum level. Two factors that cause gain deterioration are:

1. Sensitivity deterioration in the first dynode by input ions
2. Dust deposition on the secondary electron emissive surface

Figure 5-12 shows typical life characteristics for an electron multiplier tube. This is the supply voltage change required to maintain a preset gain measured with the amount of input ions and output current kept constant. As can be seen, the supply voltage increases as the accumulated output charge increases.

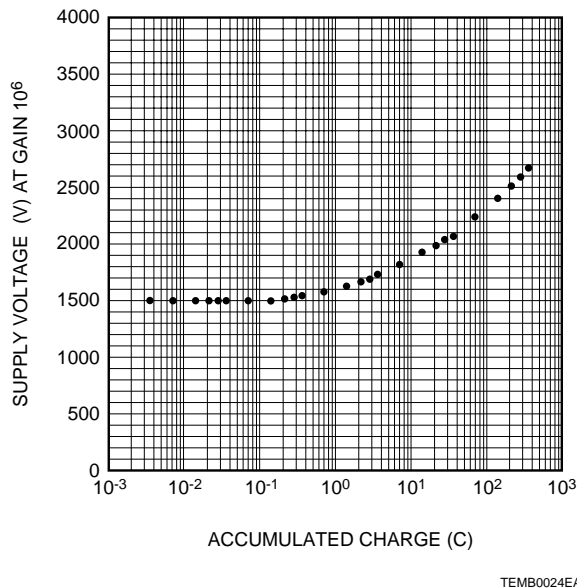


Figure 5-12: Typical life characteristics for gain of an electron multiplier tube

### References in Chapter 5

- 1) S. Araki: Mass Spectroscopy, 3rd Edition, Modern Chemistry Series 2, Tokyo Chemical Coterie.
- 2) M. Tsuchiya, M. Ohashi, T. Ueno: New Development of Mass Spectrometry, Modern Chemical, Extra Number 15, Tokyo Chemical Coterie.
- 3) T. Ueno, K. Hirayama, K. Harada: Biological Mass Spectrometry, Modern Chemical, Extra Number 31, Tokyo Chemical Coterie.

# **CHAPTER 6**

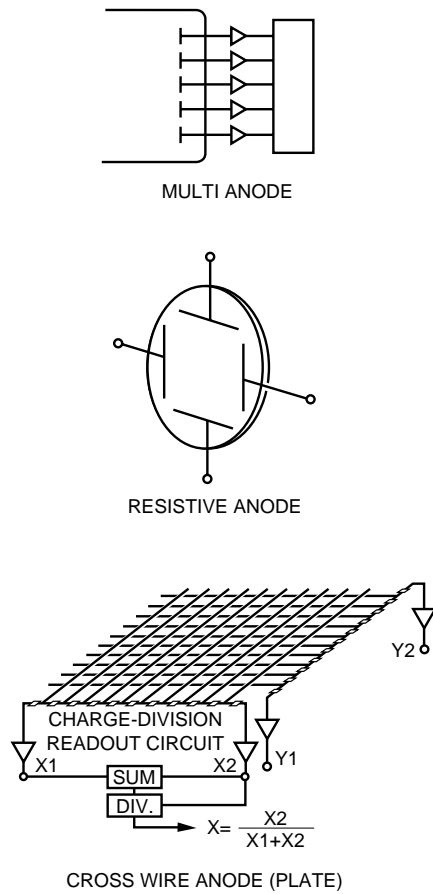
## **POSITION-SENSITIVE PHOTOMULTIPLIER TUBES**

*Applicability of photomultiplier tubes to low-light-level measurement greatly relies on the current multiplication mechanism offered by dynodes. As explained earlier, there are various types of dynode structures available for different photometric purposes.*

*Popular dynode structures are the box-and-grid type, linear-focused type, circular-cage type and venetian-blind types. Furthermore, the MCP (microchannel plate) is now in use as a dynode with high-speed response.*

*Two new dynode structures are introduced in this chapter: the "metal channel dynode"<sup>1) 2) 3)</sup> and "fine mesh dynode".<sup>4) 5) 6)</sup> These dynodes provide wide dynamic range, high gain and high position resolution, and are currently used in position-sensitive photomultiplier tubes.*

*Common methods of reading out the output electron bunch from a position-sensitive photomultiplier tube are illustrated in Figure 6-1. In a multianode, the output signal is read out from independent multiple anodes. The resistive anode has a uniformly distributed resistive layer that allows reading out the signal by means of center-of-gravity detection. The cross-wire (or plate) anode reads out the signal by means of current or charge-dividing center-of-gravity detection.*



TPMHC0054EA

**Figure 6-1: Anode output readout methods for position-sensitive photomultiplier tube**

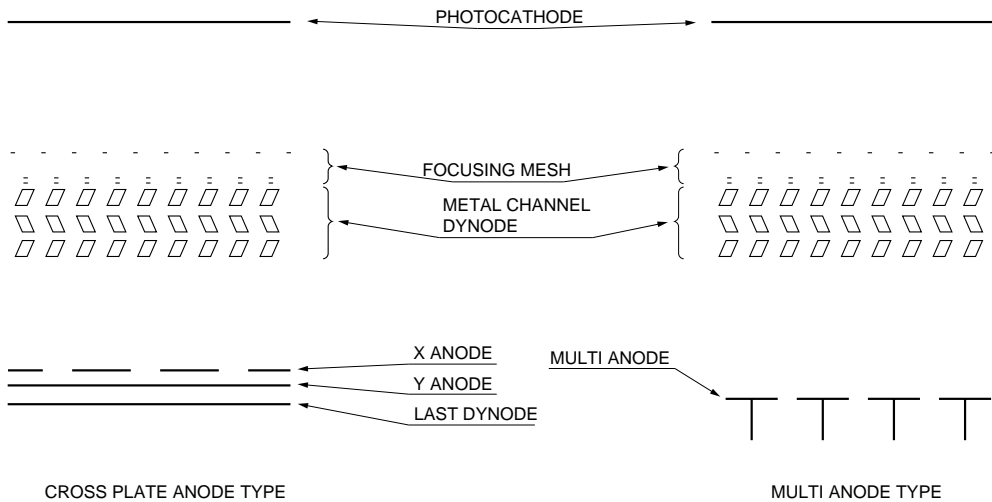
*The following sections describe position-sensitive photomultiplier tubes using "metal channel dynodes combined with a cross-plate anode", "metal channel dynodes combined with a multianode" and "fine mesh dynodes combined with a multianode"*

## 6.1 Position-Sensitive Photomultiplier Tubes Using Metal Channel Dynodes

### 6.1.1 Structure and characteristics

Figure 6-2 shows the electrode structure and electron trajectories in metal channel dynodes. One of the outstanding features offered by the metal channel dynode is very low crosstalk between multiple anodes. After photoelectrons are emitted from the photocathode, they are directed onto the first dynode by the focusing grid and then flow to the second dynode, third dynode, . . . last dynode and finally to the anode, while being multiplied with a minimum spatial spread of the electron flow. Therefore, position data is precisely maintained through the cascade multiplication process.

In addition, the overall length of the tube can be kept short because metal channel dynodes are very thin and assembled in close-proximity to each other.

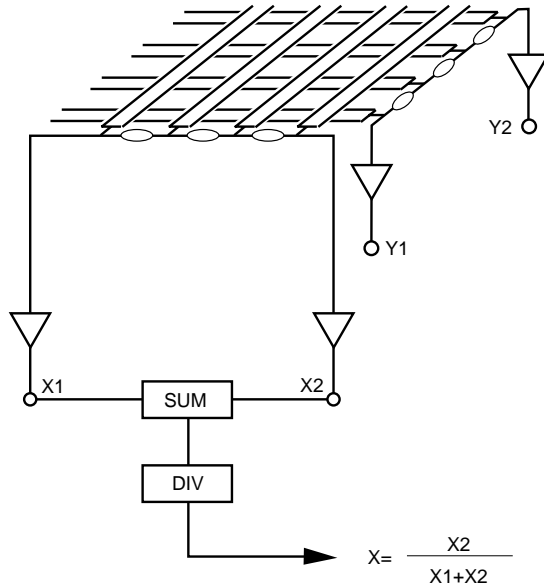


TPMHC0160EA

**Figure 6-2: Electrode structure of metal channel dynodes and electron trajectories**

Figure 6-3 illustrates the center-of-gravity detection method for reading out the output signal from a position-sensitive photomultiplier tube using a cross plate anode. The electron bunch released from the last dynode is collected by anodes linearly arranged in the X and Y directions. Since each anode in the same direction is connected by a resistor chain, the collected electrons are divided into four signal components of X1, X2, Y1 and Y2 corresponding to the anode position at which the electron bunch arrive. By inputting these signals to a summing (SUM) and divider (DIV) circuits, the center of gravity in the X and Y directions can be obtained as follows:

$$\begin{aligned} X &= X_2/(X_1+X_2) \\ Y &= Y_2/(Y_1+Y_2) \end{aligned} \dots\dots\dots \text{(Eq. 6-1)}$$



TPMHC0161EA

**Figure 6-3: Center-of-gravity detection method for position-sensitive photomultiplier tube using cross plate anodes**

Hamamatsu has developed the R5900 series position-sensitive photomultiplier tubes housed in a 1"X1" square metal package. The R5900 series uses 10 to 12 stages of metal channel dynodes and various types of multianodes as shown in Table 6-4, allowing you to make a selection to meet the particular application.

| Type No.                   | R5900-00-C8       | R5900-00-C12      | R5900-00-M4       | R5900-00-M16 (H6568) | R5900-00-L16      | R5900-00-M64 (H7546) |
|----------------------------|-------------------|-------------------|-------------------|----------------------|-------------------|----------------------|
| Anode Shape                |                   |                   |                   |                      |                   |                      |
| Number of Anodes           | 4(X)+4(Y)         | 6(X)+6(Y)         | 4                 | 16                   | 16                | 64                   |
| Number of Dynodes          | 11                | 11                | 10                | 12                   | 10                | 12                   |
| Gain (Supply voltage 800V) | 7X10 <sup>5</sup> | 7X10 <sup>5</sup> | 2X10 <sup>6</sup> | 3.3X10 <sup>6</sup>  | 2X10 <sup>6</sup> | 3X10 <sup>5</sup>    |

TPMHA0432EA

**Table 6-4: R5900 series anode patterns**

The R5900 series position-sensitive photomultiplier tube also includes an easy-to-use assembly type with built-in voltage-divider resistors. (Figure 6-5)



**Figure 6-5: R5900-00-M16 assembly (H6568)**

As mentioned, when photoelectrons are emitted from the photocathode, they are directed onto the first dynode by the focusing mesh. In this process, the photoelectron flow spreads spatially between the photocathode and the focusing mesh and also between the focusing mesh and the first dynode. Metal channel dynodes are developed to minimize this electron spread.

Figures 6-6 (1) and (2) show typical spatial resolution of the R5900-00-C8 (cross plate multianode type) using the center-of-gravity detection method. This data is measured by irradiating the photocathode surface with a 3mm diameter collimated light beam from a tungsten lamp and plotting the output distribution of each anode. (The light beam is moved along each of the XY directions with the tube axis viewed as the center.)

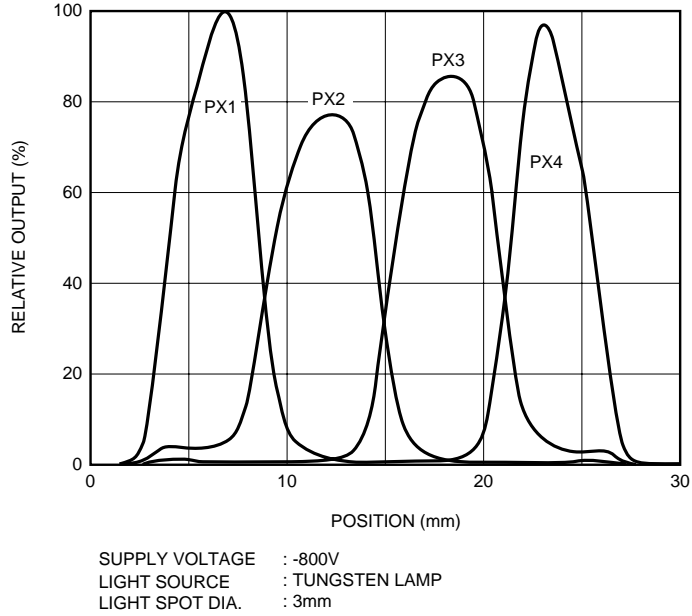


Figure 6-6 (1): Multianode spatial resolution in the X direction (R5900-00-C8)

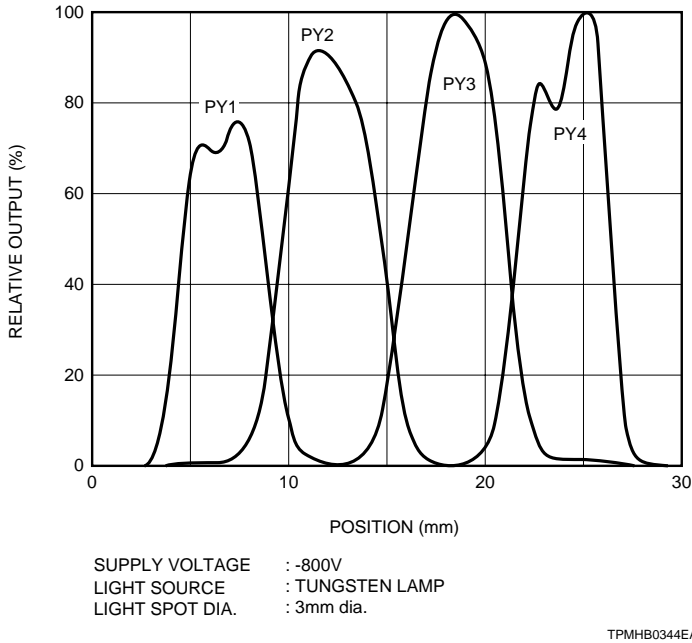


Figure 6-6 (2): Multianode spatial resolution in the Y direction (R5900-00-C8)

As one sample application, Figure 6-7 (1) shows the measurement diagram for scintillation imaging of 511keV gamma-rays, using the R5900-00-C8 coupled BGO scintillators (arranged in a mosaic pattern of  $8 \times 7 = 56$  pieces). An actual image that was taken is shown in Figure 6-7 (2).

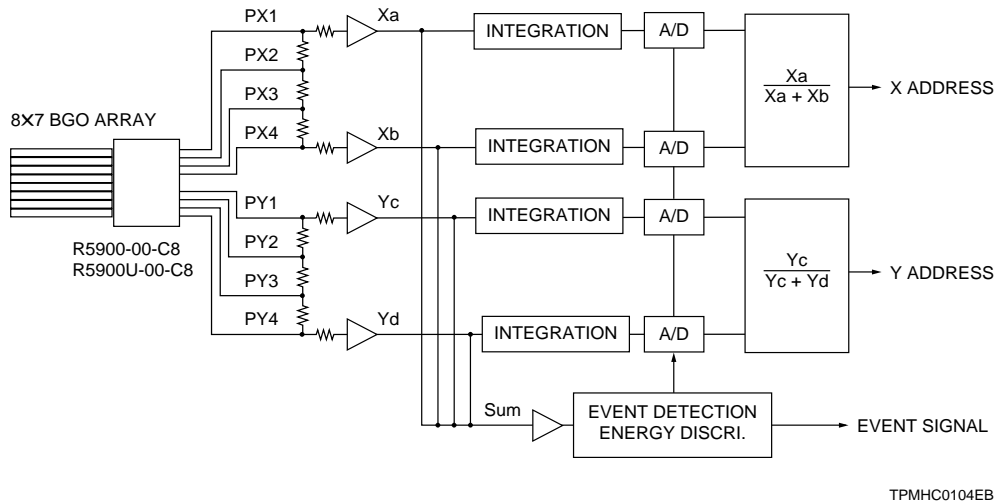
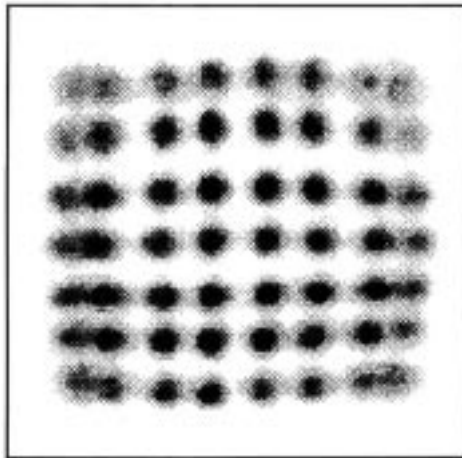


Figure 6-7(1): Scintillation imaging of gamma-rays entering a mosaic pattern of BGO scintillators

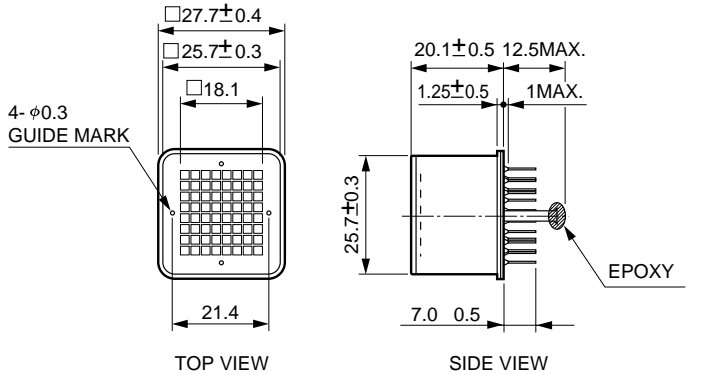


Position data after calculation when gamma-rays at 511keV were incident on the 8X7 BGO array (2.8mmX2.8mmX30mm)

Figure 6-7(2): Scintillation imaging of gamma-rays entering a mosaic pattern of BGO scintillators

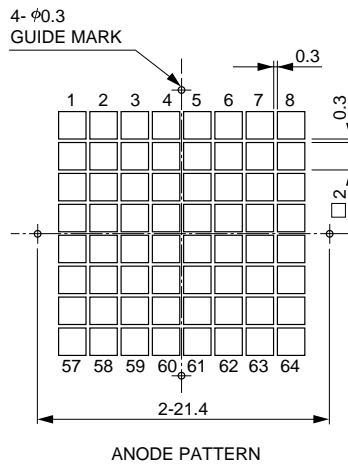
This scintillation imaging is now possible with position-sensitive photomultiplier tubes. Off-axis distortion in the image can be corrected to some extent by an electronic circuit.

Figure 6-8 shows the external dimensions of the R5900-00-M64 (8X8 multianode<sup>8)</sup>), and Figure 6-9 the anode pattern.



TPMHA0405EA

**Figure 6-8: R5900-00-M64 external dimensions**



TPMHA0404EA

**Figure 6-9: R5900-00-M64 anode pattern**

Multianode photomultiplier tubes are mainly developed for applications requiring multipoint measurements. Before they are put into practical use, multiple small diameter photomultiplier tubes were used in close arrangement, so that the total cost for using many of these tubes could not be ignored (particularly in huge equipment used in high energy physics experiments and for nuclear medical imaging systems). Simply speaking, one anode of a multianode corresponds to one photomultiplier tube, so using multianode photomultiplier tubes will contribute to a significant reduction in the total cost.

The following paragraphs explain basic characteristics of the R5900-00-M64, such as crosstalk, magnetic immunity and uniformity.<sup>9)</sup>

Crosstalk is a measure to indicate how accurately the light (signal) incident on a certain position of the photocathode is detected with the position information still retained. In photomultiplier tube operation, crosstalk is mainly caused by the broadening of electron flow when light is converted into electrons and those electrons

are multiplied in the dynode section. The incident light spread within the faceplate is another probable cause of crosstalk. A typical setup for measuring crosstalk is shown in Figure 6-10 and the measurement data in Figure 6-11.

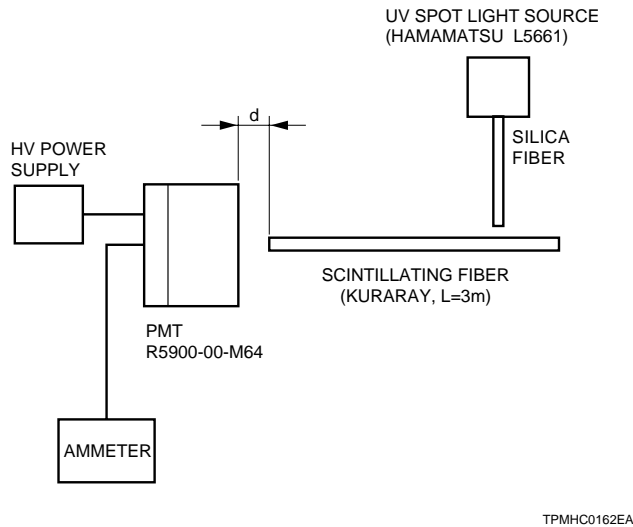


Figure 6-10: Crosstalk measurement method

|     |     |     |
|-----|-----|-----|
| 0.3 | 1.4 | 0.4 |
| 0.8 | 100 | 1.2 |
| 0.2 | 1.1 | 0.3 |

SCINTILLATING FIBER (1.0mm dia.)  
 SUPPLY VOLTAGE: 800(V)  
 d (DISTANCE): 0mm

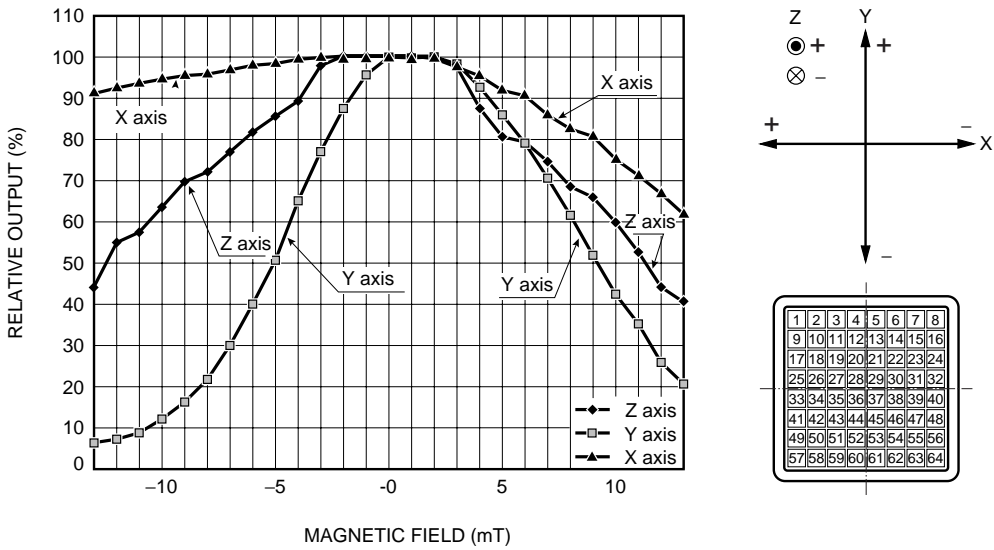
|     |     |     |
|-----|-----|-----|
| 0.4 | 2.6 | 0.6 |
| 1.5 | 100 | 1.9 |
| 0.3 | 1.8 | 0.4 |

SCINTILLATING FIBER (1.0mm dia.)  
 SUPPLY VOLTAGE: 800(V)  
 d (DISTANCE): 0.5mm

Figure 6-11: Crosstalk measurement examples

Data shown in Figure 6-11 is measured by irradiating a light spot (signal) on the photomultiplier tube faceplate, through a 1mm diameter optical fiber placed in close contact with the faceplate. The output of each anode is expressed as a relative value, with 100% being equal to the peak anode output produced from the incident light spot. The results show that crosstalk is "0.2% to 1.4% when the 1mm diameter scintillating fiber is positioned in tight contact with the photomultiplier tube faceplate. However, the crosstalk degrades by 0.3% to 2.6% when the scintillating fiber is placed 0.5mm away from the faceplate. This is of course due to light spread at the scintillating fiber exit. Bringing the optical fiber into tight contact with the photomultiplier tube faceplate is therefore recommended to make accurate measurements using scintillation fibers.

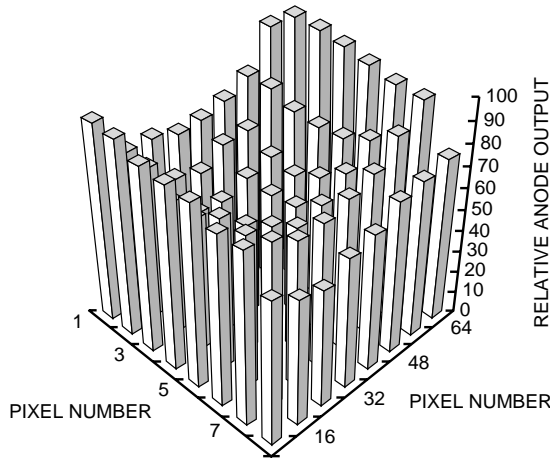
Next, let's discuss magnetic characteristics. The R5900 series photomultiplier tubes have excellent immunity to magnetic fields. This is because all parts except the photocathode are housed in a metal package and also because the distance between dynode electrodes is very short. Figure 6-12 shows how the anode output is adversely affected by external magnetic fields applied to the R5900-00-M16 along the three directions (X, Y, Z). Each data is plotted as a relative output value, with 100% corresponding to an output with no magnetic field applied. It is clear that the output is still maintained as high as 60% versus 13mT of the magnetic field in the X direction.



TPMHB0488EA

Figure 6-12: Effects of external magnetic fields on anode output (anode channel No. 29)

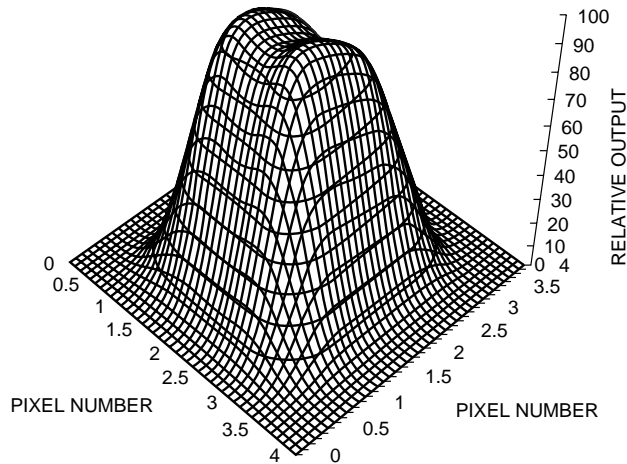
Figure 6-13 shows typical uniformity data obtained from each anode when uniform light is illuminated over the entire photocathode of the R5900-00-M64. The non-uniformity observed here probably originates from gain variations in the secondary electron multiplier because the photocathode itself has good uniformity. At the current stage, non-uniformity between each anode is about "1:3" on average.



TPMHB0489EA

Figure 6-13: R5900-00-M64 anode output uniformity

Uniformity of one anode (one pixel) is shown in Figure 6-14. This data is measured by input of weak DC light to an anode of 2X2mm per pixel through a 1mm diameter optical fiber, while scanning the optical fiber every 0.1mm on the photocathode. There are two output peaks as graphically represented. This means that the electrons (signals) extracted from one anode (one pixel) arrive at the anode through the two adjacent paths in the metal channel dynode.



TPMHB0490EA

Figure 6-14: Anode output uniformity per pixel

## 6.1.2 Applications

As stated earlier, position-sensitive photomultiplier tubes delivers accurate position information about light falling on the photocathode by center-of-gravity processing. These photomultiplier tubes can be used for scintillation imaging in combination with scintillators. Some recent applications are explained below.

### (1) Biometabolic activity imaging using PET (Positron Emission Tomography)<sup>10) 11) 12)</sup>

Nuclear medical instruments (such as gamma cameras and PET systems) have been developed and are now used in hospital facilities. Ordinary gamma cameras use a detector composed of a large scintillator and a number of photomultiplier tubes. To achieve even higher resolution and a smaller instrument, research and development of compact gamma cameras is now under way, using a flat-shaped NaI(Tl), mosaic arrangement of YAP and CsI(Na) scintillators.

PET uses a number of small position detectors arranged to surround the subject and creates tomographic images by detecting gamma rays generated from positron annihilation using the coincidence technique. Recently, scintillation detectors made up of a scintillator coupled to a position-sensitive photomultiplier tube are becoming used as detectors in PET. Major characteristics required of these photomultiplier tubes are high sensitivity, good energy resolution and excellent time resolution. By utilizing position-sensitive photomultiplier tubes having these characteristics, more compact PET systems with better spatial and time resolutions will be available.

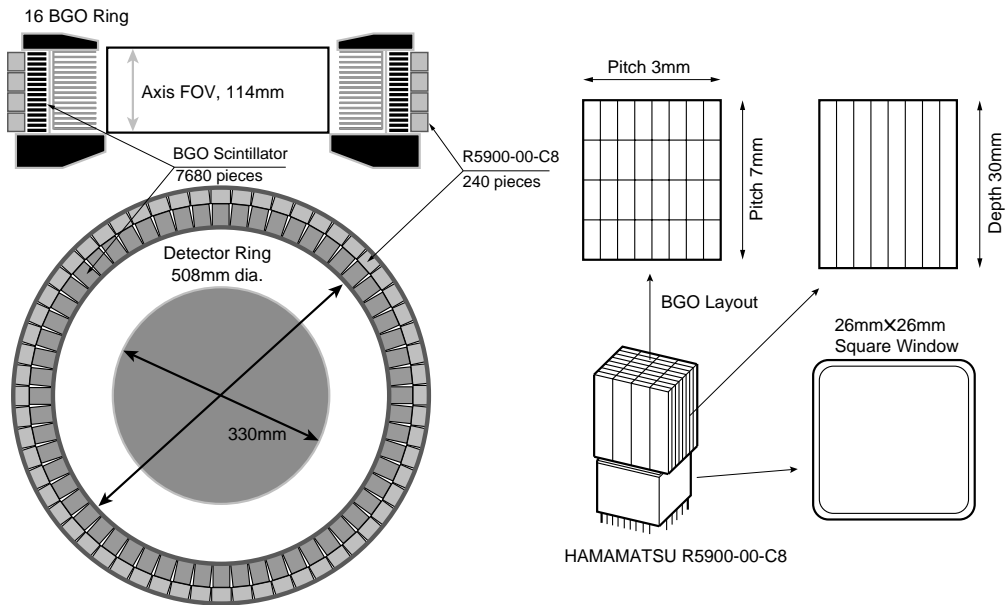
As a specific example, Figure 6-15 shows the PET system (Hamamatsu SHR-7700) designed for laboratory animals, which has been already put on the market. This PET system is used for animal studies in pharmacodynamics which are difficult to conduct with the human body, and also for development of new medicines and evaluation of pharmaceutical effects of general medicines. Laboratory animals often used with PET are mice, rats, monkeys and baboons.

Because these animal organs are relatively small, PET for animal studies must provide high resolution. The SHR-7700 uses scintillation detectors each of which consists of 32 BGO scintillators coupled to a R5900-00-08 position-sensitive photomultiplier (cross-wire anode type). Since 240 photomultiplier tubes are installed in the SHR-7700, a total of 7680 BGO scintillators are required. The SHR-7700 provides unprecedented performance with a center resolution of 2.6mm and effective field-of-view of 330mm diameter  $\times$  114mm. Fig. 6-15 shows the external view of the SHR-7700.



Figure 6-15: External view of the SHR-7700 (PET system for laboratory animals)

The detector ring and detector unit of the SHR-7700 are shown in Figures 6-16 and 6-17. As a typical example taken with the SHR-7700, Fig. 6-18 shows oxygen metabolic activity images of a monkey brain.



TPMHC0163EA

Figure 6-16: Cross section of the SHR-7700 detector ring



Figure 6-17: Detector unit

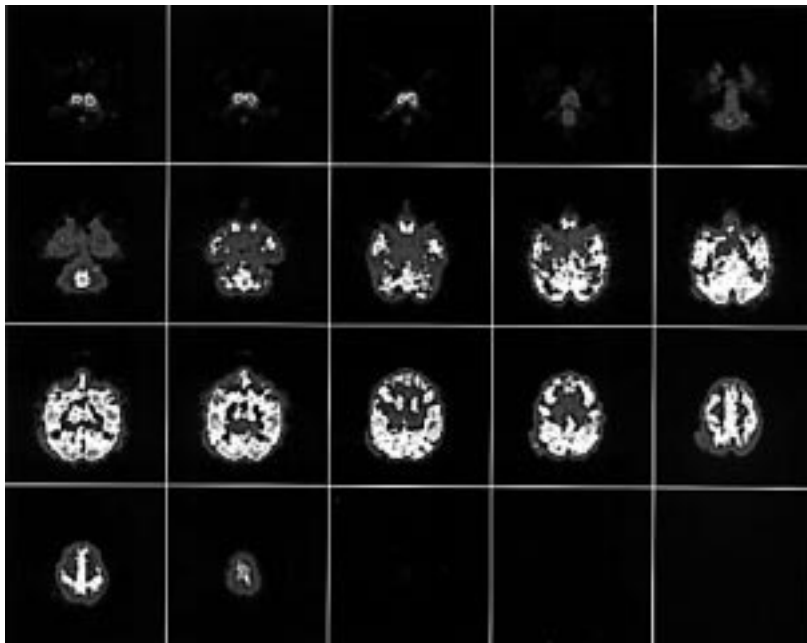
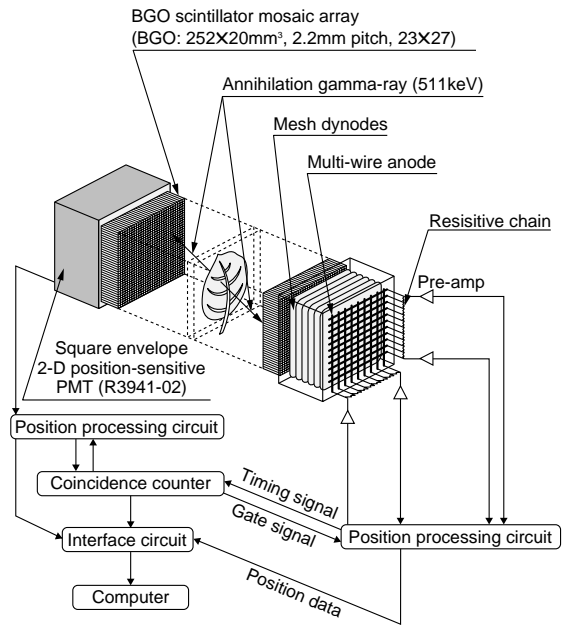


Figure 6-18: Oxygen metabolic activity images of monkey brain (positron imaging system)

As one application for position-sensitive photomultiplier tubes using grid dynodes, let's take a brief look at a planar detector system for positron imaging developed for studies on metabolism activity inside living plants. The detectors used in this system consists of a BGO scintillator array coupled to a 3-inch square envelope position-sensitive photomultiplier tube. The BGO scintillator array is made up of  $27 \times 23$  independent scintillators each of which has a prismatic shape measuring  $2\text{mm} \times 2\text{mm} \times 20\text{mm}$ . As shown in Figure 6-19, a pair of detectors are placed so that they face each other at the front and back of a planar sample such as a plant leaf. To measure real-time images of biological functions within the sample, a positron-emitting tracer is injected into the sample and annihilation gamma-rays emitted from it are captured with the two detectors by coincidence counting technique. Two-dimensional images can be produced by projecting the obtained data onto the same plane (focal plane imaging method).



TPMHC0168EA

**Figure 6-19: Planar detector system for positron imaging of metabolic functions inside plant**

A 50 minute integrated image of a rose flower whose stem was cut and given water containing  $^{18}\text{F}$  for 2 minutes. Higher concentrations can be seen in the calyxes.

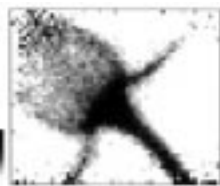


**Figure 6-20: Image of metabolic functions inside a plant**

One minute images of the stem/leaf separating area of a rose flower whose stem was cut and given water containing  $^{18}\text{F}$  for 2 minutes. It is observed that water can be seen to first flow towards the leaf.

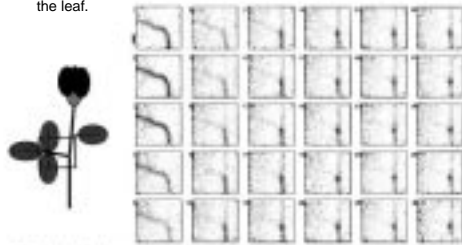


**Figure 6-21: Visualization of "water" flow inside a plantflow inside a plant**

## 6.2 Position-Sensitive Photomultiplier Tubes Using Fine-Mesh Dynodes

Position-sensitive photomultiplier tubes using fine-mesh dynodes and a multianode have been developed and put on the market.<sup>13)14)</sup> These photomultiplier tubes can be operated near large magnetic field, making them well suited for use in particle track detectors and calorimeters in high energy physics experiments.

### 6.2.1 Structure

Figure 6-22 shows the sectional view of a photomultiplier tube using fine-mesh dynodes. This tube is constructed with an input window, a photocathode, fine-mesh dynodes and an anode. The details of a fine-mesh dynode are illustrated in Figure 6-23. When an electron impinges on the upper part of the mesh, multiple secondary electrons are emitted from the secondary emissive surface deposited on the mesh. This process is repeated through the last dynode stage and finally electrons are multiplied up to a million times.

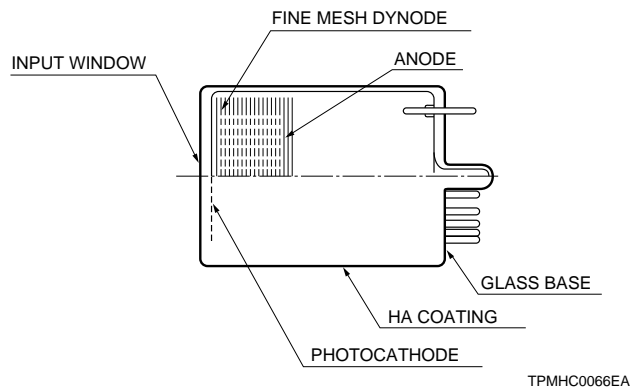


Figure 6-22: Structure of a photomultiplier tube using fine-mesh dynodes

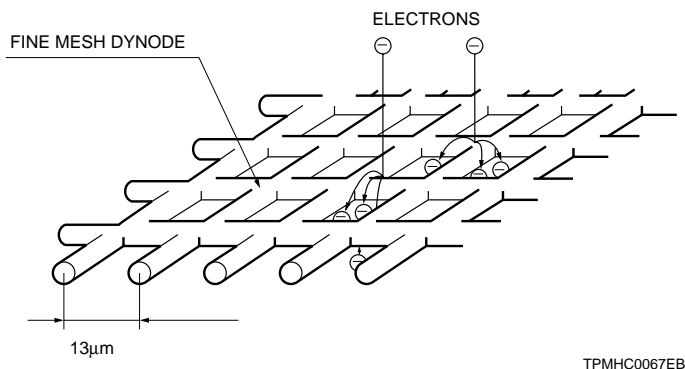


Figure 6-23: Details of a fine-mesh dynode

Figure 6-24 is a photograph of this type of photomultiplier tube. It provides a gain of  $10^6$  with 16 dynode stages and  $10^7$  with 19 dynode stages. Table 6-1 shows typical photomultiplier tubes using fine-mesh dynodes and their major characteristics. A variety of tubes have been marketed, including 1-inch, 1.5-inch, 2-inch, 2.5-inch, 3-inch and 5-inch diameter tubes with 15, 16 or 19 dynode stages.



Figure 6-24: External view of R5924

| Size                         | Type No.                              | Effective Photo-cathode | Number of Dynodes | Rise Time        | TTS              | Pulse Linearity |
|------------------------------|---------------------------------------|-------------------------|-------------------|------------------|------------------|-----------------|
| 25mm Dia.<br>(1 inch dia.)   | R5505<br>(UV R5506)                   | 17.5mm Dia.             | 15                | 1.5ns<br>(2000V) | 350ps<br>(2000V) | 180mA           |
| 38mm Dia.<br>(1.5 inch dia.) | R5946<br>(Silica R6149)<br>(UV R6148) | 27mm Dia.               | 16                | 1.9ns<br>(2000V) | 350ps<br>(2000V) | 350mA           |
| 52mm Dia.<br>(2 inch dia.)   | R5924<br>(Silica R6609)<br>(UV R6608) | 39mm Dia.               | 19                | 2.5ns<br>(2000V) | 440ps<br>(2000V) | 500mA           |
| 64mm Dia.<br>(2.5 inch dia.) | R6504<br>(UV R6505)                   | 51mm Dia.               | 19                | 2.7ns<br>(2000V) | 470ps<br>(2000V) | 700mA           |
| 78mm Dia.<br>(3 inch dia.)   | R5542<br>(UV R5543)                   | 64mm Dia.               | 19                | 2.9ns<br>(2000V) | 500ps<br>(2000V) | 1,000mA         |

Table 6-1: Photomultiplier tubes using fine-mesh dynodes

## 6.2.2 Characteristics

The greatest advantage offered by fine-mesh dynodes is that they can be operated in a magnetic field. Figure 6-25 shows the relative output of a photomultiplier tube using fine-mesh dynodes with respect to magnetic flux density. Although the output decreases with increasing magnetic flux density, this tube can be used up to near 1.5 Tesla. This performance is due to the fine-mesh structure with its very minute diameter and also to the close-proximity spacing between dynodes, so that the electron trajectories of the secondary electrons emitted from the fine-mesh dynodes are resistant to external magnetic fields.

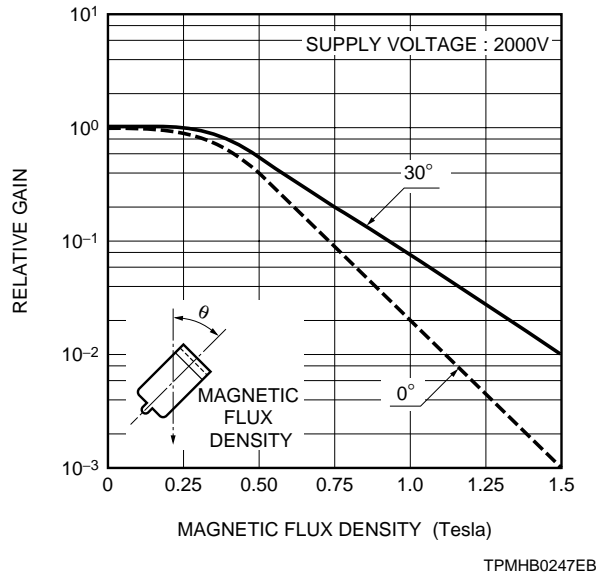
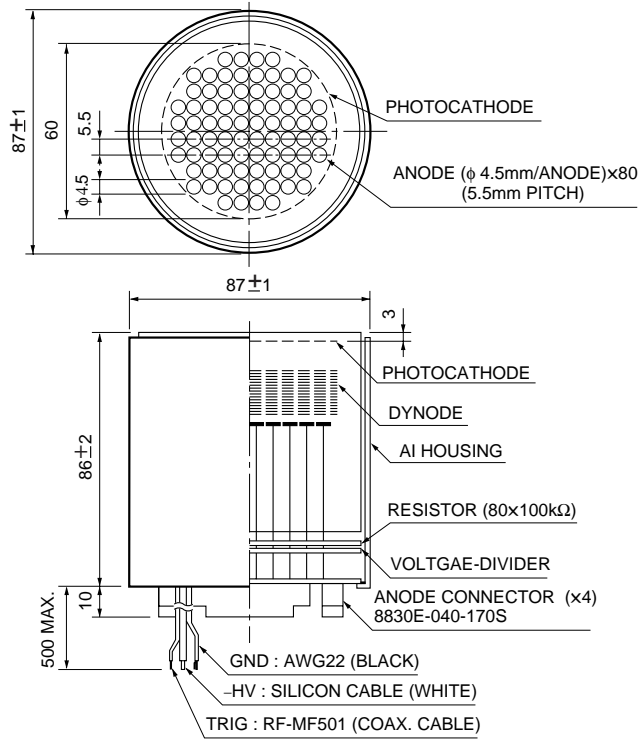


**Figure 6-25: Gain vs. magnetic flux density**

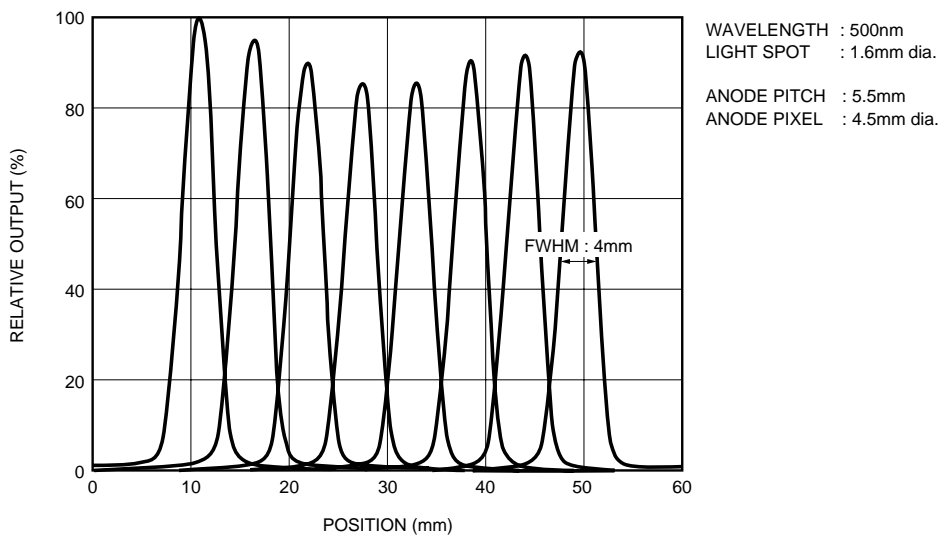
Next, let us introduce a position-sensitive photomultiplier tube that combines fine-mesh dynodes with a multianode. The configurations of this tube are illustrated in Figure 6-26. The number of fine-mesh dynodes is 19 stages, the multianode consists of 80 independent anodes and these elements are incorporated in a 3-inch diameter cylindrical envelope. A gain of approximately  $5 \times 10^6$  can be obtained with this tube. Figure 6-27 shows the spatial resolution of this tube when a 2mm light spot is scanned over the input window along the direction of a row of the anodes. This data was measured with the photomultiplier tube operated in a non-magnetic field and indicates a spatial resolution of approximately 4mm (FWHM).



TPMHA0201EE

**Figure 6-26: Dimensions and internal structure of a multianode photomultiplier tube using fine-mesh dynodes**

Figure 6-28 is the photograph of the multianode photomultiplier tube using fine-mesh dynodes described in this section. Figure 6-29 shows the external view of a modular type of photomultiplier tube using fine-mesh dynodes and multianode.



TPMHB0195EC

**Figure 6-27: Spatial resolution of H5828 (R5635 Assembly) in non-magnetic field**



**Figure 6-28: Multianode photomultiplier tube using fine-mesh dynodes**



**Figure 6-29: Modular type of multianode photomultiplier tube using fine-mesh**

Table 6-2 shows a list of major assembly modules of position-sensitive photomultiplier tubes using fine-mesh dynodes and a multianode. In addition to incorporating a voltage-divider circuit, these tubes are equipped with a multiconnector that allows easy connection of the multianode output to an external circuit. The anode configuration of each tube is also listed in this table, 8X8, 16X16 and 80 multianodes are available for tubes with a 3-inch circular and square faceplate.

| Size                            | Type No. | Remarks  |
|---------------------------------|----------|--|
| 75mm, Circular<br>(3 inch dia.) | H5828    | No. of Anodes : 80<br>Anode Size : f4.5mm<br>Anode Pitch : f5.5mm          |
| 75X75mm, Square<br>(3X3 inch)   | H4140-20 | No. of Anodes : 16X16 (256)<br>Anode Size : f1.8mm<br>Anode Pitch : 2.54mm |
| 75X75mm, Square<br>(3X3 inch)   | H4139-20 | No. of Anodes : 64<br>Anode Size : f4.2mm<br>Anode Pitch : 5.08mm          |

**Table 6-2: Multianode photomultiplier tube using fine-mesh dynodes**

### 6. 2. 3 Applications

Main applications of the fine-mesh dynode photomultiplier tubes include calorimeters and particle track detectors used in conjunction with scintillators in high energy physics experiments. Figure 6-30 shows a drawing of time resolution measurement using  $\pi$ -mesons at 2GeV and the combination of a rectangular plastic scintillator (Pilot U of 2cm $\times$ 1cm $\times$ 1cm) with a pair of fine-mesh dynode photomultiplier tubes.<sup>15)</sup>

In this measurement, it is anticipated that several thousands of photoelectrons are produced at each photomultiplier tube. The output of each photomultiplier tube is fed into a CFD (constant fraction discriminator) circuit for measurement.

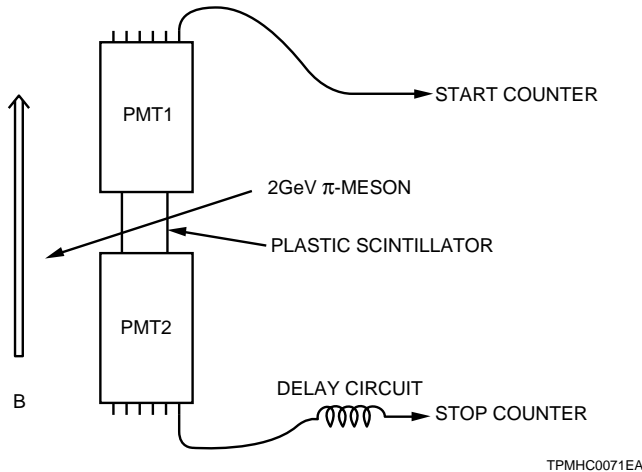


**Figure 6-30: Schematic drawing for time resolution measurement using  $\pi$ -mesons**

Figure 6-31 shows the time resolution plot obtained with this measurement as a function of magnetic flux density. The time resolution is approximately 100 picoseconds without a magnetic field, and approximately 200 picoseconds in a magnetic field at 0.78 Tesla.

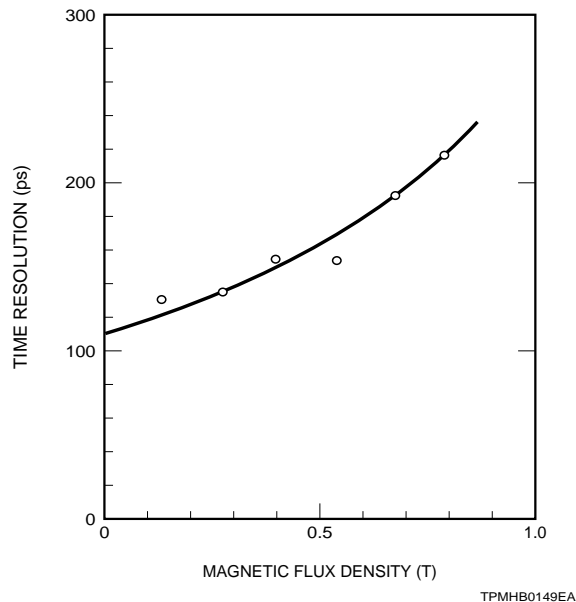


**Figure 6-31: Time resolution vs. magnetic flux density**

When the same measurement is made using fast response photomultiplier tubes in place of the fine-mesh dynode photomultiplier tubes, a time resolution of approximately 100 picoseconds is attained. This proves that fine-mesh dynode photomultiplier tubes can be used either in non-magnetic fields or in highly magnetic fields. But it should be noted that as the magnetic field intensity increases, the current amplification of the photomultiplier tube decreases, resulting in deterioration of the time resolution.

Because of their high immunity to magnetic fields and position-detection capability, these photomultiplier tubes find applications in particle track detectors and calorimeters. Figure 6-32 gives an example of a charged particle track detector consisting of a position-sensitive photomultiplier tube with a multianode in combination with a plastic scintillation fiber bundle.<sup>16)</sup>

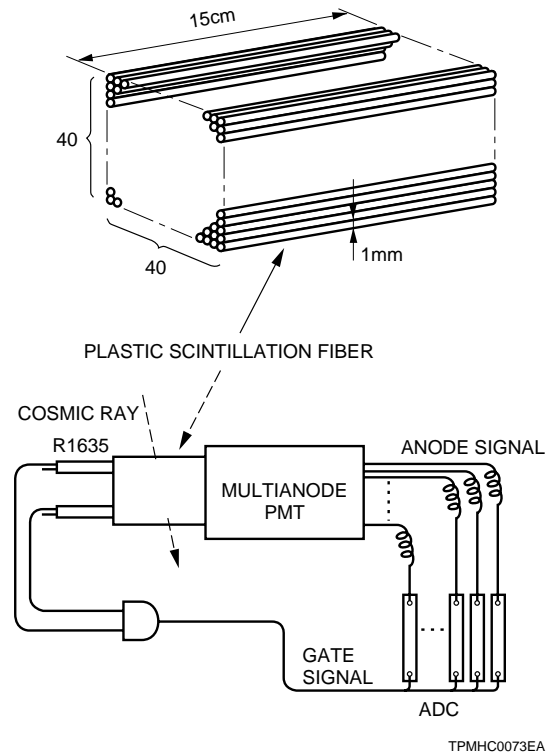
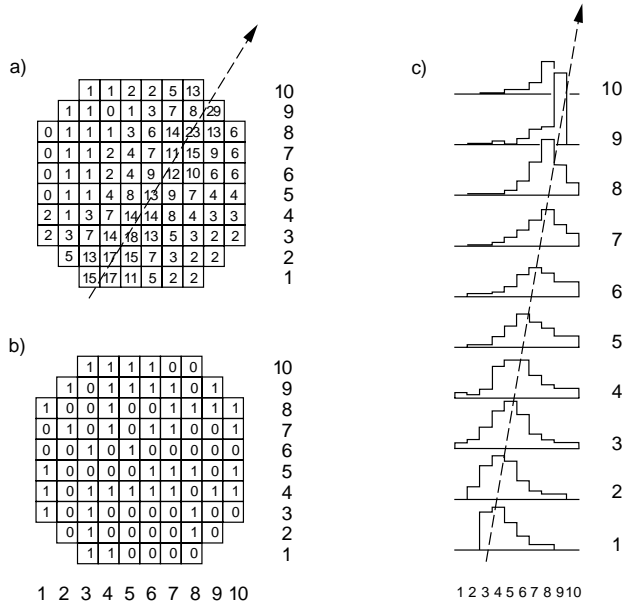


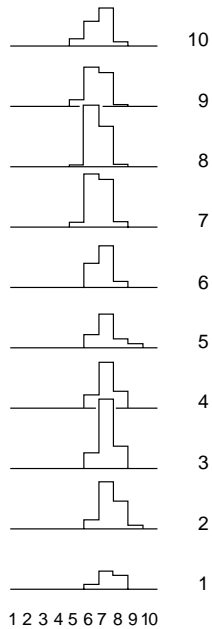
**Figure 6-32: Drawing of a particle track detector**

This detector uses a fiber bundle measuring 40mm(W)×40mm(H)×150mm(L) comprised of individual scintillation fibers (1 millimeter diameter). Figure 6-33 shows the results when the track of cosmic rays is measured with this detector. In the figure, a) are the anode outputs obtained when the photomultiplier tube is operated at 2200 volts, while b) are those at 0 volts. As shown in this figure, a multianode of an 88-matrix array is employed. Here, c) is the output profile of each row of the multianode, indicating the movement of the track. In this case, since no magnetic field is applied to the photomultiplier tube, the electrons broaden to an area equal to three anodes (approximately 8 millimeters). On the other hand, Figure 6-34 shows the results obtained when a magnetic field of 0.05 Tesla is applied to the photomultiplier tube in the direction of the tube axis. Due to the focusing effects of the magnetic field, the electron spread is suppressed to a small area equal to one anode channel (approximately 2.6 millimeters) thus assuring high resolution for the cosmic-ray track measurement.<sup>16)</sup>



TPMHC0074EA

**Figure 6-33: Cosmic-ray track measurements with a position-sensitive PMT having fine-mesh dynodes and a multianode (in no magnetic field)**



TPMHC0075EA

**Figure 6-34: Cosmic-ray track measurements with a position-sensitive PMT having fine-mesh dynodes and a multianode (in magnetic field of 0.05 Tesla)**

## References in Chapter 6

- 1) H. Kyushima, Y. Hasegawa, A. Atsumi, K. Nagura, H. Yokota, M. Ito, J. Takeuchi, K. Oba: IEEE Nucl. Sci. Symp., 41, 725-730(1994).
- 2) M. Watanabe, T. Omura, H. Kyushima, Y. Hasegawa and T. Yamashita: IEEE Nucl. Sci. Symp. and Medical Imaging Conference. Norfolk, Virginia, Nov.1994.
- 3) K. Nakanue, H. Kyushima: RADIOISOTOPES, Vol. 45, No.1, Jan. 1996.
- 4) Hamamatsu Photonics Technical Data Sheet: New Mesh PMTs for High Magnetic Environments.
- 5) A. Sawaki, S. Ohsuka, T. Hayashi: IEEE Trans. Nucl. Sci. NS-31, 1, 442(1984).
- 6) S. Suzuki, T. Nakaya, A. Suzuki, H. Suzuki, K. Yoshioka, Y. Yoshizawa: Submitting to IEEE. Trans. Nucl. Sci. Vol.NS-40(1993).
- 7) Hamamatsu Photonics Technical Data Sheet: R5900-00-C8.
- 8) Hamamatsu Photonics Technical Data Sheet: R5900-00-M64.
- 9) Y. Yoshizawa, H. Ohtsu, N.Ota, T. Watanabe, J. Takeuchi: The Development and The Study of R5900-00-M64 for Scintillating/Optical Fiber Read Out, Hamamatsu Technical Information, No.TPMH9002E01.
- 10) H. Uchida, M. Iida, T. Yamashita: MEDICAL IMAGING TECHNOLOGY 4, 314 (1986).
- 11) M. Watanabe, H. Okada, K. Shimizu, T. Omura, E. Yoshikawa, T. Kosugi, S. Mori, T. Yamashita: IEEE Trans. Nucl. Sci. Vol.44, No.3, June 1997.
- 12) E. Tanaka: RADIOISOTOPES, Vol. 46, No.10, Oct. 1997.
- 13) Hamamatsu Photonics Technical Data Sheet: H4139/H4140/R4549-01/R2490-05.
- 14) Hamamatsu Photonics Technical Data Sheet: R3384.
- 15) F. Takasaki, K. Ogawa and K. Tobimatsu: Nucl. Instrum. Methods. A228, 369(1985).
- 16) F. Takasaki, H. Saito, T. Fukui, T. Matsushita and T. Suzuki: Nucl. Instrum. Methods. A260, 447(1987).

# MEMO

# **CHAPTER 7**

## **HOW TO USE PHOTOMULTIPLIER TUBES AND ASSOCIATED CIRCUITS**

*This chapter explains how to use basic circuits and accessories necessary to operate a photomultiplier tube properly.<sup>1)</sup>*

## 7.1 Voltage-Divider Circuits

### 7.1.1 Basic operation of voltage-divider circuits

For photomultiplier tube operation, a high voltage from 500 to 3000 volts is usually applied across the cathode (K) and anode (P), with a proper voltage gradient set up between the photoelectron focusing electrode (F), dynodes and, depending on tube type, an accelerating electrode (accelerator). This voltage gradient can be set up using independent multiple power supplies as shown in Figure 7-1, but this is usually not practical.

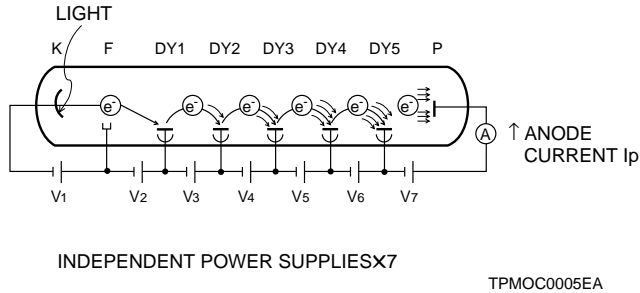


Figure 7-1: Schematic diagram of photomultiplier tube operation

In practice, as shown in Figure 7-2, the interstage voltage for each electrode is supplied by using voltage-dividing resistors (sometimes along with Zener diodes) connected between the anode and cathode. This circuit is known as a voltage-divider circuit or bleeder circuit.

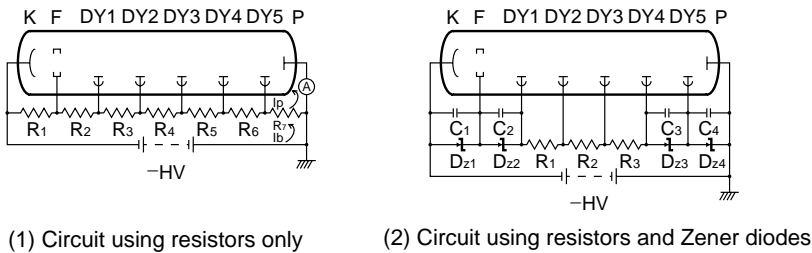


Figure 7-2: Voltage-divider circuits

The current I<sub>b</sub> flowing through the voltage-divider circuits shown in Figures 7-2 (1) and (2) is called divider current, and closely related to the output linearity described later. The divider current I<sub>b</sub> is approximately the applied voltage V divided by the sum of resistor values as follows:

$$I_b = \frac{V}{(R_1 + R_2 + \dots + R_6 + R_7)} \dots\dots\dots \text{(Eq. 7-1)}$$

The Zener diodes (D<sub>z</sub>) shown in (2) are used to maintain the interstage voltages at constant values for stabilizing the photomultiplier tube operation regardless of the magnitude of the cathode-to-anode supply voltage. The capacitors C<sub>1</sub>, C<sub>2</sub>, C<sub>3</sub> and C<sub>4</sub> connected in parallel with the Zener diodes serve to minimize noise generated by the Zener diodes. This noise becomes significant when the current flowing through the Zener diodes is insufficient. Thus care is required at this point, as this noise can affect the signal-to-noise ratio of the photomultiplier tube output.

### 7.1.2 Anode grounding and cathode grounding

As shown in Figure 7-2, the general technique used for voltage-divider circuits is to ground the anode and apply a large negative voltage to the cathode. This scheme eliminates the potential voltage difference between the external circuit and the anode, facilitating the connection of circuits such as ammeters and current-to-voltage conversion operational amplifiers to the photomultiplier tube. In this anode grounding scheme, however, bringing a grounded metal holder, housing or magnetic shield case near the bulb of the photomultiplier tube, or allowing it to make contact with the bulb can cause electrons in the photomultiplier tube to strike the inner bulb wall. This may possibly produce glass scintillation, resulting in a significant increase in noise.

Also, for head-on photomultiplier tubes, if the faceplate or bulb near the photocathode is grounded, the slight conductivity of the glass material causes a small current to flow between the photocathode and ground. This may cause electric damage to the cathode, possibly leading to considerable deterioration. For this reason, extreme care must be taken when designing the housing for a photomultiplier tube and when using an electromagnetic shield case. In addition, when wrapping the bulb of a photomultiplier tube with foam rubber or similar shock-absorbing materials before mounting the tube within its electromagnetic shield case at ground potential, it is very important to ensure that the materials have sufficiently good insulation properties.

The above problems concerning the anode grounding scheme can be solved by coating the bulb surface with black conductive paint and connecting it to the cathode potential. This technique is called "HA coating", and the conductive bulb surface is protected by a insulating cover for safety. In scintillation counting, however, because the grounded scintillator is usually coupled directly to the faceplate of a photomultiplier tube, the cathode is grounded with a high positive voltage applied to the anode, as shown in Figure 7-3. With this grounded cathode scheme, a coupling capacitor ( $C_c$ ) must be used to separate the positive high voltage (+HV) applied to the anode from the signal, making it impossible to extract a DC signal. In actual scintillation counting using this voltage-divider circuit, a problem concerning base-line shift may occur if the counting efficiency increases too much, or noise may be generated if a leakage current is present in the coupling capacitor. Thus care should be taken regarding these points.

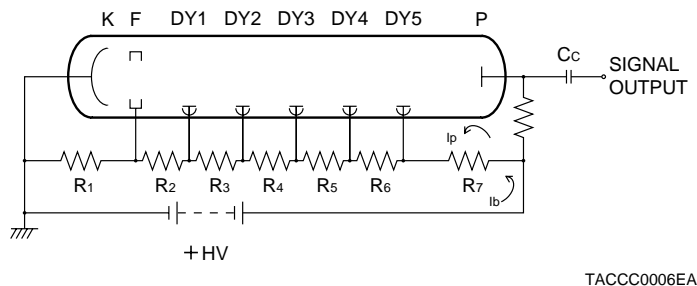


Figure 7-3: Grounded-cathode voltage-divider circuit

### 7.1.3 Voltage-divider current and output linearity

In either the anode grounding or cathode grounding scheme or either DC or pulse operation, when the light level incident on the photocathode is increased to raise the output current as shown in Figure 7-4, the relationship between the incident light level and the anode current begins to deviate from the ideal linearity at a certain current level (region B) and eventually, the photomultiplier tube output goes into saturation (region C).

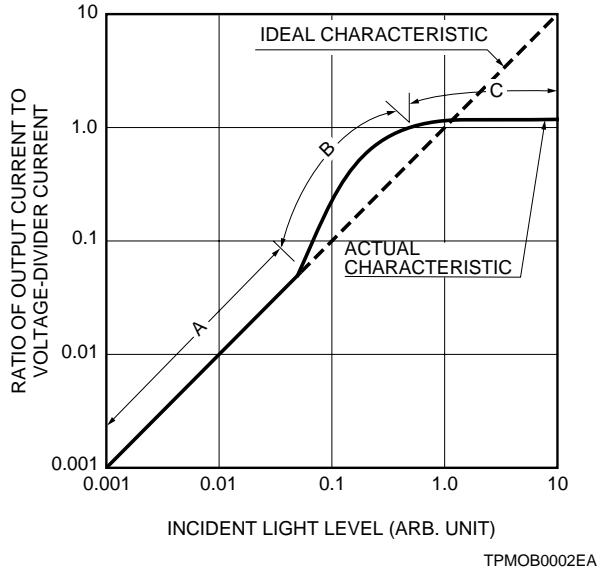


Figure 7-4: Output linearity of a photomultiplier tube

### (1) DC-operation output linearity and its countermeasures

In deriving a DC output from a photomultiplier tube using the basic operating circuit shown in Figure 7-5, the current which actually flows through a voltage-divider resistor, for example the current flowing across resistor  $R_7$ , equals the difference between the divider current  $I_b$  and the anode current  $I_p$  which flows in the opposite direction through the circuit loop of P-Dy<sub>5</sub>-R<sub>7</sub>-P. Likewise, for other voltage-divider resistors, the actual current is the difference between the divider current  $I_b$  and the dynode current  $I_{Dy}$ , flowing in the opposite direction through the voltage-divider resistor. The anode current and dynode current flow act to reduce the divider current and the accompanying loss of the interstage voltage becomes more significant in the latter dynode stages which handle larger dynode currents. Although the dynode current includes current components flowing in the same direction as the divider current  $I_b$ , they are of very small amounts and therefore not discussed here.

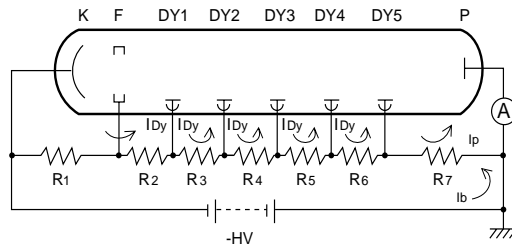
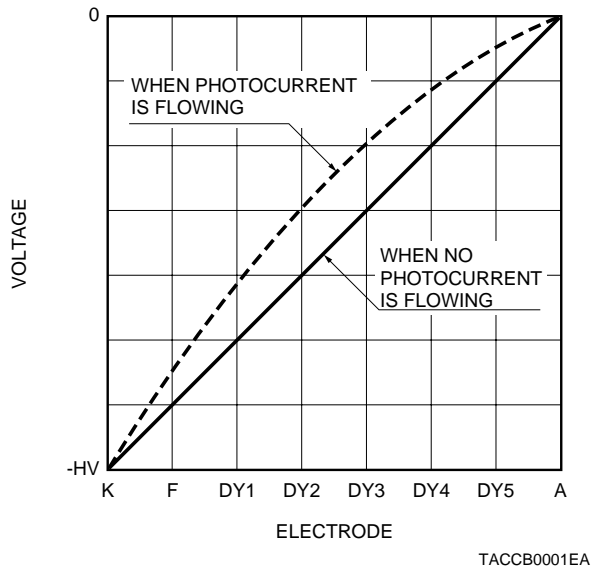


Figure 7-5: Basic operating circuit for a photomultiplier tube

The reduction of the divider current can be ignored if the anode output current is small. However, when the incident light level is increased and the resultant anode and dynode currents are increased, the voltage distribution for each dynode varies considerably as shown in Figure 7-6. Because the overall cathode-to-anode voltage is kept constant by the high-voltage power supply, the loss of the interstage voltage at the latter stages is redistributed to the previous stages so that there will be an increase in the interstage voltage.



**Figure 7-6: Influence of photocurrent on voltage applied to each electrode**

The loss of the interstage voltage by the multiplied electron current appears most significantly between the last dynode ( $DY_5$  in Figure 7-5) and the anode, but the voltage applied to this area does not contribute to the secondary emission ratio of the last dynode. Therefore, the shift in the voltage distribution to the earlier stages results in a collective increase in current amplification, as shown at region B in Figure 7-4. If the incident light level is increased further so that the anode current becomes quite large, the secondary-electron collection efficiency of the anode degrades as the voltage between the last dynode and the anode decreases. This leads to the saturation phenomenon like that shown at region C in Figure 7-4.

While there are differences depending on the type of photomultiplier tube and divider circuit being used, the maximum practical anode current in a DC output is usually 1/20th to 1/50th of the divider current. If linearity better than  $\pm 1$  percent is required, the maximum output must be held to less than 1/100th of the divider current.

To increase the maximum linear output, there are two techniques: one is to use a Zener diode between the last dynode and the anode as shown in Figure 7-2 (2) and, if necessary, between the next to last or second to last stage as well, and the other is to lower the voltage-divider resistor values to increase the divider current. However, with the former technique, if the divider current is insufficient, noise will be generated from the Zener diode, possibly causing detrimental effects on the output. Because of this, it is essential to increase the divider current to an adequate level and connect a ceramic capacitor having good frequency response in parallel with the Zener diode for absorbing the possible noise. It is also necessary to narrow the subsequent circuit bandwidth as much as possible, insofar as the response speed will permit. With the latter technique, if the voltage-divider resistors are located very close to the photomultiplier tube, the heat emanating from their resistance may raise the photomultiplier tube temperature, leading to an increase in the dark current and possible fluctuation in the output. Furthermore, since this technique requires a high-voltage power supply with a large capacity, it is inadvisable to increase the divider current more than necessary. To solve the above problems in applications where a high linear output is required, individual power supplies may be used in place of the voltage-divider resistors at the last few stages.

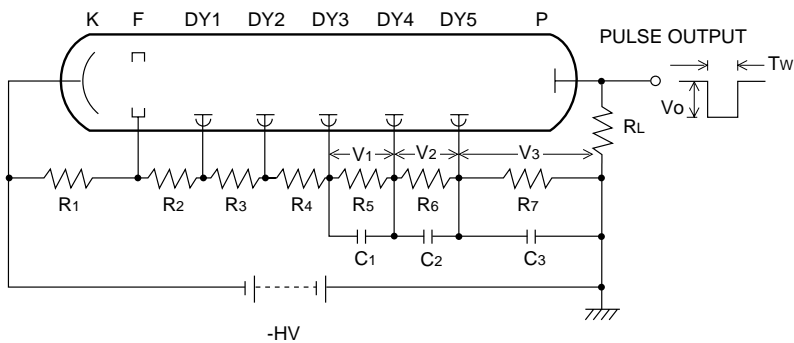
**(2) Pulse-operation output linearity and its countermeasures**

When a photomultiplier tube is pulse-operated using the voltage-divider circuit shown in Figure 7-2 (1) or Figure 7-3, the maximum linear output is limited to a fraction of the divider current just as in the case of DC operation. To prevent this problem, decoupling capacitors can be connected to the last few stages, as shown in Figures 7-7 (1) and (2). These capacitors supply the photomultiplier tube with an electric charge during the pulse duration and restrain the voltage drop between the last dynode and the anode, thus resulting in a significant improvement in pulse linearity. If the pulse width is sufficiently short so that the duty cycle is small, this method makes it possible to derive an output current up to the saturation level which is caused by the space charge effects in the photomultiplier tube dynodes discussed in Section 3.2, (2) of Chapter 3. Consequently, a high peak output current, more than several thousand times as large as the divider current can be attained.

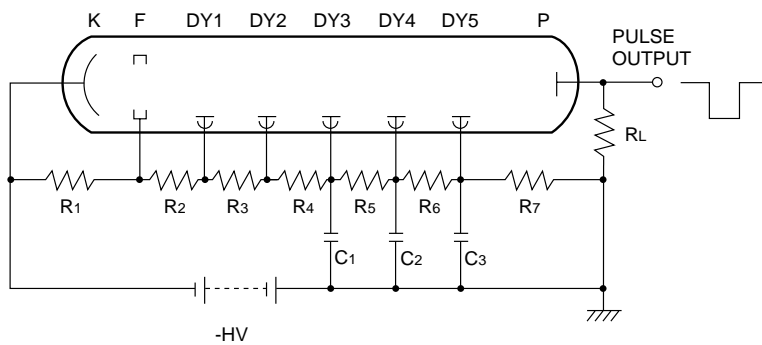
There are two methods of using the decoupling capacitors: a serial connection method and a parallel connection method as illustrated in Figure 7-7 below. The serial connection is more commonly used because the parallel connection requires capacitors which can withstand a high voltage.

The following explains the procedure for calculating the capacitor values, using the circuit shown in Figure 7-7 (1) as an example.

**(1) Serial-connected decoupling capacitors**



**(2) Parallel-connected decoupling capacitors**



TACCC0007EA

**Figure 7-7: Voltage-divider circuits with decoupling capacitors added**

First of all, if we let the output-pulse peak voltage be  $V_0$ , and the pulse width be  $T_w$  and the load resistance be  $R_L$ , the output pulse charge  $Q_0$  per pulse is expressed by Eq. 7-22), as follows:

$$Q_0 = T_w \frac{V_0}{R_L} \dots\dots\dots (Eq. 7-2)$$

Next, let us find the capacitance values of the decoupling capacitors  $C_1$  to  $C_3$ , using  $Q_0$ . If we let the charge stored in capacitor  $C_3$  be  $Q_3$ , then to achieve good output linearity of better than  $\pm 3$  percent, the following relation should generally be established:

$$Q_3 \geq 100 Q_0 \dots\dots\dots (\text{Eq. 7-3})$$

From the common relation of  $Q=CV$ ,  $C_3$  is given by Eqs. 7-4 and 7-5.

$$C_3 \geq 100 \frac{Q_3}{V_3} \dots\dots\dots (\text{Eq. 7-4})$$

then

$$C_3 \geq 100 \frac{Q_3}{I_b \cdot R_7} \dots\dots\dots (\text{Eq. 7-5})$$

Normally, the secondary emission ratio  $\delta$  per stage of a photomultiplier tube is 3 to 5 at the interstage voltage of 100 volts. However, considering occasions in which the interstage voltage drops to about 70 or 80 volts, the charges  $Q_2$  and  $Q_1$  stored in  $C_2$  and  $C_1$  respectively are calculated by assuming that  $\delta$  between each dynode is 2, as follows:

$$Q_2 = \frac{Q_3}{2} \quad Q_1 = \frac{Q_2}{2} = \frac{Q_3}{4}$$

Then, the capacitance values of  $C_2$  and  $C_1$  can be obtained in the same way as in  $C_3$ .

$$C_2 \geq 50 \frac{Q_0}{V_2} = 50 \frac{Q_0}{I_b \cdot R_6}$$

$$C_1 \geq 25 \frac{Q_0}{V_1} = 25 \frac{Q_0}{I_b \cdot R_5}$$

In cases where decoupling capacitors need to be placed in the dynode stages earlier than  $Dy_3$  in order to derive an even larger current output, the same calculation can also be used.

Here, as an example, with the output pulse peak voltage  $V_0=50\text{mV}$ , pulse width  $T_w=1\mu\text{s}$ , load resistance  $R_L=50\Omega$ , interstage resistor values  $R_5=R_6=R_7=100\text{k}\Omega$  and divider current  $I_b=1\text{mA}$ , each capacitor value can be calculated in the following steps: First, the amount of charge per output pulse is obtained as follows:

$$Q_0 \geq \frac{50\text{mV}}{50\Omega} \times 1\text{mA} = 1\text{nC}$$

The capacitance values required of the decoupling capacitors  $C_3$ ,  $C_2$  and  $C_1$  are calculated respectively as follows:

$$C_3 \geq 100 \frac{1\text{nC}}{100\text{k}\Omega \times 1\text{mA}} = 1\text{nF}$$

$$C_2 \geq 50 \frac{1\text{nC}}{100\text{k}\Omega \times 1\text{mA}} = 0.5\text{nF}$$

$$C_1 \geq 25 \frac{1\text{nC}}{100\text{k}\Omega \times 1\text{mA}} = 0.25\text{nF}$$

The above capacitance values are minimum values required for proper operation. Therefore it is usually suggested that the voltage-divider circuit be designed with a safety margin in the capacitance value, of about 10 times larger than the calculated values. If the output current increases further, additional decoupling capacitors should be connected as necessary to the earlier stages, as well as increasing the capacitance values of  $C_1$  to  $C_3$ . As with the DC operation, it should be noted that in pulse operation, even with the above countermeasures provided, the output deviates from the linearity range when the average output current exceeds 1/20th to 1/50th of the divider current. In particular, care is required at high counting rates even if the output peak current is low.

## 7.1.4 Voltage distribution in voltage-divider circuits

### (1) Voltage distribution in the anode and latter stages

Even under conditions where adequate countermeasures for pulse output linearity have been taken by use of decoupling capacitors, output saturation will occur at a certain level as the incident light is increased while the interstage voltage is kept fixed. This is caused by an increase in the electron density between the electrodes, causing space charge effects which disturb the electron current. This saturated current level varies, depending on the electrode structures of the anode and last few stages of the photomultiplier tube and also on the voltage applied between each electrode. As a corrective action to overcome space charge effects, the voltage applied to the last few stages, where the electron density becomes high, should be set at a higher value than the standard voltage distribution so that the voltage gradient between those electrodes is enhanced. For this purpose, a so-called tapered voltage-divider circuit is often employed, in which the interstage voltage is increased in the latter stages. But, sufficient care must be taken with regard to the interelectrode voltage tolerance capacity.

As an example, Figure 7-8 shows a tapered voltage-divider circuit used for a 5-stage photomultiplier tube. In this voltage-divider circuit, the  $Dy_5$ -to-anode voltage is set at a value lower than the  $Dy_4$ -to- $Dy_5$  voltage. This is because the electrode distance between the last dynode and the anode is usually short so that an adequate voltage gradient can be obtained with a relatively low voltage.

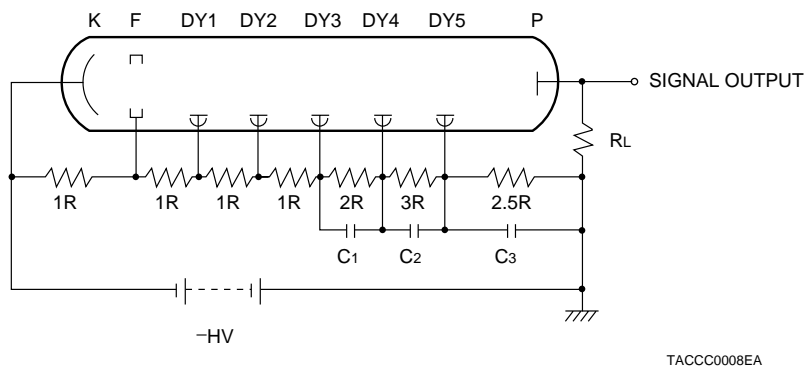


**Figure 7-8: Pulse output linearity countermeasures using decoupling capacitors and tapered voltage-divider circuit**

The voltage distribution ratio for a voltage-divider circuit that provides optimum pulse linearity depends on the type of photomultiplier tube. In high energy physics applications, a higher pulse output is usually required. Our catalog "Photomultiplier Tubes and Assemblies for Scintillation Counting and High Energy Physics" lists the recommended voltage distribution ratios of individual voltage-divider circuits intended for high pulse linearity (tapered voltage-dividers) and their maximum output current values. Use of these recommended voltage-divider circuits improves pulse linearity 5 to 10 times than that obtained with normal voltage-divider circuits (equally divided circuits). Figure 7-9 shows a comparison of pulse linearity characteristics measured with a tapered voltage-divider circuit and with a normal voltage-divider circuit. It is obvious that pulse linearity is improved about 10 times by using the tapered voltage-divider circuit. Note that when this type of tapered voltage-divider circuit is used, the anode output lowers to about 1/5th in comparison with the normal voltage-divider anode output. Therefore, adjustment is required to increase the supply voltage for the photomultiplier tube.

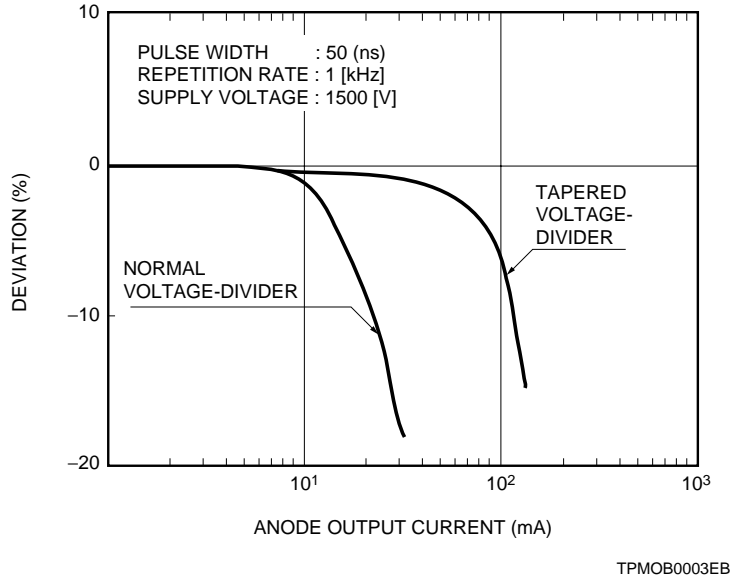


**Figure 7-9: Linearity characteristic using a tapered and a normal voltage-divider circuit**

The above methods for improving pulse output linearity by use of decoupling capacitors and tapered voltage-divider circuits are also applicable for the voltage-divider circuits with the cathode at ground potential and the anode at a high positive voltage.

The tapered voltage-divider circuit will also prove effective in special applications where a high output voltage is required. For instance, with an anode output current of  $I_p=100\mu\text{A}$  and  $R_L=1\text{M}\Omega$ , the output voltage will be 10 volts and the anode potential will drop 10 volts accordingly. This means that the anode-to-last-dynode voltage must be sufficiently greater than 10 volts in order to prevent the output linearity from deviating. Use of a tapered voltage-divider circuit can maintain the anode-to-last-dynode voltage at an adequate level and thus provides a higher output voltage compared to normal voltage-divider circuits.

## (2) Voltage distribution for the cathode and earlier stages

As mentioned above, the voltage distribution ratio for the latter stages near the anode is an important factor that determines the output linearity of a photomultiplier tube. In contrast, the voltage distribution between the cathode, focusing electrode and first dynode has an influence on the photoelectron collection efficiency and the secondary emission ratio of the first dynode. These parameters are major factors in determining the output signal-to-noise ratio, pulse height dispersion in the single and multiple photon regions, and also electron transit time spread (TTS).

Furthermore, the voltage distribution at the earlier stages affects the cathode linearity, energy resolution in scintillation counting and magnetic characteristics of a photomultiplier tube, and therefore its setting requires care just as in the case of the latter stages. In general, the voltage distribution ratios for the earlier stages listed in our catalog are determined in consideration of the electron collection efficiency, time properties and signal-to-noise ratio. Note that since they are selected based on the recommended supply voltage, proper corrective actions may be required in cases in which the supply voltage becomes less than one-half that of the recommended voltage. For example, increasing the voltage distribution ratio at the earlier stages or using Zener diodes to hold the dynode voltage constant are necessary. For more information on the photoelectron collection efficiency, output signal-to-noise ratio and other characteristics, refer to Chapter 3.

Figure 7-10 shows a variant of the voltage-divider circuit shown in Figure 7-10, which provides the above measures for the cathode to the first dynode.

It is quite essential to apply the correct voltage to the cathode, focusing electrode and the first dynode or earlier dynode stages with precision resistors. In applications such as in a magnetic field, or in very low-light-level measurement where shot noise may create a problem, or in single photon counting and in TOF (time-of-flight) trigger counters or hodoscopes requiring good time properties.

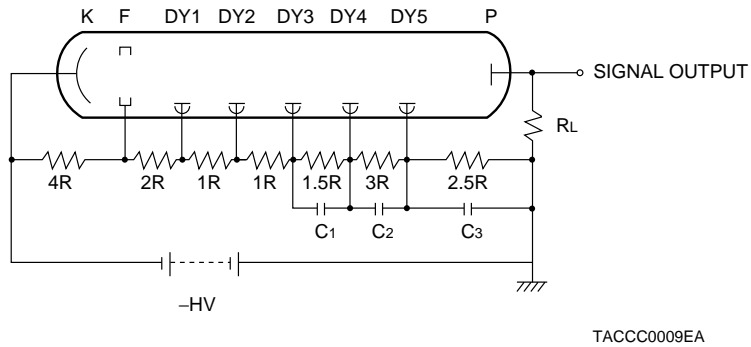
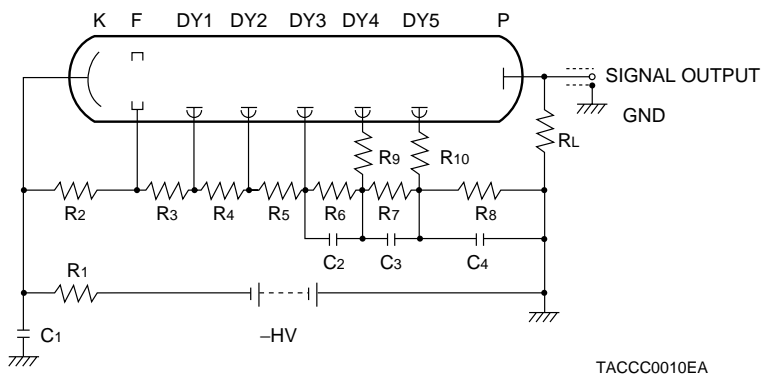


**Figure 7-10: Voltage-divider circuit with tapered configurations at both the earlier and latter stages**

The recommended voltage distribution ratios listed in our catalog are selected for general-purpose applications, with consideration primarily given to the gain. Accordingly, when the photomultiplier tube must be operated at a lower supply voltage or must provide a higher output current, selecting a proper voltage distribution ratio that matches the application is necessary. As to the resistance values actually used for the voltage-divider circuit, they should basically be selected in view of the photomultiplier tube supply voltage, output current level and required linearity. It should be noted that if the resistance values are unnecessarily small, the resulting heat generation may cause various problems, such as an increase in the dark current, temperature drift in the output and lack of capacity in the power supply. Therefore, avoid allowing excessive divider current to flow.

### 7.1.5 Countermeasures for fast response circuits

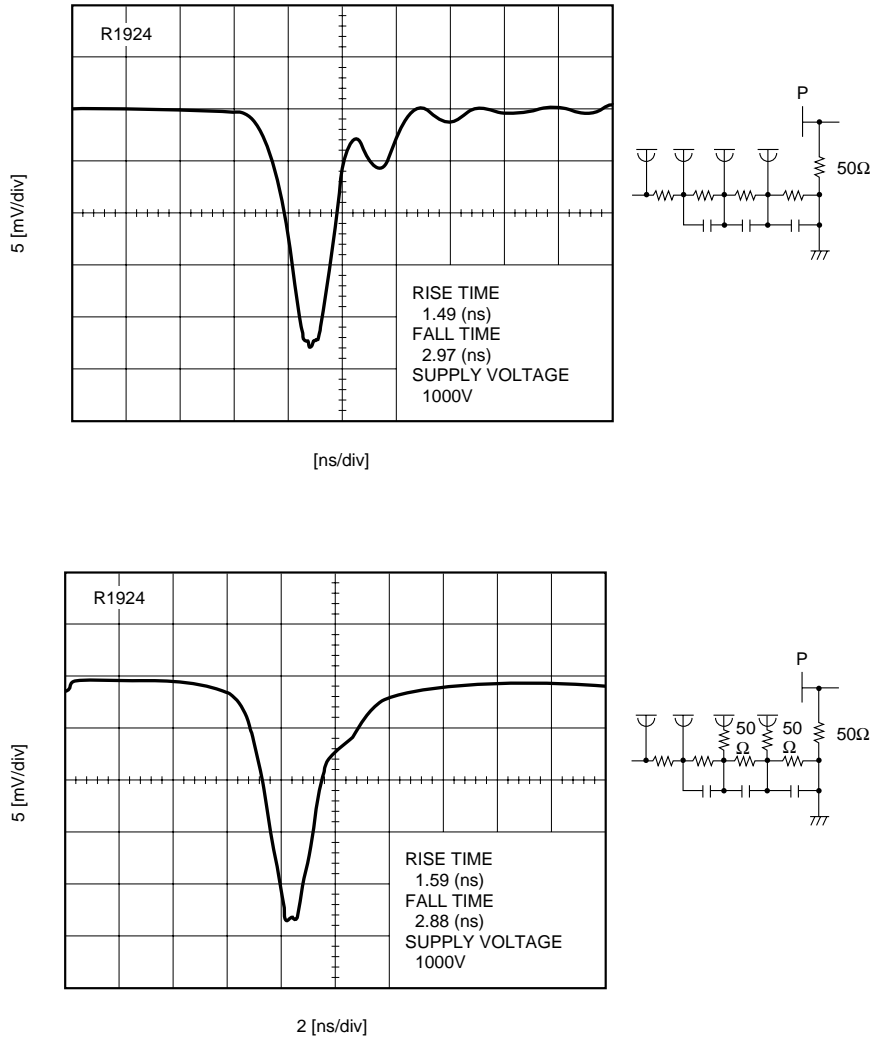
As shown in Figure 7-11, inserting a lowpass filter comprised of  $R_1$  and  $C_1$  into the high-voltage supply line is also effective in reducing noise pickup from the high-voltage line. The transistor  $R_1$  is usually several tens of kilohms, and a ceramic capacitor of 0.005 to 0.05 microfarads which withstands high voltage is frequently used as  $C_1$ .



**Figure 7-11: Voltage-divider circuit with countermeasure against pulse output linearity, ringing and high-voltage power supply noise**

In applications handling a fast pulsed output with a rise time of less than 10 nanoseconds, inserting damp-

ing resistors  $R_{10}$  into the last dynode as shown in Figure 7-11 and if necessary,  $R_9$  into the next to last dynode can reduce ringing in the output waveform. As damping resistors, noninduction type resistors of about 10 to 100 ohms are used. If these values are too large, the time response will deteriorate. Minimum possible values should be selected in the necessary range while observing the actual output waveforms. Figure 7-12 shows typical waveforms as observed in a normal voltage-divider circuit with or without damping resistors. It is clear that use of the damping resistors effectively reduces ringing.



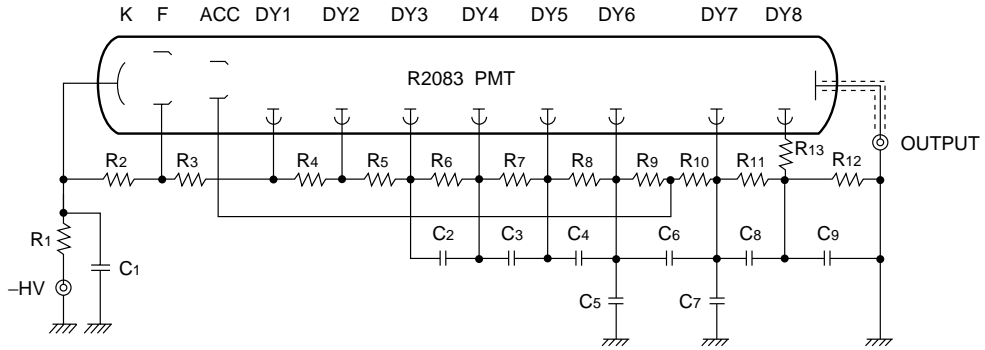
TACCB0002EA

Figure 7-12: Effect of damping resistors on ringing

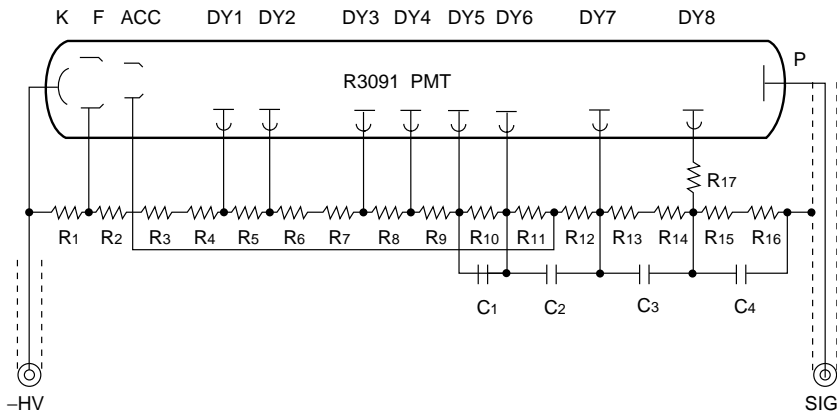
### 7. 1. 6 Practical fast-response voltage-divider circuits

The circuit diagrams of the Hamamatsu H2431 and H3284 photomultiplier tube assemblies are shown in Figure 7-13 below as practical examples of fast-response voltage-divider circuits which have been designed based on the description in the preceding section.

(a) H2431 circuit diagram



(b) H3284 circuit diagram



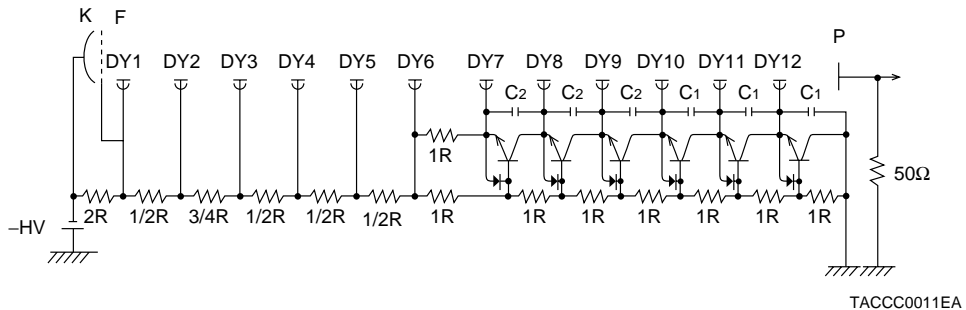
TPMHC0016EA

Figure 7-13: Fast-response voltage-divider circuits

### 7.1.7 High output linearity voltage-divider circuit (1)

In pulse applications such as scintillation counting, when a photomultiplier tube is operated at a high count rate, the output sometimes encounters linearity problems. In this case, use of transistors in place of the voltage-divider resistors at the latter stages can improve the output linearity degradation resulting from the divider current limitation.

As an example, Figure 7-14 shows a voltage-divider circuit for the Hamamatsu R329 photomultiplier tube, devised by FNAL (Fermi National Accelerator Laboratories)<sup>3)</sup>.



**Figure 7-14: Voltage-divider circuit using transistors**

In the circuit shown in Figure 7-14, a photoelectron current first flows into the first dynode, then secondary electrons flow through the successive dynodes and into the collector of each transistor. As a result, the emitter potential of each transistor increases while the collector current decreases along with a decrease in the base current. At this point, the decrease in the collector current is nearly equal to the current flowing through the photomultiplier tube and accordingly, the transistors supply the current for the photomultiplier tube.

When using these transistors, the following points must be taken into consideration.

1. Choose transistors having a large  $h_{fe}$  so that sufficient current can flow into the collector.
2. Choose transistors having good frequency characteristics.
3. Use capacitors having good frequency characteristics.
4. The number of stages to which transistors are added should be determined in view of the operating conditions of the photomultiplier tube to be used.

### 7. 1. 8 High output linearity voltage-divider circuit (2)

As shown in Figure 7-15, this circuit utilizes a Cockcroft-Walton voltage multiplier circuit in which an array of diodes is connected in series. Along each side of the alternate connection points, capacitors are connected in series. If the reference voltage  $V$  is placed at the input, this circuit provides voltage potentials of  $2V$ ,  $3V$  and so on at each connection point. Therefore, this power supply circuit functions just like a conventional resistive voltage-divider circuit. In addition, this circuit achieves good linearity for both DC and pulsed currents yet with low power consumption, making it suitable for use in compact circuits. As Figure 7-16 shows, the Cockcroft-Walton circuit assures higher DC linearity than that obtained with a resistive voltage-divider circuit.

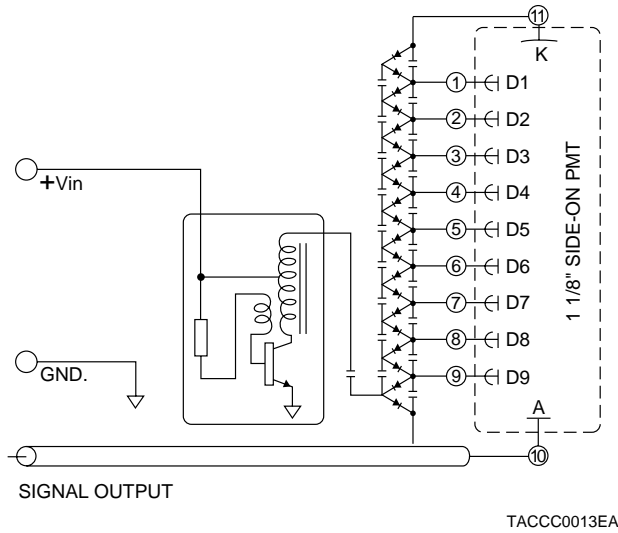


Figure 7-15: Cockcroft-Walton circuit

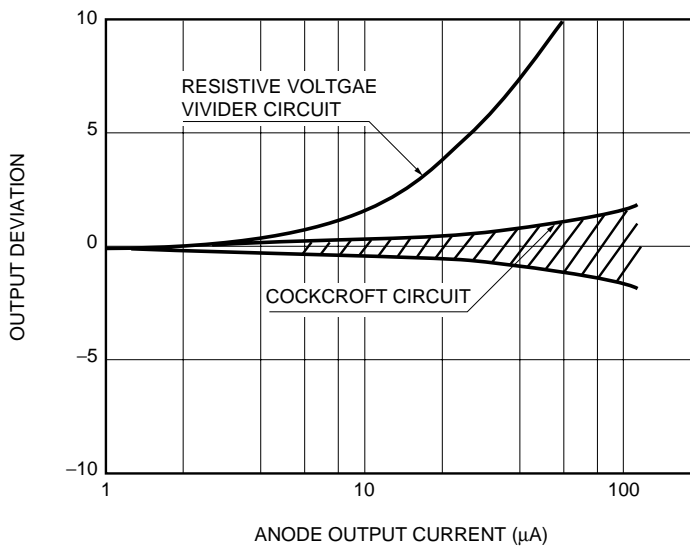
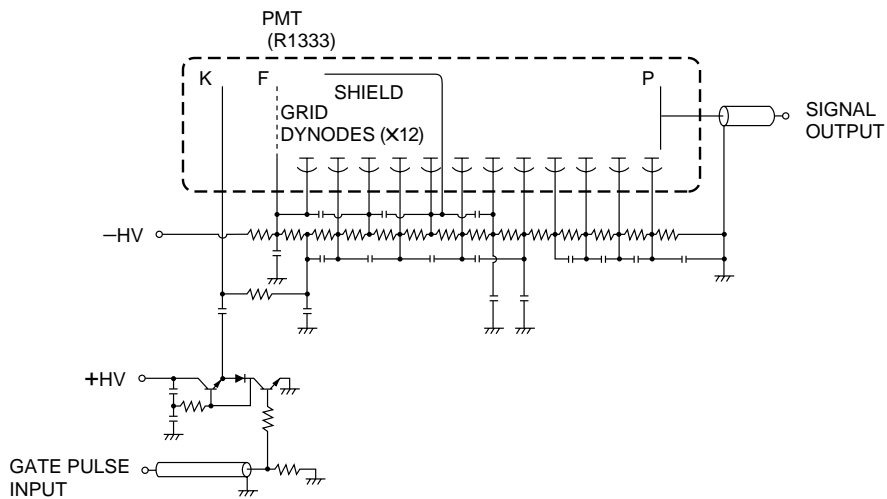


Figure 7-16: Output linearity

### 7.1.9 Gating circuit

Next, let us introduce gating circuits as a variant of voltage-divider circuits.

In general, in such applications as fluorescence measurement, plasma electron temperature measurement utilizing Thomson scattering, Raman spectroscopy and detection of defects in optical transmission paths, the signal light to be measured is extremely weak in comparison with primary light levels such as the excitation light. For this reason, the detector system is set up to have extremely high sensitivity. If even part of the primary light enters the detector system as stray light, it may cause saturation in the photomultiplier tube output and in the subsequent circuits, degrading their performance. This problem could be solved if only the excessive light was blocked by use of an ultra-fast shutter such as a liquid crystal. But this is not yet practical. A practical technique commonly used is “gating” by which a photomultiplier tube is electronically switched to eliminate the output during unnecessary periods when excess light may be present.



TACCC0014EA

**Figure 7-17: Circuit diagram of the C1392 socket assembly with a gating circuit**

Figure 7-17 shows the circuit diagram of the Hamamatsu C1392 socket assembly with a gating circuit.<sup>4)</sup> The C1392 is a "normally OFF" type which normally sets the photomultiplier tube output to OFF, and when a gate signal is inputted, sets the photomultiplier output to ON. Also available are variant models with reverse operation, i.e., a "normally ON" type which sets the output to OFF by input of a gate signal.

The following explains the basic operation of the C1392 socket assembly used in conjunction with a photomultiplier tube.

If the photomultiplier tube output is OFF at a gate input of 0V, a reverse bias of about 10 volts with respect to the focusing electrode and first dynode is supplied to the cathode, thereby preventing photoelectrons, if emitted from the cathode, from reaching the dynode section. Here, if a pulse signal of +3 to +4 volts is applied to the gate input terminal, the driver circuit gives a forward bias to the cathode via capacitance coupling, and sets the photomultiplier tube output to ON during the period determined by the gate pulse width and the time constant of the capacitance-coupled circuit. This gating circuit provides a switching ratio (or extinction ratio) of  $10^4$  or more. The capacitors are connected from the first through the center dynode to absorb the switching noises often encountered with this type of gating circuit.

### 7.1.10 Output control circuit

The photomultiplier tube output is usually controlled by changing the supply voltage. In some applications, however, a single power supply is used to operate two or more photomultiplier tubes or an output control circuit is added to the voltage-divider circuit if the variable range of the high-voltage power supply and amplifier is narrow. The following explains how to provide an output control circuit, using the circuits shown in Figure 7-18 as examples.

With the circuits shown in Figure 7-18, there are three techniques for controlling the photomultiplier tube output. The first is, as shown in both (1) and (2) in the figure, to use a variable resistor connected between the cathode and the negative high-voltage power supply so that the overall voltage applied to the photomultiplier tube can be varied. With this technique, depending on the conditions, the photomultiplier tube gain can be varied within a considerably wide range (up to 10 times). The high voltage supplied from the power supply is divided across this variable resistor and each resistor in the voltage-divider circuit. If the resistance value of the variable resistor is known, the change in the voltage applied to the photomultiplier tube can also be found, thus the signal variation can be predicted. Therefore, this technique is frequently used in many applications. It should be borne in mind that the higher the voltage-divider resistance value, the higher the variable resistance value should be and, in some cases, it might be difficult to obtain a high-quality resistor with high resistance and large rated capacity. On the other hand, if the voltage-divider resistor value is too small, a variable resistor with high rated capacity is required, and problems with contact failure in the variable resistor tend to occur.

Moreover, when a negative high voltage is applied to the cathode as shown in the figure, a high voltage is also impressed on the variable resistor. Thus the housing that contains the photomultiplier tube and associated circuits must also be designed to have sufficiently high dielectric resistance.

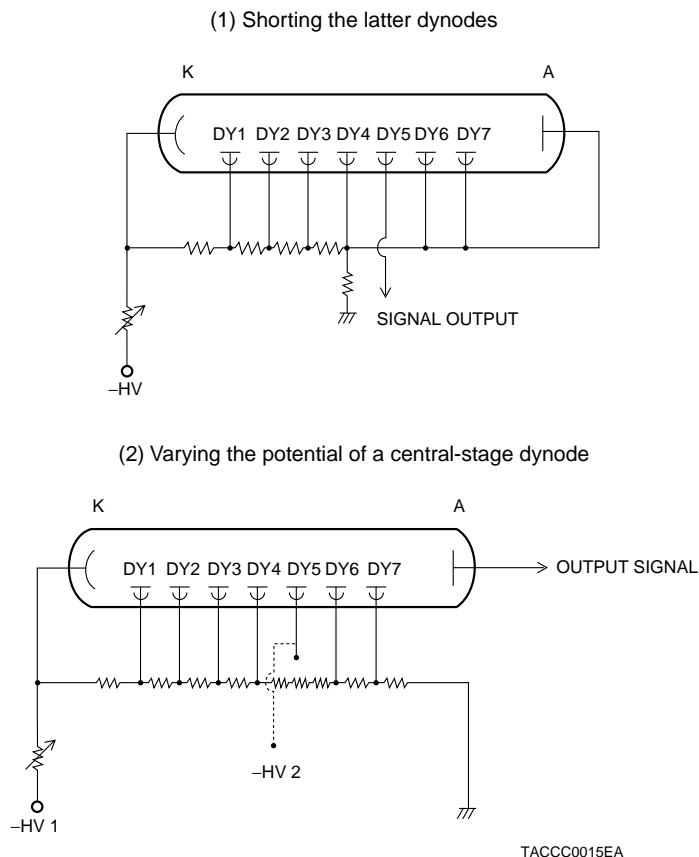
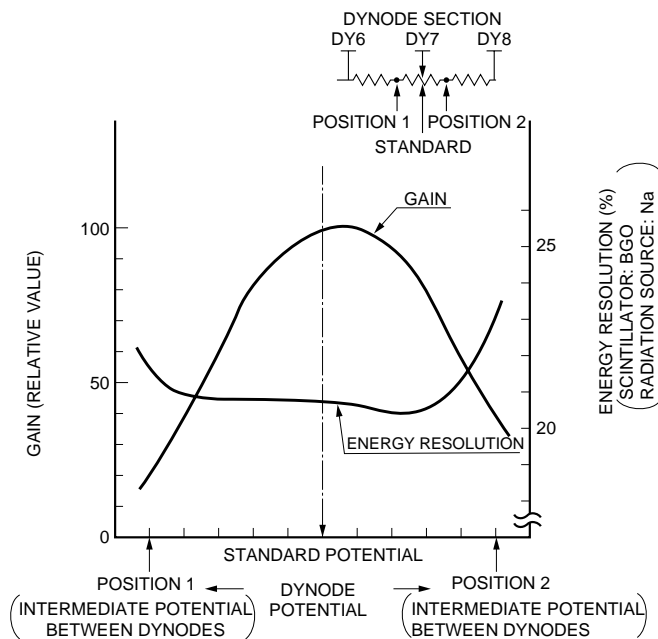


Figure 7-18: Output control circuits

The second technique is to short the latter dynode stages and anode so that the signal is derived from a middle dynode. This is effective in cases in which the photomultiplier tube gain is so high that the supply voltage may drop considerably and the resultant decrease in the interstage voltage degrades the collection efficiency and secondary electron emission ratio. Shorting the latter dynode stages as shown in (1), that is, essentially, reducing the number of dynode stages, assures a higher interstage voltage and results in an improvement in the signal-to-noise ratio. However, this is accompanied by a sacrifice in linearity characteristics because the output is fetched from an earlier dynode. Furthermore, since the number of stages being used is changed, the gain versus supply voltage characteristic also varies accordingly. The degree of this variation is different from tube to tube, and it is therefore best to select a photomultiplier tube with characteristics optimized for the particular application rather than using this technique.

The third technique is performed by varying the potential of a mid-stage dynode, as shown in Figure 7-18 (2). This makes use of the fact that with a varying dynode potential, the number of secondary electrons released from the dynode decreases and also the collection efficiency between dynodes drops. There are two methods of adjusting the dynode potential. In one method a variable resistor is added between the front and rear adjacent dynodes. The other method is to use an external power supply directly connected to the central dynode. Although both are relatively easy to implement, there is a disadvantage that the signal-to-noise ratio may deteriorate if the dynode potential is varied too much. Figure 7-19 dictates the gain variation and energy resolution of a photomultiplier tube when the dynode potential is varied continuously. It can be seen that the energy resolution begins to deteriorate near the points at which the gain drops by more than 50 percent. This behavior is not constant but differs depending on individual photomultiplier tubes. In addition, the variable gain range is not so wide.



**Figure 7-19: Gain variation and energy resolution as a function of dynode potential**

As discussed above, it should be noted that using the voltage-divider circuit for controlling the photomultiplier tube output is not recommended. We advise using normal methods by which the power supply voltage is directly changed for controlling the photomultiplier tube output.

### 7.1.11 Precautions when fabricating a voltage-divider circuit

In the previous sections, the functions of various voltage-divider circuits and their design consideration have been discussed. This section describes the precautions for actually fabricating a voltage-divider circuit.

#### (1) Selecting the parts used for a voltage-divider circuit

Since the voltage-divider circuit has a direct influence on the photomultiplier tube operation, careful selection of parts is necessary.

##### Resistors

Because photomultiplier tubes are very susceptible to changes in the supply voltage and interstage voltage, metal-film resistors with a minimum temperature coefficient should be used. Preferably, use the same type of resistor for all stages, but if not available, select resistors with temperature coefficients which are close to each other. These resistors should also have good temperature characteristics, but their accuracy is not so critical. If non-uniformity between each resistor is held within  $\pm 5$  percent, it will work sufficiently. This is because the photomultiplier tube gain varies to some degree from tube to tube and also because a voltage difference of several volts will not affect the electron trajectories very much. If possible, we recommend using resistors with sufficient rated power and dielectric resistance, for example, respectively at least 1.7 times and 1.5 times higher than necessary. As a rough guide, the resistance value per stage is typically from 100 kilohms to 1 megohm. For damping resistance and load resistance, use noninduction type resistors designed for use at high frequency.

##### Decoupling capacitors

In pulsed light applications where a fast response photomultiplier tube handles the output with a rise time of less than 10 nanoseconds, decoupling capacitors are connected between dynodes. For these decoupling capacitors, use ceramic capacitors with sufficiently high impedance at a high frequency range and adequate dielectric resistance at least 1.5 times higher than the maximum voltage applied between dynodes. To prevent the actual capacitance from being lower than the designed value during operation, select capacitors with a minimum minus (-) tolerance.

For the bypass capacitor used to eliminate noise from the power supply connected to the high-voltage input terminal of a photomultiplier tube, use a ceramic capacitor having high impedance at high frequencies and adequate dielectric resistance.

##### Coupling capacitors

For the coupling capacitor which separates the signal from a positive high voltage applied to the anode in a grounded-cathode voltage-divider circuit, use a ceramic capacitor having minimum leakage current (which may also be a source of noise) as well as having superior frequency response and sufficient dielectric resistance.

##### PC boards for voltage-divider circuits

When a voltage-divider circuit is assembled not on a photomultiplier tube socket but on a PC board, use a high-quality PC board made of glass epoxy or similar materials which exhibit low leakage current even at a high voltage. If both sides of the PC board are used for assembly, select a board with adequate thickness.

On a glass epoxy board, the wiring space between patterns necessary to hold a potential difference of 1 kilovolt is typically 1 millimeter or more.

## Leads

For high voltage circuits, use teflon or silicone leads which can withstand a high voltage, or use coaxial cable such as RG-59B/U. In either case, take sufficient care with regard to the dielectric resistance of leads or conductor wires.

For signal output lines, use of a coaxial cable such as RG-174/U and 3D-2V is recommended. For high-speed circuits, in particular, a 50-ohm coaxial cable is commonly used to provide the good impedance match with the measurement equipment. However, if the signal current to be derived is not very low (several microamperes or more) and the lead length is no longer than 20 centimeters, using normal leads does not create any problem in practice, as long as a noise source is not located near the photomultiplier tube.

## (2) Precautions for mounting components

This section describes precautions to be observed when mounting components on a voltage-divider circuit. Refer to Figure 7-11 while reading the following precautions.

### Voltage-divider resistors

Considering heat dispersion, provide adequate space between voltage-divider resistors so as not to allow them to make contact with each other. When a low resistance is used or in low-light-level measurement where an increase in the dark current resulting from temperature rise may create a significant problem, avoid direct connections of voltage-divider resistors to the lead pins of the photomultiplier tube or to the socket so that Joule heat generated from the voltage-divider circuit is not directly conducted to the photomultiplier tube. Be sure to allow a distance between the photomultiplier tube and the voltage-divider circuit.

### Decoupling capacitors

The lead length of decoupling capacitors used for fast pulse operation affects the photomultiplier tube time properties and also causes ringing due to the lead inductance. Therefore lead length should be kept as short as possible. Even when mounting voltage-divider resistors remote from a photomultiplier tube, the decoupling capacitors must be mounted directly to the lead pins of the photomultiplier tube or to the socket.

### Signal output line

The wiring length of a signal output line including load resistance should be as short as possible. It must be wired away from the high voltage lines and the components to which a high voltage is applied. In particular, when handling fast pulse signals, grounding of the signal circuitry and power supply circuitry, as shown in Figure 7-11, is essential. If extra-low output currents are to be derived from a photomultiplier tube, attention must also be paid to shielding the signal line and to preventing ohmic leakage.

## 7.2 Photomultiplier Tube Voltage Dependence and High-Voltage Power Supply

Photoelectrons emitted from the photocathode of a photomultiplier tube are guided by the focusing electrode or accelerating electrode and impinge on the first dynode where several times this number of electrons are released as secondary electrons. These secondary electrons are further multiplied in the successive dynodes and finally a large number of electrons, 0.1 to 10 million times the initial number of photoelectrons, reach the anode. As detailed in Section 2.2 of Chapter 3, when a voltage  $V$  is applied between the cathode and the anode of a photomultiplier tube having  $n$  dynode stages, the overall current gain  $\mu$  is expressed in the following relation.

$$\mu = A \cdot V^{kn}$$

Typical photomultiplier tubes employ about 10 stages of dynodes and as shown in Figure 7-20, the current amplification is proportional to the 6th to 10th power of the voltage applied between the cathode and the anode. This means that the photomultiplier tube output is extremely susceptible to variations in the applied voltage and that the power supply used for photomultiplier tubes must be stable.

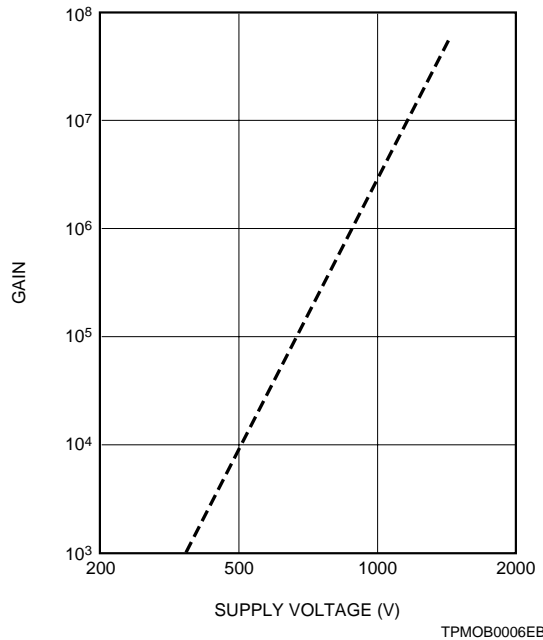


**Figure 7-20: Current amplification vs. supply voltage**

Including drift, ripple, temperature dependence, input regulation and load regulation, the power supply must provide collective stability which is at least 10 times as stable as the output stability required of the photomultiplier tube.

Series-regulator types regulated high-voltage power supplies optimized for photomultiplier tubes, are extensively used and have gained a good reputation. Recently, a variety of switching-regulator types have been put on the market and are becoming widely used. Most of the switching-regulator type power supplies offer compactness and light weight, yet provide high voltage and high current. However, with some models, the switching noise is superimposed on the AC input and high voltage output or the noise is radiated. Thus, sufficient care is required when selecting this type of power supply, especially in low-light-level detection, measurement involving fast signal processing, and photon counting applications.

## 7.3 Connection to The External Circuit

### 7.3.1 Observing an output signal

To observe the output signal of a photomultiplier tube, various methods are used depending on the operating conditions as illustrated in Figures 7-21 to 7-23.

As described in Section 7.1.2 in this chapter, there are two schemes for voltage-divider circuit operation: the anode grounding and the cathode grounding schemes. The anode grounding scheme permits both DC and pulse operation as shown in Figures 7-21 and 7-22. On the other hand, the cathode grounding scheme uses a coupling capacitor to separate the high voltage applied to the anode, so that only pulse operation is feasible. This scheme eliminates DC components produced by such factors as background light.

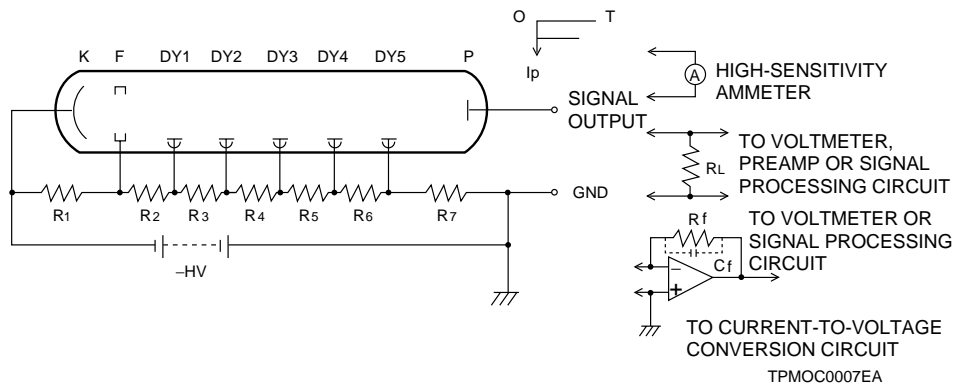


Figure 7-21: Anode grounding scheme in DC operation

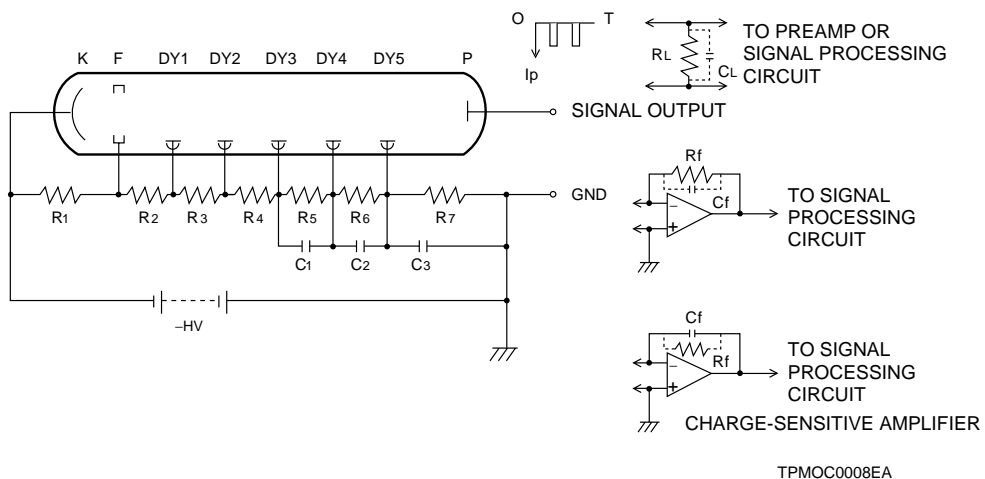
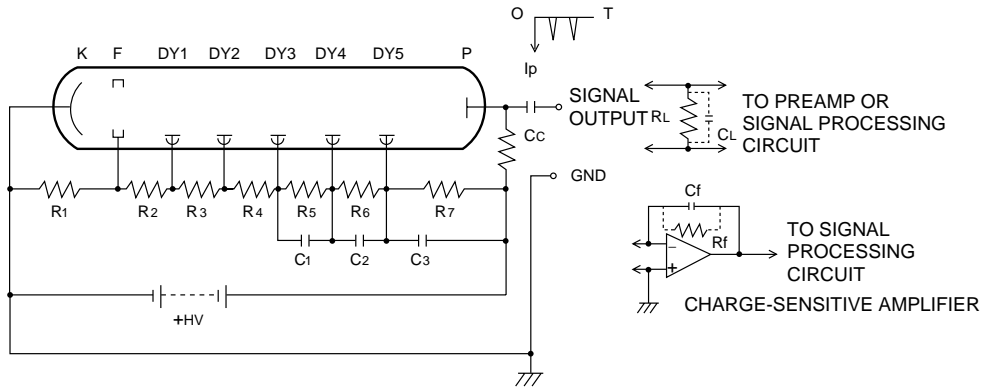


Figure 7-22: Anode grounding scheme in pulse operation



TPMOC009EA

**Figure 7-23: Cathode grounding scheme in pulse operation**

It should be noted that when wiring the photomultiplier tube output to an amplifier circuit, the amplifier circuit must be wired before turning on the high-voltage power supply. When a high voltage is applied to the voltage-divider circuit even in a dark state, the possible dark current creates a charge on the anode. If the voltage-divider circuit is wired to the amplifier circuit under this condition, the charge will instantaneously flow into the amplifier, thus probably leading to damage of the amplifier circuit. Care should particularly be taken when using high speed circuits, as they are more susceptible to damage.

### 7.3.2 Influence of a coupling capacitor

A coupling capacitor, required by the cathode grounding scheme, can also be used in the anode grounding scheme in order to eliminate the DC components. This section describes precautions for using a voltage-divider circuit to which a coupling capacitor is connected.

#### Output waveform

When a photomultiplier tube is operated with the circuit shown in Figure 7-24, if the anode output pulse width  $P_w$  is sufficiently shorter than the time constant  $CR$  ( $R$  is parallel resistance of  $R_a$  and  $R_L$ ), the impedance of the coupling capacitor can be ignored and thus the signal pulse current is divided to flow into  $R_L$  and  $R_a$ . In this case, the input waveform is transmitted to the output waveform without distortion, regardless of the capacitance value of the coupling capacitor. However, if  $P_w$  is close to or longer than  $CR$ , the output will have a differential waveform.

Because the coupling capacitor is merely used as a coupling element between the voltage-divider circuit and the amplifier circuit,  $P_w$  must be at least several tens of times shorter than  $C_R$  so that the output waveform has good fidelity to the input waveform. If the output waveform is differentiated, the output pulse height is influenced by the capacitance value and temperature characteristic of the coupling capacitor. In particular, when a 50-ohm resistor is used for  $R_a$  to optimize fast response operation, the time constant  $C_R$  becomes small and thus care should be taken of this point.

In the case of low frequency applications, the impedance of the coupling capacitor cannot be ignored. Since its impedance  $Z_c = \frac{1}{2\pi f C}$ , the output signal decays by 3dB (approximately to 7/10th of the pulse height) at a frequency  $f = 1/2\pi C R_a$ .

**Base-line shift**

As stated above, the amount of the signal passing through the coupling capacitor is stored as a corresponding charge on the capacitor. This stored charge  $Q$  generates a voltage of  $E_0=Q/C$  across both sides of the capacitor in the reverse direction of the signal. This voltage  $E_0$  attenuates by a factor of  $V=E_0e^{-t/RC}$  related to the time constant  $CR$  which is determined by the capacitance value  $C$  and the serial resistance value  $R$  of  $R_a$  and  $R_L$ . The voltage induced in the capacitor is divided by  $R_a$  and  $R_L$ , and the output voltage  $V_a$  is given by the following equation:

$$V_a = E_0e^{-t/RC} \times \frac{R_a}{R_a+R_L} \dots\dots\dots \text{(Eq. 7-6)}$$

Here, if the signal repetition rate increases, the base line does not return to the true zero level. This is known as base-line shift, and can be minimized by reducing the time constant  $CR$ . In this case, reducing the capacitor value increases the initial voltage  $E_0$ , but shortens the discharge time. Decreasing the resistor value also shortens the discharge time, but this is accompanied by a decrease in the signal voltage, causing a problem with the signal-to-noise ratio. In contrast, increasing the resistor value produces a larger output and results in an improvement in the signal-to-noise ratio, but a base-line shift tends to occur due to the long time constant. If  $R_a$  is large, it lowers the anode potential, thus care is required when excessive current including DC current flows.

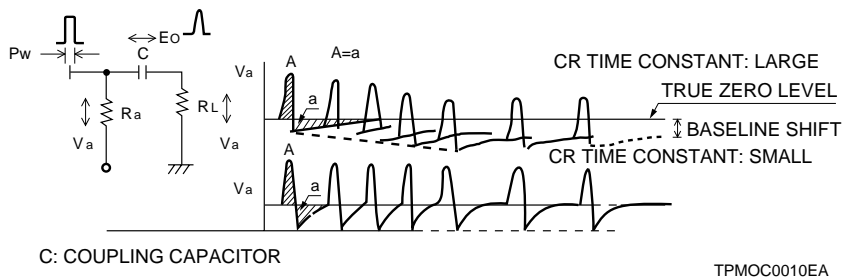


**Figure 7-24: Base-line shift**

Eventually, when the amount of charge stored on the capacitor (portion A in Figure 7-24) is discharged in a certain time period (portion a in Figure 7-24), the area of portion A is equal to the area of portion a, regardless of the discharge time constant. In general, the circuit time constant is longer than the signal pulse width, so this discharge time will have less effect on the pulse height. However, when the signal repetition rate is extremely high or accurate information on the output pulse height is needed, the discharge time cannot be neglected. If a base-line shift occurs, the signal is observed at an apparently lower level. Therefore, when designing the circuit it is necessary to select the optimum resistor and capacitor values such that the output pulse height exhibits no fluctuations even if the signal repetition rate is increased.

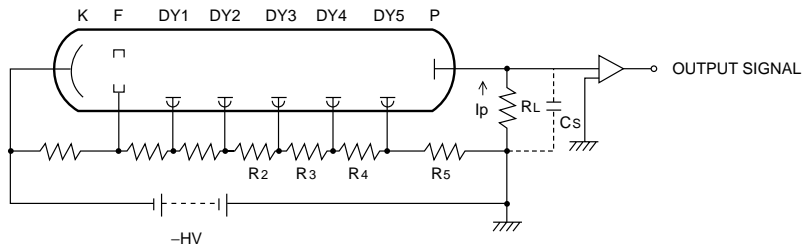
Furthermore, when multiple pulses enter the measurement system including an amplifier, these pulses are added to create a large pulse, and a so-called "pile-up" problem occurs. Because of this, in applications where a pulse height discriminator is used to discern the height of individual pulses, it is important to take into account the time resolution of the measurement device.

### 7.3.3 Current-to-voltage conversion for photomultiplier tube output

The output of a photomultiplier tube is a current (charge), while the external signal processing circuit is usually designed to handle a voltage signal. Therefore, the current output must be converted into a voltage signal by some means, except when the output is measured with a high-sensitivity ammeter. The following describes how to perform the current-to-voltage conversion and major precautions to be observed.

#### (1) Current-to-voltage conversion using load resistance

One method for converting the current output of a photomultiplier tube into a voltage output is to use a load resistance. Since the photomultiplier tube may be thought of as an ideal constant-current source at low output current levels, a load resistance with a considerably large value can theoretically be used. In practice, however, the load resistance value is limited by such factors as the required frequency response and output linearity as discussed below.



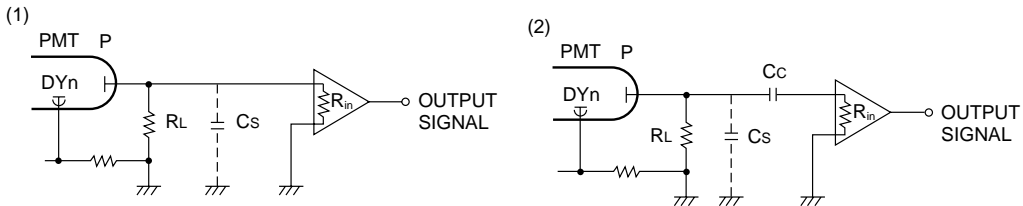
TACCC0016EA

Figure 7-25: Photomultiplier tube and output circuit

If, in the circuit of Figure 7-25, we let the load resistance be  $R_L$  and the total electrostatic capacitance of the photomultiplier tube anode to all other electrodes including stray capacitance such as wiring capacitance be  $C_s$ , then the cutoff frequency  $f_c$  is given by the following equation:

$$f_c = \frac{1}{2\pi C_s R_L} \text{ (Hz)} \dots\dots\dots \text{(Eq. 7-7)}$$

From this relation, it can be seen that, even if the photomultiplier tube and amplifier have fast response, the response is limited to the cutoff frequency  $f_c$  determined by the subsequent output circuits. In addition, as described in Section 7.1.4 in this chapter, if the load resistance is made unnecessarily large, the voltage drop by  $I_p \cdot R_L$  at the anode potential is increased accordingly, causing the last-dynode-to-anode voltage to decrease. This will increase the space charge effect and result in degradation of output linearity.



TACCC0017EA

Figure 7-26: Amplifier internal input resistance

When selecting the optimum load resistance, it is also necessary to take account of the internal input resistance of the amplifier connected to the photomultiplier tube. Figure 7-26 shows equivalent circuits of the photomultiplier tube output when connected to an amplifier. In this figure, if the load resistance is  $R_L$  and the input resistance is  $R_{in}$ , the resultant parallel output resistance  $R_0$  is calculated from the following relation:

$$R_0 = \frac{R_{in} \cdot R_L}{R_{in} + R_L} \dots\dots\dots \text{(Eq. 7-8)}$$

This value of  $R_0$ , less than the  $R_L$  value, is then the effective load resistance of the photomultiplier tube. The relation between the output voltage  $V_0$  at  $R_{in} = \infty \Omega$  and the output voltage  $V_0'$  when the output was affected by  $R_{in}$  is expressed as follows:

$$V_0' = V_0 \times \frac{R_{in}}{R_{in} + R_L} \dots\dots\dots \text{(Eq. 7-9)}$$

With  $R_{in} = R_L$ ,  $V_0'$  is one-half the value of  $V_0$ . This means that the upper limit of the load resistance is actually the input resistance  $R_{in}$  of the amplifier and that making the load resistance greater than this value does not have a significant effect. Particularly, when a coupling capacitor  $C_c$  is placed between the photomultiplier tube and the amplifier, as shown in Figure 7-26, an unnecessarily large load resistance may create a problem with the output level.

While the above description assumed the load resistance and internal input resistance of the amplifier to be purely resistive, in practice, stray capacitance and stray inductance are added. Therefore, these circuit elements must be considered as compound impedances, especially in high frequency operation.

Summarizing the above discussions, the following guides should be used in determining the load resistance:

1. When frequency and amplitude characteristics are important, make the load resistance value as small as possible. Also, minimize the stray capacitance such as cable capacitance which may be present in parallel with the load resistance.
2. When the linearity of output amplitude is important, select a load resistance value such that the output voltage developed across the load resistance is several percent of the last-dynode-to-anode voltage.
3. Use a load resistance value equal to or less than the input impedance of the amplifier connected to the photomultiplier tube.

## (2) Current-to-voltage conversion using an operational amplifier

The combination of a current-to-voltage conversion circuit using an operational amplifier and an analog or digital voltmeter enables accurate measurement of the output current from a photomultiplier tube, without having to use an expensive, high-sensitivity ammeter. A basic current-to-voltage conversion circuit using an operational amplifier is shown in Figure 7-27.

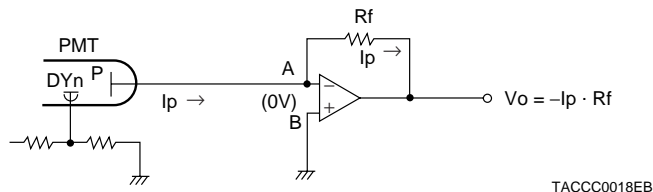


Figure 7-27: Current-to-voltage conversion circuit using an operational amplifier

With this circuit, the output voltage  $V_0$  is given by

$$V_0 = -I_p \cdot R_f \text{ ..... (Eq. 7-10)}$$

This relation can be understood as follows:

Since the input impedance of the operational amplifier is extremely high, the output current of the photomultiplier tube is blocked from flowing into the inverting input terminal (-) of the operational amplifier at point A in Figure 7-27. Therefore, most of the output current flows through the feedback resistance  $R_f$  and a voltage of  $I_p \cdot R_f$  is developed across  $R_f$ . On the other hand, the operational amplifier gain (open loop gain) is as high as  $10^5$ , and it always acts so as to maintain the potential of the inverting input terminal (point A) at a potential equal to that (ground potential) of the non-inverting input terminal (point B). (This effect is known as an imaginary short or virtual ground.) Because of this, the operational amplifier outputs voltage  $V_0$  which is equal to that developed across  $R_f$ . Theoretically, use of a preamplifier performs the current-to-voltage conversion with an accuracy as high as the reciprocal of the open loop gain.

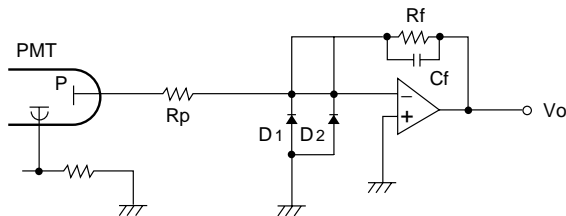
When a preamplifier is used, factors that determine the minimum measurable current are the preamplifier offset current ( $I_{OS}$ ), the quality of  $R_f$  and insulating materials used, and wiring methods.

To accurately measure a very low current on the order of picoamperes ( $10^{-12}$ A), the following points should be noted in addition to the above factors:

1. Connect the photomultiplier tube anode directly to the signal output cable without using any repeater.
2. Use a low-noise type coaxial cable with sufficiently high insulating properties for the signal output cable.
3. Select a connector with adequate insulating properties, for example, a teflon connector.
4. For connection of the photomultiplier tube anode to the input signal pin of the preamplifier, do not use a trace on the printed circuit board but use a teflon standoff instead.
5. For the actual output  $V_0 = -(I_p + I_{OS})R_f + V_{OS}$ , if the  $R_f$  value is large,  $I_{OS}$  may cause a problem. Therefore, select a FET input preamplifier which has a small  $I_{OS}$  of less than 0.1 picoamperes and also exhibits minimum input conversion noise and temperature drift.
6. Provide adequate output-offset adjustment and phase compensation for the preamplifier.
7. Use a metal-film resistor with a minimum temperature coefficient and tolerance for the feedback resistance  $R_f$ . Use clean tweezers to handle the resistor so that no dirt or foreign material gets on its surface. In addition, when the resistance value must be  $10^9$  ohms or more, use a glass-sealed resistor that assures low leakage current.
8. Carbon-film resistors are not suitable as a load resistance because of insufficient accuracy and temperature characteristics and, depending on the type, noise problems. When several feedback resistors are used to switch the current range, place a ceramic rotary switch with minimum leakage current or a high-quality reed relay between the feedback resistance and the preamplifier output. Also connect a low-leakage capacitor with good temperature characteristics, for example a styrene capacitor, in parallel with the feedback resistors so that the frequency range can be limited to a frequency permitted by the application.
9. Use a glass-epoxy PC board or other boards with better insulating properties.

On the other hand, since the maximum output voltage of a preamplifier is typically 1 to 2 volts lower than the supply voltage, multiple feedback resistors are usually used for switching to extend the measurement current range. In this method, grounding the non-inverting input terminal of the preamplifier for each range, via a resistor with a resistance equal to the feedback resistance while observing the above precautions can balance the input bias current, so that the offset current  $I_{OS}$  between the input terminals can be reduced.

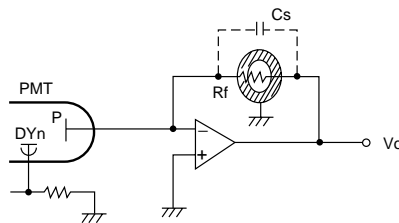
If high voltage is accidentally emitted by the photomultiplier tube, a protective circuit consisting of a resistor  $R_p$  and diodes  $D_1$  and  $D_2$  as shown in Figure 7-28 is effective in protecting the preamplifier from being damaged. In this case, these diodes should have minimum leakage current and junction capacitance. The B-E junction of a low-signal-amplification transistor or FET is commonly used. If  $R_p$  in Figure 7-28 is too small, it will not effectively protect the circuit, but if too large, an error may occur when measuring a large current. It is suggested that  $R_p$  be selected in a range from several kilohms to several tens of kilohms.



TACCC0019EB

**Figure 7-28: Protective circuit for preamplifier**

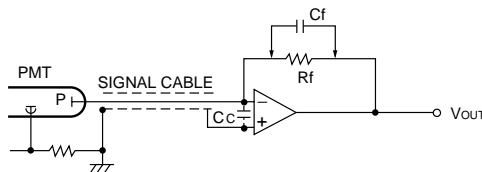
When a feedback resistance,  $R_f$ , and of as high as  $10^{12}$  ohms is used, if a stray capacitance,  $C_s$ , exists in parallel with  $R_f$  as shown in Figure 7-26, the circuit exhibits a time constant of  $C_s \cdot R_f$ . This limits the bandwidth. Depending on the application. This may cause a problem. As illustrated in the figure, passing  $R_f$  through a hole in a shield plate can reduce  $C_s$ , resulting in an improvement of the response speed.



TACCC0020EA

**Figure 7-29: Canceling the stray capacitance  $C_s$**

The output cable for a photomultiplier tube has an its equivalent capacitance  $C_c$  when the cable is long, the  $C_c$  and  $R_f$  create a rolloff in the frequency response of the feedback loop. This rolloff may be the cause of oscillations. Connecting  $C_f$  in parallel with  $R_f$  is used in canceling out the rolloff and avoiding this oscillation, but degradation of the response speed is inevitable.



TACCC0021EA

**Figure 7-30: Canceling the signal cable capacitance**

**(3) Charge-sensitive amplifier using an operational amplifier**

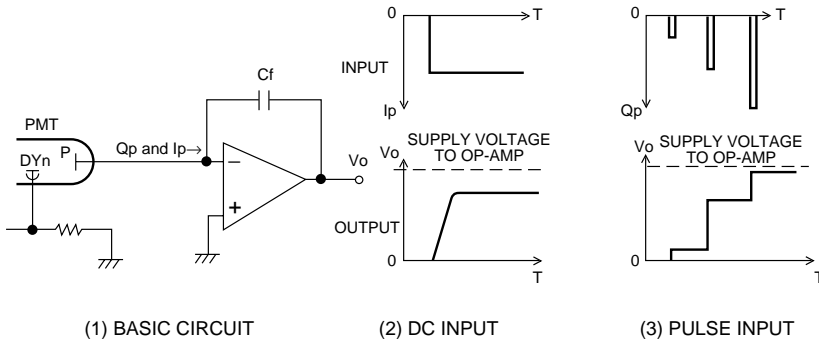
Figure 7-31 (1) shows the basic circuit of a charge-sensitive amplifier using an operational amplifier. The output charge  $Q_p$  of a photomultiplier tube is stored in  $C_f$ , and the output voltage  $V_0$  is expressed by the

$$V_0 = -\int_0^t Q_p \cdot dt \dots\dots\dots (Eq. 7-11)$$

Here, if the output current of the photomultiplier tube is  $I_p$ ,  $V_0$  becomes

$$V_0 = -\frac{1}{C} \int_0^t I_p \cdot dt \dots\dots\dots (Eq. 7-12)$$

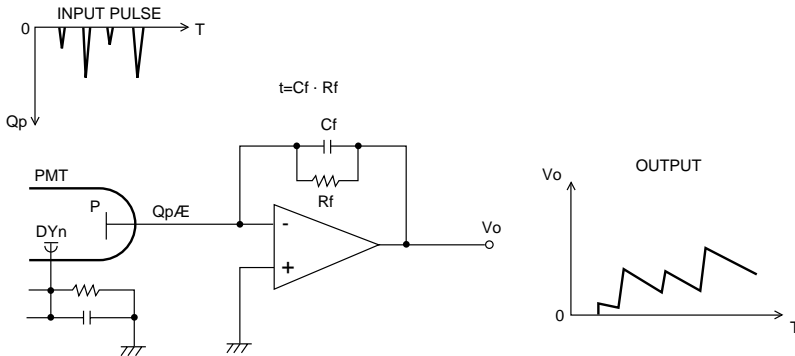
When the output charge is accumulated continuously,  $V_0$  finally increases up to a level near the supply voltage for the preamplifier, as shown in Figure 7-31 (2) and (3).



TACCC0022EA

**Figure 7-31: Charge-sensitive amplifier circuit and its operation**

In Figure 7-31 (1), acts as an integrator that stores the output charge during the measurement time, regardless of whether the photomultiplier tube output is DC or pulse. If a FET switch is added in parallel to  $C_f$ , the charge stored in  $C_f$  can be discharged at the beginning of a measurement. In scintillation counting or photon counting, the individual output pulses of a photomultiplier tube must be converted into corresponding voltage pulses. Therefore,  $R_f$  is connected in parallel with  $C_f$  as shown in Figure 7-32, so that a circuit having a discharge time constant  $\tau=C_f R_f$  is used.<sup>5)</sup>



TACCC0023EA

**Figure 7-32: Pulse input type charge-sensitive amplifier**

If the time constant  $\tau$  is made small, the output  $V_0$  is more dependent on the pulse height of the input current. Conversely, if  $\tau$  is made large,  $V_0$  will be more dependent on the input pulse charge and eventually approaches the value of  $-Q_p/C_f$ . In scintillation counting, from the relation between the circuit time constant  $\tau=RC$  and the fluorescent decay constant of the scintillator  $\tau_s$ , the output-pulse voltage waveform  $V(t)$  is given by<sup>5)</sup>

$$V(t) = \frac{Q_p \cdot t}{t - \tau_s} (e^{-t/\tau} - e^{-t/\tau_s}) \dots\dots\dots \text{(Eq. 7-13)}$$

when  $\tau \gg \tau_s$ ,  $V(t)$  becomes

$$V(t) \approx \frac{Q_p}{C} (e^{-t/\tau} - e^{-t/\tau_s}) \dots\dots\dots \text{(Eq. 7-14)}$$

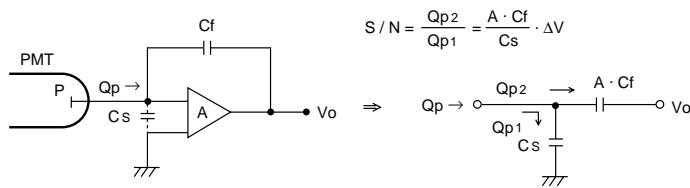
While, when  $\tau \ll \tau_s$ ,  $V(t)$  is

$$V(t) \approx \frac{Q_p}{C} \cdot \frac{t}{\tau_s} (e^{-t/\tau_s} - e^{-t/\tau}) \dots\dots\dots \text{(Eq. 7-15)}$$

When the circuit time constant  $\tau$  is larger than the scintillator decay constant  $\tau_s$ , the rise of the output waveform depends on  $\tau_s$ , while the fall depends on  $\tau$ , with the maximum pulse height given by  $Q/C$ . In contrast, when the circuit time constant  $\tau$  is smaller than  $\tau_s$ , the rise of the output waveform depends on  $\tau$ , while the fall depends on  $\tau_s$ , with the maximum pulse height given by  $Q/C \cdot \tau/\tau_s$ . In most cases, the condition of  $\tau \gg \tau_s$  is used since higher energy resolution can be expected. This is because the output pulse has a large amplitude so that it is less influenced by such factors as noise, temperature characteristics of the scintillator and variations of the load resistance. In this case, it should be noted that the pulse width becomes longer due to a larger  $\tau$  and, if the repetition rate is high, base-line shift and pile-up tend to occur. If measurement requires a high counting rate, reducing  $\tau$  is effective in creating an output waveform as fast as the scintillator decay time. However, the output pulse height becomes lower and tends to be affected by noise, resulting in a sacrifice of energy resolution. Under either condition, the output voltage  $V(t)$  is proportional to the output charge from the photomultiplier tube anode. Generally, the load capacitance is reduced to obtain higher pulse height as long as the operation permits, and in most cases the resistor value is changed to alter the time constant. When a NaI(Tl) scintillator is used, the time constant is usually selected to be from several microseconds to several tens of microseconds.

As explained above, noise generated in the charge-sensitive amplifier degrades the energy resolution. This noise mainly originates from the amplifier circuit elements, but care should also be taken of the cable capacitance  $C_s$  indicated in Figure 7-33 because the output charge of the photomultiplier tube is divided and stored in  $C_f$  and  $C_s$ . The  $C_s$  makes the charge of  $C_f$  smaller as compared to the amount of charge without  $C_s$ . Thus, it is necessary to increase the value of  $A \cdot C_f / C_s$  in order to improve the signal-to-noise ratio. In actual operation, however, since  $A \cdot C_f$  cannot be made larger than a certain value due to various limiting conditions, the value of  $C_s$  is usually made as small as possible to improve the signal-to-noise ratio.

In scintillation counting measurements, a common method of reducing the cable capacitance is to place the preamplifier in the vicinity of the photomultiplier tube, remote from the main amplifier.



TACCC0024EA

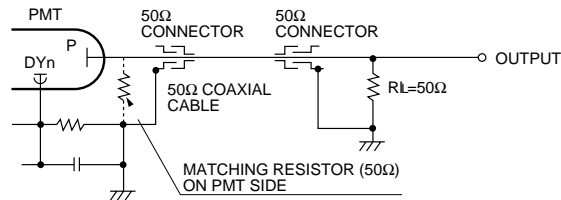
Figure 7-33: Influence of input distribution capacitance

### 7.3.4 Output circuit for a fast response photomultiplier tube

For the detection of light pulses with fast rise and fall times, a coaxial cable with 50-ohm impedance is used to make connection between the photomultiplier tube and the subsequent circuits.

To transmit and receive the signal output waveform with good fidelity, the output end must be terminated in a pure resistance equal to the characteristic impedance of the coaxial cable. This allows the impedance seen from the photomultiplier tube to remain constant, independent of the cable length, thus making it possible to reduce "ringing" which may be observed in the output waveform. However, when using an MCP-PMT for the detection of ultra-fast phenomena, if the cable length is made unnecessarily long, distortion may occur in signal waveforms due to a signal loss in the coaxial cable.

If a proper impedance match is not provided at the output end, the impedance seen from the photomultiplier tube varies with frequency, and further the impedance value is also affected by the coaxial cable length, as a result, ringing appears in the output. Such a mismatch may be caused not only by the terminated resistance and the coaxial cable but also by the connectors or the termination method of the coaxial cable. Thus, sufficient care must be taken to select a proper connector and also to avoid creating impedance discontinuity when connecting the coaxial cable to the photomultiplier tube or the connector.



TACCC0025EA

**Figure 7-34: Output circuit impedance match**

When a mismatch occurs at the coaxial cable ends, all of the output signal energy is not dissipated at the output end, but is partially reflected back to the photomultiplier tube. If a matching resistor is not provided on the photomultiplier tube side, the photomultiplier tube anode is viewed as an open end, thus the signal will be reflected from the anode and returned to the output end again. This reflected signal is observed as a pulse which appears after the main pulse with a time delay equal to the round trip through the coaxial cable. This signal repeats its round trip until its total energy is dissipated, as a result, ringing occurs at the output end. To prevent this, providing an impedance match not only at the output end but also at the photomultiplier tube side is effective to some extent, although the output voltage will be reduced to one-half in comparison with that obtained when impedance match is done only at the output end. When using a photomultiplier tube which is not a fast response type or using a coaxial cable with a short length, an impedance matching resistor is not necessarily required on the photomultiplier tube side. Whether or not to connect this resistor to the photomultiplier tube can be determined by doing trial-and-error impedance matching. Among photomultiplier tubes, there are special types having a 50-ohm matched output impedance. These tubes do not require any matching resistor.

Next, let us consider waveform observation of fast pulses using an oscilloscope. A coaxial cable terminated with a matching resistor offers the advantage that the cable length will not greatly affect the pulse shape. Since the matching resistance is usually as low as 50 to 100 ohms, the output voltage is reduced. While this situation can be corrected by use of a wide-band amplifier with high gain, the inherent noise of such an amplifier makes it difficult to measure low-level signals. In this case, to achieve the desired output voltage, it is more advantageous, as shown in Figure 7-35, to bring the photomultiplier tube as close as possible to the amplifier to reduce the stray capacitance and also to use as a large load resistance as a possible without effecting the frequency response.

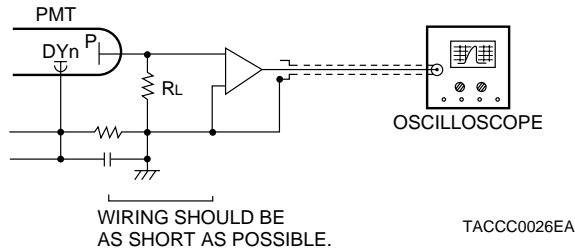


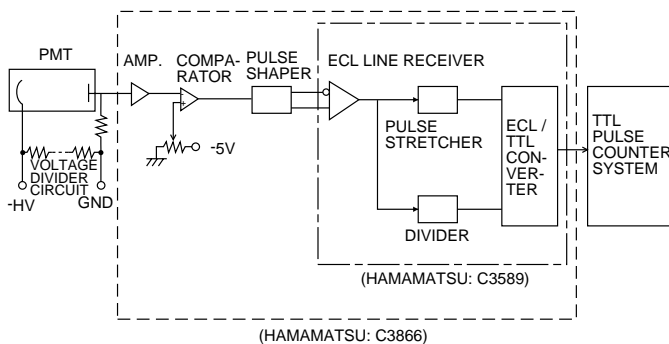
**Figure 7-35: Waveform observation using an oscilloscope**

It is relatively simple to operate a fast amplifier with a wide bandwidth using a video IC or pulse type IC. However, in exchange for such design convenience, these ICs tends to reduce performance, such as introducing noise. For optimum operation, it is therefore necessary to know their performance limits and take corrective action.

As the pulse repetition rate increases, a phenomenon called "base-line shift" creates another reason for concern. This base-line shift occurs when the DC signal component has been eliminated from the signal circuit by use of a coupling capacitor. If this occurs, the zero reference level shifts from ground to an apparent zero level equal to the average of the output pulses. Furthermore, when multiple pulses enter within the time resolution of the measuring system including the amplifier, they are integrated so that a large output pulse appears. This is known as "pile-up". Special care should be taken in cases where a pulse height discriminator is used to discern the amplitude of individual pulses.

### 7.3.5 Photon counting circuits

Because the basic operating principles of photon counting have already been detailed in Section 3.4 of Chapter 3, this section briefly explains how to connect a photomultiplier tube to the photon counting circuits available from Hamamatsu Photonics. The block diagram of the photon counting circuits connected between the photomultiplier tube anode and a TTL counter is shown in Figure 7-36.



TACCC0027EB

**Figure 7-36: Photon counting circuits**

After passing through the comparator and pulse shaper, the output signals become ECL output pulses. These are then fed to the ECL line receiver and the pulse width is extended by the pulse stretcher so that the signals are compatible with a TTL counter. If a high-speed counter is not available, use of a prescaler enables photon counting operation without impairing the linearity.

## 7.4 Housing

A photomultiplier tube housing is primarily used to contain and secure in place a photomultiplier tube, but it also provides the following functions:

1. To shield extraneous light
2. To eliminate the effect of external electrostatic fields
3. To reduce the effect of external magnetic fields

The following sections explain each of these functions

### 7.4.1 Light shield

Since a photomultiplier tube is an extremely high-sensitivity photodetector, the signal light level to be detected is very low and therefore particular care must be exercised in shielding extraneous light. For instance, when a connector is used for signal input/output, there is a possibility of light leakage through the connector itself or through its mounting holes and screw holes. Furthermore, light leakage may occur through seams in the housing.

As a corrective action, when mounting connectors or other components in the housing, use black silicone rubber at any location where light leakage may occur. It is also important to use black soft tape or an O-ring so as to fill in any gaps around the components attached to the housing. In addition, it is necessary to coat the inside of the housing with black mat paint in order to prevent reflection of scattered light.

### 7.4.2 Electrostatic shield

Since photomultiplier tube housings are made of metal such as aluminum, maintaining the housing at ground potential provides an effective shield with respect to external electrostatic fields. The inside of the housing is usually coated with black paint to prevent diffuse reflection of light, so care is required to be certain that the paint does not interfere with the contact of the ground line. As stated previously, if any object at ground potential is brought close to the bulb of a photomultiplier tube, noise increases, so that the housing should have sufficient separation from the photomultiplier tube.

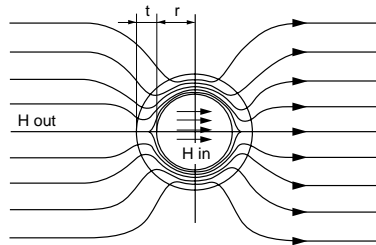
### 7.4.3 Magnetic shield

As will be described in Section 3.3 of Chapter 8, photomultiplier tubes are very sensitive to a magnetic field. Even terrestrial magnetism will have a detrimental effect on the photomultiplier tube performance<sup>6)</sup>. Therefore, in precision photometry or in applications where the photomultiplier tube must be used in a highly magnetic field, the use of a magnetic shield case is essential. However, unlike the electrostatic shield, there exists no conductors that carry the magnetic flux. It is not possible to shield a magnetic field completely. One common technique for reducing the effect of an external magnetic field is to wrap a metal shield having high permeability around the photomultiplier tube bulb, but such a metal shield cannot completely block the magnetic field. It is also necessary to select an optimum shielding material and method, based on both the strength and frequency of the magnetic fields.

In general applications, it is not necessary to fabricate the entire housing from high-permeability materials. Instead, a photomultiplier tube can be wrapped into a cylindrical shield case. Among shielding materials, "Permalloy" is the best and is widely used. The effect of a magnetic shield is described below.

**(1) Shielding factor of magnetic shield case and orientation of magnetic field**

Photomultiplier tubes are very sensitive to an external magnetic field, especially for head-on types, the output varies significantly even with terrestrial magnetism. To eliminate the effect of the terrestrial magnetism or to operate a photomultiplier tube more stably in a magnetic field, a magnetic shield case must be used. (Also refer to Section 3.3 of Chapter 8.) Utilizing the fact that a magnetic field is shunted through an object with high permeability, it is possible to reduce the influence of an external magnetic field by placing the photomultiplier tube within a magnetic shield case, as illustrated in Figure 7-37.



TACCC0028EA

**Figure 7-37: Shielding effect of a magnetic shield case**

Let us consider the shielding effect of a magnetic shield case illustrated in Figure 7-37. As stated, the magnetic shield case is commonly fabricated from metal with high-permeability such as Permalloy. The shielding factor S of such a magnetic shield case is expressed as follows:

$$S = \frac{H_{out}}{H_{in}} = \frac{3t\mu}{4r} \dots\dots\dots \text{(Eq. 7-16)}$$

where  $H_{in}$  and  $H_{out}$  are the magnetic field strength inside and outside the shield case respectively,  $t$  is the thickness of the case,  $r$  is the radius of the case and  $\mu$  is the permeability. When two or more magnetic shield cases with different radii are used in combination, the resultant shielding factor  $S'$  will be the product of the shielding factor of each case, as expressed in the following equation:

$$S' = S_1 \times S_2 \times S_3 \dots S_n$$

$$= \frac{3t_1\mu_1}{4r_1} \times \frac{3t_2\mu_2}{4r_2} \times \frac{3t_3\mu_3}{4r_3} \times \dots \times \frac{3t_n\mu_n}{4r_n} \dots\dots\dots \text{(Eq. 7-17)}$$

When a magnetic shield case is used, the magnetic field strength inside the case  $H_{in}$ , which is actually imposed on the photomultiplier tube, is reduced to a level of  $H_{out}/S$ . For example, if a magnetic shield case with a shielding factor of 10 is employed for a photomultiplier tube operated in an external magnetic field of 30 milliteslas, this means that the photomultiplier tube is operated in a magnetic field of 3 milliteslas. In practice, the edge effect of the shield case, as will be described later, creates a loss of the shielding effect. But this approach is basically correct.

Figure 7-38 shows the output variations of a photomultiplier tube with and without a magnetic shield case which is made of "PC" materials with a 0.6 millimeter thickness. It is obvious that the shielding is effective for both X and Y axes. For these axes the shielding factor of the magnetic shield case must be equal. However, the Y axis exhibits better magnetic characteristics than the X axis when not using a magnetic shield case, so that the Y axis provides a slightly better performance when used with the magnetic shield case. In the case of the Z axis which is parallel to the tube axis, the photomultiplier tube used with the magnetic shield case shows larger output variations. It is thought that, as described in the section on the edge effect, this is probably due to the direction of the magnetic field which is bent near the edge of the shield case.

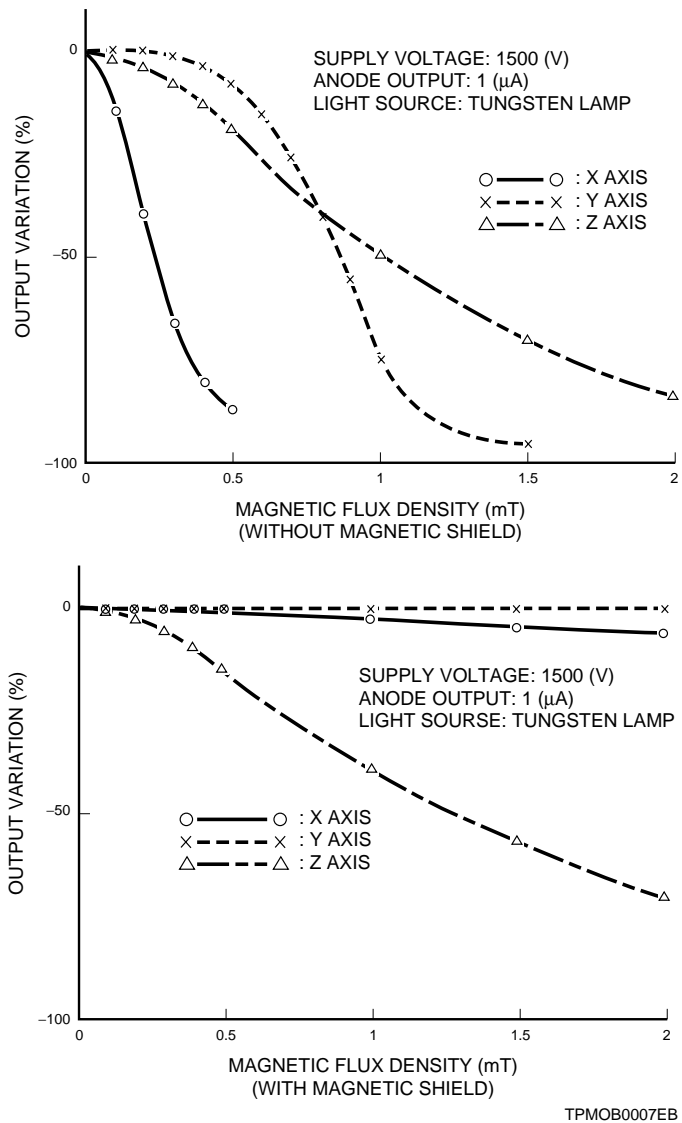
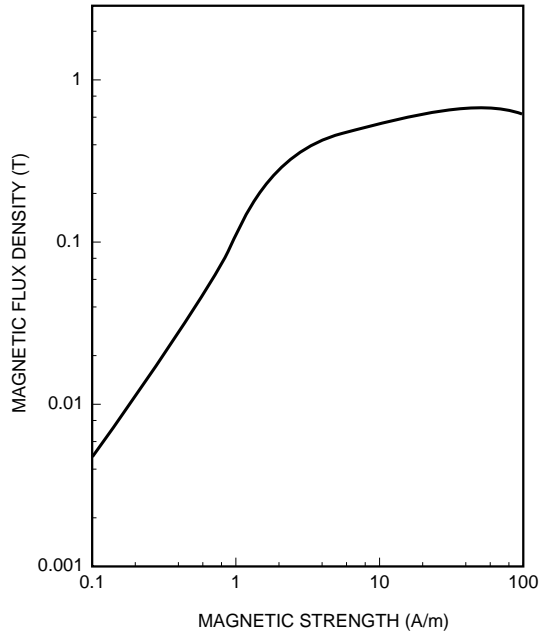


Figure 7-38: Magnetic characteristics of a photomultiplier tube

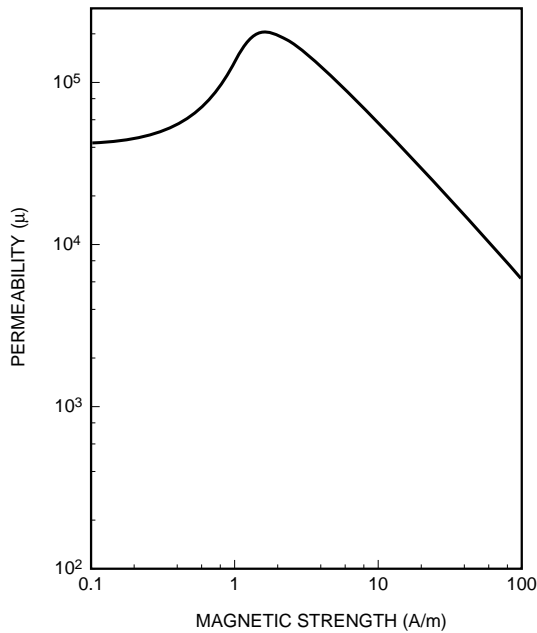
## (2) Saturation characteristics

When plotting a B-H curve which represents the relationship between the external magnetic field strength (H) and the magnetic flux density (B) traveling through a magnetic material, a saturation characteristic is seen as shown in Figure 7-39.



TPMOB0008EB

Figure 7-39: DC magnetization curve (B-H curve)

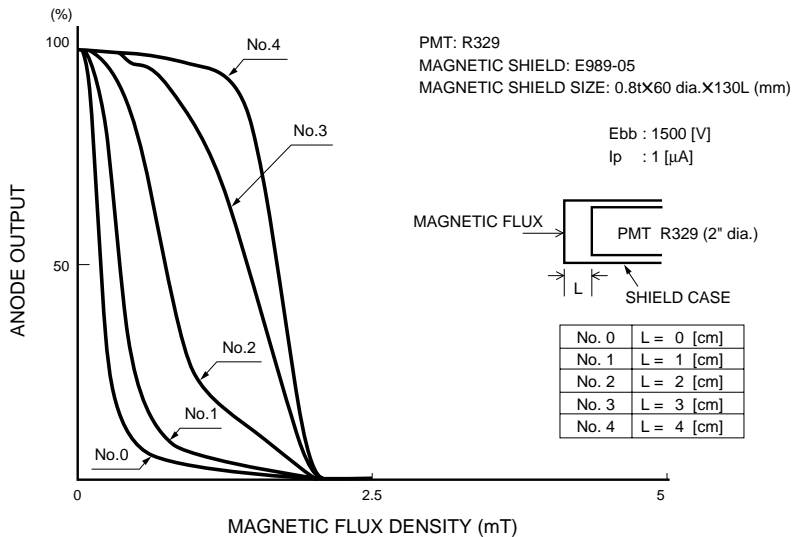


TPMOB0009EB

Figure 7-40: Permeability and external magnetic field

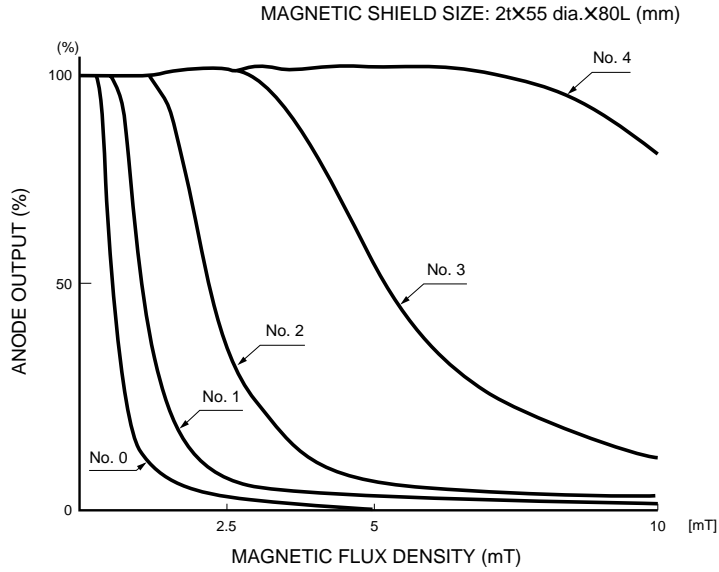
Since the permeability  $\mu$  of a magnetic material is given by the B/H ratio,  $\mu$  varies with H as shown in Figure 7-40 with a peak at a certain H level and above it, both  $\mu$  and the shielding factor degrade sharply. Data shown in Figures 7-39 and 7-40 are measured using a magnetic shield case E989 (0.8 millimeter thick) manufactured by Hamamatsu Photonics when a magnetic field is applied in the direction perpendicular to the shield case axis.

The Hamamatsu E989 series magnetic shield cases are made of a "PC" material which contains large quantities of nickel. This material assures very high permeability, but exhibits a rather low saturation level of magnetic flux density. In a weak magnetic field such as from terrestrial magnetism, the "PC" material provides good shielding factor as high as  $10^3$  and thus proves effective in shielding out terrestrial magnetism. In contrast, "PB" material which contains small quantities of nickel offers high saturation levels of magnetic flux density, though the permeability is lower than that of the "PC" material. Figure 7-41 shows the anode output variations of a photomultiplier tube used with a magnetic shield case made of "PC" or "PB" material. As the magnetic flux density is increased, the anode output of the photomultiplier tube used with the "PC" material shield case drops sharply while that used with the "PB" material shield case drops slowly. Therefore, in a highly magnetic field, it is necessary to use a "PC" material shield case in conjunction with a shield case made of high-permeability metal such as soft-iron, with a thickness of 3 to 10 millimeters.



(1) PC MATERIAL

Figure 7-41: Magnetic characteristics of a photomultiplier tube used with magnetic shield case (1)



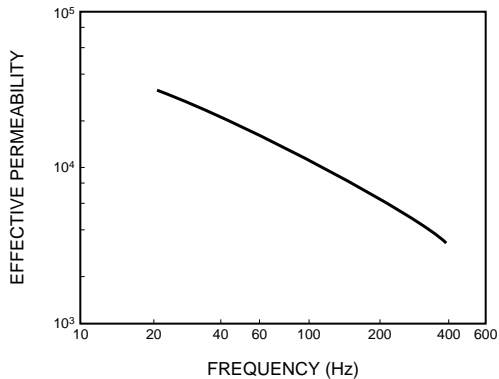
(2) PB MATERIAL

TPMOB0010EB

Figure 7-41: Magnetic characteristics of a photomultiplier tube used with magnetic shield case (2)

### (3) Frequency characteristics

The above description concerning the effect of magnetic shield cases, refers entirely to DC magnetic fields. In AC magnetic fields, the shielding effect of a magnetic shield case decreases with increasing frequency as shown in Figure 7-42. This is particularly noticeable for thick materials, so it will be preferable to use a thin shield case of 0.05 to 0.1 millimeter thickness when a photomultiplier tube is operated in a magnetic field at frequencies from 1kHz to 10kHz. The thickness of a magnetic shield case must be carefully determined to find the optimum compromise between the saturated magnetic flux density and frequency characteristics.



TACCB0003EA

Figure 7-42: Frequency characteristics of a magnetic shield case

#### (4) Edge effect

The shielding effect given by  $3t \mu/4r$  applies to the case in which the magnetic shield case is sufficiently long with respect to the overall length of the photomultiplier tube. Actual magnetic shield cases have a finite length which is typically only several millimeters to several centimeters longer than the photomultiplier tube, and their shielding effects deteriorate near both ends as shown in Figure 7-43. Since the photocathode to the first dynode region is most affected by a magnetic field, this region must be carefully shielded. For example, in the case of a head-on photomultiplier tube, the tube should be positioned deep inside the magnetic shield case so that the photocathode surface is hidden from the shield case edge by a length equal to the shield case radius.

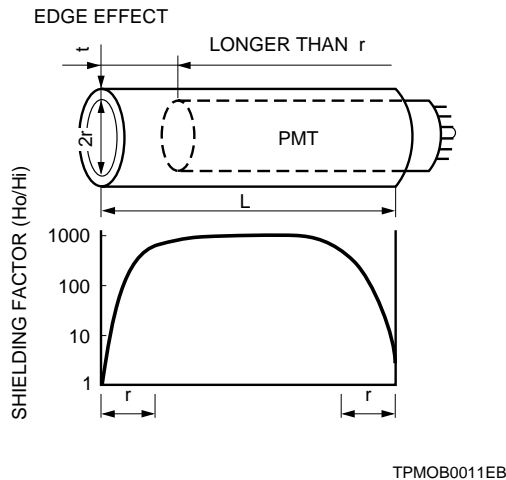


Figure 7-43: Edge effect of a magnetic shield case

Figures 7-44 (1) to (4) show the output variations of a head-on photomultiplier tube operated in magnetic fields in the respective directions of X, Y and Z axes. Also shown in these figures are the output variations measured using a magnetic shield wrapping and a magnetic shield case while moving the photomultiplier tube along the shield case axis at positions a, b and c. When used with the magnetic shield case, in either axis of the magnetic field, the longer the distance from the edge of the shield case to the photocathode, the more the output variations improve. For the Y axis, however, since the photomultiplier tube originally exhibits better magnetic characteristics, no output variations occur, as seen from (2), up to 3 milliteslas even if the photocathode is positioned near the edge of the magnetic shield case. For the Z axis, on the other hand, if the photocathode is positioned at the open edge of the magnetic shield case, the output variations are increased. This is often larger than the case even without using a magnetic shield case, as shown in (3). The reason for this is thought to be that the magnetic field applied along the shield case axis is bent near the open edge, and this bent magnetic field adversely affects the photoelectron collection efficiency from the photocathode to the first dynode. In addition, as shown in (1), the photomultiplier tube output is significantly affected by the magnetic field along the X axis. Therefore, even if the magnetic field along the Z axis is reduced, the resultant magnetic field which is generated along the X axis can cause output variations. This problem will be solved by positioning the photomultiplier tube deeper than the open edge of the magnetic shield case.

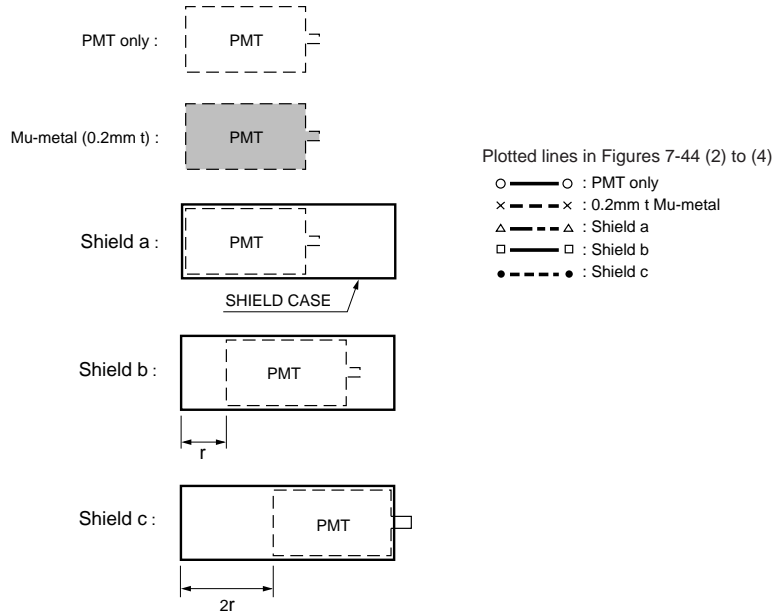


Figure 7-44 (1): Photomultiplier tube shield conditions for magnetic characteristic measurements

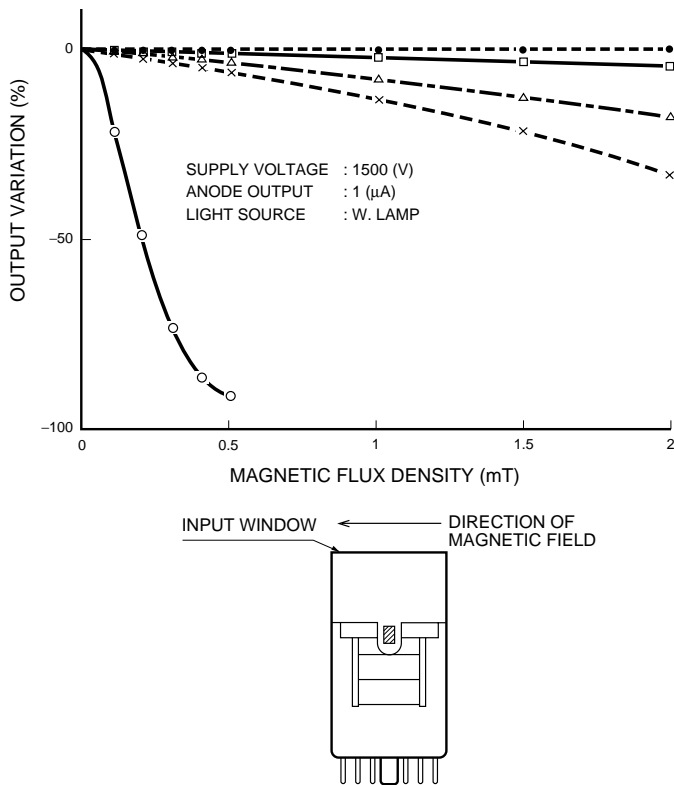
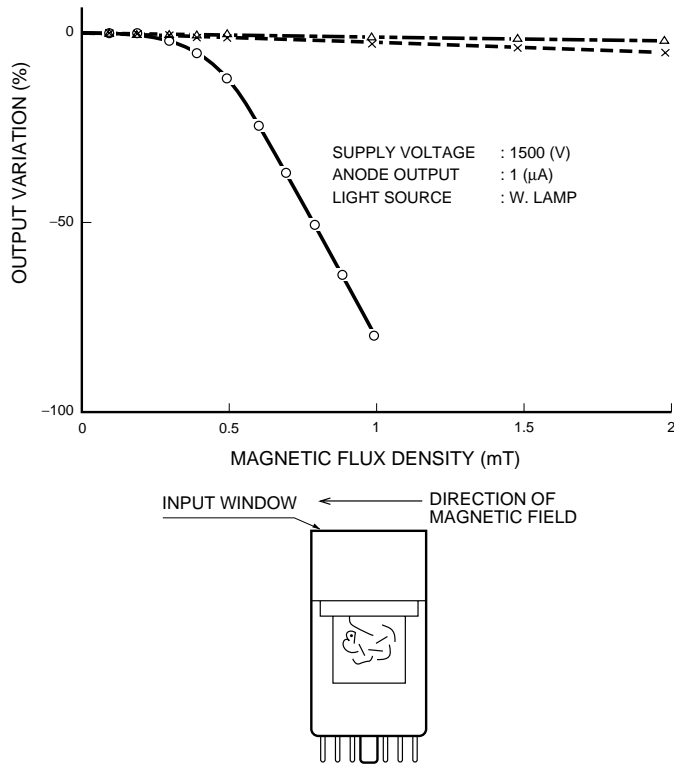
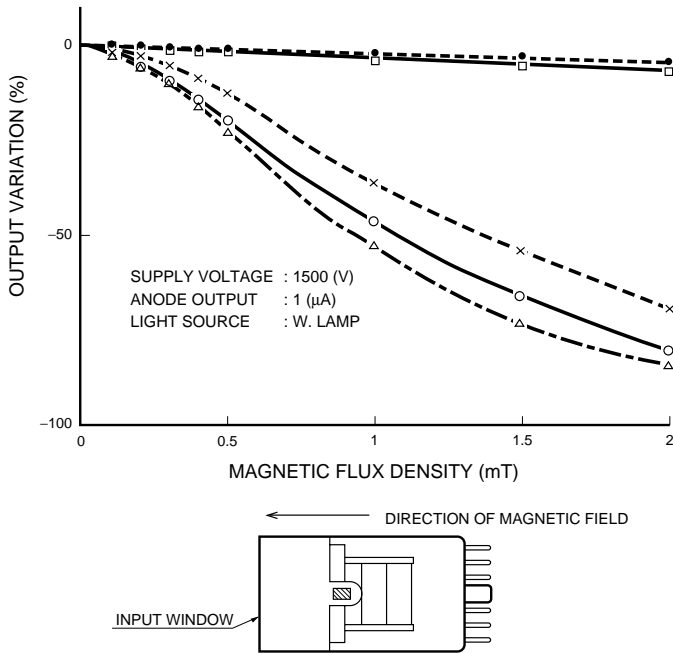


Figure 7-44 (2): Magnetic characteristics of a photomultiplier tube



TPMOB0012EB (2)

Figure 7-44 (3): Magnetic characteristics of a photomultiplier tube



TPMOB0012EB (3)

Figure 7-44 (4): Magnetic characteristics of a photomultiplier tube

(5) Photomultiplier tube magnetic characteristics and shielding effect

Figures 7-45 (a) to (e) show magnetic characteristics of typical photomultiplier tubes (anode output variations versus magnetic flux density characteristics) and the shielding effects<sup>7)</sup> of magnetic shield cases (Hamamatsu E989 series). It can be seen from these figures that use of a shield case can greatly reduce the influence of magnetic fields of less than one hundred milliteslas.

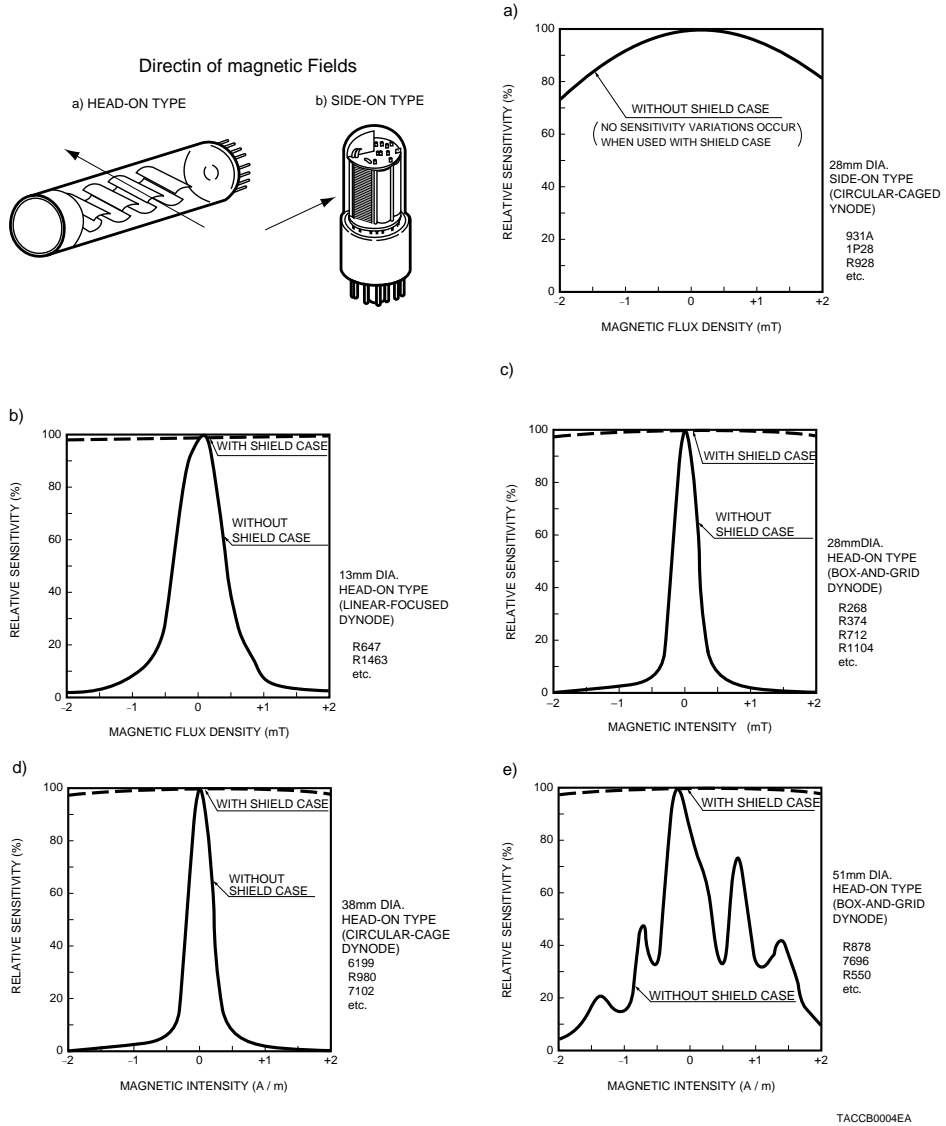


Figure 7-45: Effect of magnetic shield case

## (6) Handling the magnetic shield case

Magnetic shield cases are subject to deterioration in performance due to mechanical shock and deformation therefore sufficient care must be exercised during handling. Once the performance has deteriorated, a special annealing process is required to effect a recovery. In particular, since the permeability characteristics are more susceptible to external shock and stress, avoid any alteration, for example such as drilling and machining the shield case.

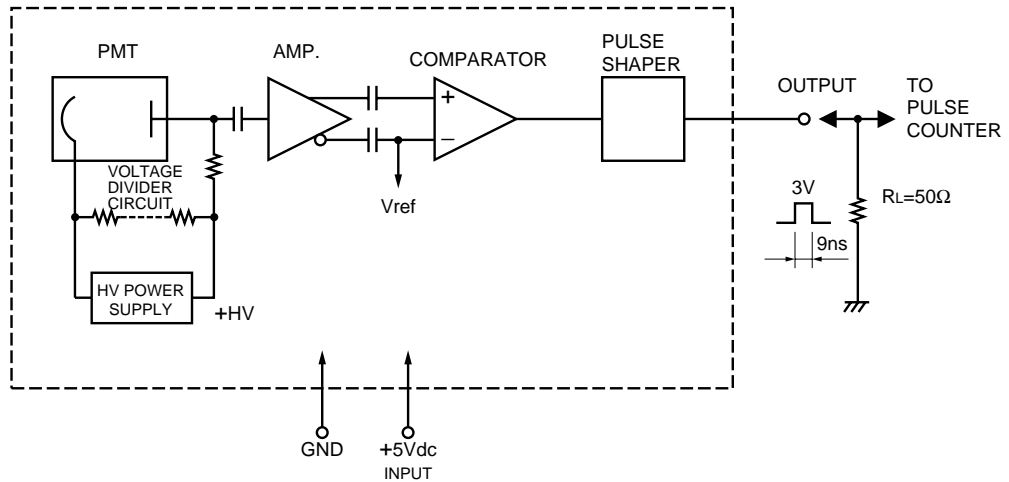
As stated in Chapter 3, if any object at ground potential is brought close to the bulb of a photomultiplier tube, the photomultiplier tube noise increases considerably. Therefore, it is advisable to use a magnetic shield case larger than the photomultiplier tube diameter. In this case, positioning the photomultiplier tube in the center of the shield case is important, otherwise an electrical problem may occur. Foam rubber or similar materials with good buffering and insulating properties can be used to hold the photomultiplier tube in the shield case.

It is recommended for safety and also for noise suppression measures that the magnetic shield case be grounded via a resistor of 5 to 10 megohms, although this is not mandatory when a HA-coating photomultiplier tube or a photomultiplier tube with the cathode at ground potential and the anode at a positive high voltage is used. In this case, sufficient care must be taken with regards to the insulation of the magnetic shield case.

## 7.5 Detector Head Assemblies

A compact detector head assembly can be configured, by integrating a voltage-divider circuit, signal processing amplifier and high-voltage power supply into a housing along with a photomultiplier tube. As examples, this section explains the Hamamatsu H6180-01 and H5784 detector head assemblies and their circuit configurations.

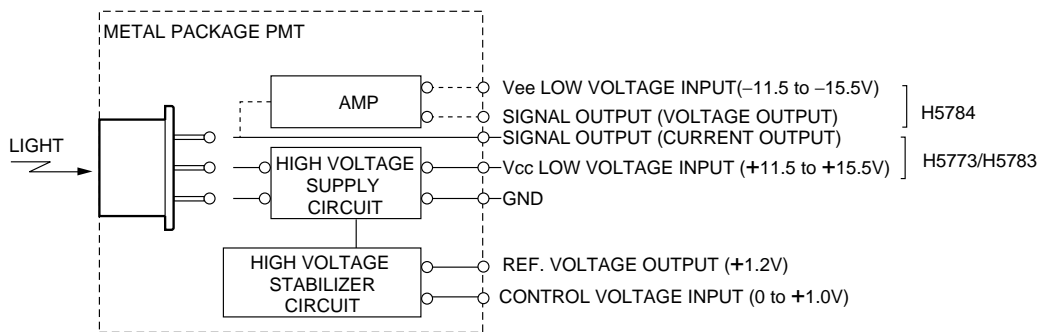
As Figure 7-46 shows, the H6180-01 incorporates a signal processing amplifier and circuit components designed for photon counting. Since a comparator and pulse shaper are included, measurement can be easily performed by simply connecting the output to a commercially available pulse counter. In addition, the built-in high-voltage power supply generates a high voltage inside the housing by input of +5 volts in order to operate the photomultiplier tube and signal processing amplifier.



TPHOC0024EB

Figure 7-46: Internal circuit diagram of the H6180-01

In the H5784, a low-noise current-to-voltage conversion amplifier is used as a signal processing amplifier. To make this assembly as compact as possible, a metal package photomultiplier tube connected to a Cockcroft-Walton circuit as a high-voltage power supply is used. By simply supplying +12 volts, a high voltage is internally generated allowing operation of the photomultiplier tube and signal processing amplifier.



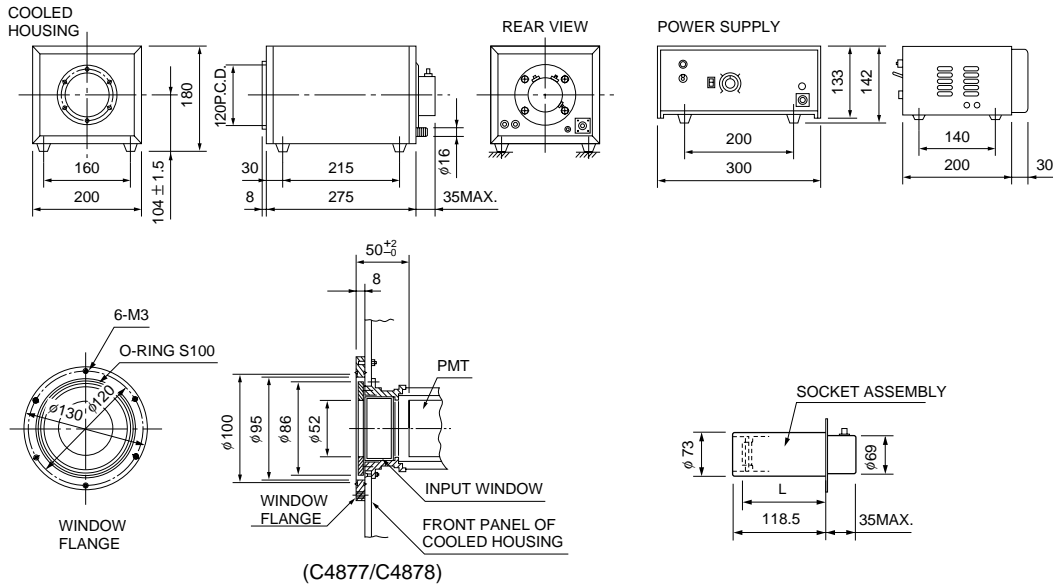
TACCC0048EA

Figure 7-47: Internal circuit diagram of the H5784

## 7.6 Cooling

As described in Section 3.6 of Chapter 3, thermionic emission of electrons is a major cause of dark current. It is especially predominant when the photomultiplier tube is operated in a normal supply voltage range. Because of this, cooling the photomultiplier tube can effectively reduce the dark current and the resulting noise pulses, thus improving the signal-to-noise ratio and enhancing the lower detection limit. However, the following precautions are required for cooling a photomultiplier tube.

Photomultiplier tube cooling is usually performed in the range from 0°C to -30°C according to the temperature characteristic of the dark current. When a photomultiplier tube is cooled to such a temperature level, moisture condensation may occur at the input window, bulb stem or voltage-divider circuit. This condensation may cause a loss of light at the input window and an increase in the leakage current at the bulb stem or voltage-divider circuit. To prevent this condensation, circulating dry nitrogen gas is recommended, but the equipment configuration or application often limits the use of liquid nitrogen gas. For efficient cooling, Hamamatsu provides thermoelectric coolers having an evacuated double-pane quartz window with a defogger and also air-tight socket assemblies.<sup>8)</sup> An example of thermoelectric coolers is shown in Figure 7-48, along with a suitable socket assembly.



TACCA0018EB

**Figure 7-48: Thermoelectric cooler (manufactured by Hamamatsu Photonics)**

The cooler shown in Figure 7-48 is identical with the Hamamatsu C4877 and C4848 coolers. The C4877 is designed for 2-inch or 1.5-inch diameter head-on photomultiplier tubes, while the C4848 is for MCP-PMTs. Either model can be cooled down to -30°C by thermoelectric cooling.

If a socket made by other manufacturers is used with a Hamamatsu photomultiplier tube, the bulb stem of the photomultiplier tube may possibly crack during cooling. This is due to the difference in the thermal expansion coefficient between the socket and the bulb stem. Be sure to use the mating socket available from Hamamatsu. Stem cracks may also occur from other causes, for example, a distortion of the stem. When the bulb stem is to be cooled below -50°C, the socket should not be used, instead, the lead pins of the photomultiplier tube should be directly connected to wiring leads. To facilitate this, use of socket contacts, as illustrated

in Figure 7-49, will prove helpful. (The socket contact shown in the figure is Winchester 100-2520S.)

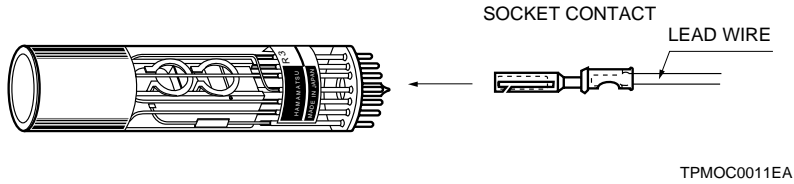


**Figure 7-49: Connecting the lead pins to the socket contacts**

Thermionic electrons are emitted not only from the photocathode but also from the dynodes. Of these, thermionic emissions that actually affect the dark current are those from the photocathode,  $Dy_1$  and  $Dy_2$ , because the latter-stage dynodes contribute less to the current amplification. Therefore cooling the photocathode,  $Dy_1$ , and  $Dy_2$  proves effective in reducing dark current and besides, this is advantageous in view of possible leakage currents which may occur due to moisture condensation on the bulb stem, base or socket.

The interior of a photomultiplier tube is a vacuum and thus heat is conducted through it very slowly. Therefore, it is recommended that the photomultiplier tube be left for one hour or longer after the ambient temperature has reached a constant level, so that the dark current and noise pulses will become constant. Another point to be observed is that, since heat generated from the voltage-divider resistors may heat the dynodes, the voltage-divider resistor values should not be made any smaller than necessary.

## References in Chapter 7

- 1) Hamamatsu Photonics Catalog: Accessories for Photomultiplier Tubes.
- 2) McGRAW-HILL: Electronic Circuits Discrete and Integrated, International Student Edition.
- 3) Ref. to "Kerns-type PM base" Produced by R.L. McCarthy.
- 4) Hamamatsu Photonics Catalog: Accessories for Photomultiplier Tubes.
- 5) Hamamatsu Photonics Technical Information: Photomultiplier Tubes for Use in Scintillation Counting.
- 6) Hamamatsu Photonics Catalog: Accessories for Photomultiplier Tubes.  
Ref. to "Improvement of 20-inch diameter photomultiplier tubes" published by A. Suzuki (KEK, Tsukuba) and others.
- 7) Hamamatsu Photonics Catalog: Accessories for Photomultiplier Tubes.
- 8) Hamamatsu Photonics Catalog: Accessories for Photomultiplier Tubes.

## **CHAPTER 8 ENVIRONMENTAL RESISTANCE AND RELIABILITY**

*Photomultiplier tube characteristics, for example, sensitivity and dark current, are susceptible to environmental conditions such as ambient temperature, humidity and magnetic fields.<sup>1)</sup> To obtain the fullest capabilities from a photomultiplier tube, it is necessary to know how environmental conditions affect the photomultiplier tube and to take corrective action. This chapter discusses these points and also describes operating stability over time and reliability.*

## 8.1 Effects of Ambient Temperature

### 8.1.1 Temperature characteristics

The photomultiplier tube is more susceptible to ambient temperature than ordinary electronic components (such as resistors and capacitors). In precision measurement therefore, the photomultiplier tube must be operated with temperature control or comparative photometric techniques so that the effects of ambient temperature are minimized. When performing temperature control, note that the interior of a photomultiplier tube is a vacuum and thereby heat is conducted through it very slowly. The photomultiplier tube should be left for one hour or longer until the photomultiplier tube reaches the same level as the ambient temperature and its characteristics become stable.

#### (1) Sensitivity

Temperature characteristics of anode sensitivity can be divided into those for cathode sensitivity (photocathode) and gain (dynode). Temperature characteristics for cathode sensitivity are dependent on the wavelength. In general, the temperature coefficient of cathode sensitivity varies significantly from a negative value to a positive value near the long wavelength limit. In contrast, temperature characteristics of gain have virtually no dependence on wavelength or on supply voltage. Figure 8-1 shows temperature coefficients of major photomultiplier tubes as a function of wavelength, with the abscissa representing wavelength and the ordinate expressing temperature coefficients of anode sensitivity.

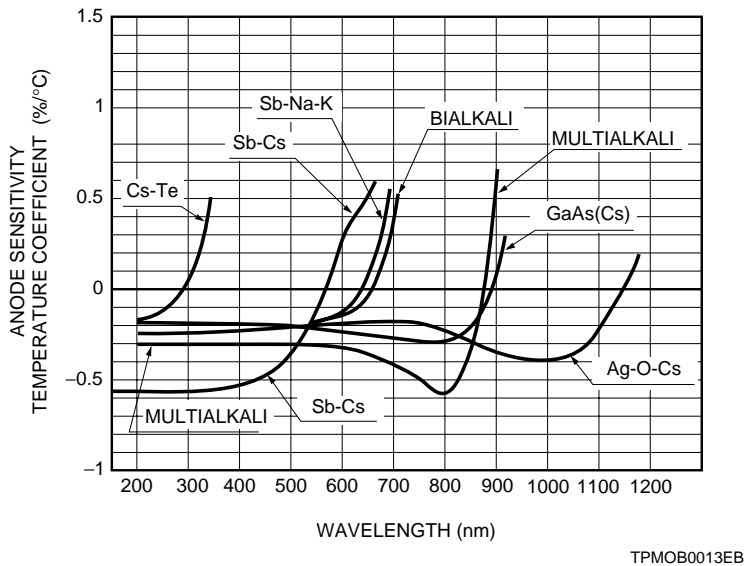


**Figure 8-1: Photocathode types and temperature coefficients**

When a photomultiplier tube with a transmission mode photocathode is used at very low temperatures, the subsequent increase in the photocathode surface resistance may cause a cathode current saturation effect, resulting in a loss of output linearity with respect to the incident light level. This effect appears drastically with certain types of bialkali photocathodes and thus care is required when using such photomultiplier tubes.

Typical cathode saturation currents for bialkali and multialkali photocathodes are shown in Figure 8-2.

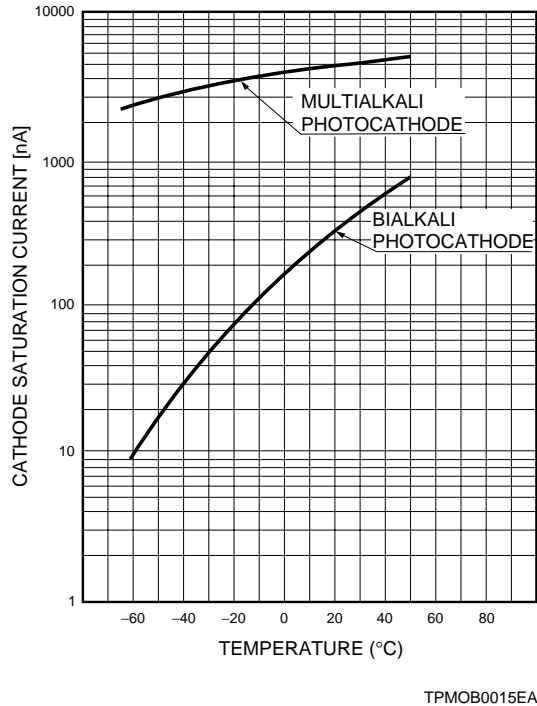
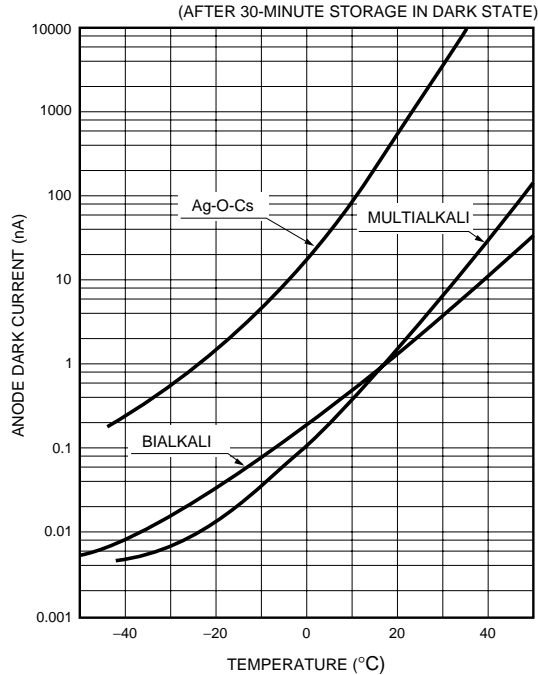


Figure 8-2: Cathode saturation current vs. temperature

## (2) Dark current

A photocathode consists of materials having small energy gap and electron affinity so that photoelectrons can be released efficiently. This means that dark current is very sensitive to the ambient temperature. It greatly increases with temperature as shown in Figure 8-3. In low-light-level detection, this effect of the ambient temperature on the dark current is an important factor to consider.

Cooling a photomultiplier tube is most effective in reducing the dark current and improving the signal-to-noise ratio, especially for photomultiplier tubes with high sensitivity in the red to near infrared region. Conversely, using a photomultiplier tube at a high temperature invites signal-to-noise ratio deterioration. If a photomultiplier tube must be operated at a high temperature, use of a special photocathode (Sb-Na-K) is recommended. Figure 8-3 shows dark current versus temperature characteristics of photomultiplier tubes having major photocathodes.



TPMOB0065EB

Figure 8-3: Temperature characteristics of anode dark current

## 8. 1. 2 Storage temperature and cooling precautions

Photomultiplier tube sensitivity varies somewhat during storage, even at room temperatures. This is probably due to the movement of alkali elements activating the photocathode and dynode surfaces. If a photomultiplier tube is left at a high temperature, this sensitivity variation will be accelerated. It is therefore recommended that the photomultiplier tube be stored at or below room temperatures.

In the case of PMT assemblies, do not store them in a place where the temperature falls below the specified storage temperature (generally  $-20^{\circ}\text{C}$ ).

As explained in (2), "Dark current" in the preceding section "8.1.1", photomultiplier tubes using a photocathode with high red-to-white sensitivity such as multialkali, GaAs(Cs), InGaAs and Ag-O-Cs are often cooled during operation to reduce the dark current. In this case, the following precautions should be observed, otherwise the difference in thermal expansion coefficient between the photomultiplier tube bulb, socket and adhesive (epoxy resin) may cause bulb rupture.

1. Avoid using a photomultiplier tube with a plastic base when cooling to  $-30^{\circ}\text{C}$  or below.
2. Assemble a voltage-divider circuit on a PC board and connect it to the socket using thin, soft wires, so that excessive force is not applied to the lead pins.
3. Avoid subjecting a photomultiplier tube to drastic temperature changes.

## 8. 2 Effects of Humidity

### 8. 2. 1 Operating humidity

Since the photomultiplier tube is operated at high voltages and handles very low current in the order of micro to picoamperes, leakage current between the lead pins may create a significant problem. This leakage current sometimes increases by several orders of magnitude due to a rise in the ambient humidity. It is advisable that the photomultiplier tube be operated at a humidity below 60 percent.

### 8. 2. 2 Storage humidity

If a photomultiplier tube is left at a high humidity for a long period of time, the following problems may occur: an increase in the leakage current on the bulb stem surface, contact failure due to rust formed on the lead pin surface and, for UV glass, a loss of transmittance. Therefore, the photomultiplier tube must be stored in locations of low humidity. In addition, since dirt on the photomultiplier tube surface may be a cause of increased leakage current and rust formation on the leads, avoid touching the bulb stem, lead pins and especially around the anode pin of a plastic base with bare hands. These portions must be kept clean but, if they become contaminated, use anhydrous alcohol for cleaning.

## 8. 3 Effects of External Magnetic Fields

### 8. 3. 1 Magnetic characteristics<sup>2)</sup>

In photomultiplier tube operation, because low-energy electrons travel along a long path in a vacuum, their trajectories are affected by even a slight magnetic field such as terrestrial magnetism, causing an anode sensitivity variation. A prime reason for this sensitivity variation is that the electron trajectories influenced by the magnetic fields cannot precisely focus the photoelectrons onto the first dynode. This means that photomultiplier tubes having a long distance between the photocathode and the first dynode or a small first-dynode opening in comparison with the photocathode area are more vulnerable to effects of a magnetic field.

For most head-on photomultiplier tubes, the anode sensitivity will be reduced by as much as 50 percent by a magnetic flux density of below 0.1 to several milliteslas. The sensitivity is most vulnerable to a magnetic flux in the direction parallel to the photocathode surface (X axis). Side-on photomultiplier tubes exhibit less sensitivity variations since the distance from the photocathode to the first dynode is short. The magnetic flux density at which the anode sensitivity reduces 50 percent is approximately 3.5 milliteslas for 1-1/8 inch side-on types. Recently developed metal-can type photomultiplier tubes (R5600 series) offer excellent immunity to magnetic fields because they have a short distance from the photocathode to the first dynode. Figure 8-4 shows the effects of magnetic fields on typical photomultiplier tubes.<sup>3)</sup> Note that the higher the supply voltage to a photomultiplier tube, the less the effects of magnetic fields.

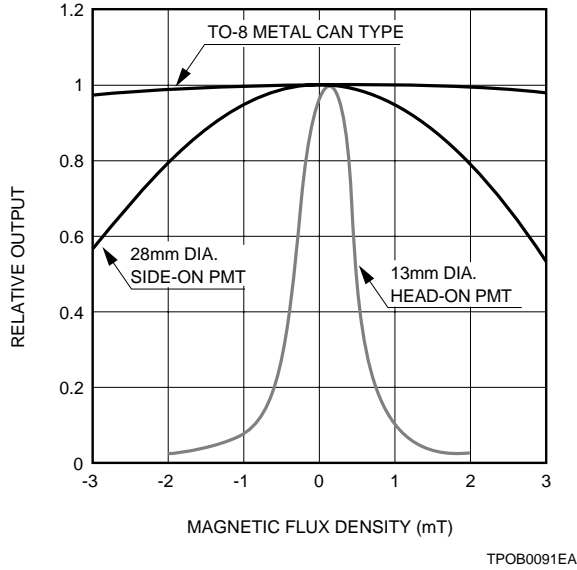
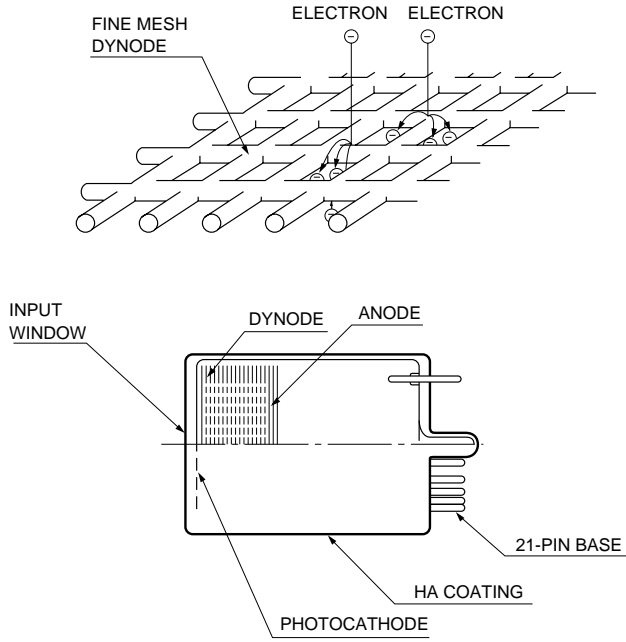


Figure 8-4: Magnetic characteristics of typical photomultiplier tubes

As can be seen from Figure 8-4, photomultiplier tubes are susceptible to magnetic fields. It is advisable that the photomultiplier tube be used in locations where no magnetic source is present. In particular, avoid using the photomultiplier tube near such devices as transformers and magnets. If the photomultiplier tube must be operated in a magnetic field, be sure to use a magnetic shield case. Refer to Section 7.4 of Chapter 7 for more details and specific usage of magnetic shield cases.

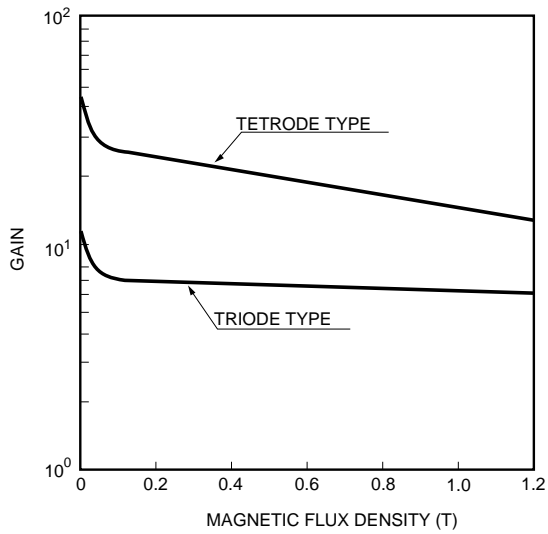
### 8.3.2 Photomultiplier tubes for use in highly magnetic fields

As stated previously, normal photomultiplier tubes exhibit a large variation in a magnetic field, for example, sensitivity reduces at least one order of magnitude in a magnetic field of 10 milliteslas. In high-energy physics applications, however, photomultiplier tubes capable of operating in a magnetic field of more than one tesla are demanded. To meet these demands, special photomultiplier tubes with fine-mesh dynodes have been developed and put into use. These photomultiplier tubes include a "triode" type using a single stage dynode, a "tetrode" type using a two-stage dynode and a high-gain type using multiple dynode stages (8 to 19 stages).<sup>4)</sup> The structure of this photomultiplier tube is illustrated in Figure 8-5. Figure 8-6 shows (1) current gain versus magnetic field perpendicular to the photocathode (tube axis) for a tetrode and triode types, and (2) relative output of a 19-stage photomultiplier tube versus magnetic field at different angles.



TPMOC0012EA

Figure 8-5: Structure of a photomultiplier tube designed for use in highly magnetic fields



TPMHB0247EB-(1)

Figure 8-6 (1): Magnetic characteristics of photomultiplier tubes for highly magnetic fields

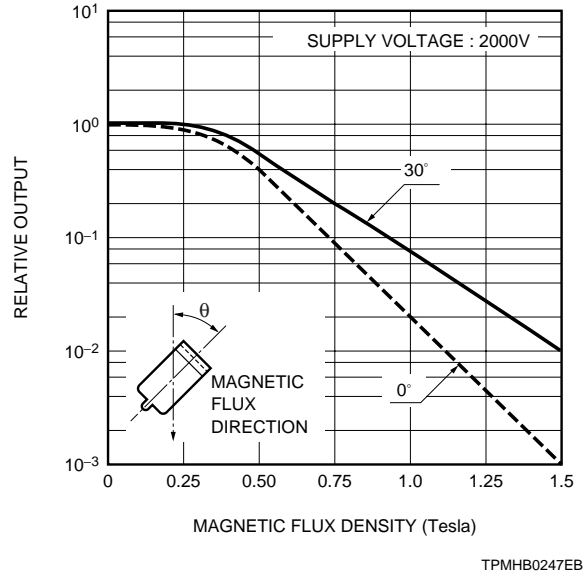


Figure 8-6 (2): Magnetic characteristics of photomultiplier tubes for high magnetic fields

### 8. 3. 3 Magnetization

The dynode substrate is commonly made from nickel with magnetic properties, and the photomultiplier tube leads and electrodes are also made from similar metals which can be magnetized. There will be no problem as long as the photomultiplier tube is operated in a weak magnetic field such as from terrestrial magnetism. If the magnetic field strength increases and exceeds the initial permeability of the dynode substrate and electrode materials, they will remain magnetized even after the magnetic field has been removed (residual magnetism). Thus the gain after the magnetic field has once been applied will differ from that before the magnetic field is applied. If magnetized, they can be demagnetized by applying an AC magnetic field to the photomultiplier tube and gradually attenuating it.

### 8. 3. 4 Photomultiplier tubes made of nonmagnetic materials

In applications where a photomultiplier tube must be used in a highly magnetic field or magnetization of the tube is unwanted, photomultiplier tubes made of nonmagnetic materials are sometimes required. Hamamatsu Photonics offers photomultiplier tubes assembled using nonmagnetic materials for the dynode substrate. However, the stem pins and hermetically-sealed portions still must be made from magnetic materials. Fortunately, stems made of a nonmagnetic material has been developed recently for use in special applications. It will soon become possible to manufacture a whole photomultiplier tube with nonmagnetic materials.

## 8. 4 Vibration and Shock

Resistance to vibration and shock can be categorized into two conditions: one is under non-operating conditions, for example, during transportation or storage and the other is under conditions when the tube is actually installed and operated in equipment. Except for special tubes designed for such applications as rocket-borne space research and geological surveys, photomultiplier tubes should not be exposed to vibration and shock during operation.

### 8. 4. 1 Resistance to vibration and shock during non-operation

Most photomultiplier tubes are designed to withstand several G of vibration and several hundred G of shock. However, if excessive vibration and shock are applied to a photomultiplier tube, its characteristics may vary and the bulb envelope may break.

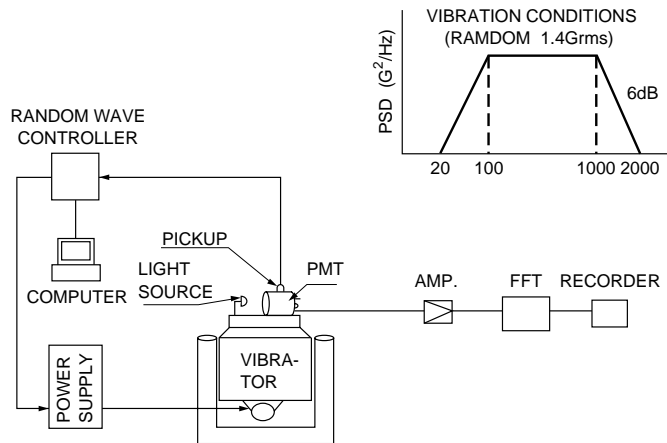
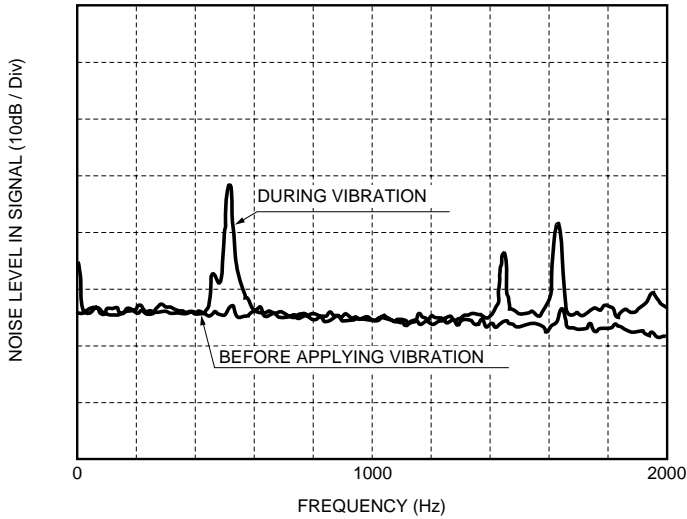
In general, photomultiplier tubes with a smaller size, lighter weight and shorter overall length exhibit better resistance to vibration and shock. Even so, sufficient care must be exercised when handling. The following table shows the maximum vibration and shock values which photomultiplier tubes can withstand.

| PMT Type            | Maximum Vibration  | Maximum Shock |
|---------------------|--------------------|---------------|
| 1/2 inch side-on    | 15G (10 to 2000Hz) | 200G (6ms)    |
| 1-1/8 inch side-on  | 10G (10 to 500Hz)  | 100G (11ms)   |
| 1/2 inch head-on    | 10G (10 to 500Hz)  | 100G (11ms)   |
| 1-1/8 inch head-on  | 5G (10 to 500Hz)   | 100G (11ms)   |
| 2 inch head-on type | 5G (10 to 500Hz)   | 75G (11ms)    |
| 3 inch head-on type | 5G (10 to 500Hz)   | 75G (11ms)    |

The photomultiplier tube envelope is made of glass, so it is vulnerable to direct mechanical shock. Envelopes with silica windows are especially vulnerable to shock on the bulb side because of a graded glass seal. Sufficient care must be taken in handling this type of tube. Furthermore, photomultiplier tubes designed for liquid scintillation counting use a very thin faceplate of 0.5 millimeters thick. Some of them may be broken even by a slight shock. Since the photomultiplier tube is a vacuum tube, if the envelope is broken, implosion may cause it to fly apart in fragments. Thus care is required, especially in handling a large diameter tube of more than 8 inches.

### 8. 4. 2 Resistance to vibration and shock during operation (resonance)

The photomultiplier tube is not normally designed to receive vibration and shocks during operation, except for specially-designed ruggedized tubes. If a photomultiplier tube suffers vibration or shocks during operation, problems such as variations of the signal level and an increase in the microphonic noise may occur. Attention should be given to the mounting method and arrangement of the tube. Moreover, the photomultiplier tube may have a resonance at a certain frequency, but this resonant frequency differs from tube to tube. If vibration is increased at this resonance, the above problems will be more noticeable, leading to the breakage of the envelope. Figure 8-7 shows the variations in the frequency spectrum of photomultiplier tube output subjected to vibration, along with the measurement block diagram.



TPMOB0019EA

**Figure 8-7: Resonance noise of photomultiplier tube output subjected to vibration**

In this experiment, the photomultiplier tube is subjected to random vibration (1.4G rms) from 20Hz to 2000Hz and its output signal is frequency-analyzed using a FFT (fast fourier transform). It is obvious from Figure 8-7 that the noise sharply increases at frequencies near 500Hz, 1450Hz and 1600Hz.

When measurement is made at extremely low light levels, even a slight vibration caused by the table on which the equipment is placed may be a source of noise. Precautions should be taken to ensure the equipment is installed securely and also the cable length to the preamplifier should be checked.

### 8. 4. 3 Testing methods and conditions

There are two vibration test methods<sup>5)</sup>: sinusoidal-wave and random-wave application tests. The sinusoidal wave used for vibration tests is determined by the frequency range, displacement (amplitude), acceleration, vibration duration and sweep time. The frequency sweep method commonly employed is a logarithmic sweep method. The random wave is determined by the acceleration, power spectrum density ( $G^2/Hz$ ), and the vibration duration, and is expressed in terms of the RMS value. This method allows tests to be performed under the conditions close to the actual environment. In Figure 8-8 (A) and (B), vibration waveform examples created by sinusoidal wave and random wave are shown.

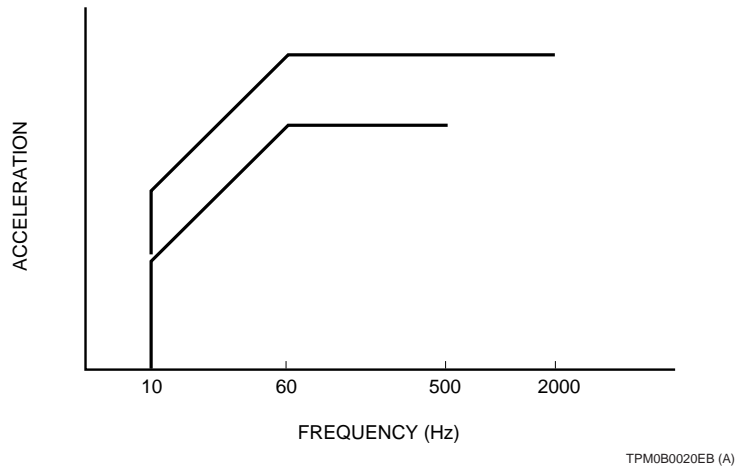


Figure 8-8 (A): Sinusoidal wave vibration pattern example

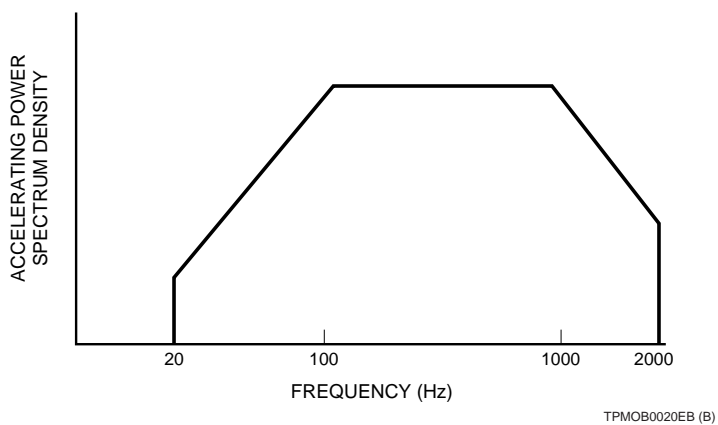
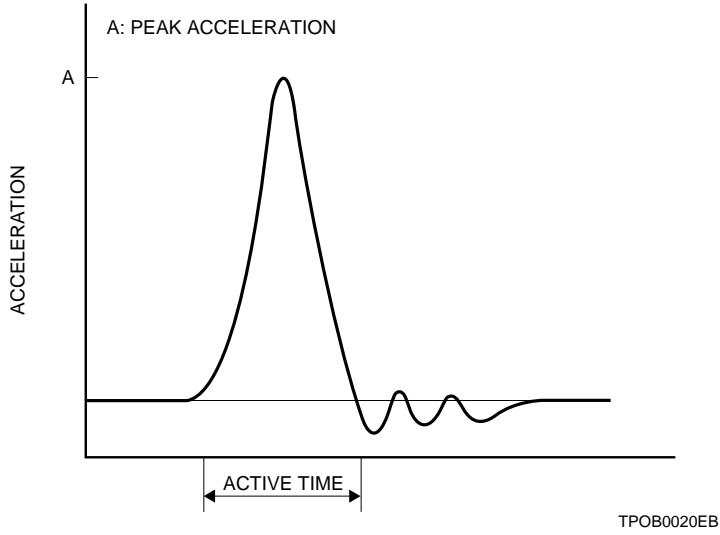


Figure 8-8 (B): Random vibration pattern example

Various methods are used in shock tests such as half-wave sinusoidal pulses, sawtooth wave pulses, and trapezoidal wave pulses. Hamamatsu Photonics performs shock tests using half-wave sinusoidal pulses. The test conditions are determined by the peak acceleration, shock duration, and the number of shocks applied. A typical shock-application pattern is shown in Figure 8-8 (C).

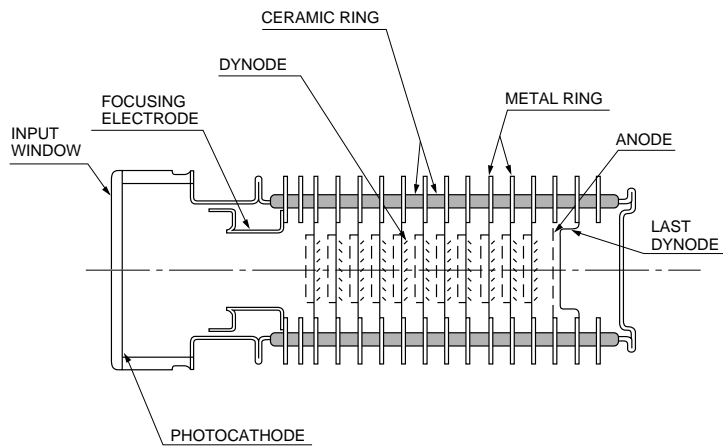


**Figure 8-8 (C): Shock-application pattern (half-wave sinusoidal pulse)**

Official standards for vibration and shock test methods include IEC Pub. 68, JIS-C0040 (vibration), JIS-C0041 (shock), MIL STD-810E and MIL STD-202F.<sup>6)</sup> Hamamatsu Photonics performs the vibration and shock tests in conformance to these official standards. The above data for vibration and shock tests were measured under these official conditions. For instance, the shock tests were carried out along three orthogonal axes for a shock duration period of 11 milliseconds, three times each in the plus and minus directions, and thus shocks were applied a total of 18 times. Accordingly, even if the test proves that a photomultiplier tube withstands a shock of 100G, this does not mean that it will survive such shocks dozens or hundreds of times.

### 8. 4. 4 Ruggedized photomultiplier tubes<sup>7)</sup>

In geological surveys such as oil well logging or in space research in which photomultiplier tubes are launched in a rocket, extremely high resistance to vibration and shock is required.<sup>8)</sup> To meet these applications, ruggedized photomultiplier tubes have been developed, which can operate reliably during periods of 20G to 50G vibration and 100G to 1000G shock. A variety of ruggedized types are available ranging in diameter from 1/2 to 2 inches and are also available with different dynode structures. Most ruggedized photomultiplier tubes have been devised based on conventional glass-envelope photomultiplier tubes by improving their electrode supports, lead pins and dynode structure so that they will withstand severe shock and vibration. These ruggedized photomultiplier tubes with a diameter of 2 inches or less can withstand vibrations up to 20G. If even higher performance is required, specially-designed ruggedized photomultiplier tubes having a stacked ceramic bulb are used. Figure 8-9 shows the cross section of this type of ruggedized photomultiplier tube.



TPMOC0013EA

**Figure 8-9: Cross section of a ruggedized photomultiplier tube using a stacked ceramic bulb.**

As illustrated in Figure 8-9, each dynode electrode of this ruggedized photomultiplier tube is securely welded to a ceramic ring. This structure resists electrical discontinuity, contact failure and envelope rupture even under severe vibration and shock. This is because the dynodes resist deformation and peeling. No lead wires, ceramic spacers or cathode contacts are required, and few fragile glass parts need to be used. The voltage-divider resistors can be soldered on the outside of the metal rings which are fused to the ceramic rings, assuring high ruggedness even after the voltage-divider circuit has been assembled on the tube. The typical maximum vibration and shock for a stacked-ceramic photomultiplier tube using a high-temperature bialkali photocathode and a 12-stage dynode multiplier is as follows:

|                         |                    |
|-------------------------|--------------------|
| Resistance to vibration | 50G (50 to 2000Hz) |
| Resistance to shock     | 1000G (0.5ms)      |

## 8.5 Effects of Helium Gas

It is well known that helium gas permeates through glass.<sup>9)</sup> The extent of helium permeation through glass depends on the glass materials, their composition and ambient temperature. Photomultiplier tubes designed for UV light detection usually employ silica glass for the input window. Helium gas permeates through silica glass more than through other window materials. So if such a photomultiplier tube is stored or operated in environments where helium gas is present, a gas increase occurs inside the tube, leading to an increase in dark current and promoting a degradation of the breakdown voltage level. This eventually results in breakdown and end of the tube service life. For example, if a photomultiplier tube with a silica bulb is placed in helium gas at one atmosphere, a drastic increase of afterpulse due to helium gas will be seen in about 30 minutes, making the tube unusable. Thus this must be avoided. To reduce the effects of helium gas, it is best to store the tube in helium-free environments such as argon gas and nitrogen gas.

Helium gas exists on the earth at a partial pressure of about 0.5 pascals. As stated above, the permeability of helium through silica glass is extremely high, as much as  $10^{-19}$  cm<sup>2</sup>/s (at a pressure difference of  $1.013 \times 10^5$  pascals) at room temperatures. Because of this, the helium pressure inside the photomultiplier tube gradually increases and finally reaches a level close to the helium partial-pressure in the atmosphere. The time needed to reach that level depends on the surface area and thickness of the silica glass. For instance, if a side-on photomultiplier tube (1-1/8 inch diameter type) with a silica bulb is left in the atmosphere, the helium partial-pressure inside the tube will increase to  $9 \times 10^{-2}$  pascals after one year. (Refer to Figure 8-10.) In practice however, if the helium partial-pressure inside the tube increases to a level equal to the helium partial-pressure in the atmosphere, no significant problem will immediately occur and the tube is still usable.

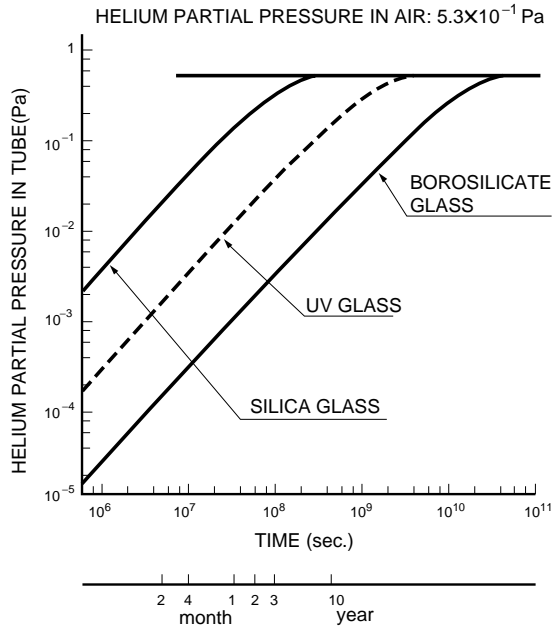


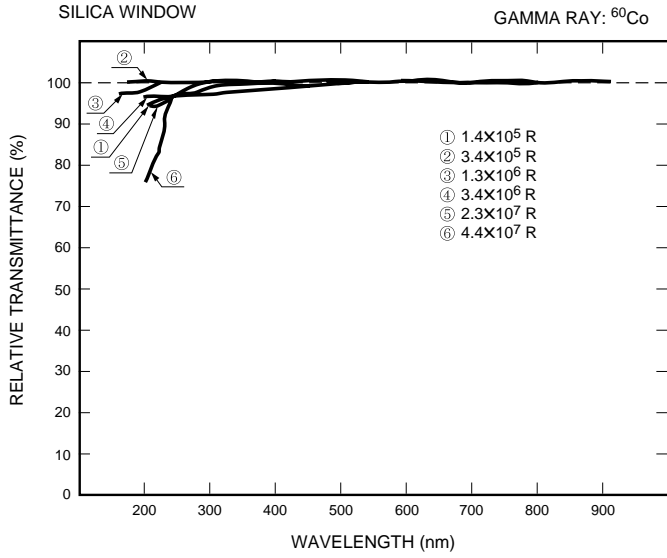
Figure 8-10: Bulb materials and variations in helium partial-pressure inside a tube

## 8. 6 Effects of Radiation

Photomultiplier tube applications are constantly expanding, as stated previously, to such fields as high energy physics, nuclear medicine, X-ray applied instrumentation, and space research. In these environments, photomultiplier tubes are usually exposed to radiation (X-rays, alpha rays, beta rays, gamma rays, neutrons, etc.) which somewhat affect the performance characteristics of photomultiplier tubes.<sup>10)</sup> Such radiation is detected by the photomultiplier tube photocathode and converted into useful signals, but it also causes deterioration of the glass envelope, metals, insulators, and materials used to construct the photomultiplier tube. The following sections describe the effects of radiation.

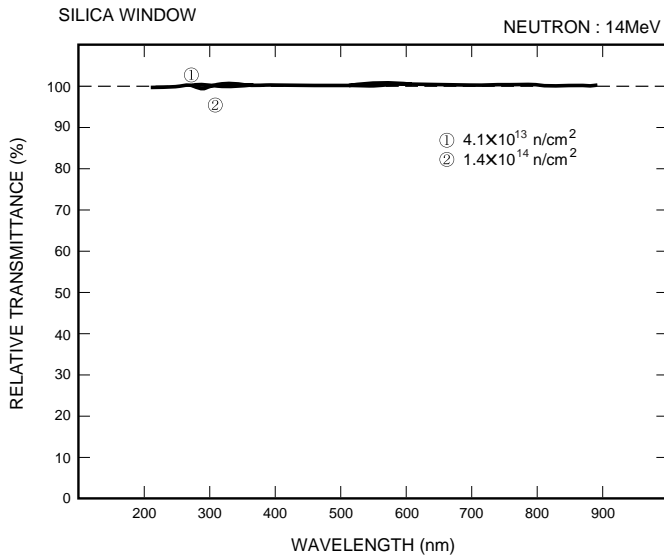
### 8. 6. 1 Deterioration of window transmittance

Even when a photomultiplier tube is exposed to radiation, the cathode sensitivity and secondary emission ratio exhibit very little variation. Sensitivity variation chiefly results from a loss of transmittance through the window due to coloring of the glass, which is an essential part of the photodetector.<sup>11)</sup> Figures 8-11 to 8-13 show variations in the window transmittance when photomultiplier tubes are irradiated by gamma rays from a <sup>60</sup>Co radiation source and also by neutrons (14MeV).



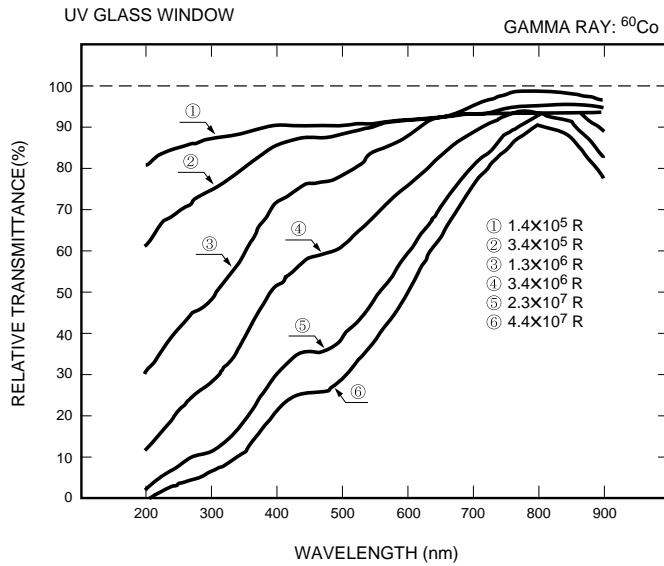
TPMOB0022EB (a)

Figure 8-11 (a): Transmittance variations of synthetic silica window when irradiated by gamma rays



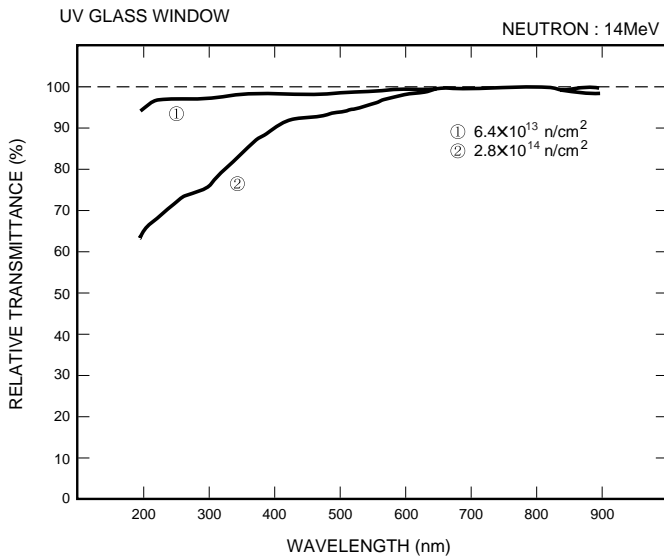
TPMOB0022EB (b)

Figure 8-11 (b): Transmittance variations of synthetic silica window when irradiated by neutrons



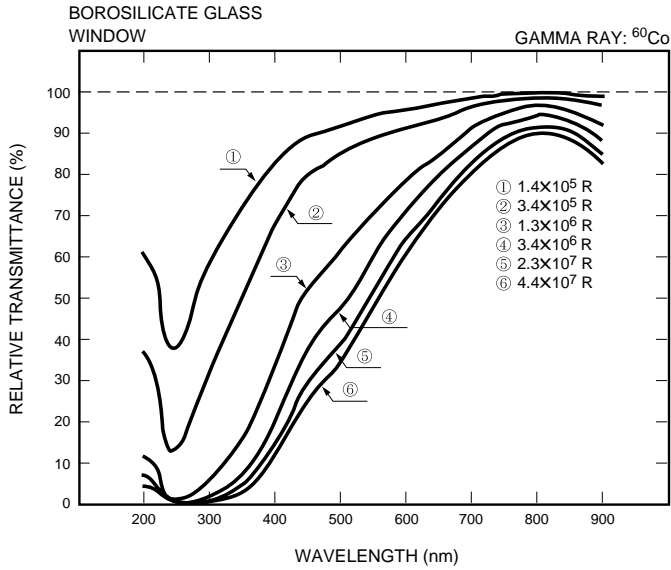
TPMOB0023EB (a)

Figure 8-12 (a): Transmittance variations of UV glass window when irradiated by gamma rays



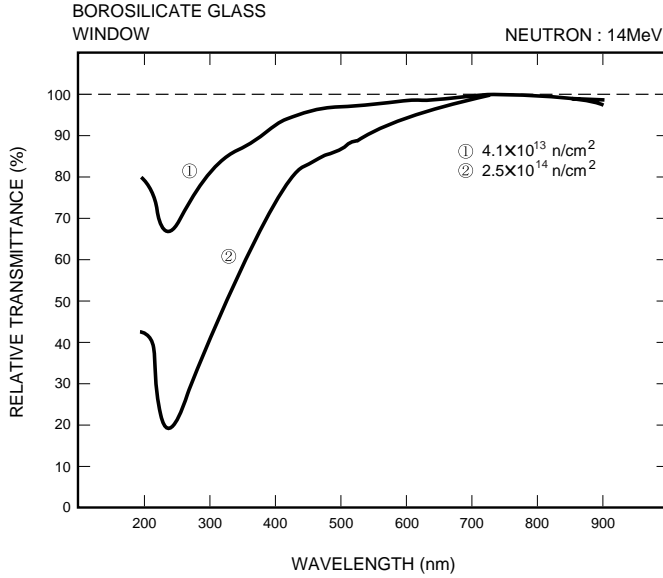
TPMOB0023EB (b)

Figure 8-12 (b): Transmittance variations of UV glass window when irradiated by neutrons



TPMOB0024EB (a)

Figure 8-13 (a): Transmittance variations of borosilicate glass window when irradiated by gamma rays



TPMOB0024EB (b)

Figure 8-13(b): Transmittance variations of a borosilicate glass window when irradiated by neutrons

As can be seen from these figures showing the data on a synthetic silica, UV glass and borosilicate glass respectively, a loss of the transmittance occurs more noticeably in the UV region. The synthetic silica glass is least affected by radiation and virtually no variation is seen after irradiation of gamma rays of  $4.4 \times 10^7$  roentgens and neutrons of  $1.4 \times 10^{14}$  n/cm<sup>2</sup>. There are two types of silica glass: synthetic silica and fused silica. The synthetic silica exhibits a higher resistance to radiation than the fused silica. A loss of transmittance begins to occur from near  $5 \times 10^4$  roentgens for the UV glass, and near  $1 \times 10^4$  roentgens for the borosilicate glass. However, this tendency is not constant even for the same type of glass, because the composition differs depending on the fabrication method. In general, the radiation-resistance characteristic is superior in the order of silica, UV glass and borosilicate glass. When the transmittance has dropped due to exposure to radiation, it will recover to some extent after storage. This recovery is more effective when the tube is stored at higher temperatures.

### 8. 6. 2 Glass scintillation

The photomultiplier tube is slightly sensitive to radiation and produces a resultant noise. This is primarily due to unwanted scintillation of the glass window caused by beta and alpha rays or scintillation of the glass window and electron emission from the photocathode and dynodes caused by gamma rays and neutrons.<sup>12)</sup>

Of these, the scintillation of the glass window likely has the largest contribution to noise, but, as described in Section 3.11 of Chapter 3, the amount of scintillation differs depending on the type of glass. Glass scintillation further causes a continual fluorescence or phosphorescence to occur even after radiation has been removed, resulting in yet another source of noise. Figure 8-14 shows a variation in the dark current when a tube is irradiated by gamma rays, indicating that it takes 40 to 60 minutes to reach a steady level. In the case of neutron irradiation, it has been confirmed that the dynode materials are made radioactive through nuclear reaction (n, p) (n, n, p).

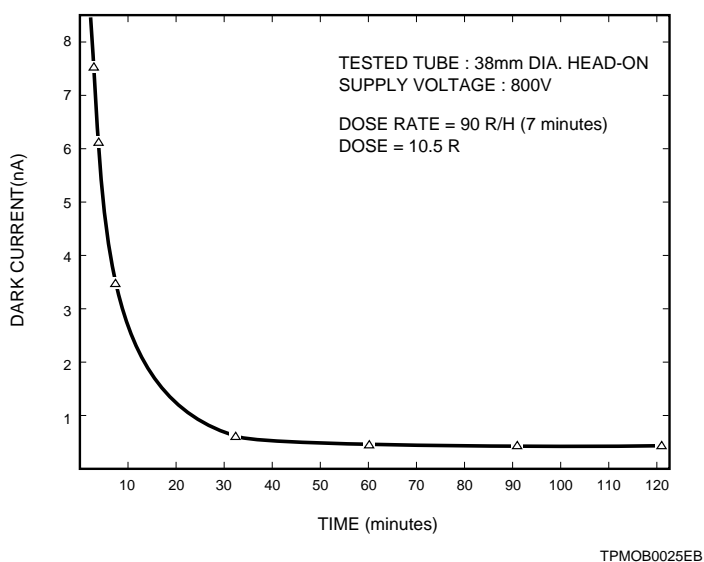


Figure 8-14: Dark current variation after gamma-ray irradiation

## 8.7 Effects of Atmosphere

The photomultiplier tube may be used in environments not only at one atmosphere but also at very low pressures or in depressurized areas such as in aircraft and scientific satellite.

When there is a pressure drop from the atmospheric pressure down to a near vacuum, there is a possibility of a discharge occurring in the photomultiplier tube. This phenomenon is known as the Paschen's law. The law states that the minimum sparking potential between two electrodes in a gas is a function of the product of the distance between the electrodes and the gas pressure, if the electric field is uniform and the ambient temperature is constant.

The distance between the leads on the outside base and on the socket is set to an interval so that no discharge occurs in environments at one atmosphere or in vacuum. However, these structures tend to discharge most frequently at pressures from 100 to 1000 pascals\*. If the tube is to be operated in this pressure range, sufficient precautions must be taken in the designing and wiring of the parts to which a high voltage is applied.

(\* 133 pascals equal one torr.)

In high-energy physics applications such as proton decay experiments and cosmic ray detection, photomultiplier tubes are sometimes operated while underwater or in the sea. In this case, a pressure higher than one atmosphere is applied to the photomultiplier tube. The breaking pressure depends on the configuration, size and bulb material of the photomultiplier tube. In most cases, smaller tubes can withstand a higher pressure. However, large diameter (8 to 20 inches) photomultiplier tubes, specifically developed for high energy physics experiments, have a hemispherical shape capable of withstanding a high pressure. For example, 8-inch diameter tubes can withstand up to 7 atmospheres and 20-inch diameter tubes up to 6 atmospheres.

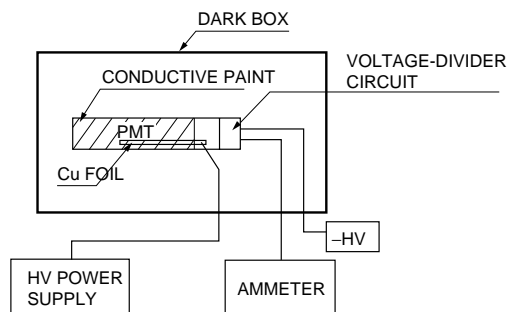
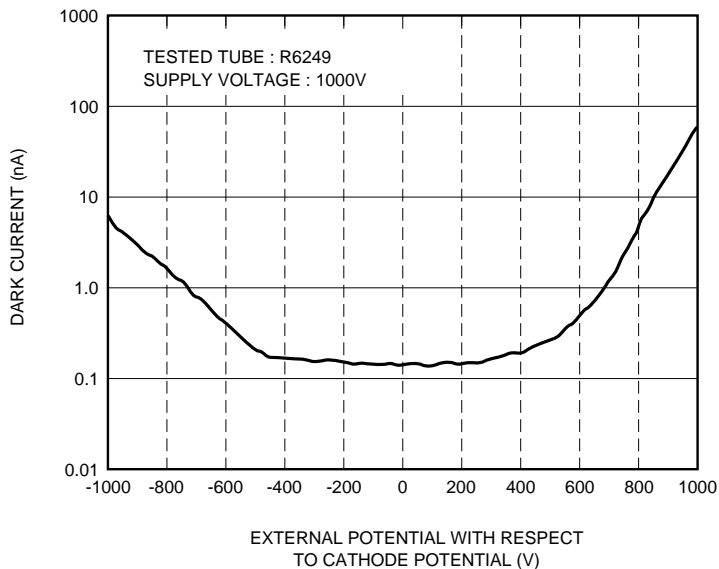
As for the bulb materials, photomultiplier tubes using a silica bulb provide lower pressure-resistance due to the graded seal. There are various shapes of input windows used for head-on photomultiplier tubes, including a plano-plano type (both the faceplate and photocathode are flat), a plano-concave type (the faceplate is flat but the photocathode is concave) and a convex-concave type (the faceplate is convex but the photocathode is concave). Compared to the plano-plano type, the plano-concave and convex-concave types offer higher pressure-resistance.

## 8.8 Effects of External Electric Potential

Glass scintillation occurs upon exposure to radioactive rays or UV light, as explained in Section 8.6.2 of Chapter 8. It also occurs when a strong electric field is inside the glass. These glass scintillations cause the dark current to increase.

### 8.8.1 Experiment

Figure 8-15 shows the dark current variations of a photomultiplier tube whose side bulb is coated with conductive paint, measured while changing the electric potential of this coating with respect to the cathode potential.

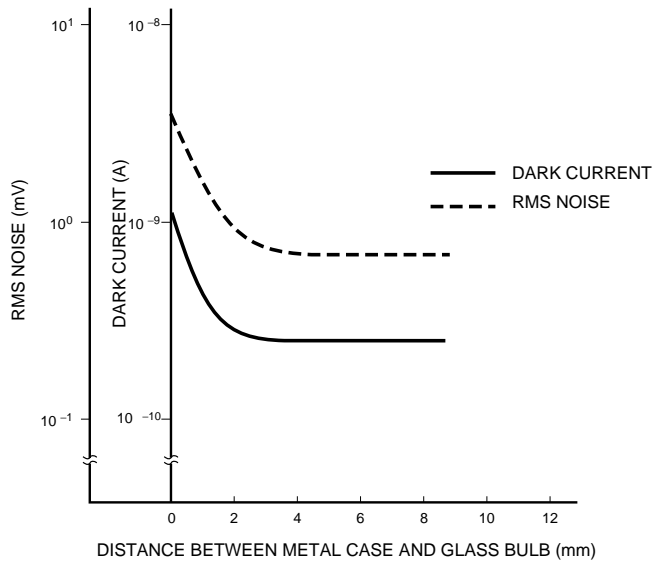
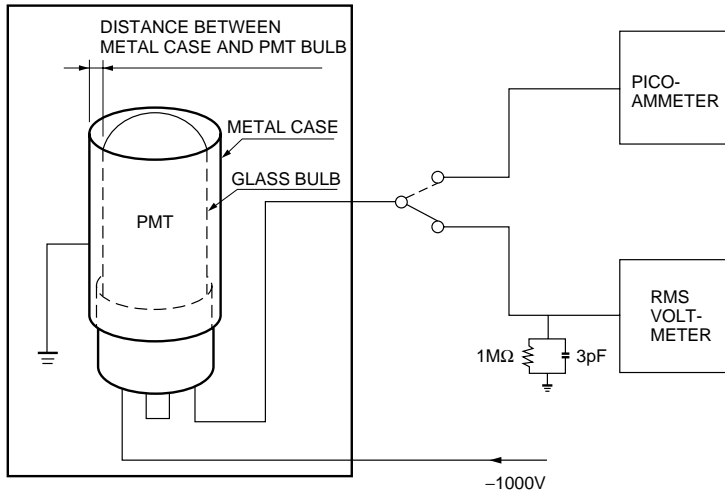


TPOB0026EB

**Figure 8-15: Dark current vs. external electric potential**

It is clear that the larger the potential difference with respect to the cathode, the higher the dark current. The reason for this effect is that the inner surface of the bulb near the cathode is aluminum-coated and maintained at the cathode potential as explained in Chapter 2, and if the outside of the bulb has a large potential difference with respect to the cathode, glass scintillation occurs there. This scintillation light is reflected into the photocathode, causing an increase in the dark current.

The housing in which the photomultiplier tube is installed is usually grounded. If the photomultiplier tube is operated in the anode grounding scheme with the cathode at a negative high voltage and is installed close to the wall of the housing, the dark current may increase for the same reason. This problem can be solved by allowing an adequate distance between the photomultiplier tube and the inside of the housing. Figure 8-16 shows the dark current variations while the distance between the photomultiplier tube and the grounded case is changed, proving that there is no increase in the dark current when the separation is 4 millimeters or more.

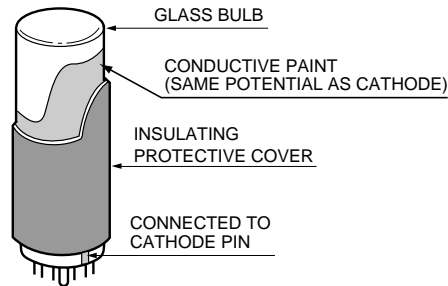


TPMOC0014EB

Figure 8-16: Dark current vs. distance to the grounded case

## 8. 8. 2 Taking corrective action

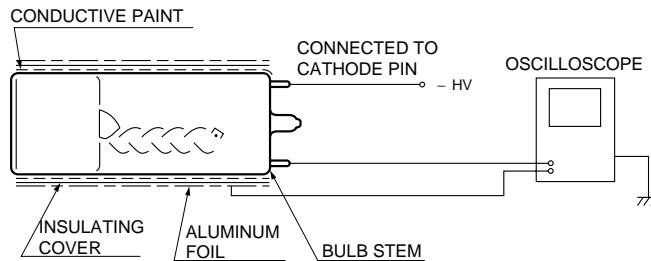
The above effects of external electric potential can be eliminated by use of the cathode grounding scheme with the anode at a positive high voltage, but photomultiplier tubes are frequently operated in the anode grounding scheme with the cathode at a negative high voltage. In this case, a technique of applying a conductive paint around the outside of the bulb and connecting it to the cathode potential can be used, as illustrated in Figure 8-17.<sup>13)</sup>



TPMOC0015EA

**Figure 8-17: HA coating**

This technique is called "HA coating" by Hamamatsu Photonics and, since a negative high voltage is applied to the outside of the bulb, the whole bulb is covered with an insulating cover (heat-shrinkable tube) for safety. The noise problem caused by the external electric potential can be minimized by use of an HA coating. Even so, in cases where a metal foil at ground potential is wrapped around the tube, minute amounts of noise may still occur. This effect can be observed using a setup like that shown in Figure 8-18. This noise is probably caused by a small discharge which may sometimes occur due to dielectric breakdown in the insulating cover, which then produces a glass scintillation reaching the photocathode. This problem can be reduced by shifting the metal foil wrapped around the glass scintillation away from the photocathode toward the bulb stem.



TPMOC0016EA

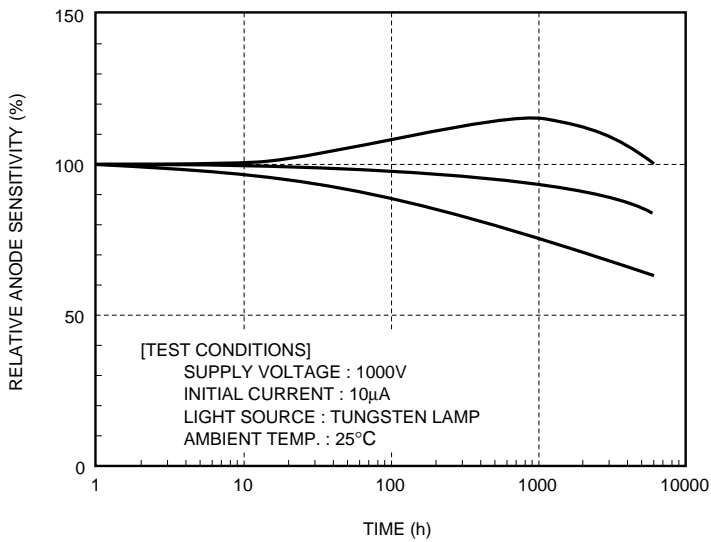
**Figure 8-18: Observing the effect of external electric potential on HA coating**

As mentioned above, the HA coating can be effectively used to eliminate the effects of external potential on the side of the bulb. However, if a grounded conductive object is located on the photocathode faceplate, there are no effective countermeasures and what is worse, scintillation occurring in the faceplate has a larger influence on the noise. Therefore, any grounded object, even insulating materials, should not make contact with the faceplate. If such an object must make contact with the faceplate, it is necessary to select one with high insulating properties such as teflon. Another point to be observed is that a grounded object located on the faceplate can cause not only a noise increase but also deterioration of the photocathode sensitivity. Once deteriorated, the sensitivity will never recover to the original level. Thus, particular care must be exercised with regard to the mounting method of the photomultiplier tube. Taking account of the above effects of external electric potential it is recommended, if possible, that the photomultiplier tube be operated in the cathode grounding scheme with the anode at a positive high voltage.

## 8.9 Reliability

### 8.9.1 Stability over time (life characteristic)

Stability over time of a photomultiplier tube exhibits a somewhat specific pattern according to the type of photocathode and the dynode materials, but greatly depends on the operating conditions (especially on the output current) and the fabrication process. Also, stability over time widely varies from tube to tube even among the same tube family. In normal operation, the cathode current flowing through the photocathode is on the order of picoamperes, and the photocathode fatigue can virtually be ignored. Accordingly, the operating stability of the dynodes is an important factor that largely affects the stability over time of the photomultiplier tube. Figure 8-19 shows typical data for time stability when photomultiplier tubes are operated at an anode current of  $10\mu\text{A}$ .

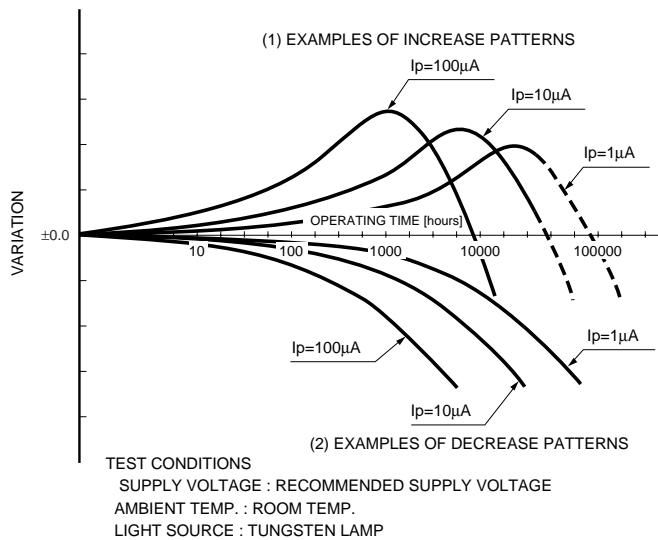


TPOB0027EB

Figure 8-19: Typical time stability of photomultiplier tubes

### 8.9.2 Current stress and stability

As mentioned in the preceding section, time stability of a photomultiplier tube varies with the operating conditions. In general, the larger the current stress, the earlier and more significant the variation that occurs. Figure 8-20 shows typical time stability of photomultiplier tubes when their operating anode currents  $I_p$  are set to 1, 10 and 100 microamperes, indicating both increasing and decreasing patterns.

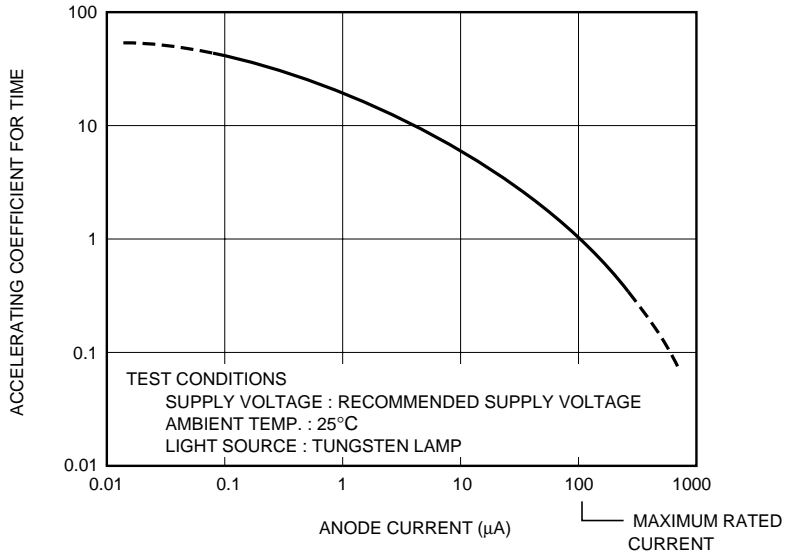


TPMOB0028EA

**Figure 8-20: Typical time stability of photomultiplier tubes (at different anode currents)**

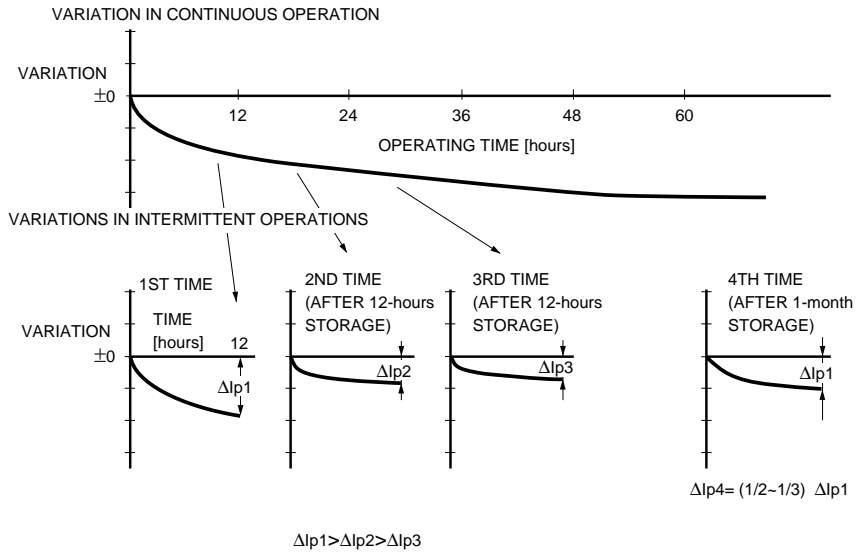
Figure 8-21 shows a typical acceleration factor over time with respect to the anode current. Stability over time can be improved to some extent by aging the tube. Figure 8-22 shows the initial output variations when a photomultiplier tube is intermittently operated. It is obvious from the figure that a large variation during the initial operation can be reduced to nearly half, during the second or later operations.

When the photomultiplier tube is left for long periods of time, stability will return to its original values. In applications where high stability is prerequisite, we recommend the tube be aged before use.



TPOB0029EB

Figure 8-21: Typical acceleration factor over time with respect to anode current



TPMOB0030JB

Figure 8-22: Effects of intermittent operation (aging effect)

### 8.9.3 Reliability

Photomultiplier tube applications are constantly expanding to such fields as scintillation counting, high energy physics, nuclear medicine, X-ray applied instrumentation, and aerospace fields. In these application fields, a large number of photomultiplier tubes (sometimes hundreds or occasionally even thousands of tubes) are used in one instrument. It is therefore extremely important in these applications to predict and verify the reliability of the photomultiplier tubes.

#### (1) Failure mode

Failure mode for photomultiplier tubes is roughly classified into gradual failure and breakdown failure. The main failure mode is gradual failure, which includes cathode sensitivity degradation, a loss of gain, an increase in dark current and a decrease in dielectric resistance. Breakdown failure includes cracks in the faceplate, bulb envelope and stem portion, and also air leakage through microscopic cracks. Breakdown failure fatally damages the photomultiplier tube, making it permanently unusable.

Since Hamamatsu photomultiplier tubes undergo stringent screening both in the manufacturing and inspection process, most possible failures and their causes are eliminated before shipping. As a result of in-house reliability tests, we have found most of the failure mode causes lie in a loss (or variation) of gain. This means that the photomultiplier tube can still be properly used by adjusting the operating voltage.

#### (2) Failure rate

Failure rate<sup>(15) 16)</sup> is defined as the probability of failure per unit time. Failure rate is generally estimated by using the following two kinds of data:

1. In-house reliability test data
2. Field data

Actual results obtained from field data prove that the photomultiplier tube failure rate is at a level of  $2 \times 10^{-7}$  to  $2 \times 10^{-6}$  failures/hour with operating conditions at room temperatures, a rated supply voltage and an anode output current of 100 nanoamperes. In particular, it is predicted that those tubes which have undergone screening provide a failure rate as small as  $5 \times 10^{-7}$  failures/hour.

#### (3) Mean life

There is a measure of reliability which is commonly referred to as MTBF<sup>(15) 16)</sup> (mean time between failure) or MTTF (mean time to failure). Stated simply, this is the average hours of time until any failure occurs, in other words, mean life.

Since the definition and fundamental calculation of these terms are described in detail in various papers, this section only briefly explains these terms.

The relation between the failure rate ( $\lambda$ ) and the mean life ( $\theta$ ) can be expressed on the assumption that it has failure distribution in accordance with exponential distribution, as follows:<sup>(15) 16)</sup>

$$\theta \Delta = 1 / \lambda$$

Therefore, the reciprocal of the failure rate is the mean life.

As an example, when a photomultiplier tube is operated in room environments with the anode output current of about 100 nanoamperes, a mean life of  $5 \times 10^5$  to  $5 \times 10^6$  hours can be predicted based on the failure rate explained above. For those tube which have passed screening, the mean life would be more than  $2 \times 10^6$  hours.

**(4) Reliability**

Based on the fundamental calculation for stability data, reliability R is defined as follows.<sup>15) 16)</sup>

$$R(t) = e^{-t\lambda}$$

t: operating time in hours

$\lambda$ : failure rate

Therefore, using a typical failure rate  $\lambda$  of photomultiplier tubes of  $2 \times 10^{-6}$  to  $2 \times 10^{-7}$  failures/time, reliability R becomes as follows:

| Elapsed time in operation | Reliability R(t)                |                                 |
|---------------------------|---------------------------------|---------------------------------|
|                           | at $\lambda = 2 \times 10^{-6}$ | at $\lambda = 2 \times 10^{-7}$ |
| One year (8760 hours)     | 98.3%                           | 99.8%                           |
| 2 years (17520 hours)     | 96.6%                           | 99.7%                           |
| 3 years (26280 hours)     | 94.9%                           | 99.5%                           |
| 4 years (35040 hours)     | 93.2%                           | 99.3%                           |
| 5 years (43800 hours)     | 91.6%                           | 99.1%                           |

The above results can be used as a reference in determining reliability levels of photomultiplier tubes, and prove that the photomultiplier tube provides considerably high reliability levels tube when operated under favorable conditions.

### 8.9.4 Reliability tests and criteria used in Hamamatsu Photonics

Hamamatsu Photonics performs in-house reliability tests by setting the following test conditions and failure criteria to obtain the failure rate.

#### Reliability test conditions

- 1) Environmental stress conditions  
Room temperature (25°C) and high temperature (60°C) (10°C above the maximum rating)
- 2) Test procedures  
Storage and operating life
- 3) Operating conditions (photomultiplier tubes)  
Supply voltage: catalog-listed standard operating voltage 1000 to 1250V  
Anode output current: catalog-listed maximum rating 10 to 100µA

#### Failure criteria

- 1) Anode sensitivity judged as the end of life:  $\pm 50\%$  variation
- 2) Anode sensitivity during non-operation (storage):  $\pm 25\%$  variation
- 3) Cathode sensitivity:  $\pm 25\%$  variation
- 4) Anode dark current (DC): more than 500 times increase, faulty dielectric-resistance
- 5) Breakdown failure: discharge, crack, anode leakage current, etc.

Notice that the above criteria are specified by Hamamatsu Photonics for evaluation and do not necessarily indicate that a tube outside these standards is unusable.

Hamamatsu Photonics has continually performed reliability tests under the above conditions over extended periods of time and has collected large amounts of data. Our evaluation results show that the failure rate of photomultiplier tubes ranges from  $1 \times 10^{-3}$  to  $1 \times 10^{-4}$  failures/hour and thus the mean time is from 1000 up to 10000 hours. Based on these results, the ratio of the failure rate at room temperatures and an anode output current of 100 nanoamperes, to the failure rate under operating conditions at a maximum rating (10 to 100 microamperes) will be approximately 500 times. This means that our in-house test conditions have an acceleration factor approximately 500 times that of the field data.

## References in Chapter 8

- 1) Hamamatsu Photonics Catalog: Photomultiplier Tubes.
- 2) Hamamatsu Photonics Catalog: Accessories for Photomultiplier Tubes.
- 3) Hamamatsu Photonics Catalog: Accessories for Photomultiplier Tubes.
- 4) Hamamatsu Photonics Technical Data Sheet: T-101.
- 5) Special Committee for Measurement and Research into Vibration and Shock, Society of Electricity: Measurement: Electric/Electronic Equipment and Vibration/Shock, Corona-sha.
- 6) IEC Publication 68-2: Basic Environmental Testing Procedures.
- 7) Hamamatsu Photonics Catalog: Ruggedized High-Temperature Photomultiplier Tubes TPMHOOO1EA.
- 8) Bicron Corp.: Ruggedized High-Temperature Detector Technology.
- 9) J.R. Incandela, S.P. Ahlen, J. Beatty, A. Ciocio, M. Felcini, D. Levin, D. Ficenec, E. Hazen, A. Marin, J.L. Stone, L.R. Sulac, W. Worstell: Nucl. Instrum. & Methods, Phys. Res. A269, 237-245 (1988).
- 10) L.W. Howell, H.F. Kenne: Optical Engineering, 25, 4, 545 (1986).  
M.M. Brinbaum, R.L. Bunker, J. Roderick, K. Stephenson: AIAA Guidance And Control Conference (1984).
- 11) S. Sakubana, T. Kyono, K. Takahashi: Glass Handbook, 825, Asakura Shoten.
- 12) W. Viehamann, A.G. Eubanks, G.F. Pieper, J.H. Bredekamp: Applied Optics, 14,9, 2104 (1975).
- 13) Hamamatsu Photonics Catalog: Photomultiplier Tubes.

# **CHAPTER 9**

## **APPLICATIONS**

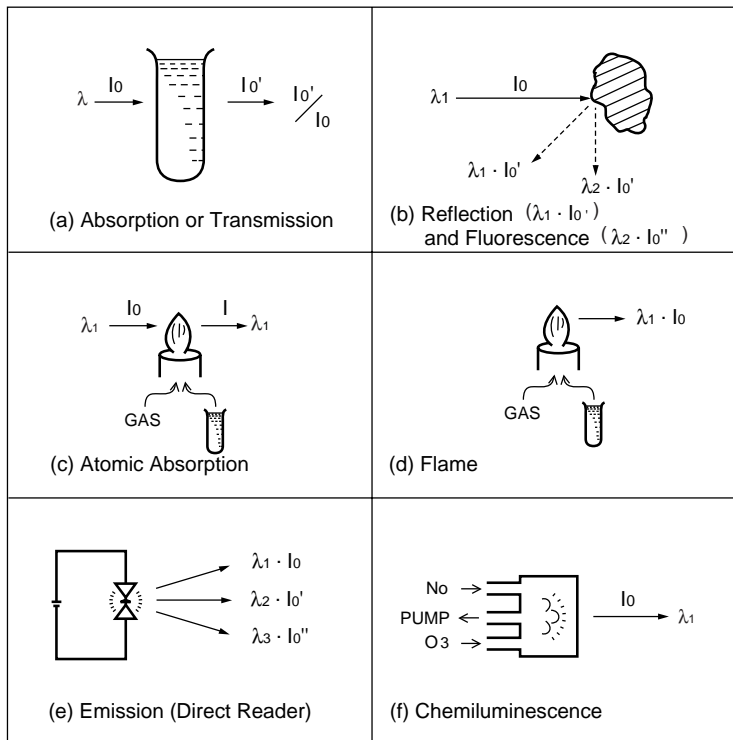
*Photomultiplier tubes (PMTs) are extensively used as photodetectors in various measuring equipment in fields such as chemical analysis, medical diagnosis, scientific research and industrial measurement. This chapter introduces major applications of photomultiplier tubes and describes the principle and detection methods of each application.*

*This chapter also explains the types of photomultiplier tubes which are most suited for each application as well as the major performance characteristics required of the photomultiplier tubes and their measurement methods.*

## 9.1 Spectrophotometry

### 9.1.1 Overview

Spectrophotometry is a study of the transmission and reflection properties of material samples as a function of wavelength, but the term commonly means chemical analysis of various substances utilizing photometry. Photometric instruments used in this field are broadly divided into two methods: one utilizes light absorption, reflection or polarization at specific wavelengths and the other uses external energy to excite a sample and measures the subsequent light emission. Photomultiplier tubes have been most widely used in this field for years. Major principles used in spectrophotometry are classified as illustrated in Figure 9-1 below.



TPMOC0017EB

**Figure 9-1: Major principles of spectrophotometry**

Specific photometric instruments currently used are:

- 1) Visible to UV spectrophotometers (absorption, reflection)
  - 2) Infrared spectrophotometers (absorption, reflection)
  - 3) Far UV spectrophotometers (absorption, reflection)
  - 4) Emission spectrophotometers
  - 5) Fluorescence spectrophotometers
  - 6) Atomic absorption spectrophotometers
  - 7) Azimuthal, circular dichroism meters
  - 8) Raman spectrophotometers
  - 9) Densitometers, colorimeters and color analyzers
- etc.

## 9.1.2 Specific applications

The following paragraphs explain major, specific applications of spectrophotometers, divided into two methods utilizing absorption or emission.

### (1) Utilizing Absorption

#### A. UV, visible and infrared spectrophotometers

When light passes through a substance, the light energy causes changes in the electronic state of the substance (electron transition) or induces characteristic vibration of the molecules, resulting in a loss of partial energy. This is referred to as absorption, and quantitative analysis can be performed by measuring the extent of absorption.

The principle and simplified block diagram<sup>1)</sup> of an absorption spectrophotometer are shown in Figure 9-2.

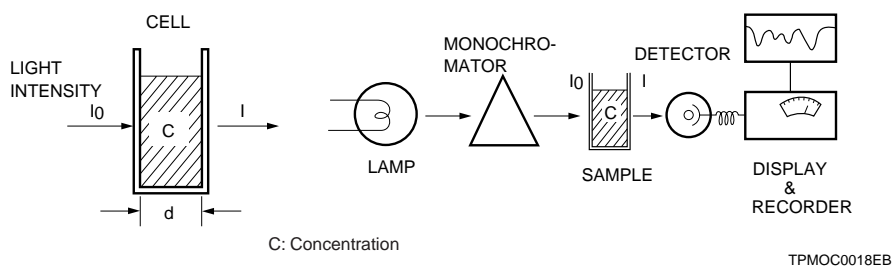


**Figure 9-2: Principle and block diagram of an absorption spectrophotometer**

There are various optical systems in use today for spectrophotometers. Figure 9-3 illustrates the optical system<sup>2)</sup> of a spectrophotometer using sequential plasma emission as the light source for covering from the ultraviolet to visible and infrared range.

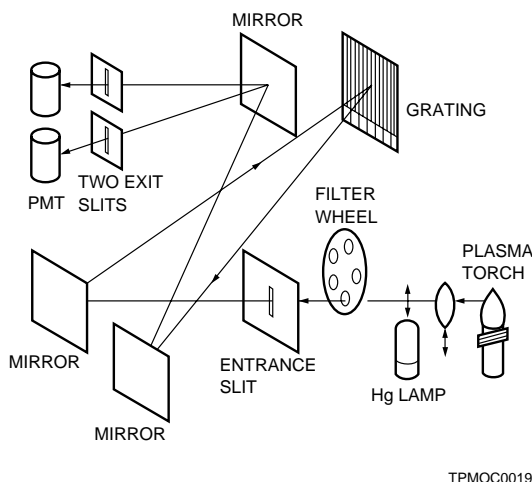


**Figure 9-3: Optical system of a UV to visible spectrophotometer**

## B. Atomic absorption spectrophotometers

The atomic absorption spectrophotometer employs special light sources (hollow cathode lamps) constructed for the respective elements to be analyzed. A sample is dissolved in solvent and burned for atomization, and light from the specific hollow cathode lamp is passed through the flame. The amount of light that is absorbed is proportional to the concentration of the sample material. Therefore, by comparing the extent of absorption between the sample to be analyzed and a standard sample measured in advance, it is possible to know the concentration of the specific element contained in the sample. A typical optical system<sup>3)</sup> used for atomic absorption spectrophotometers is shown in Figure 9-4.

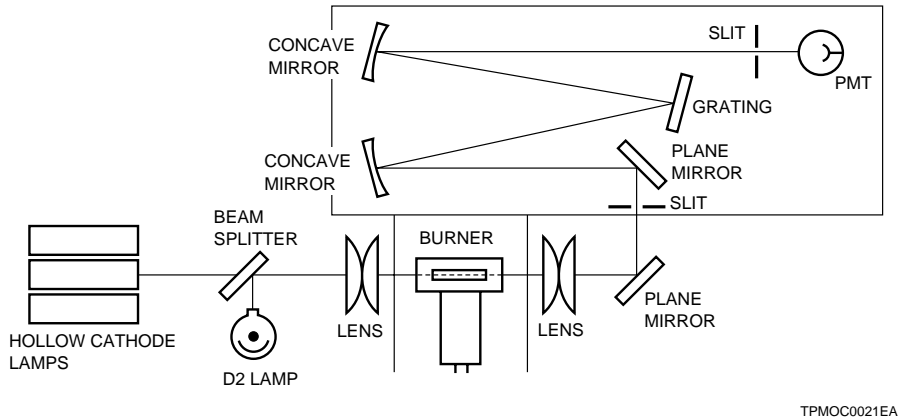


Figure 9-4: Optical system used for atomic absorption spectrophotometers

## (2) Utilizing Emission

### A. Photoelectric emission spectrophotometers (direct readers)

When external energy is applied to a sample, light emission occurs from the sample. Dispersing this emission using a monochromator, into characteristic spectral lines of elements and measuring their presence and intensity simultaneously, enables rapid qualitative and quantitative analysis of the elements contained in the sample. Figure 9-5 illustrates the block diagram<sup>4)</sup> of a photoelectric emission spectrophotometer in which multiple photomultiplier tubes are used.

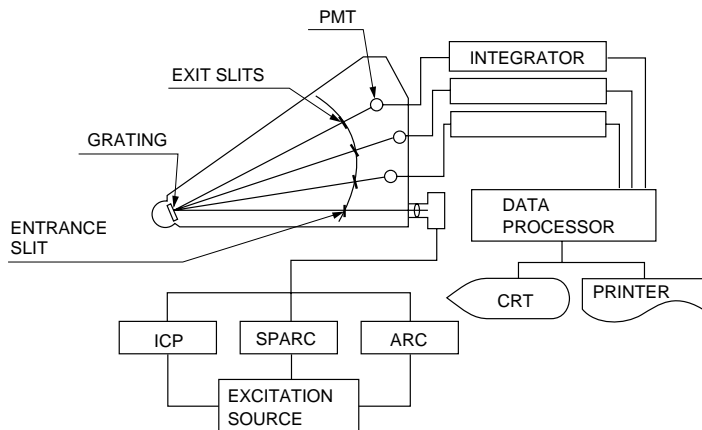
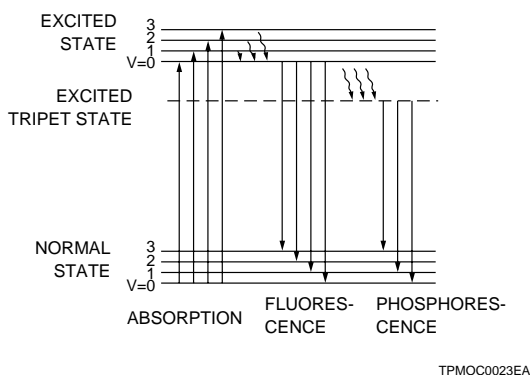


Figure 9-5: Block diagram illustrating a photoelectric emission spectrophotometer

## B. Fluorospectrophotometers

The fluorospectrophotometer is mainly used for chemical analysis in biochemistry, especially in molecular biology. When a substance is illuminated and excited by visible or ultraviolet light, it may emit light with a wavelength longer than that of the excitation light. This light emission is known as fluorescence and its emission process<sup>5)</sup> is shown in Figure 9-6. Measuring the fluorescent intensity and spectra allows quantitative and qualitative analysis of the elements contained in the substance.



**Figure 9-6: Fluorescent molecular energy levels**

Figure 9-7 shows the structure<sup>6)</sup> of a fluorospectrophotometer using photomultiplier tubes as the detectors. This instrument roughly consists of a light source, excitation monochromator, fluorescence monochromator and fluorescence detector. A xenon lamp is commonly used as the light source because it provides a continuous spectrum output over a wide spectral range. The excitation and fluorescence monochromators use the same diffraction grating or prism, as are used in general-purpose monochromators.

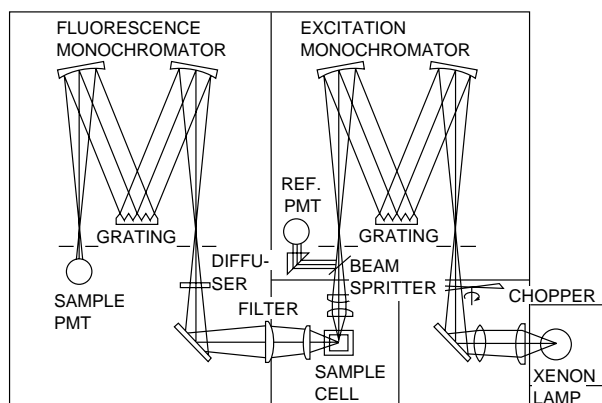


**Figure 9-7: Fluorospectrophotometer structure**

### 9. 1. 3 Characteristics required of photomultiplier tubes

The following photomultiplier tube characteristics are required in this application.

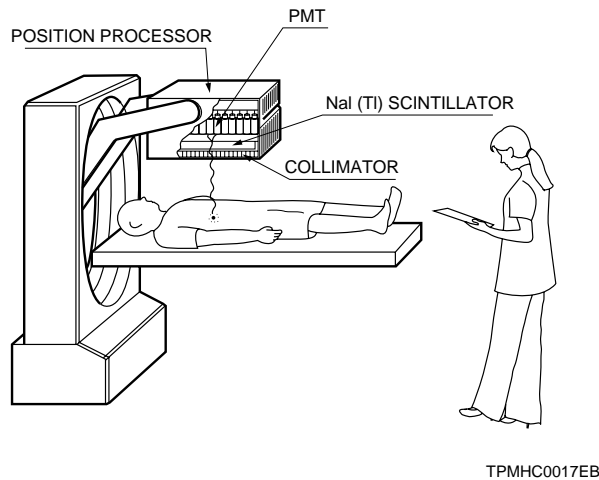
- a) High stability
- b) Low dark current
- c) High signal-to-noise ratio
- d) Wide spectral response (ultraviolet to infrared)
- e) Low hysteresis
- f) Excellent polarization properties

Side-on and head-on photomultiplier tubes having a multi-alkali photocathode and silica window are most frequently used in these applications.

## 9.2 Gamma Cameras

### 9.2.1 Overview

Imaging equipment utilizing a radioactive isotope (RI) first appeared as a scintillation scanner before undergoing successive improvements leading to the currently used gamma camera developed by Anger (U.S.A.). Recently, even more sophisticated equipment called SPECT (single photon emission computed tomography) utilizing the principle of the gamma camera, has been developed and is now coming into wide use. An external view of a gamma camera is shown in Figure 9-8.



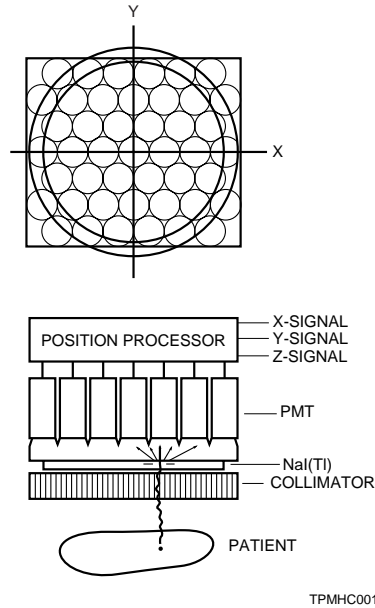
**Figure 9-8: External view of a gamma camera**

Figure 9-9 shows sectional views of a detector used in gamma cameras, in which dozens of photomultiplier tubes are installed in a honeycomb arrangement. Each photomultiplier tube is coupled, via a light-guide, to a large-diameter scintillator made from a thallium-activated sodium-iodide (NaI(Tl) scintillator), serving as a gamma-ray detector.

Three prime features of gamma cameras are:

1. High sensitivity
2. Broad, static field-of-view
3. High spatial resolution

These features lead to advantages such that rapid changes in the RI distribution can be measured and the length of diagnostic time shortened.

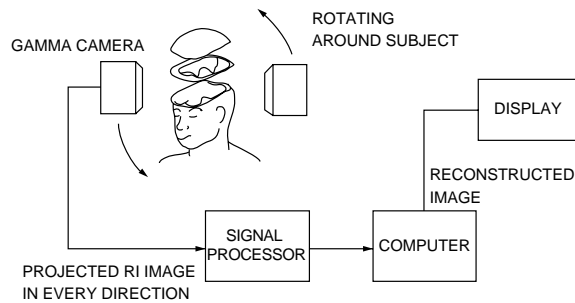


**Figure 9-9: Sectional views of a detector used in gamma cameras**

To make more effective use of these advantages, a variety of gamma-ray nuclide drugs have been developed for use with the gamma cameras. In addition, improvements in the position processing circuit have achieved higher resolution, making gamma cameras more popular in medical diagnosis. Major nuclides used for nuclear medical imaging are listed in Table 9-1 and the principle of SPECT equipment utilizing gamma cameras is shown in Figure 9-10.

Recently, a SPECT equipped with two or three camera heads is often used to improve sensitivity. Moreover, a PET-SPECT with two camera heads has now been developed which is capable of simultaneous counting of gamma-ray pairs released from a positron-emitting nuclide.

| Nuclide           | Gamma-ray energy (keV)           | Half-life |
|-------------------|----------------------------------|-----------|
| $^{99m}\text{Tc}$ | 141 (no $\beta$ )                | 6.01h     |
| $^{133}\text{Xe}$ | 81( $\beta$ :346)                | 5.243d    |
| $^{67}\text{Ga}$  | 93(37%), 185(20%), 300(17%)      | 78.3h     |
| $^{201}\text{Tl}$ | 70.8(Hg-X), 16.7(11%), 135(2.8%) | 72.91h    |
| $^{131}\text{I}$  | 364(81%)( $\beta$ :606)          | 8.04d     |
| $^{123}\text{I}$  | 159(83%)                         | 13.2h     |
| $^{81m}\text{Kr}$ | 190(67%)                         | 13s       |
| $^{111}\text{In}$ | 245(94%), 171(90%)               | 2.83d     |

**Table 9-1: Major nuclides used for nuclear medical imaging**

TPMHC0019EB

**Figure 9-10: Principle of SPECT**

### 9.2.2 Major characteristics required of photomultiplier tubes

The following characteristics are required particularly for photomultiplier tubes used in gamma cameras and SPECT equipment.

- a) High energy resolution or pulse height resolution (PHR)
- b) Excellent uniformity (especially azimuth uniformity; refer to Section 3.5.2)
- c) High stability
- d) Uniform RPH (relative pulse height) gain between each tube

Energy resolution is one of the most important characteristics required of photomultiplier tubes used in gamma cameras. As explained in (1) in 3-5-2, the photomultiplier tube photocathode must have a high quantum efficiency in the spectral range where NaI(Tl) scintillator emission occurs and high collection efficiency of photoelectrons onto the first dynode. Since these photomultiplier tube characteristics greatly affect the spatial resolution of gamma cameras, the use of photomultiplier tubes with good energy resolution usually improves the spatial resolution of gamma cameras. Photomultiplier tube uniformity also has an effect on the position linearity and uniformity which are computed by a gamma camera.

With the recent progress in digital technology using computers, it is becoming possible to correct the position linearity and uniformity of gamma cameras. Even so, these are still important characteristics for concern. The most important factor that affects gamma camera performance is photomultiplier tube stability. Because the position and energy information is obtained from the pulse height of photomultiplier tube output, if the output pulse height varies due to the amount of input gamma-rays or extended operating time, this may cause problems with output pulse height measurement. (Refer to Section 3.3.4, "Stability") Figure 9-11 shows typical long-term stability characteristics for the Hamamatsu R1306 photomultiplier tube specifically devel-

oped for gamma cameras.

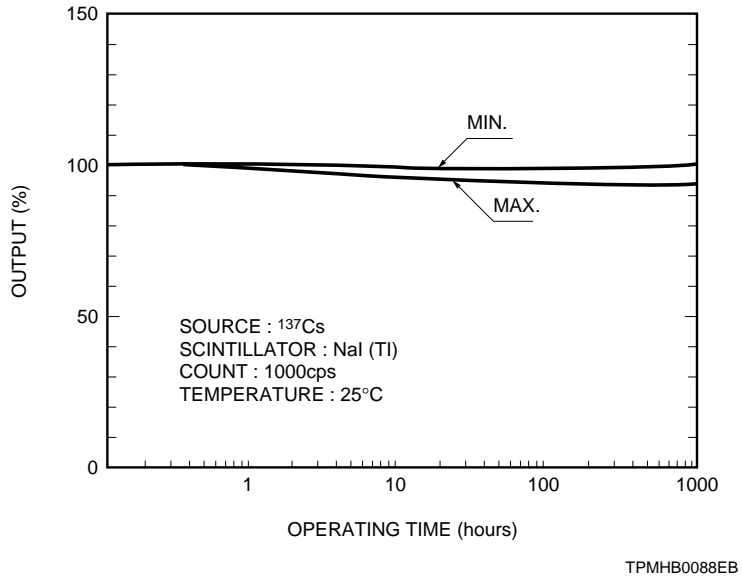


**Figure 9-11: Typical long-term stability of a photomultiplier tube**

## 9.3 Positron Emission Tomography (PET)

### 9.3.1 Overview

In addition to gamma cameras and SPECT described previously, much attention has recently been focused on positron emission tomography (PET) as an application of nuclear medical diagnosis using photomultiplier tubes. This section explains specific examples of PET. The schematic diagram<sup>7)</sup> of a PET system is illustrated in Figure 9-12, the external view in Figure 9-13, and the cutaway view of the detector section in Figure 9-14.

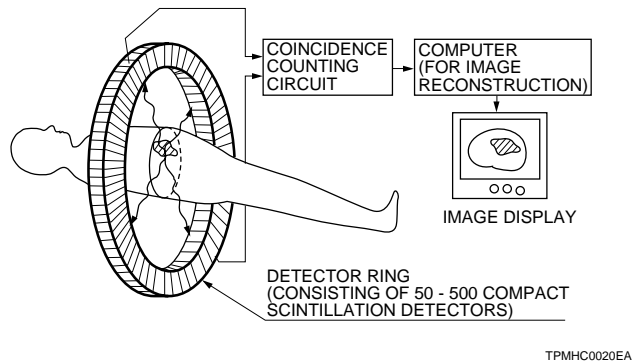


Figure 9-12: Concept view of a PET system



Figure 9-13: External view of a PET system

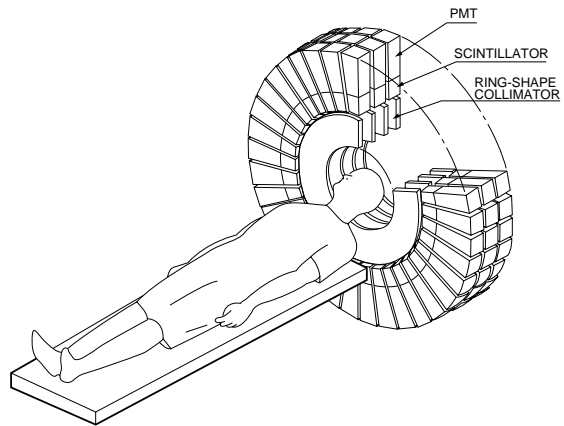


Figure 9-14: Cutaway view of a PET system

PET provides tomographic images of a living body in the active state, by injecting pharmaceuticals labeled with positron-emitting radioisotope into the body and measuring their concentrations. Typical positron-emitting radioisotopes used in PET are  $^{11}\text{C}$ ,  $^{13}\text{N}$ ,  $^{15}\text{O}$  and  $^{18}\text{F}$ .

When positrons are emitted within the body, they combine with the electrons in the neighboring tissues, releasing a pair of gamma-rays at 180 degrees opposite each other. Multiple rings of detectors surrounding the subject detect and measure these gamma rays by coincidence technique. The principle of this measurement is shown in Figure 9-15. By arranging the acquired transaxial data at each angle, the PET system then creates a tomographic image by image reconstruction technique in the same manner as used in X-ray computed tomography (X-ray CT).

A prime feature of PET is that quantitative measurement of physiological or biochemical information such as metabolism, blood flow and neural transmission within the body can be performed. Up until now, PET has been chiefly used in research and study on brain functions and other organ mechanisms. Recently, PET is gradually being put to active use in medical diagnosis, proving effective in diagnosing cardiac diseases and cancer.

A detector used in PET consists of a compact photomultiplier coupled to a scintillator. To efficiently detect gamma-rays of high energy (511keV) released from inside the body, scintillators with high stopping power versus gamma-rays, such as BGO crystals are commonly used.

Another type of measurement technique is now being studied, which utilizes TOF (time-of-flight) of gamma-rays generated by positron annihilation. This measurement uses high-speed photomultiplier tubes and scintillators with a short emission decay.

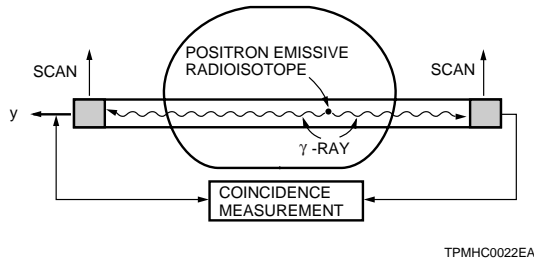


**Figure 9-15: Principles of PET measurement**

| Scintillator     | Density ( $\text{g}/\text{cm}^3$ ) | Relative Emission Intensity | Emission Time (ns) | Wavelength of Peak Emission (nm) |
|------------------|------------------------------------|-----------------------------|--------------------|----------------------------------|
| BaF <sub>2</sub> | 4.89                               | 5/26                        | 0.8/620            | 220/320                          |
| BGO              | 7.13                               | 20                          | 60/300             | 480                              |
| LSO              | 7.35                               | 72                          | 40                 | 420                              |
| GSO              | 6.71                               | 20                          | 60/600             | 430                              |
| NaI(Tl)          | 3.67                               | 100                         | 230                | 410                              |

**Table 9-2: Characteristics of major scintillators**

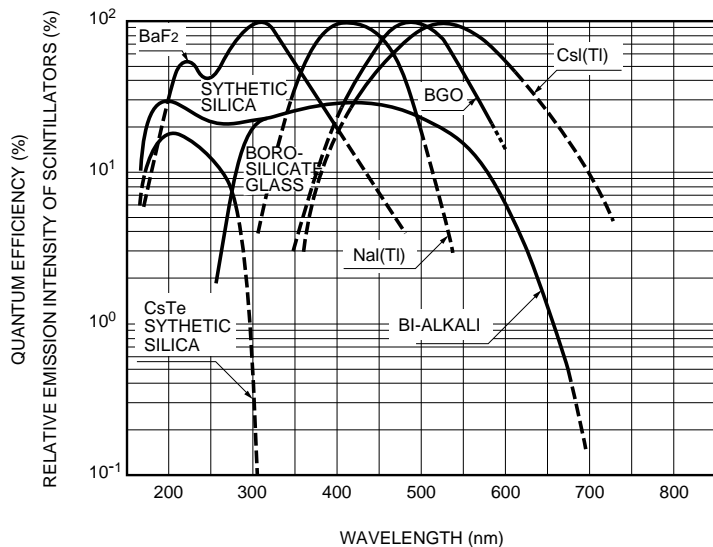
### 9.3.2 Major characteristics required of photomultiplier tubes

Photomultiplier tubes used in PET systems must have the following characteristics.

- a) High energy resolution or pulse height resolution (PHR)
- b) High gain and minimal variations between individual tubes
- c) Excellent CRT (coincidence resolving time)
- d) High level of stability
- e) Compact size

#### (1) Photomultiplier tubes coupled to BGO ( $\text{Bi}_4\text{Ge}_3\text{O}_{12}$ ) scintillators

This application requires high energy resolution of the photomultiplier tube. For this purpose, the photomultiplier tube must have high photocathode quantum efficiency at the emission wavelength (480 nanometers) of the BGO scintillator (See Figure 9-16), high secondary emission ratio ( $\delta$ ) of the first dynode and excellent photoelectron collection efficiency ( $\alpha$ ). Moreover, because many photomultiplier tubes are used at the same time in one system, it is also important that the photomultiplier tubes be compact and have adequate gain in order to improve position resolution.



TPMHB0089EA

**Figure 9-16: Scintillator emission spectra and photocathode spectral response of photomultiplier tubes**

Figure 9-17 shows a cutaway view of the structure of a low-profile photomultiplier tube (R5900-c8) recently developed for PET. This tube has a unique structure of cross plate anode intended to improve position resolution. Position is identified with this anode by calculating the center of gravity, making it compatible with small scintillator segments. Its compact configuration allows increasing the installation density of scintillators, thus reducing the dead space and leading to high sensitivity in PET.

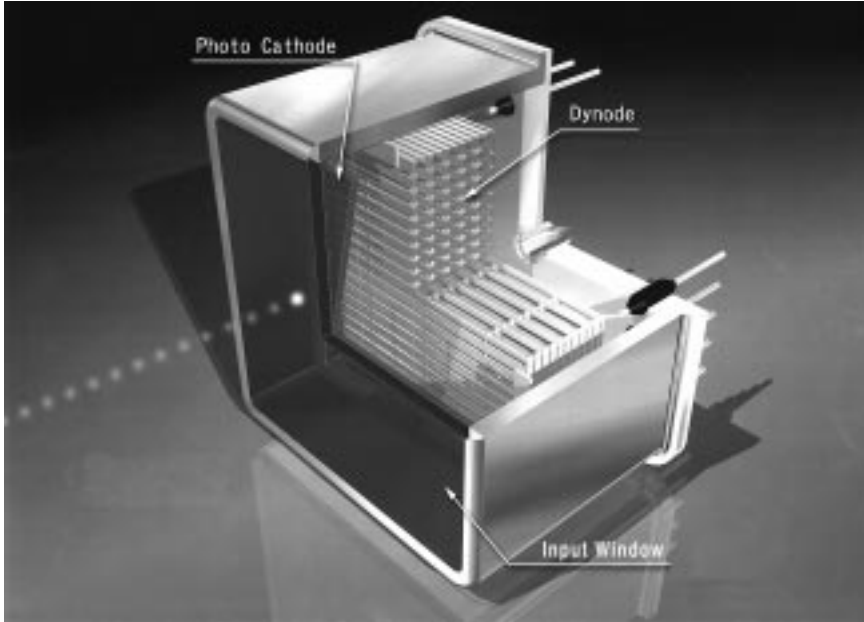
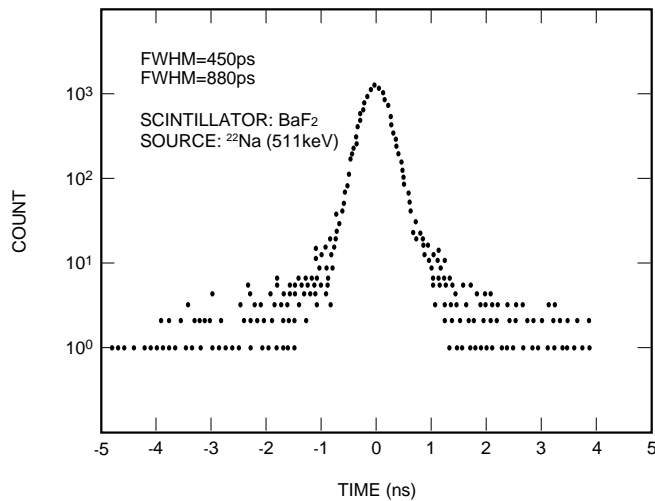


Figure 9-17: Cutaway view of R5900-c8 photomultiplier tube developed for positron CT

## (2) Photomultiplier tubes coupled to barium fluoride ( $\text{BaF}_2$ ) scintillators

Barium fluoride ( $\text{BaF}_2$ ) scintillators offer an extremely short emission decay compared to other scintillators and are used particularly for radiation detectors requiring high speeds. One application is positron imaging that utilizes TOF (time of flight) of gamma-rays. Photomultiplier tubes in this application should have characteristics equivalent to those used with BGO scintillators. In addition, the photocathode quantum efficiency must be high at the peak wavelength of fast emission components (220 nanometers) of  $\text{BaF}_2$  scintillators (see Figure 9-16) and the CRT (coincidence resolving time) as fast as possible. (See Figure 9-18 and 3.3.1, "Time characteristics".) Better CRT provides more accurate TOF information to acquire high-quality tomographic images, making it possible to perform dynamic studies. Another characteristic required of photomultiplier tubes is high gain.

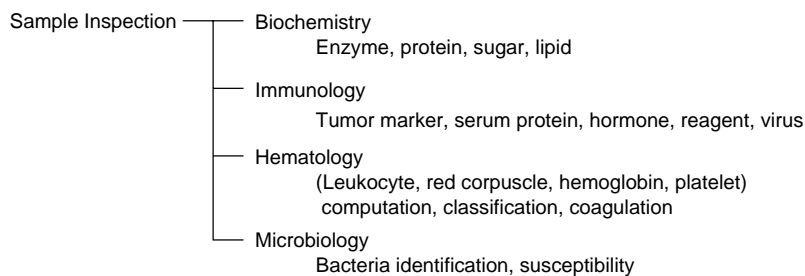


TPMHB0090EA

Figure 9-18: CRT spectrum of R2496 obtained at energy threshold of 140keV

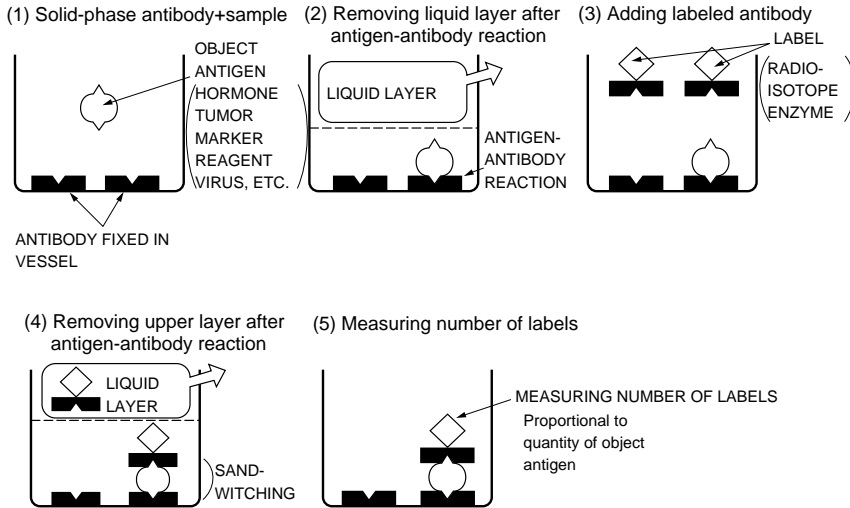
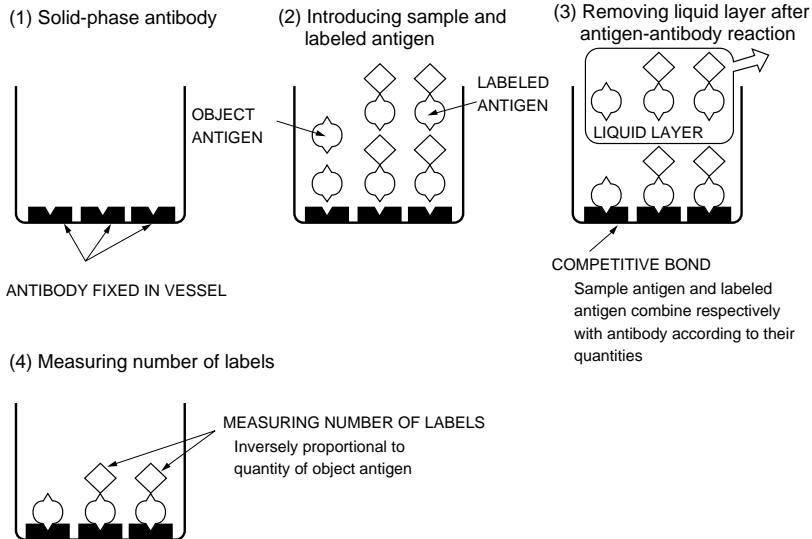
## 9.4 In-vitro Assay

The analysis and inspection of blood or urine samples collected out of a living body is referred to as in-vitro assay. It is used for physical checkups, diagnosis, and evaluation of drug potency. The in-vitro assay can be classified as shown in Table 9-3. Of these, the concentrations of most tumor markers, hormones, drugs and viruses which are classified under immunological assay are exceedingly low. This requires extremely high-sensitivity inspection equipment for frequently requiring use of photomultiplier tubes.



**Table 9-3: Classification of in-vitro inspection**

Immunoassay, a measurement technique making use of specificity of the antigen-antibody reaction, is widely used. The principles of immunoassay<sup>9)</sup> are illustrated in Figure 9-19 below, and the procedures of each method are explained in the subsequent paragraphs.

**(a) Sandwich Method****(b) Competitive Method**

TPMHC0023EA

**Figure 9-19: Principles of immunoassay**

Figure 9-19 (a) is a technique known as the sandwich method. Step (1): Samples are introduced into a vessel in which antibodies responding to object antigens (hormones, tumor markers, etc.) are fixed (solid-phase antibody). Step (2): Antigen-antibody reaction occurs, and each object antigen combines with a solid-phase antibody. This reaction has an extremely high singularity and hardly ever occurs with a different antigen. After antigen-antibody reaction, the liquid layer is removed leaving the combined antigen and antibody. Step (3): Labeled antibodies are added, which combine with object antigens. Step (4): Antigen-antibody reaction occurs again so that the object antigen is sandwiched between the antibodies. Then the liquid layer is removed. Step (5): The quantity of labels is optically measured using a photomultiplier tube.

Figure 9-19 (b) is another technique called the competitive method. Step (1): Antibodies responding to object antigens are fixed on the bottom of a vessel. Step (2): Samples are added along with the labeled object antigens. Step (3): Competitive reaction in which object antigens and labeled antigens combine with labeled antibodies in proportional to their concentration, reaching a state of equilibrium. After the antigen-antibody reaction, the unnecessary upper layer is removed. Step (4): The quantity of labels is measured using a photomultiplier tube. In the sandwich method, the higher the concentration of object antigens, the larger the signal. Conversely, in the competitive method, the higher the concentration of the object antigens, the lower the signal.

Immunoassay can be further categorized according to the material used for labeling as follows

- (1) Using radioactive isotopes for labeling  
(Radioimmunoassay)
- (2) Using enzymes for labeling  
(Enzymeimmunoassay)

### 9.4.1 RIA (Radioimmunoassay) method

#### (1) Overview

Radioactive isotope (RI) is used for the labeling as was explained above, and radiation (gamma or beta rays) emitting from the RI labels is detected by the combination of a scintillator and a photomultiplier tube, so that the object antigen can be quantitatively measured. Radioactive isotopes most frequently used for labeling are  $^3\text{H}$ ,  $^{14}\text{C}$ ,  $^{57}\text{Co}$ ,  $^{75}\text{Se}$ ,  $^{125}\text{I}$  and  $^{131}\text{I}$ . (See Table 9-4.)<sup>10)</sup> Of these,  $^{125}\text{I}$  offers useful characteristics for labeling and is very widely used. Because radioactive isotopes other than  $^3\text{H}$  and  $^{14}\text{C}$  emit gamma rays, sodium iodide crystals are used as a scintillator, providing a high conversion efficiency.

| Radioisotope     | Half-life   | Energy          | Detection Method      |
|------------------|-------------|-----------------|-----------------------|
| $^3\text{H}$     | 12.26 years | $\beta$         | Liquid scintillation  |
| $^{14}\text{C}$  | 5730 years  | $\beta$         | Liquid scintillation  |
| $^{57}\text{Co}$ | 270 days    | $\gamma$        | Scintillation crystal |
| $^{75}\text{Se}$ | 120.4 days  | $\gamma$        | Scintillation crystal |
| $^{125}\text{I}$ | 60 days     | $\gamma$        | Scintillation crystal |
| $^{137}\text{I}$ | 8 days      | $\beta, \gamma$ | Scintillation crystal |

**Table 9-4: Radioactive isotopes used for labeling in radioimmunoassay**

Recently, for in-vitro assays, the quantity of samples and the number of items to be measured are rapidly increasing. To meet this trend, the equipment for radioimmunoassay has been automated. A typical piece of automated equipment in use today is the well scintillation counter<sup>11)</sup> that makes use of sodium iodide scintillators having a well-like hole to enhance the conversion efficiency of the radiation into light. Measurements are made by automatically inserting test tubes, which contain a mixture of antigens and antibodies including labels, into each hole in the scintillator. (See Figure 9-20.) Each detector section including a scintillator is covered by lead shield to block extraneous radiation.

Isotopes  $^3\text{H}$  and  $^{14}\text{C}$  can be used for labeling; however, because they emit extremely low-energy beta rays, a liquid scintillation counter explained in Section 9.5, is used to make measurements with these two isotopes.

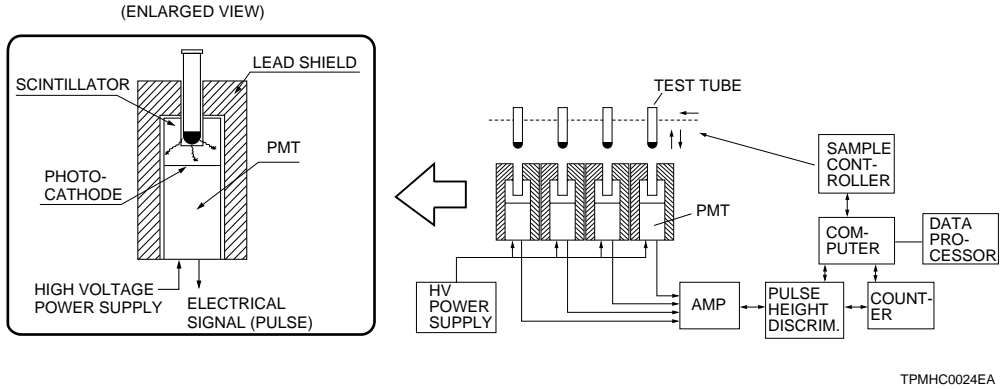


Figure 9-20: Schematic block diagram illustrating a well scintillation counter

## (2) Major characteristics required of photomultiplier tubes

Photomultiplier tubes used in RIA must have the following characteristics.

- a) High energy resolution or pulse height resolution (PHR)
- b) High level of stability
- c) Low noise

To obtain high energy resolution, the photomultiplier tube should have high quantum efficiency at the peak emission wavelength (410 nanometers) of the sodium iodide (NaI(Tl)) scintillator. (See Figure 9-16.) In addition, because this application field deals with quite a few samples that emit extremely small amounts of radiation, it is also very important that the photomultiplier tube exhibits sufficiently low noise.

## 9. 4. 2 EIA (Enzymeimmunoassay) method

### (1) Overview

An enzyme is used as a label utilizing the antigen-antibody reaction. As Figure 9-21<sup>12)</sup> shows, RIA offers exceptionally high sensitivity among various immunoassay techniques. However, because it uses radioactive isotopes, various restrictions are imposed on its use. On the other hand, though its sensitivity is inferior to RIA, EIA is more popular because of its easy use. EIA sensitivity is gradually increasing due to improvements in reagents and detection method.

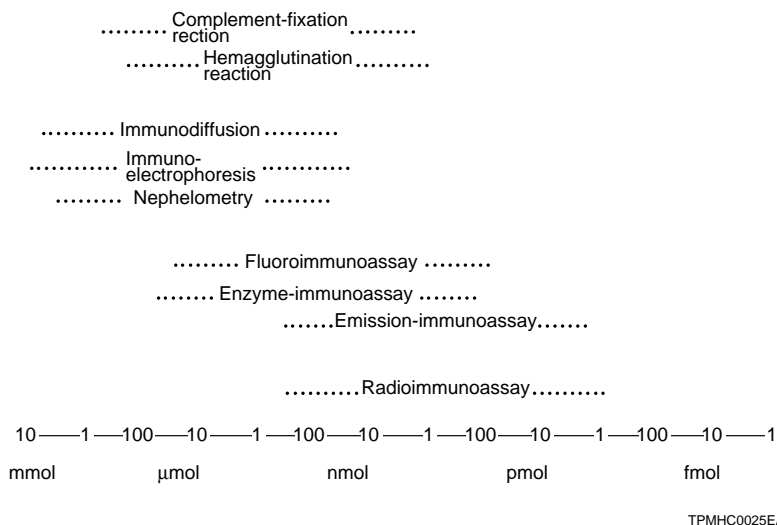
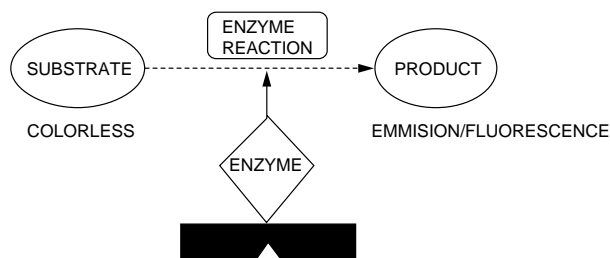


**Figure 9-21: Comparison of various immunoassay techniques and measurable concentration range (Use this comparison data just for a general guide.)**

In the EIA procedure, an enzyme used as a label in the antigen-antibody mixture in the last step in Figure 9-19 is activated to create a product. Then, color or fluorescence emitted from the product is detected by a photomultiplier tube. (See Figure 9-22.)<sup>13)</sup> The extent of color or fluorescent intensity is proportional to the quantity of enzyme (enzyme concentration).



TPMHC0026EA

**Figure 9-22: Label enzyme reaction**

## (2) Major characteristics required of photomultiplier tubes

- High sensitivity at the wavelength of color or fluorescence emitted from the product of the enzyme reaction
- Low dark current
- High signal-to-noise ratio
- Compact size

### 9. 4. 3 Other immunoassay methods

#### (1) Overview

Besides EIA, several non radioactive immunoassay techniques not using radioisotopes are under research and development.

One of these is fluoroimmunoassay in which a fluorescent substance is used for labeling. The final remaining mixture of antigens and antibodies is irradiated by an excitation light and the resulting fluorescence is measured with regard to the intensity, wavelength shift and polarization. This technique offers slightly higher sensitivity than that of EIA. Figure 9-23 shows the schematic of a fluorescence-polarization photometer,<sup>14)</sup> which is used for fluoroimmunoassay.

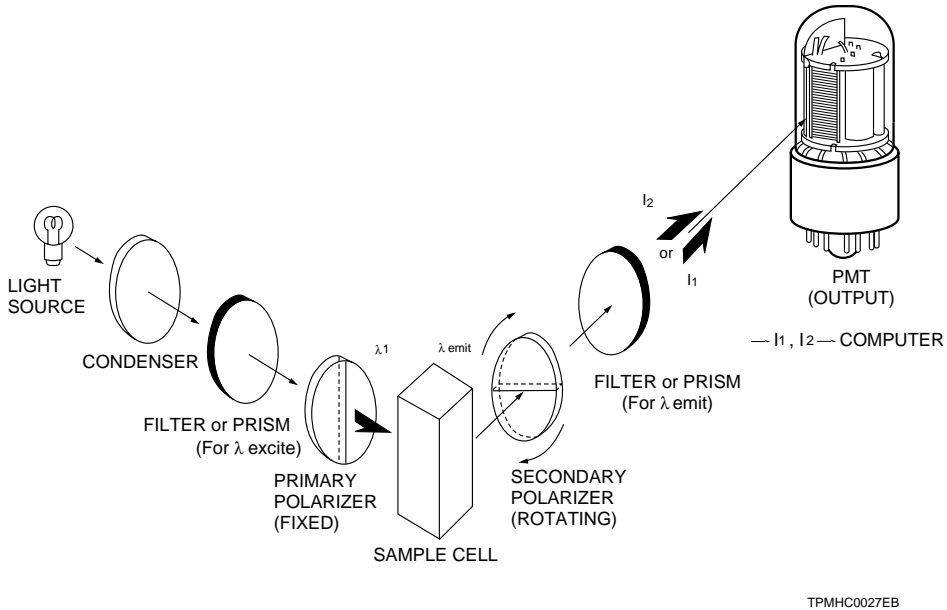


**Figure 9-23: Schematic presentation of a fluorescence-polarization photometer**

To achieve high sensitivity equal to RIA by using non-radioactive immunoassay, intensive research and development of emission-immunoassay has been carried out. This immunoassay uses a chemiluminous substance or bioluminescent substance for labeling and allows the final remaining mixture of antigens and antibodies to emit light, which is detected by a photomultiplier tube. There are three types of emission-immunoassay methods, as follows:

- 1) Use of a chemiluminous substance such as luminol and acridinium for labeling
- 2) Use of chemiluminescence or bioluminescence for activation of the label enzyme used in EIA
- 3) Use of a catalyst for the bioluminescence reaction

Methods 2) and 3) can be thought of as kinds of EIA techniques. As shown in Figure 9-21 previously, emission-immunoassay is a high sensitivity equivalent to RIA.

---

**(2) Major characteristics required of photomultiplier tubes****Fluoroimmunoassay**

- a) High sensitivity at fluorescent wavelengths
- b) High level of stability
- c) Low dark current
- d) High signal-to-noise ratio
- e) Compact size

**Emission-immunoassay**

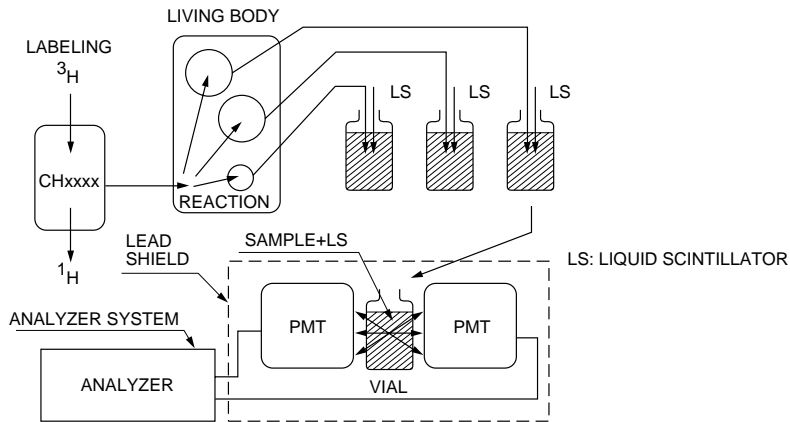
- a) High sensitivity at emission wavelengths
- b) Excellent single-photoelectron pulse height distribution
- c) Low dark current pulse
- d) High gain
- e) Compact size

## 9.5 Liquid Scintillation Counting Systems

### 9.5.1 Overview

Among the various radiation detecting methods, the liquid scintillation counting system is primarily used for detection of alpha and beta rays. This is because this system provides higher sensitivity to alpha and beta rays compared to other methods and also offers low background, enabling highly accurate measurement. Photomultiplier tubes are essential for detecting exceptionally low level light resulting from low-energy alpha and beta rays.

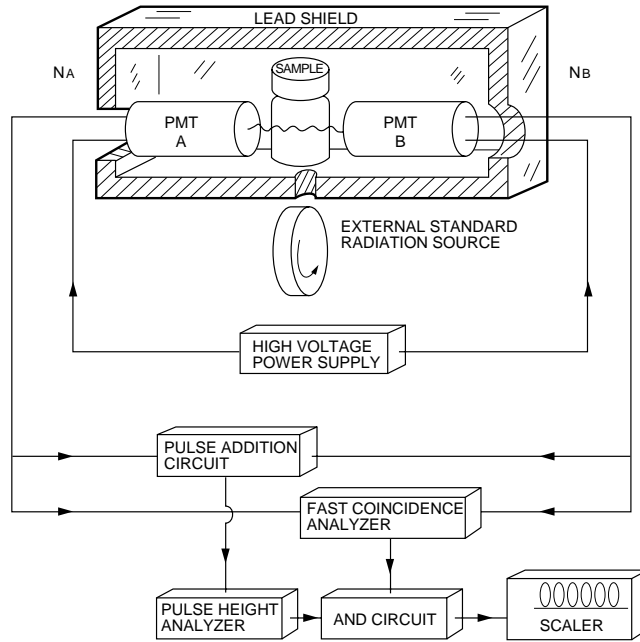
Liquid scintillation counting systems are used in diverse applications. One of their major applications is in tracer analysis using radioactive isotopes such as  $^3\text{H}$  and  $^{14}\text{C}$  as a label, which is referred to in Section 9.4.1, "RIA (Radioimmunoassay)". This tracer analysis is effectively used for diagnosis of biofunctions and diseases. The schematic block diagram of a liquid scintillation counting system is shown in Figure 9-24.



TPMHC0028EA

**Figure 9-24: Schematic construction of the tracer analysis (liquid scintillation counting system)**

There are many other applications of liquid scintillation counting, including Cherenkov radiation detection, age measurement and rock analysis. Beta energy released from  $^3\text{H}$  or  $^{14}\text{C}$  is very low and, moreover, the corresponding emission from the liquid scintillator is also extremely low in comparison with those from crystal scintillators. For this reason, photomultiplier tube background noise has a large influence on the measurement accuracy. A coincidence counting circuit is used to eliminate this background noise. As Figure 9-25<sup>15)</sup> shows, the coincident outputs from a pair of photomultiplier tubes are counted as a signal from the sample. Because the possibility that noise from individual photomultiplier tubes will simultaneously enter the coincidence counting circuit is extremely low, the signal can be separated from the noise with a high degree of accuracy.



TPMHC0029EB

Figure 9-25: Basic construction of a liquid scintillation counting system

### 9.5.2 Major characteristics required of photomultiplier tubes

The following photomultiplier tube characteristics are important in liquid scintillation counting systems.

- a) Low thermionic emission noise
- b) Low scintillation of the faceplate or side bulb of a photomultiplier tube
- c) High-speed time response
- d) High quantum efficiency
- e) Excellent linearity
- f) High gain

Liquid scintillation counting places even more stringent demands on photomultiplier tube characteristics in comparison with other applications. For instance, item b) above, is not so severe in other applications but is extremely important for liquid scintillation counting as it determines the system performance. As shown in Figure 9-25, the pulse counting technique known as the coincidence counting is effectively used to reduce noise to as low a level as 15cpm (counts per minute). Even so, if glass scintillation occurs and a resulting noise of several cpm is generated, the signal-to-noise ratio will significantly deteriorate. Therefore, glass bulbs causing minimum scintillation are selected. Because such scintillation from the glass is mainly caused by radioisotope elements contained in the glass, these glass bulbs must contain very small amounts of such elements. For this purpose, silica glass bulbs which basically contain no impurities are often used.

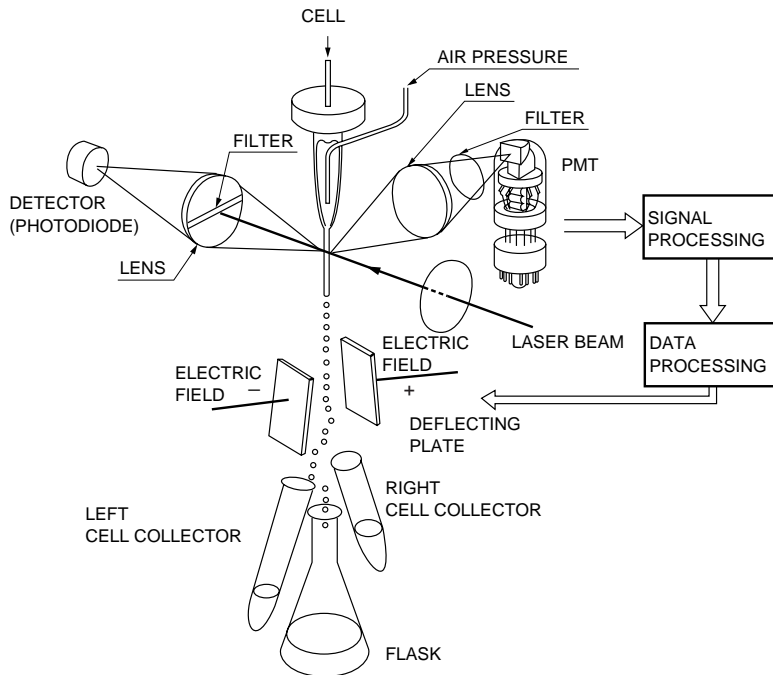
## 9.6 Biotechnology

In life science applications, photomultiplier tubes are mainly used for detection of fluorescence and scattered light. Major equipment used for life science includes cell sorters, fluorometers and DNA sequencers.

### 9.6.1 Overview

#### (1) Cell sorters

When light is irradiated onto a rapidly flowing solution which contains cells or chromosomes, a scattered light or fluorescence is released from the cells or chromosomes. By analyzing this scattered light or fluorescence, it is possible to elucidate cell properties and structures and separate the cells based on these properties. This field is known as flow cytometry. A cell sorter like the one illustrated in Figure 9-26 is most frequently used. The cell sorter is an instrument that selects and collects only specific cells labeled by a fluorescent substance from a mixture of cells in a solution.



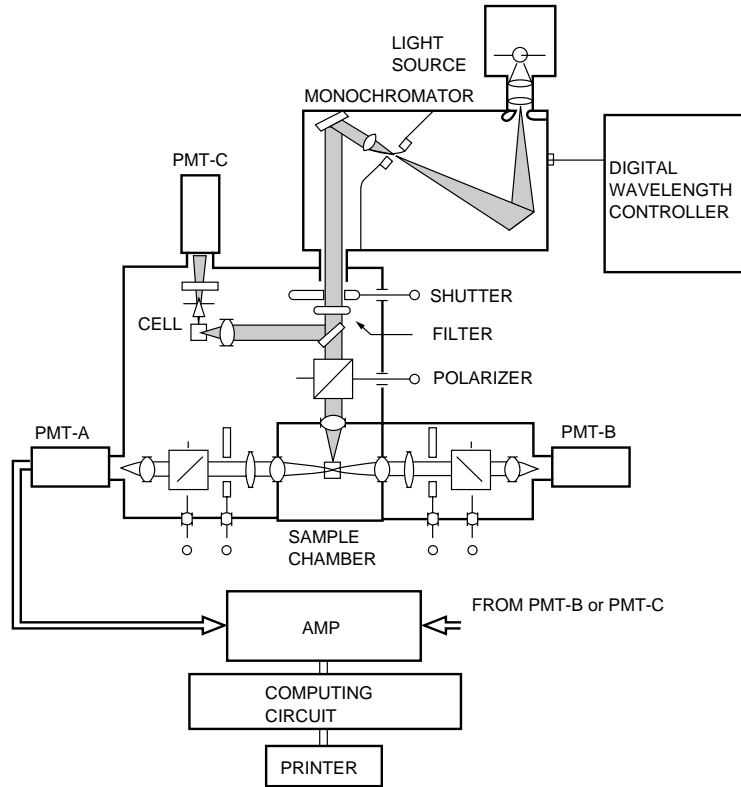
TPMOC0025EA

**Figure 9-26: Major components for a cell sorter**

In a cell sorter, a fluorescent probe is first attached to the cells. The cells pass through a thin tube at a fixed velocity. When each cell passes through a small area onto which an intense laser beam is focused, the fluorescence is emitted from the cell and is detected by a photomultiplier tube. The photomultiplier tube outputs an electrical signal in proportion to the number of fluorescent molecules attached to each cell. At the same time, the laser beam light is scattered forward by the cell, and detecting this scattered light gives information on the cell volume. After processing these two signals, the cell sorter creates an electrical pulse that deflects a drop of liquid, containing the desired cell into one of the collection tubes.

## (2) Fluorometers

While the ultimate purpose of the cell sorter explained above is to separate cells, the fluorometer<sup>16)</sup> is used to analyze cells and chemical substances by measuring the fluorescence or scattered light from a cell or chromosome with regard to such factors as the fluorescence spectrum, fluorescence quantum efficiency, fluorescence anisotropy (polarization) and fluorescence lifetime. (See Figure 9-27.)



TPMOC0026EA

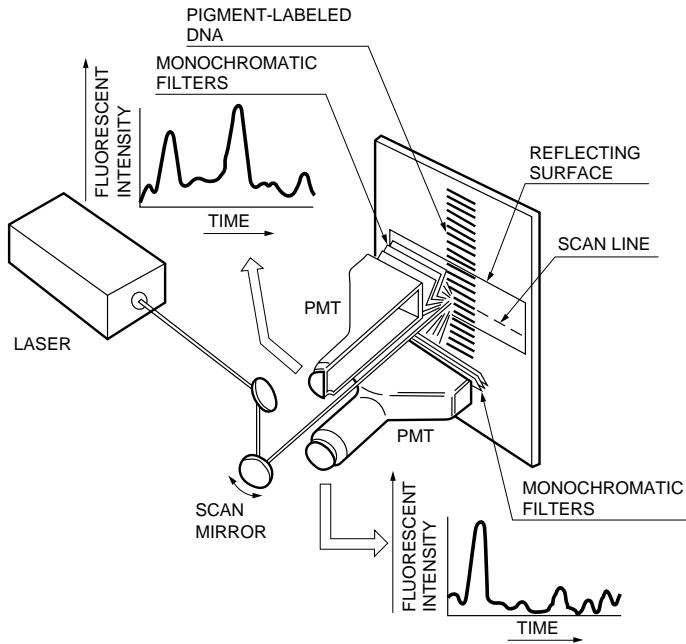
**Figure 9-27: Automatic fluorescence-depolarization photometer**

The basic configuration of the fluorometer is nearly identical with that of the fluorospectrophotometer and thus a description is omitted here. There are a variety of models of fluorometers which are roughly categorized into: filtering fluorescence photometers, spectrofluorescence photometers, compensated-spectrofluorescence photometers, fluoroanisotropy analyzers, and phase fluorescence lifetime measurement systems. Of these, the fluoroanisotropy analyzer is an instrument specially dedicated to measurement of fluorescence-depolarization.

When performing research on biological samples such as proteins, nucleic acid and lipid membranes, rotational relaxation of a fluorescent molecule takes place only slowly and the fluorescence is polarized in most cases. It is still necessary to compensate for the effect of fluorescence depolarization when measuring quantum efficiency and spectrum. For this purpose, the automatic fluorescence-depolarization photometer uses a pair of photomultiplier tubes which detect the two polarized components at the same time.

### (3) DNA sequencers

This is an instrument used to decode the base arrangement of DNA extracted from a cell. The principle of a DNA sequencer is shown in Figure 9-28. An extracted DNA segment is injected onto gel electrophoresis plate along with a fluorescent label which combines with the DNA. When an electric potential is applied across the gel, the DNA begins to migrate and separate based on size and charge. When the DNA segment reaches the position of the scanning line, it is excited by a laser, causing only the portion with the labeling pigment to give off fluorescence. This fluorescent light is passed through monochromatic filters and detected by photomultiplier tubes. Computer-processing of the position at which the fluorescence has occurred gives information on where the specific bases are located. The DNA sequencer is used for the genetic study of living organisms, research into the cause and treatment of genetic diseases and decoding of human genes.



TPMOC0027EA

Figure 9-28 Principle of a DNA sequencer

## 9. 6. 2 Major characteristics required of photomultiplier tubes

Because the photomultiplier tube detects very-low fluorescence emitted from a cell or DNA, the following characteristics are required as in the case of spectrophotometry.

- a) High stability
- b) Low dark current
- c) High signal-to-noise ratio
- d) Wide spectral response
- e) Low hysteresis
- f) Excellent polarization properties

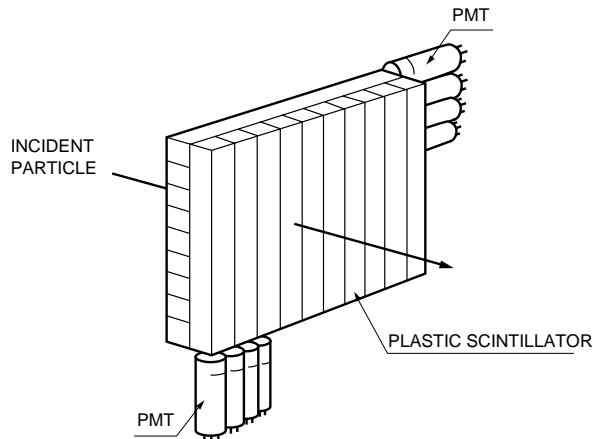
## 9.7 High-Energy Physics Experiments

Photomultiplier tubes are widely used as detectors in high-energy physics experiments. For example, when a charged particle passes through a scintillator, a light flash is given off in accordance with the particle energy. Detecting this light flash makes it possible to measure the energy, speed and direction of the charged particle. This technique is absolutely essential in high-energy physics research which is constantly aiming for the ultimate in scientific technology.

### 9.7.1 Overview

Photomultiplier tubes are used in a variety of equipment for high-energy particle detection such as a hodoscopes, TOF (time of flight) counters, Cherenkov counters and calorimeters. Photomultiplier tubes are also used in proton decay and neutrino detection where a great number of large-diameter tubes are required.

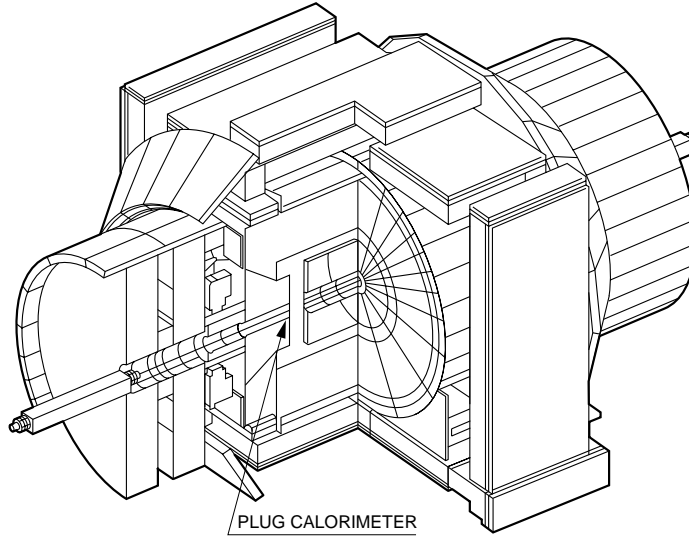
Figure 9-29 shows a simplified diagram<sup>17)</sup> of a hodoscope. Plastic scintillators are arrayed in two orthogonal layers followed by photomultiplier tubes. The position and time at which a charged particle passes through certain scintillators are detected by the corresponding photomultiplier tubes.



TPMHC0030EA

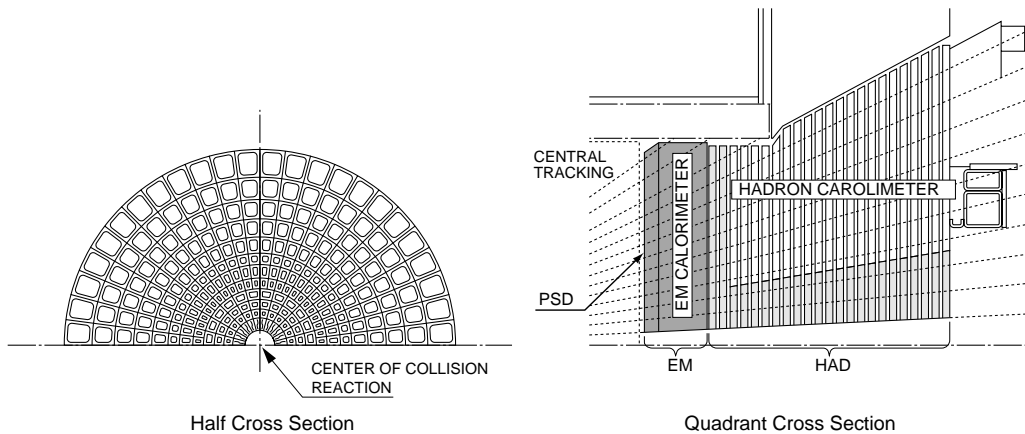
**Figure 9-29: Simplified diagram of a hodoscope**

Figure 9-30 illustrates a cutaway view of a CDF detector installed in a high energy accelerator. The CDF detector is used to measure the amount of photons, electrons and other elementary particles ( $\pi$  mesons, etc.) which are created by collision of protons and positrons.



**Figure 9-30: Cutaway view of a CDF detector**

Figure 9-31 shows end views of a calorimeter with three detecting layers designed for different targets to be measured. From the inner position near the collision reaction point, a PSD (Preshower detector for identifying photons and pi mesons), an EM (Electromagnetic calorimeter for measuring the energy of photons) and a HAD (Hadronic calorimeter for measuring the energy of  $\pi$  mesons) are radially installed. Among these, a detailed view of the PSD is shown Figure 9-32. When a particle beam passes through the scintillators, a series of scintillations are produced and detected by the respective photomultiplier tubes.



**Figure 9-31: End view of a calorimeter**

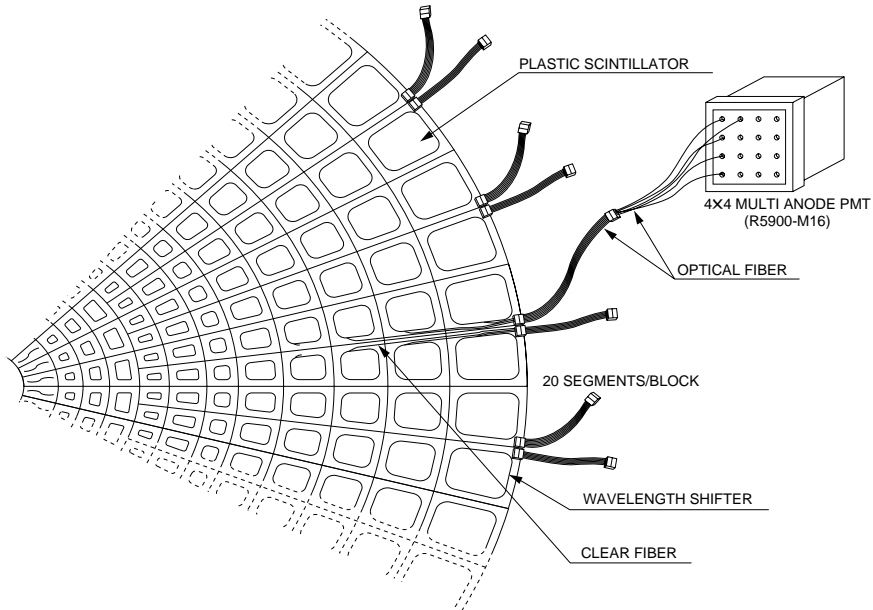


**Figure 9-32: Layout of a PSD (Preshower detector)**

In the PSD, photons detected with each of a 20-segmented plastic scintillator are guided to optical fibers by way of wavelength-shifting fibers and then collected into each channel of a multianode photomultiplier tube (R5900-M16). Since the PSD handles a great deal of signals up to a total of 960 channels, multianode photomultiplier tubes play an important role in reducing the cost per channel.

Figure 9-33 shows a schematic view of proton decay experiment presently being performed in Kamioka, Japan. Here, a 50,000-ton tank of super-purified water has been surrounded by more than ten-thousand, 20-inch diameter, hemispherical photomultiplier tubes. The photomultiplier tubes are used to constantly detect Cherenkov radiation that is supposedly emitted when proton decay occurs in water. In this experiment, neutrinos released from the sun or a supernova as it bursts have been successively detected.

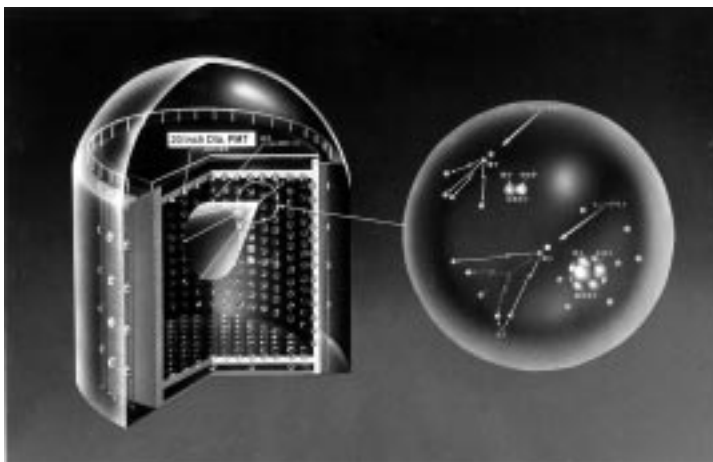


**Figure 9-33: Proton decay experiment SUPER-KAMIOKANDE, Japan**

### 9.7.2 Major characteristics required of photomultiplier tubes

The following characteristics are required of photomultiplier tubes used in the vicinity of an accelerator.

- a) High energy resolution or pulse height resolution (PHR)
- b) Good pulse linearity
- c) Excellent time characteristics
- d) High magnetic immunity
- e) Long life and high stability

For photomultiplier tubes used in proton decay and neutrino detection, the following characteristics are essential.

- f) Large diameter (wide effective field-of-view)
- g) Low noise

To obtain high energy resolution, it is important that the photomultiplier tube must have high absolute sensitivity in the emission wavelength range of the scintillator to be used. Moreover, because a wide range of light levels need to be measured at the same time in high-energy physics experiments, pulse linearity characteristics are also important. (Refer to Section 3.3.2, "Linearity" and Section 7.1.3, "Divider current and output linearity".)

In TOF counters in which the traveling time of a particle is measured, time characteristics are very important factors to consider. (Refer to Section 3.3.1, "Timing properties".) In general, photomultiplier tubes using a linear-focused dynode structure are frequently used in TOF counters because of superior time characteristics as compared to photomultiplier tubes using other dynodes.

When photomultiplier tubes are used in the vicinity of an accelerator, their magnetic characteristics are significant because stray magnetic fields may be generated there. As discussed in the section on magnetic characteristics, photomultiplier tubes using fine-mesh dynodes display high immunity to magnetic fields, thus making them suitable for use in environments where magnetic fields are present.

In proton decay and neutrino detection, because the frequency of signal occurrence is very low, exceptionally low noise qualities are required of photomultiplier tubes. Furthermore, each photomultiplier tube should cover a wide detection area, so large-diameter tubes with a wide field-of-view are required. Hemispherical photomultiplier tubes with a large diameter from 5, 8, 15 up to 20 inches are available from Hamamatsu Photonics.

Cherenkov radiation provides higher intensity at short wavelengths, thus photomultiplier tubes used for this application must have high ultraviolet sensitivity. Also, since Cherenkov radiation is very low, a photon counting technique is usually used.

## 9.8 Oil Well Logging

### 9.8.1 Overview

Special photomultiplier tubes capable of operating reliably in harsh environments including high temperature and severe vibration and shock have been developed. This section explains oil well exploration (oil well logging) as a sample application of these special tubes.

To locate an oil deposit and to determine its size, oil well logging is used. This technique makes use of photomultiplier tubes as detectors for density well logging using radiation, neutron well logging and natural gamma-ray-spectrum well logging. In these well loggings, a probe containing a neutron or gamma ray source is lowered into a well as it is being drilled. The radiation or the neutrons that are scattered by the rock surrounding the well are detected by a scintillator/photomultiplier. The amount of scattered radiation detected is indicative of the density of the rock that surrounds the well. The scattered neutrons indicate the porosity of the rock which is required to ascertain if the oil can be removed. Naturally occurring gamma rays are detected to locate shale which indicates the presence of oil or gas. Figure 9-34 shows the measurement method<sup>18)</sup> for oil well logging using radiation, and Figure 9-35 shows the cross sectional view<sup>19)</sup> of the strata layers around an oil well site.

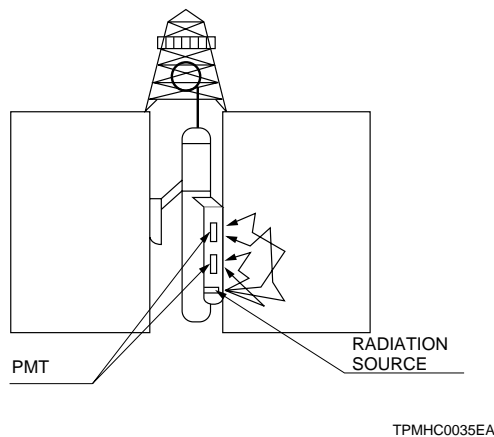


**Figure 9-34: Measurement method for oil well logging using radiation**

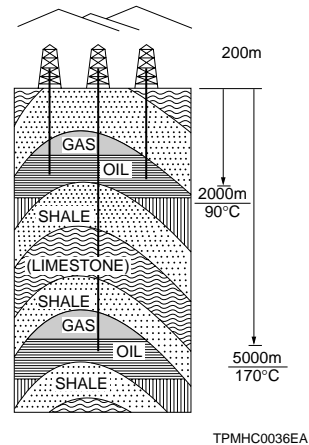


**Figure 9-35: Cross sectional view of strata layers around an oil well**

### 9.8.2 Major characteristics required of photomultiplier tubes

The depth of a trial hole may be as deep as several thousand meters where the ambient temperature reaches as high as 150 to 200°C. In addition, shock and vibration are also applied to the photomultiplier tubes, imposing an extremely severe environment on the photomultiplier tubes. Normal photomultiplier tubes cannot survive under these conditions and therefore custom-designed photomultiplier tubes are required.

To meet these requirements, various types of ruggedized, high-temperature photomultiplier tubes have been developed which ensure adequate performance even under these severe environments. These photomultiplier tubes have a special photocathode that exhibits a minimal increase in dark current even at high temperatures and, in the multiplier section, copper-beryllium (Cu-Be) dynodes capable of withstanding high temperatures are employed. Furthermore, the electrode structures are designed with careful consideration given to the effects of thermal expansion and vibration.

As typical characteristics, gain and energy resolution (pulse height resolution)<sup>20)</sup> with respect to temperature are plotted in Figure 9-36 and plateau characteristics<sup>21)</sup> at different temperatures are shown in Figure 9-37. Also, typical stability data<sup>22)</sup> of anode output current at different temperatures is shown in Figure 9-38.

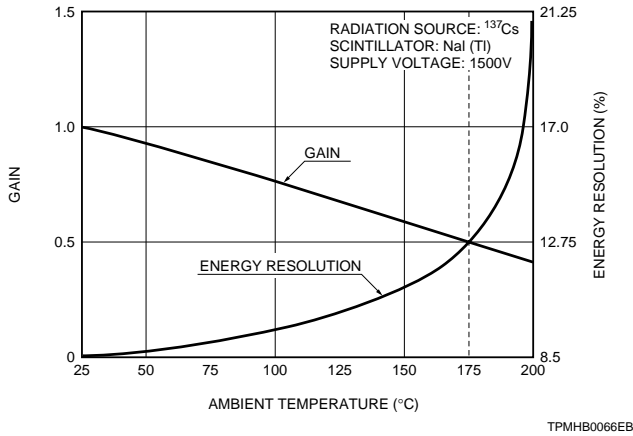


Figure 9-36: Gain and energy resolution vs. temperature

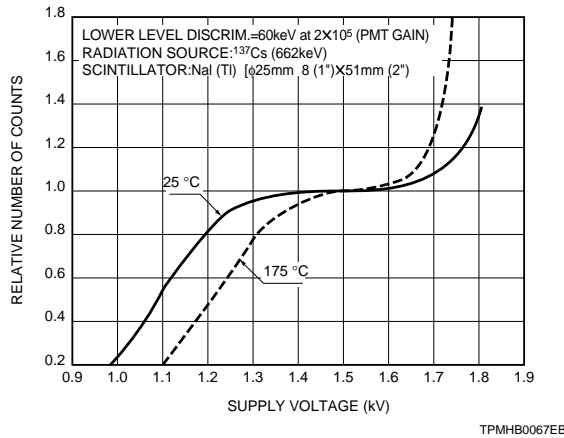


Figure 9-37: Plateau characteristics at different temperatures

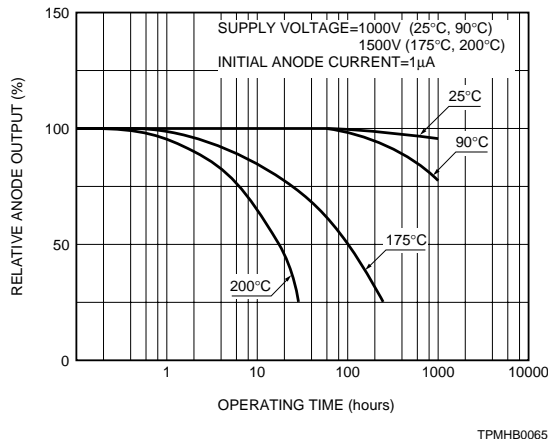


Figure 9-38: Anode current stability at different temperatures

## 9.9 Mass Spectrometry/Solid Surface Analysis

Mass spectrometry is a technique used to identify and analyze the mass, makeup and minute quantity of a sample through the measurement of the difference in mass and movement of ions by exerting electric or magnetic energy on the sample which is ionized.

Solid state surface analysis is used to examine the surface state of a sample through the measurement of photoelectrons, secondary electrons, reflected electrons, transmitting electrons, Auger electrons or X-rays which are generated as a result of interactions of incident electrons with atoms composing the sample, which take place when an electron beam or X-ray irradiates the sample.

### 9.9.1 Mass spectrometers

#### (1) Overview<sup>23) 24)</sup>

Mass spectrometers are broadly classified into two groups: one using magnetic force (magnet) and one not using magnetic force. Currently used mass spectrometers fall under one of the following four types.

- Time of flight (TOF) type
- Quadrupole (Q-Pole) or ion trap type
- Magnetic field type
- Ion cyclotron (FTICR) type

Among these, the quadrupole (Q-Pole) type mass spectrometer is most widely used and its block diagram is shown in Figure 9-39.

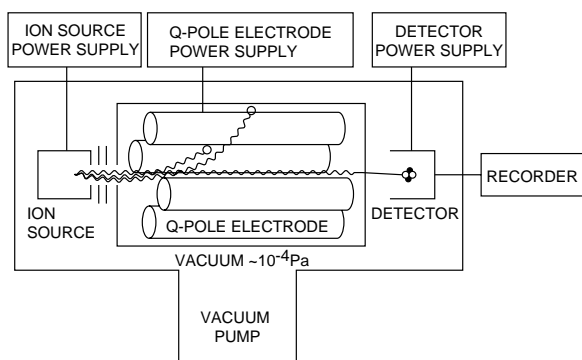
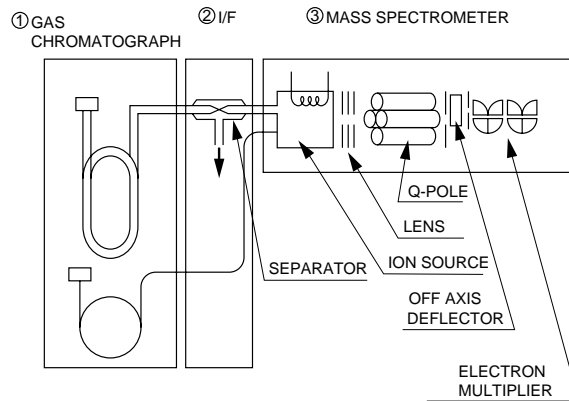


**Figure 9-39: Block diagram of a quadrupole (Q-Pole) type mass spectrometer**

When a sample is guided into the ionizer, it is ionized through the electronic ionization (EI method), chemical ionization (CI method), fast atomic bombardment (FAB method), electro-spray ionization (ESI method) or atmospheric pressure chemical ionization (APCI method). The ionized sample is sent to the analyzer section (quadrupolar electrodes) in which the sample is separated depending on the mass per charge count ( $m/z$ ) by the DC voltage and high-frequency voltage applied to the quadrupolar electrodes. After passing through the analyzer section, the ions then reach the detector section where they are detected by an electron multiplier tube.

Mass spectrometers are often combined with a gas chromatograph or liquid chromatograph to build a gas chromatograph mass spectrometer (GC-MS) or liquid chromatograph mass spectrometer (LC-MS). Mass spectrometers are used to identify, measure and analyze the composition of various samples such as petrochemicals, fragrance materials, medicines, biogenic components and substances causing environmental pollution. Figure 9-40 shows the schematic drawing of a gas chromatograph mass spectrometer.



TEM0020EA

**Figure 9-40: Schematic drawing of a gas chromatograph mass spectrometer.**

## (2) Major characteristics required of electron multiplier tubes

Since the mass spectrometer measures and analyzes the sample in minute amounts, electron multiplier tubes should have the following characteristics.

- a) High gain
- b) Low noise
- c) Long operating life

## 9.9.2 Solid surface analyzers

### (1) Overview<sup>25)</sup>

Solid surface analyzers are broadly divided into two groups: one using electron beams to irradiate a sample and the other using X-rays. Major solid surface analyzers presently used are as follows.

- Scanning electron microscope (SEM)
- Transmission electron microscope (TEM)
- Auger electron spectrometer (AES)
- Electron spectrometer for chemical analysis (ESCA)

When a sample is irradiated by electron beams, interactions of the incident electrons with atoms which compose the sample occur and generate various kinds of signals characterized by the particular atom. Figure 9-41 shows the kinds of signals obtained and the approximate depth at which each signal is generated on the surface of the sample.

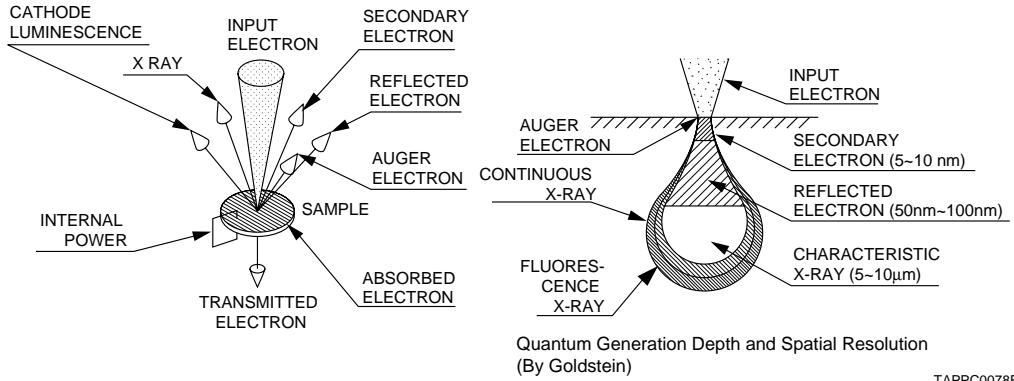


**Figure 9-41: Interactions of incident electrons with sample**

Obtained signals are chosen to extract necessary information according to measurement purpose, which is then used for analyzing the surface of the sample.

Among the four types of surface analyzers, the scanning electron microscope (SEM) is the most widely used and its structure and principle are illustrated in Figure 9-42.<sup>26)</sup>

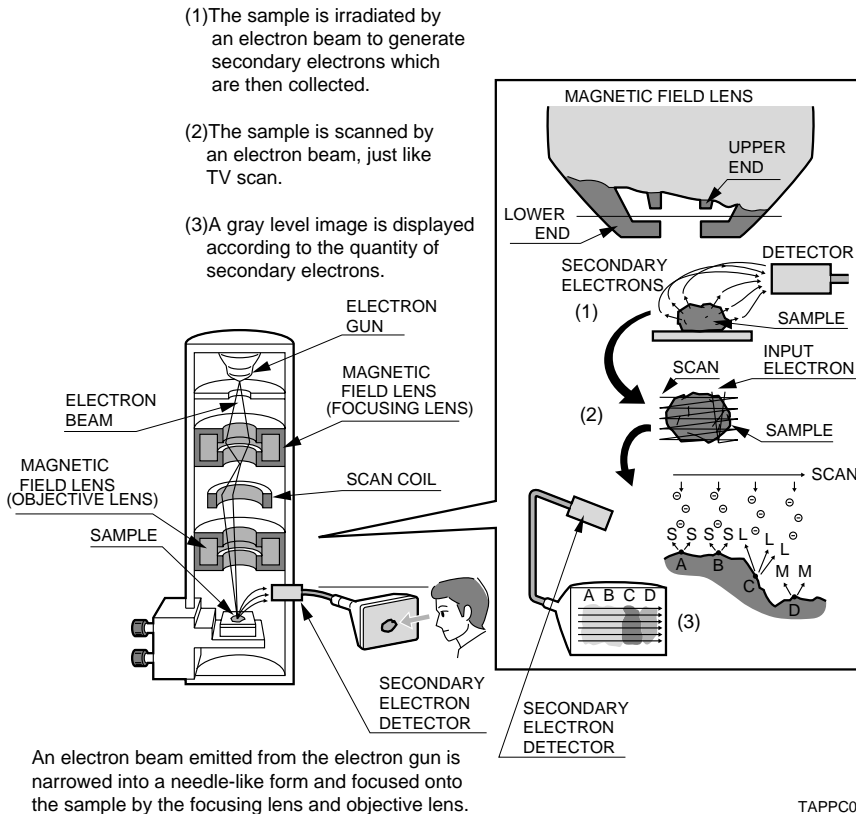
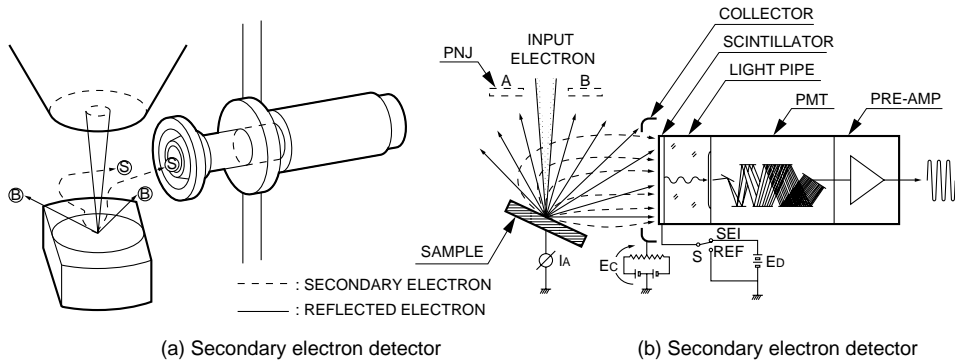


**Figure 9-42: Structure and principle of a scanning electron microscope**

An electron beam emitted from the electron gun is accelerated at a voltage of 0.5 to 30kV. This accelerated electron beam is then condensed by electromagnetic lens action of the focusing lens and objective lens, and finally formed into a very narrow beam of 3 to 100nm in diameter, irradiating on the surface of a sample. Secondary electrons are then produced from the surface of the sample where the electron beam landed, and detected with a secondary electron detector. The electron beam can be scanned in the XY directions across the predetermined area on the surface of the sample by scanning the electromagnetic lens. A magnified image can be displayed on the CRT in synchronization with the signals of the secondary electron detector. Figure 9-43 shows the structure and operation of the secondary electron detector.



TAPPC0080EA

**Figure 9-43: Structure and operation of a secondary electron detector**

A typical secondary electron detector consists of a collector electrode, scintillator, light pipe, photomultiplier tube and preamplifier. Voltage is applied to the collector electrode and scintillator at a level required to collect secondary electrons efficiently. Most of the secondary electrons produced from the sample enter the scintillator and are converted into light. This converted light then passes through the light pipe and is detected with the photomultiplier tube. Figure 9-44 shows the images of a broken surface of ceramic, observed with a scanning electron microscope.<sup>27)</sup>

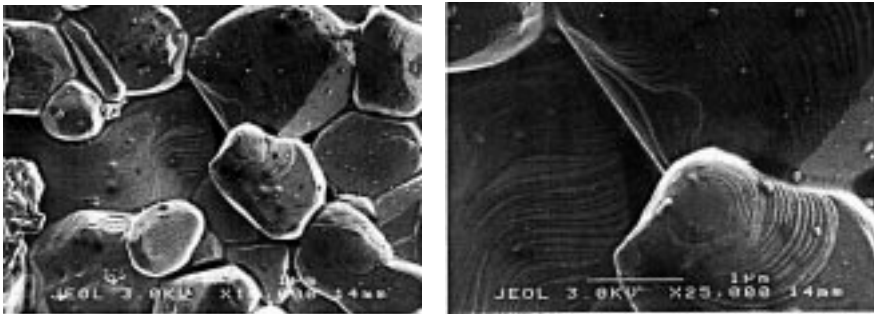


**Figure 9-44: Photographs of broken ceramic material taken with a scanning electron microscope**

## (2) Major characteristics required of photomultiplier tubes

To detect low level light emitted from the scintillator, photomultiplier tubes must have the following characteristics.

- a) High stability
- b) Low dark current
- c) High quantum efficiency

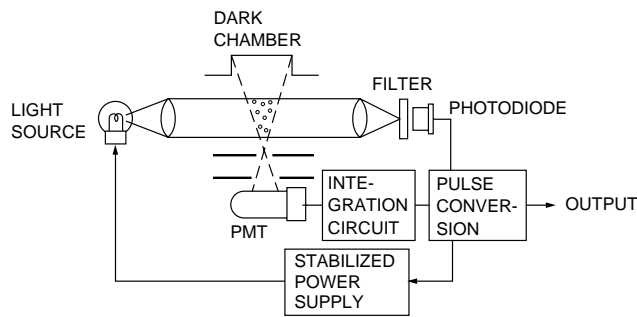
## 9.10 Environmental Measurement

Photomultiplier tubes are also used as detectors in environmental measurement equipment, for example, in dust counters used to detect dust contained in air or liquids, and radiation survey monitors used in nuclear power plants. This section explains some of these applications.

### 9.10.1 Dust counters

#### (1) Overview

A dust counter measures the concentration of floating dust in the atmosphere or inside a room by making use of principles such as light scattering and absorption of beta rays. Figure 9-45<sup>28)</sup> shows the principle of a dust counter using light scattering. If dust is present in the light path, light is scattered by the dust. The quantity of this scattered light is proportional to the quantity of dust. The scattered light is detected by a photomultiplier tube and after being integrated, the output signal is converted into a pulse signal, which then corresponds to the mass concentration. This method offers an advantage that the output signal can immediately follow changes in the concentration, making it suitable for continuous operation to monitor the change over time. However, this method has a disadvantage in that even if the mass concentration is constant, the quantity of scattered light varies with such factors as particle shape and the refractive index.



TPMSC0002EA

**Figure 9-45: Block diagram of a dust counter using light scattering**

Another dust counter makes use of the absorption of beta rays which is proportional to the mass of a substance through which the beta rays are transmitted. A filter paper is used to collect the dust, and the difference in the amount of beta-ray absorption before and after collecting the dust are compared to determine the mass.

#### (2) Major characteristics required of photomultiplier tubes

Since dust counters measure low levels of light, the following characteristics are required of photomultiplier tubes.

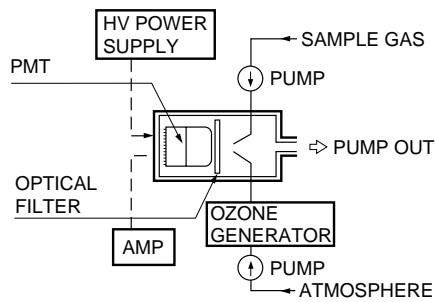
- a) Less spike noise
- b) High quantum efficiency
- c) High gain

## 9.10.2 NOx analyzers

### (1) Overview

These instruments are used to measure nitrogen oxide (NOx), an air-polluting gas contained in exhaust gases from automobiles and other internal combustion engines. NOx is a general term indicating nitrogen monoxide (NO) and nitrogen dioxide (NO<sub>2</sub>) and, in many countries, the concentration of NOx is limited by air pollution regulations so that it shall not exceed a certain level.

Figure 9-46 shows the configuration of an NOx analyzer making use of chemiluminescence.<sup>29)</sup> When NO gas reacts with ozone (O<sub>3</sub>) to become NO<sub>2</sub> gas, chemiluminescence is released. The intensity of this chemiluminescence is proportional to the concentration of NOx. Since other gases contained in the exhaust gas do not produce such luminescence, the NOx concentration can be selectively measured by detecting the intensity of this chemiluminescence.



TPMOC0028EA

Figure 9-46: NOx analyzer utilizing chemiluminescence

### (2) Major characteristics required of photomultiplier tubes

The following characteristics are required because this chemiluminescence increases at 600 nanometers and extends into the infrared region.

- a) High quantum efficiency in the infrared region
- b) Low noise

### 9.10.3 Turbidimeters

#### (1) Overview

When floating particles are contained in a liquid, light incident on the liquid is absorbed, scattered or refracted by these particles. It looks cloudy or hazy to the human eye. To express the clarity of such liquid, the term "turbidity" is used. A turbidimeter is a device that numerically measures the turbidity by using light transmission or scattering. There are various methods as explained below:

- |                             |                                       |
|-----------------------------|---------------------------------------|
| 1) Transmitted-light method | a) Transmitted-light method           |
|                             | b) Transmitted/scattered-light method |
| 2) Scattered-light method   | a) Forward scattered-light method     |
|                             | b) Backward scattered-light method    |
|                             | c) Surface scattered-light method     |

The principles of the surface scattered-light method<sup>30)</sup> and the transmitted/scattered-light method<sup>31)</sup> are shown in Figures 9-47 and 9-48, respectively. Either method uses a photomultiplier tube as the photodetector. In the surface scattered-light method, a light beam illuminates the surface of the liquid and the intensity of the light scattered from near the surface is measured. This method facilitates a wide range of measurement points by changing the position at which the light beam is incident. Since the light beam directly strikes the liquid surface, there will be less measurement errors which may otherwise be caused by reflective objects such as a window. However, errors may occur when measuring a colored liquid. The transmitted/scattered-light method measures the ratio between the transmitted and scattered light. No error occurs even when measuring a colored liquid, but dirt or stains on the window may affect the measurement accuracy.

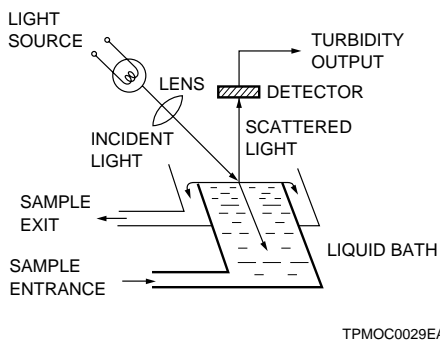


Figure 9-47: Turbidimeter using the surface scattered-light method

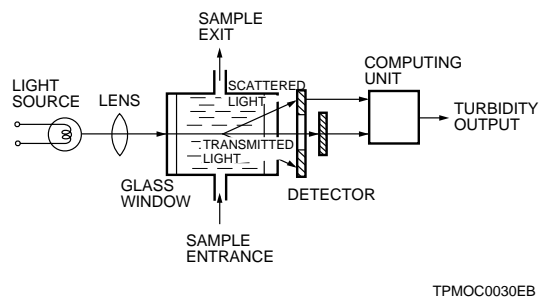


Figure 9-48: Turbidimeter using the transmitted/scattered-light method

#### (2) Major characteristics required of photomultiplier tubes

Photomultiplier tubes used for turbidimeters must provide the following factors.

- Low noise
- High quantum efficiency
- High gain

## 9.10.4 Door monitors

### (1) Overview

As the name implies, the door monitor is installed near the exit door in the monitored area of a nuclear power plant, in order to check the personnel going out of this area for contamination by radioactive material. A photomultiplier tube is used in conjunction with a scintillator to detect radiation released from the radioactive material. An example<sup>32)</sup> of a door monitor is shown in Figure 9-49. The detector section consists of an array of scintillators coupled to photomultiplier tubes, enabling simultaneous measurement of the location and extent of contamination. Since the number of signals to be detected is usually very low, a coincidence counting circuit is used as in the case of scintillation counting to minimize erroneous signal counting.

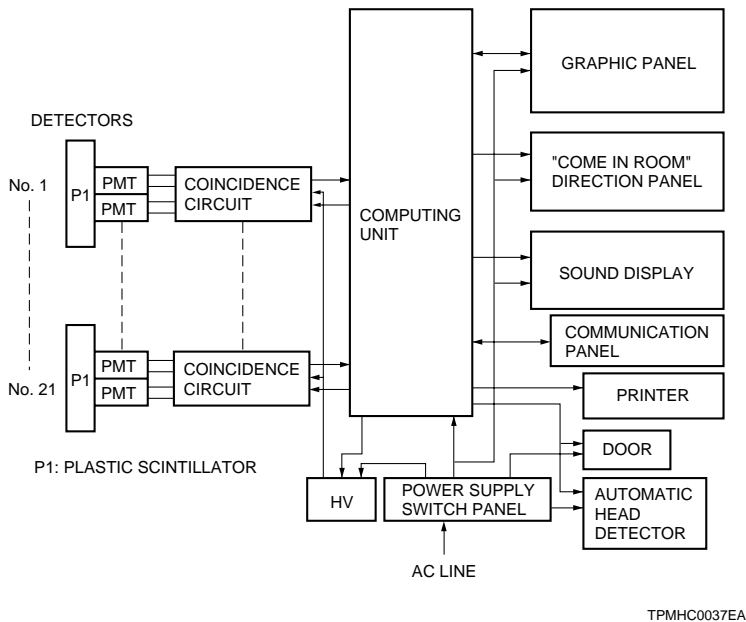


Figure 9-49: Block diagram of a door monitor

### (2) Major characteristics required of photomultiplier tubes

Because the number of signals to be detected is very low and, further, the amount of light detected by one photomultiplier tube is small, the following characteristics are required of each photomultiplier tube:

- a) High quantum efficiency
- b) Low noise
- c) High energy resolution or pulse height resolution (PHR)
- d) High gain

## 9.11 Applications to Laser Measurement

Recently, lasers are being applied to a wide range of measurement and processing applications owing to their superior advantages such as spatial or temporal coherency and high optical power.

Applications utilizing lasers can be classified as follows:

**1) Measurement**

Range finder, laser radar, holography, laser chemistry, medical measurement

**2) Data processing**

Optical communications, optical data processing

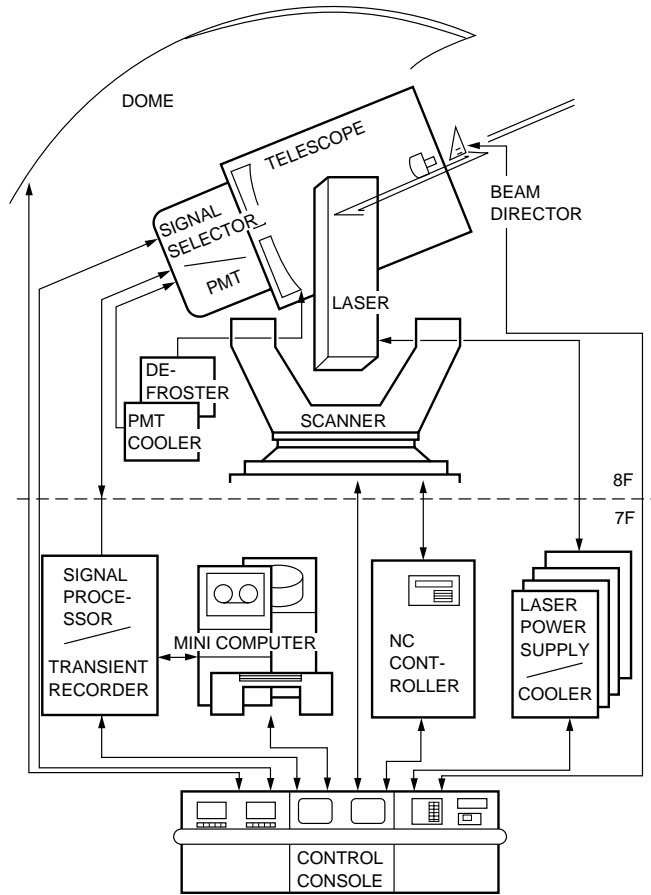
**3) Energy sources**

Laser processing, laser fusion, laser scalpel

This section explains typical applications of photomultiplier tubes used in laser measurements and major characteristics required.

### 9.11.1 Overview

Laser measurement applications using photomultiplier tubes include laser radars for rangefinding and atmospheric observation and laser spectroscopy such as fluorescence lifetime measurement. For signal processing in these measurements, the photon counting mode is widely used rather than analog mode, in order to improve the signal-to-noise ratio and enhance the detection limit. Furthermore, time correlated photon counting (TCPC) technique is employed in picosecond measurements such as fluorescence lifetime determination. Figure 9-50 illustrates the block diagram of a laser radar used for atmospheric observation,<sup>33)</sup> installed at the National Environmental Pollution Laboratory, Tsukuba, Japan.



TPMOC0031EA

Figure 9-50: Schematic construction of a laser radar for atmospheric observation

### 9.11.2 Major characteristics required of photomultiplier tubes

The following photomultiplier tube characteristics are essential in this field.

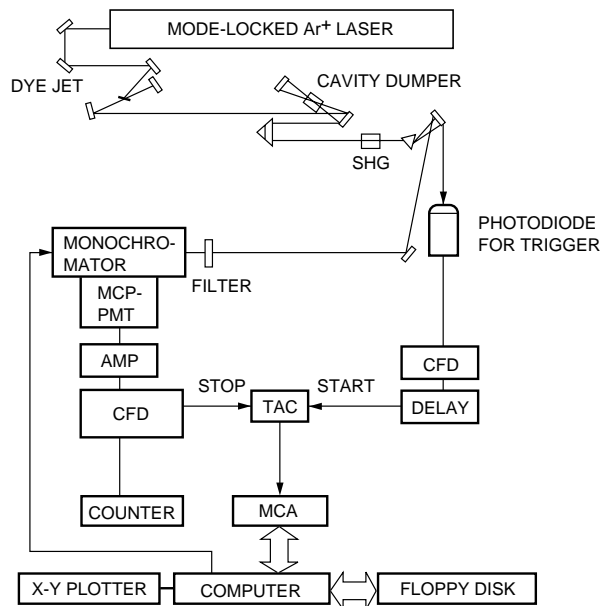
- a) Fast time response
- b) Low noise
- c) High gain

Of these, time response is the most important factor. With the development of laser technology, photomultiplier tubes with faster time response are in greater demand. In particular, electron transit time spread (TTS) is important for picosecond resolution in measuring fluorescence lifetime.

The TTS (transit time spread) is greatly affected by CTTD (cathode transit time difference) and wavelength effects (Refer to Section 3.3.1, "Time characteristics".) These effects sometimes cause significant problems in normal photomultiplier tubes using discrete dynodes, but create very few problems with an MCP-PMT. Normally, noise should be as low as possible to achieve a high signal-to-noise ratio and especially, the dark count must be small.

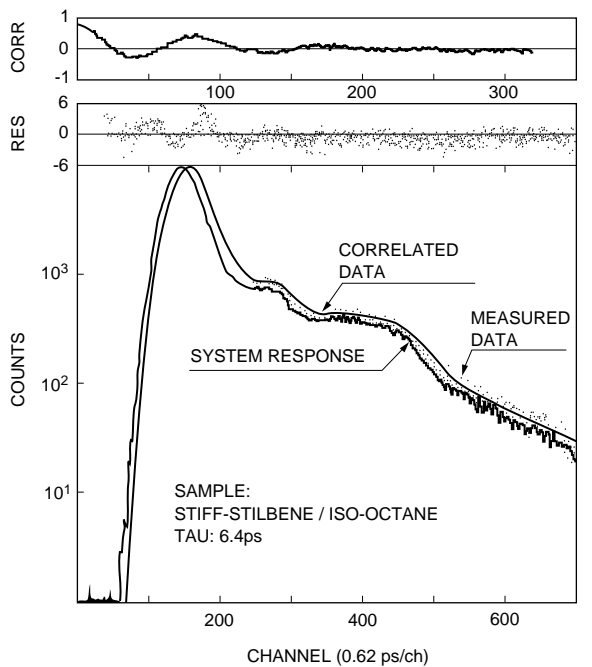
The gain should be high enough to obtain a good pulse height distribution in single photon events, in other words, a distinct valley should exist in the single-photoelectron pulse height distribution. Typically, gain of  $5 \times 10^6$  is necessary.

Figures 9-51<sup>34)</sup> and 9-52<sup>35)</sup> show a system setup for fluorescence lifetime measurement and typical results that were measured. The photomultiplier tube used for this measurement is a high-speed MCP-PMT (Hamamatsu R3809U).



TPMHC0038EA

Figure 9-51: TCPC system for fluorescence lifetime measurement



TPMHB0091EA

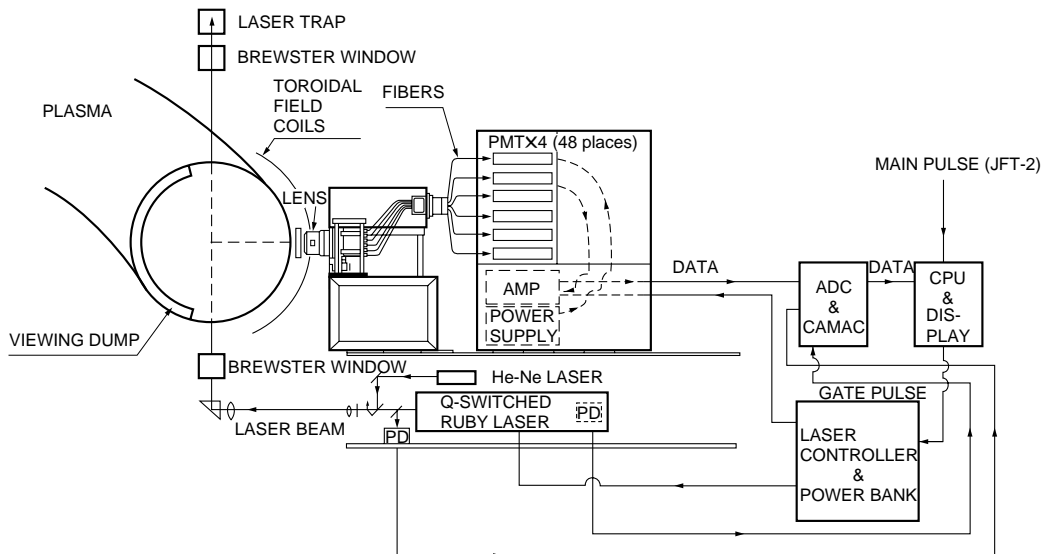
Figure 9-52: Fluorescence lifetime data of stiff-stilbene (courtesy of Prof. Yamazaki, Hokkaido University, Japan)

## 9.12 Plasma Applications

Photomultiplier tubes and MCPs (microchannel plates) are used in plasma measurements, such as plasma electron-density and electron-temperature measurement applications utilizing Thomson scattering or the Doppler effect, plasma spatial-distribution observation and plasma impurity measurements intended for controlling impurities and ions in plasma.

### 9.12.1 Overview

Figure 9-53 shows the construction of a plasma electron-density and electron-temperature measuring system,<sup>36)</sup> actually used in a Japanese tokamak-type nuclear fusion reactor "JFT-2". The detector and signal processing units used in this system are also shown in Figure 9-54<sup>37)</sup>, example of a scattered-light measuring system<sup>38)</sup> using a high-power ruby laser designed for plasma diagnosis is shown in Figure 9-55. In both systems, photomultiplier tubes are used as detectors in the ultraviolet to visible region, while multichannel spectrophotometry using a MCP is performed in the soft X-ray region.



TPMHC0039EA

**Figure 9-53: Schematic construction of a plasma electron-density and electron-temperature measuring system**

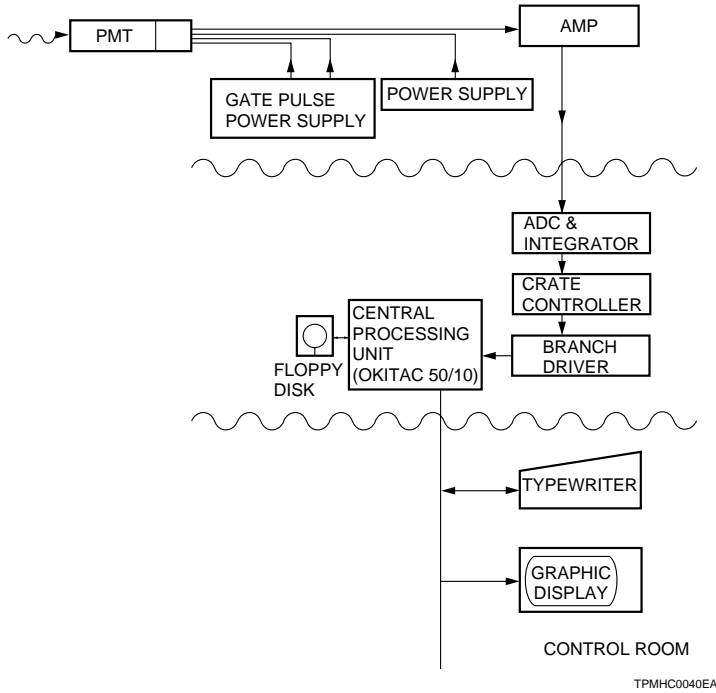


Figure 9-54: Block diagram of the detector and signal processing units used in the above system

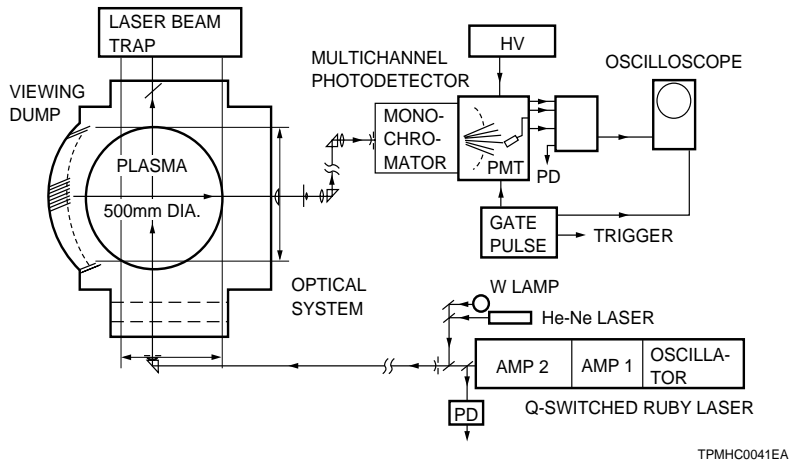


Figure 9-55: Example of a scattered-light measuring system using a ruby laser

## 9.12.2 Major characteristics required of photomultiplier tubes

- a) High photocathode sensitivity
- b) Gate operation

Photomultiplier tubes used in this field must provide gate operation to avoid damage caused by input of intense light from the excitation laser, as well as high sensitivity for detecting low light levels.

## 9.13 Color Scanners

Photomultiplier tubes are used in color scanners in photographic printing applications. The color scanner is a high-precision instrument designed to produce color-analyzed film by photoelectrically scanning an original color film or reflective print and analyzing its color balance.

### 9.13.1 Overview

Figure 9-56 shows the block diagram of a color scanner using a photomultiplier tube for each of three primary (red, green, blue) colors and black. There is another type of color scanner that uses a single photomultiplier tube for analyzing and controlling RGB colors by rotating the drum 3 times faster.

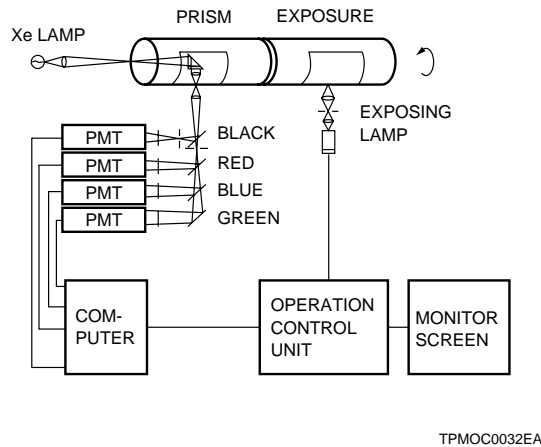


Figure 9-56: Block diagram of a color scanner

### 9.13.2 Major characteristics required of photomultiplier tubes

The following characteristics are required of photomultiplier tubes used in these applications.

- a) High quantum efficiency at each wavelength of RGB
- b) Low noise, especially no microphonic noise
- c) Fast signal-waveform fall time
- d) Good reproducibility with respect to changes in input signal
- e) High stability

Among these, fall time and reproducibility are very important factors that affect color shading and resolution of color scanners.

## 9.14 Industrial Measurement Applications

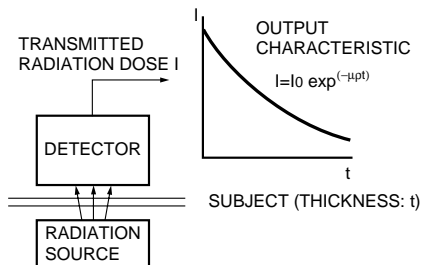
For non-contact measurement on a production line and other industrial measurement applications where rapid measurement with a high degree of accuracy and quality is essential, extensive use is made of various devices having photomultiplier tubes as detectors. These devices include thickness gauges, laser scanners and flying spot scanners, which are briefly discussed in the following paragraphs.

### 9.14.1 Thickness gauges

#### (1) Overview

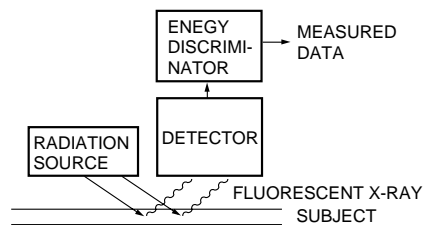
To measure the thickness of paper, plastics and steel plates on a production line, non-contact measurement techniques that use radiation such as beta rays, X rays or gamma rays are favored.

These techniques can be roughly divided into two methods: one measures the amount of beta or gamma rays transmitted through an object<sup>39)</sup> (Figure 9-57) and the other measures the amount of fluorescent X-rays<sup>40)</sup> (Figure 9-58).



TPMHC0042EA

**Figure 9-57: Principle of a transmission-mode thickness gauge**



TPMHC0043EA

**Figure 9-58: Principle of a fluorescent X-ray thickness gauge**

When the intensity of radiation incident on a material is  $I_0$ , the transmitted radiation intensity  $I$  can be expressed in the following relation:

$$I = I_0 e^{(-\mu\rho t)}$$

$t$  : thickness (m)

$\rho$  : density ( $\text{g}/\text{m}^3$ )

$\mu$  : mass absorption coefficient ( $\text{m}^2/\text{g}$ )

Since the transmitted radiation intensity is proportional to the count rate, the thickness of the material can be obtained by calculating the count rate. In general, beta rays are used to measure rubber, plastics and paper which have a small surface density (thickness  $\times$  density), while gamma rays are used to measure material with a large density such as metals. In addition, infrared radiation is also used for measurement of films, plastics and other similar materials.

Fluorescent X-rays are used to measure the film thickness of plating and deposition layers. Fluorescent X-rays are secondary X-rays generated when a material is excited by radiation and have characteristic energy of the material. By detecting and discriminating this energy, the quantitative measurement of the object material can be made.

There are a variety of detectors used in these applications, such as proportional counter tubes, GM counter tubes, photomultiplier tubes and semiconductor detectors. Photomultiplier tubes are used in conjunction with scintillators, mainly for detection of gamma rays and X-rays.

## (2) Characteristics required of photomultiplier tubes

Major characteristics required of photomultiplier tubes in these applications are as follows:

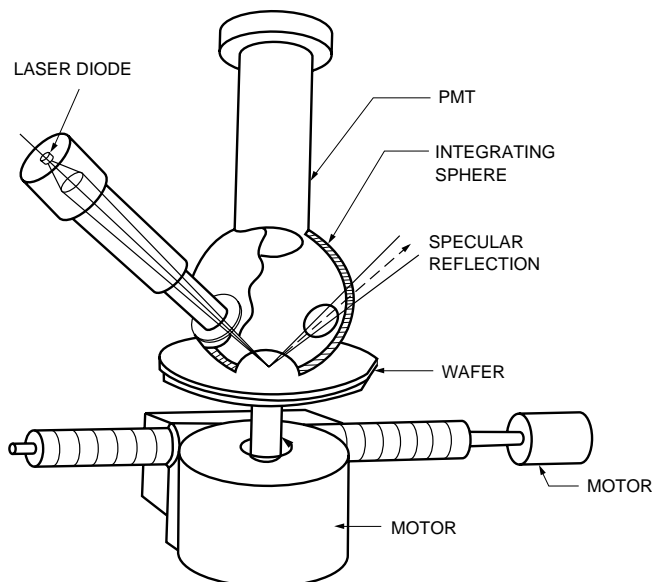
- a) Superior linearity characteristics
- b) Low hysteresis
- c) High energy resolution or pulse height resolution (PHR)
- d) Stability

## 9.14.2 Laser scanners

### (1) Overview

Laser scanners are widely used in pattern recognition such as defect inspection and mask alignment of semiconductor wafers.

In semiconductor wafer inspection systems,<sup>41)</sup> a laser beam is scanned over the wafer surface or the wafer itself is scanned while a laser beam is focused onto a fixed point. In either case, photomultiplier tubes are commonly used to detect scattered light caused by dirt, stain and defects on the wafer surface. (See Figure 9-59.)



TPMOC0034EB

Figure 9-59: Construction of the optical system for a semiconductor wafer inspection system

## (2) Characteristics required of photomultiplier tubes

The following characteristics are required of photomultiplier tubes used in laser scanners.

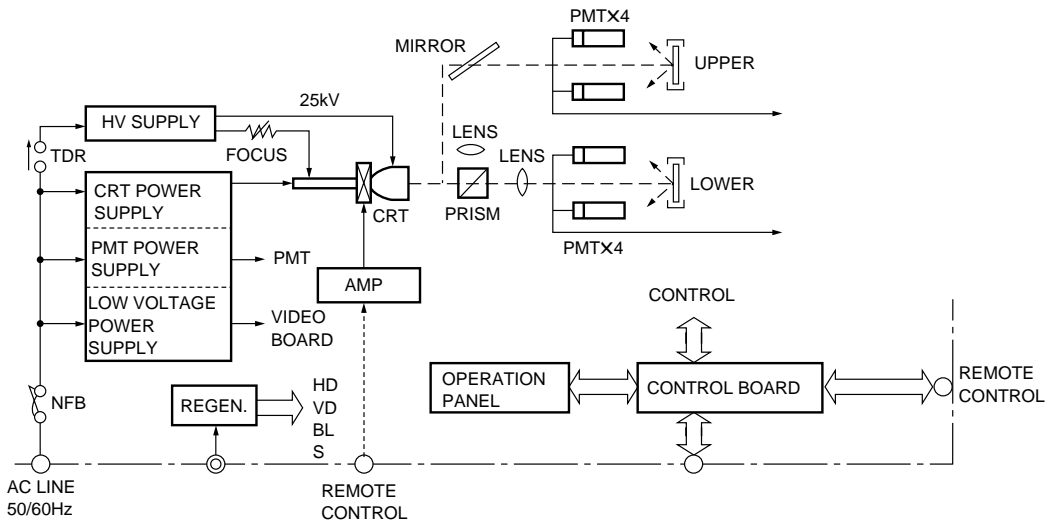
- a) Low dark current and spike noise
- b) High quantum efficiency at wavelengths to be measured
- c) Superior uniformity
- d) Superior linearity
- e) Resistance to relatively large current and good stability

### 9.14.3 Flying spot scanners

#### (1) Overview

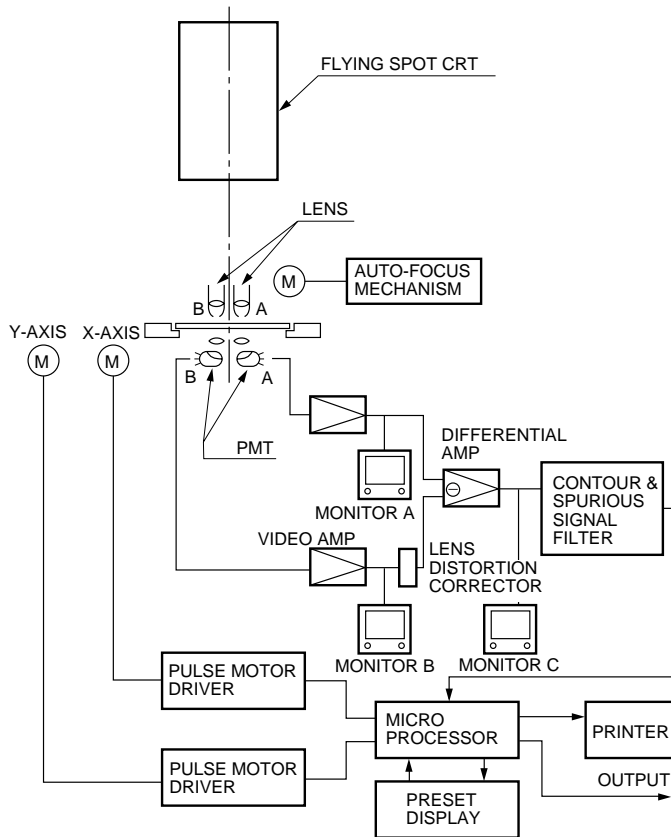
There are several methods for converting the information recorded on photographic film into electrical signals, for example, methods using a camera tube, CCD linear image sensor or flying spot scanning. Of these, flying spot scanning using photomultiplier tubes as detectors has been extensively used thanks to its advantages in processing speed, sensitivity and image quality including resolution and signal-to-noise ratio.

In a typical flying spot scanner, a special low-lag CRT (cathode-ray tube) called a flying spot tube provides a small light spot to form a raster. The raster is focused onto the film, and the transmitted or reflected light is detected by photomultiplier tubes. The block diagram<sup>42)</sup> of a typical flying spot scanner is shown in Figure 9-60. The flying spot scanner is used not only in image processing but also inspection of photolithographic masks used for fabrication of semiconductor devices. Figure 9-61 shows an example of this application.<sup>43)</sup>



TPMOC0035EA

Figure 9-60: Block diagram of a flying spot scanner



TPMOV0036EA

**Figure 9-61: Semiconductor mask inspection system utilizing a flying spot scanner**

## (2) Characteristics required of photomultiplier tubes

Photomultiplier tubes used in flying spot scanners should have the following characteristics.

- a) Low dark current and spike noise
- b) High quantum efficiency (at RGB wavelengths in the case of color operation)
- c) Wide dynamic range

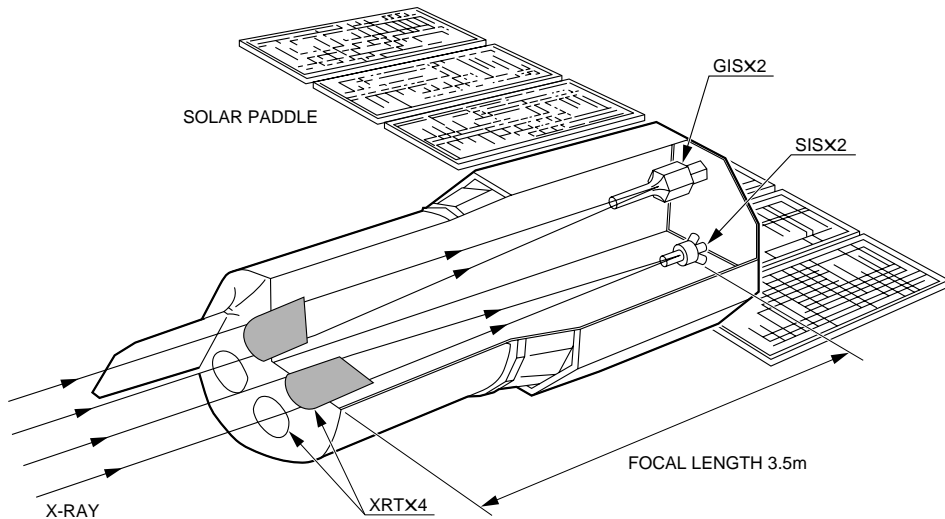
Spike noise may be a cause of a spot-like noise, and low quantum efficiency may result in an increase in shot noise, leading to deterioration of the signal-to-noise ratio.

## 9.15 Space Research Applications

Photomultiplier tubes are widely used in space research applications, for example, detection of X-rays from space, planetary observation, solar observation, environmental measurement in inner or outer space and aurora observation. In addition, photomultiplier tubes are also used for spectral measurements of various radiation in the atmosphere or outer space and measurement of X-rays from supernovas.

### 9.15.1 Overview

Figure 9-62 illustrates the structure of ASUKA launched and placed in its orbit in February 1993, as the fourth astronomical satellite for X-ray observation in Japan. A gas imaging spectrometer (GIS) is used as the detector, which consists of a gas-scintillation proportional counter coupled to a photomultiplier tube (Hamamatsu R2486X).



TPMHC0165EA

Figure 9-62: Astronomical satellite ASUKA for X-ray observation

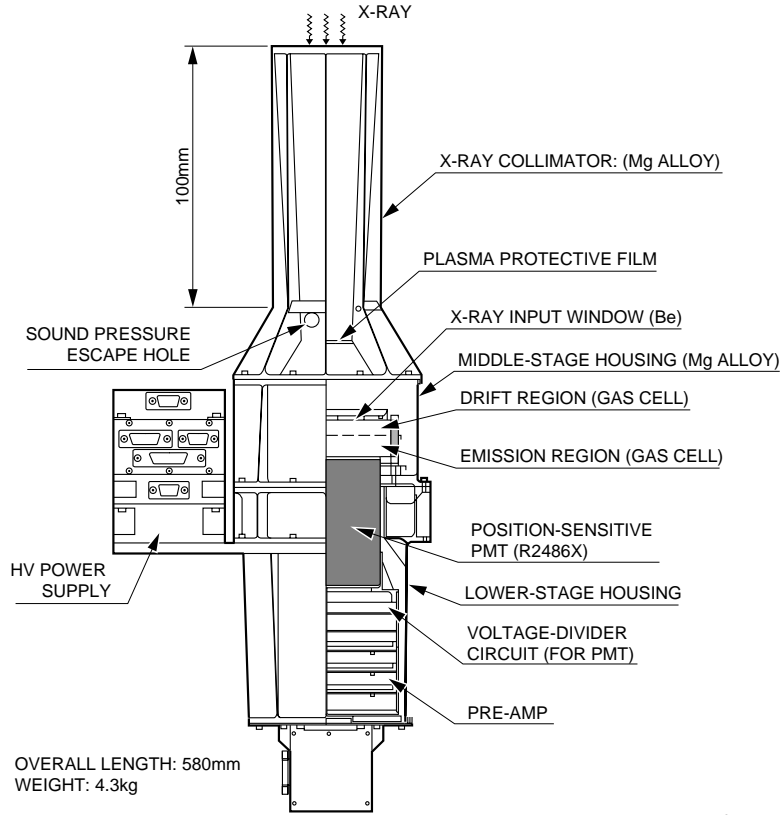


Figure 9-63: X-ray detector (GIS detector) mounted in the ASUKA

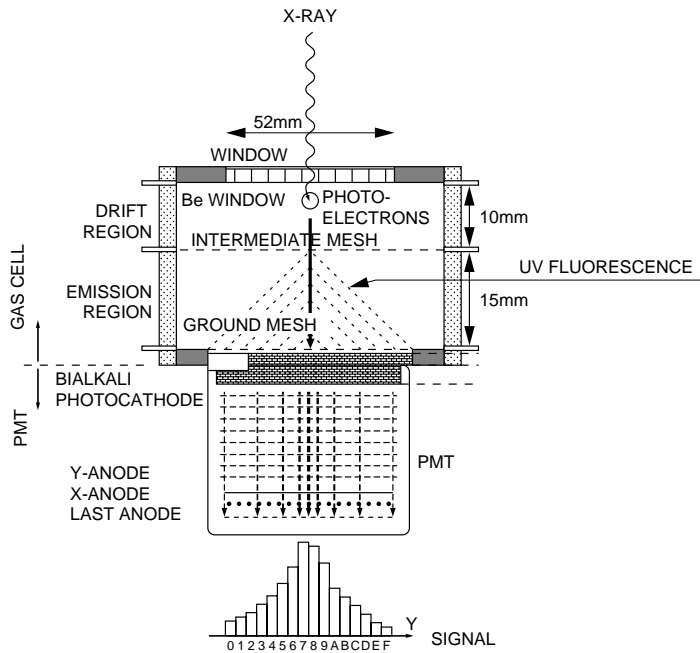


Figure 9-64: Principle of detection in the GIS detector

The ASUKA has succeeded in discovering various interesting facts, beginning from the detection of X-rays travelling from the supernova named "SN1993J", discovery of low-luminosity nucleus in the center of ordinary galaxy, and world's first detection of inverse Compton X-rays coming from a radio galaxy. Furthermore, the ASUKA successfully revealed that the low energy spectrum of CXB (cosmic X-ray background) is extending to 1keV as single photon fingers. This discovery is expected to elucidate the CXB, which is the primary object of the ASUKA.

### 9.15.2 Characteristics required of photomultiplier tubes

Photomultiplier tubes used in these applications must provide the following characteristics.

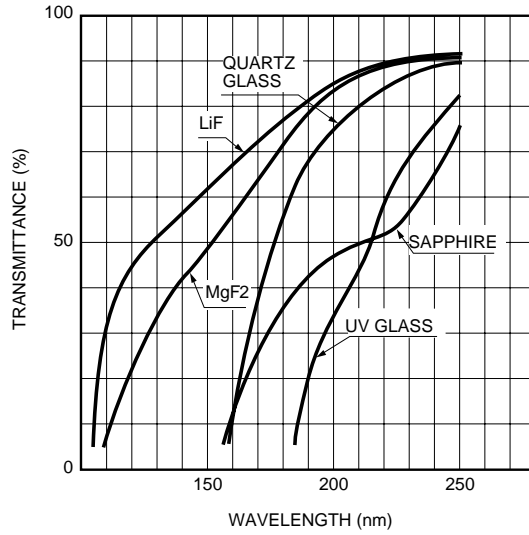
- a) High energy resolution
- b) Resistance to vibration and shock
- c) Solar blind response (in the case of vacuum UV to UV detection)

As discussed in Chapter 8, photomultiplier tube resistance to vibration and shock differs depending on the tube size and dynode structure. Normal photomultiplier tubes are resistant to a vibration of 5 to 10G, while ruggedized tubes can endure up to 15 to 30G. Table 9-5 classifies the grades of measurement conditions. Note that these grades are based on the sinusoidal vibration test, so random vibration tests should also be taken into account as well. Hamamatsu Photonics performs vibration tests according to the user's needs in order to design and manufacture vibration-proof, ruggedized photomultiplier tubes.

| Grade | Acceleration G | Frequency  | Photomultiplier Tube |
|-------|----------------|------------|----------------------|
| A     | 5.0            | 10 to 55   | Normal type          |
| B     | 5.0            | 10 to 500  | Normal type          |
| C     | 7.5            | 10 to 500  | Normal type          |
| D     | 10             | 10 to 1000 | Normal type          |
| E     | 15             | 10 to 2000 | Ruggedized type      |
| F     | 20             | 10 to 2000 | Ruggedized type      |
| G     | 25             | 10 to 2000 | Ruggedized type      |
| H     | 30             | 10 to 2000 | Ruggedized type      |

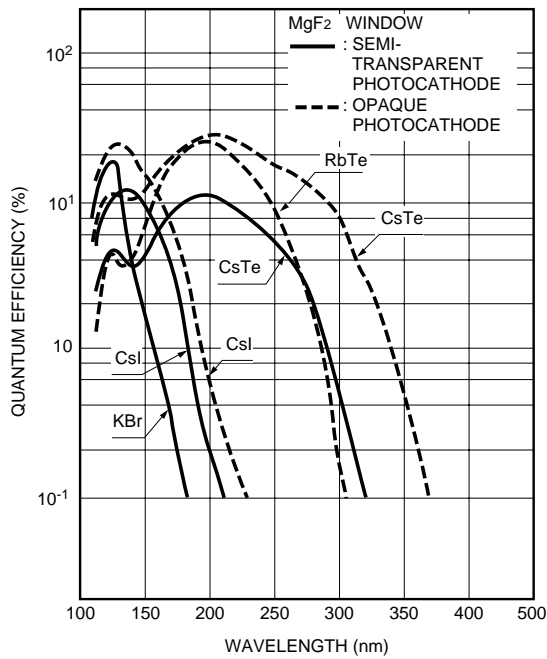
**Table 9-5: Vibration test conditions**

In the measurement of radiation traveling from space, photomultiplier tubes must have high sensitivity in the vacuum UV to UV range but also have a solar blind response. Since the detection limit on the short wavelength side is determined by the transmittance of the window material used for the photomultiplier tube, proper selection of window material is also important. Figure 9-65 shows transmittance characteristics of various window materials and Figure 9-66 shows spectral response characteristics of solar blind photocathodes specifically intended for UV detection.



TPMOB0031EA

Figure 9-65: Transmittance characteristics of various window materials



TPMOB0032EA

Figure 9-66: Spectral response characteristics of solar blind photocathodes

## 9.16 Low-Light-Level Detection

Lately, low-light-level detection is becoming increasingly important in various scientific fields. In particular, low-light-level detection techniques are in greater demand in such studies as Raman scattering, Rayleigh scattering, biology, analytical chemistry, astronomy and fluorescence analysis. The detection techniques using photomultiplier tubes include the analog DC method, analog pulse method and digital method (photon counting). Of these, the photon counting is extremely effective in low-light-level detection. The excellent characteristics of photomultiplier tubes such as high gain and low noise can be fully utilized in this field.

### 9.16.1 Overview

Low-light-level detection utilizing the superior signal-to-noise ratio of photomultiplier tubes is being applied to diverse fields including Raman scattering, biology, chemical analysis and astronomy. Figure 9-67 shows the block diagram of a laser Raman spectrophotometer.<sup>44)</sup>

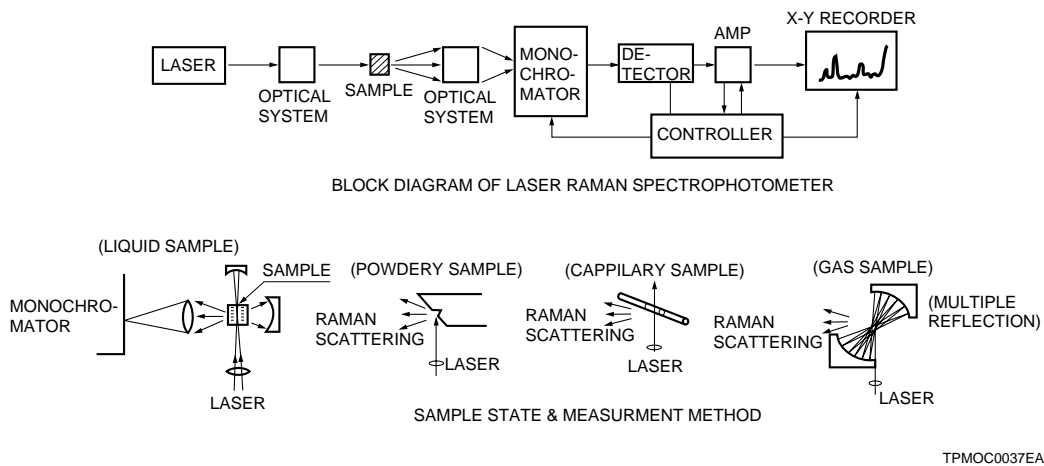
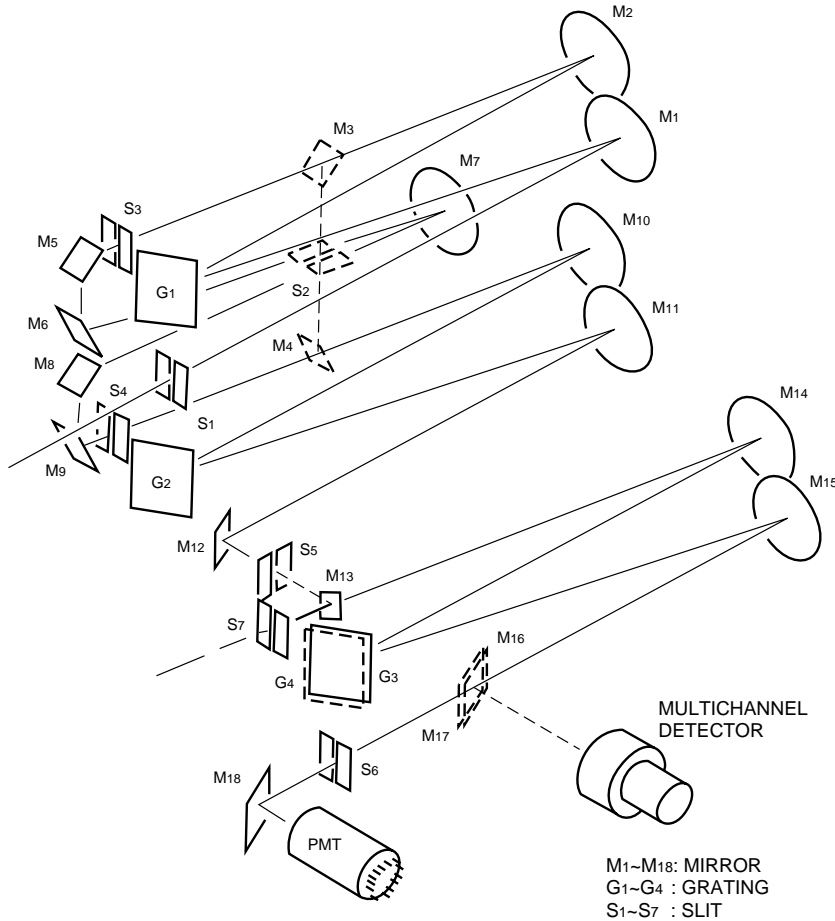


**Figure 9-67: Block diagram of a laser Raman spectrophotometer**

With recent advancements in laser technology, life science research such as a study of local protein structures utilizing Raman scattering is rapidly progressing. Because Raman scattering has an extremely low light level as compared to Rayleigh scattering (with the same wavelength as that of the excitation light), a high-quality monochromator with minimum stray light and a high-sensitivity detector must be used to separate the Raman scattering from extraneous light. A common monochromator used in Raman spectrophotometry is a double-monochromator equipped with a holographic grating or, in some cases a triple-monochromator with filter mechanism. Raman spectrophotometry requires such a complicated optical system that the incident light on the photomultiplier tube will be exceptionally low. For this reason, the photon counting method which ensures excellent signal-to-noise ratio and stability is frequently used. The monochromator and optical system used in Raman spectrophotometry must provide "minimum stray light", "high resolution" and "good light-collection efficiency". Figure 9-68 shows the optical layout<sup>45)</sup> of a laser Raman spectrophotometer. This instrument usually uses a photomultiplier tube specially selected for photon counting.



TPMOC0038EB

Figure 9-68: Optical layout of a laser Raman spectrophotometer

### 9.16.2 Characteristics required of photomultiplier tubes

The following characteristics are required of photomultiplier tubes used in photon counting.

- a) Less broadening of pulse height distribution, in other words, superior single photoelectron resolution (a sharp valley should exist so that the effects of photomultiplier tube sensitivity drift and supply voltage fluctuation can be reduced when the tube is operated over extended time periods.
- b) Less dark current pulse
- c) High gain

If linear counting is essential up to a high light level, a fast-response photomultiplier tube must be used. In this case, it is recommended that photomultiplier tubes with a linear-focused dynode or circular-cage dynode be used.

## References in Chapter 9

- 1) Japan Analytical Instruments Manufacturers' Association: Guide to Analytical Instruments, 3rd Edition, 37 (1986).
- 2) Thermo Jarrell Ash Corp. Ltd.: The Atom Scan25 Spectrometer.
- 3) H. Daidouji: The Spectroscopical Society of Japan - Measurement Method Series, 20, 129, Japanese Association of Spectroscopy (1985). (Published in Japanese)
- 4) Japan Analytical Instruments Manufacturers' Association: Guide to Analytical Instruments, 3rd Edition, 42 (1986). (Published in Japanese)
- 5) Japan Analytical Instruments Manufacturers' Association: Guide to Analytical Instruments, 3rd Edition, 45 (1986). (Published in Japanese)
- 6) K. Anan, K. Konno, Z. Tamura, M. Matsushashi, J. Matsumoto and M. Watanabe: Fundamental Biochemical Experimental Methods, 4, 32, Maruzen Corp. (1975). (Published in Japanese)
- 7) M. Yamamoto: Medical Electronics and Bioengineering, 24, 6, 54 (1986). (Published in Japanese)
- 8) M. Yamamoto: Positron CT Imaging - PET- Medical History, 127 (14), 1218-1225 (1983).
- 9) Y. Endo and K. Miyai: Protein, Nucleic Acid and Enzyme, Separate Volume 31, Enzyme Immunoassay, 13, Kyoritsu Publishing Corp. (1987). (Published in Japanese)
- 10) G. Kawashima: Introduction to Immunoassay, 29, Nanzandou (1987).
- 11) Japan Analytical Instruments Manufacturers' Association: Guide to Analytical Instruments, 3rd Edition, 228 (1986). (Published in Japanese)
- 12) G. Kawashima: Introduction to Immunoassay, 162, Nanzandou (1987). (Published in Japanese)
- 13) G. Kawashima: Introduction to Immunoassay, 83, Nanzandou (1987). (Published in Japanese)
- 14) T. Oda and H. Maeda: Protein, Nucleic Acid and Enzyme, Separate Volume 31, Enzyme Immunoassay, 243, Kyoritsu Publishing Corp. (1987). (Published in Japanese)
- 15) Association of Japanese Radiation Instrument Industry: General Guide to '84 Medical Radiation Instrument Technology. 198, Denshi Keisoku Publishing Company (1983). (Published in Japanese)
- 16) K. Kinoshita and T. Kamiyama: Fluorescence Measurement - Application to Biophysics, 83, The Spectroscopical Society of Japan (1983).
- 17) T. Hayashi: Photomultiplier Tubes For Use In High Energy Physics, 6 (1983).
- 18) Hamamatsu Photonics: Photomultiplier Tubes and Environmental Conditions (1986)
- 19) Hamamatsu Photonics: Photomultiplier Tubes and Environmental Conditions (1986)
- 20) Hamamatsu Photonics Data Sheet: Ruggedized High-Temperature Photomultiplier Tubes (1992).
- 21) Hamamatsu Photonics Data Sheet: Ruggedized High-Temperature Photomultiplier Tubes (1992).
- 22) Hamamatsu Photonics Data Sheet: Ruggedized High-Temperature Photomultiplier Tubes (1992).
- 23) M. Tsuchiya, M. Ohashi, T. Ueno: New Development of Mass Spectrometry, Modern Chemical, Extra Number 15, Tokyo Chemical Coterie.
- 24) T. Ueno, K. Hirayama, K. Harada: Biological Mass Spectrometry, Modern Chemical, Extra Number 31, Tokyo Chemical Coterie.
- 25) JEOL Ltd.: Introduction to the world of SEM (published in Japanese)
- 26) The Nikkan Kogyo Shimbun: Structure of Machine/Wonder of Technology, No. 3, 42, 1996 (published in Japanese)
- 27) JEOL Ltd.: Introduction to the World of SEM (published in Japanese)
- 28) Japan Analytical Instruments Manufacturers' Association: Guide to Analytical Instruments, 3rd Edition, 171 (1986). (Published in Japanese)
- 29) Japan Analytical Instruments Manufacturers' Association: Guide to Analytical Instruments, 3rd Edition, 179 (1986). (Published in Japanese)
- 30) Japan Analytical Instruments Manufacturers' Association: Guide to Analytical Instruments, 3rd Edition, 133 (1986). (Published in Japanese)
- 31) Japan Analytical Instruments Manufacturers' Association: Guide to Analytical Instruments, 3rd Edition, 133 (1986).
- 32) Aroka Corp.: Gated Surface Monitor.
- 33) H. Shimizu, N. Takeuchi, Y. Sasano, N. Sugimoto, I. Matsui and N. Okuda: Oyo Butsuri (Applied Physics), 50,

- 
- 11, 1154 (1984). (Published in Japanese)
- 34) Hamamatsu Photonics Data Sheet: MCP-PMTs (Microchannel Plate - Photomultiplier Tubes)
- 35) I. Yamazaki, H. Kume, N. Tamai, H. Tsuchiya, K. Oba: *Oyo Butsuri (Applied Physics)*, 50, 7, 702 (1985)
- 36) T. Yamauchi et al.: *Jpn. J. Appl. Phys.* 21, 2, 348 (1982).
- 37) T. Yamauchi et al.: *Jpn. J. Appl. Phys.* 21, 2, 350 (1982).
- 38) Y. Suzuki, A. Funabashi, A. Ogata and T. Matoba: *Measurement and Control*, 17, 1 (1977).
- 39) Japan Analytical Instruments Manufacturers' Association: *Guide to Analytical Instruments*, 3rd Edition, 143 (1986).
- 40) Japan Analytical Instruments Manufacturers' Association: *Guide to Analytical Instruments*, 3rd Edition, 143 (1986).
- 41) TOPCON: *Wafer Dust Inspection System WM-3* (1990).
- 42) Ikegami Tsushinki Co., Ltd: TKF-106.
- 43) Y. Nakada: (*Electronic Parts and Materials*) '83, Separate Volume, 189, Kogyo Chosa Kai Publishing Co., Ltd. (1983).
- 44) Japan Analytical Instruments Manufacturers' Association: *Guide to Analytical Instruments*, 3rd Edition, 46 (1986). (Published in Japanese)
- 45) Japan Spectroscopic Co., Ltd.: NR-1800.

# MEMO